Synthesis and Characterization of Tailored Photoactive Macromolecules

Scott R. Trenor

Dissertation submitted to the Faculty of the
Virginia Polytechnic Institute and State University
in partial fulfillment of the requirements for the degree of
Doctor of Philosophy
in
Macromolecular Science and Engineering

Brian J. Love, Co-chair
Timothy E. Long, Co-chair
Thomas C. Ward
David A. Dillard
Judy S. Riffle

April 16, 2004
Blacksburg, Virginia

Keywords: Polymer Photochemistry, Coumarin, Cinnamates, Alkyl Acrylates, Adhesives

Synthesis and Characterization of Tailored Photoactive Macromolecules

Scott R. Trenor

ABSTRACT:

Coumarin and cinnamate derivatives were positioned as either polymer chain ends or side groups to synthesize photoactive macromolecules and gain the ability to reversibly control molecular weight and crosslink density using UV light. The cinnamates and coumarins were reacted onto the polymers via multiple reaction pathways. Polymers were functionalized with coumarin or cinnamate groups via an esterification reaction between hydroxyl functionalities and an acid chloride derivatized coumarin group. In addition to the esterification reaction, cinnamates were also coupled to polymers via a ring opening reaction between a hydroxyl functionalized cinnamate derivative and a maleic anhydride repeat unit copolymerized into the polymer. Both functional groups undergo a [$2\pi + 2\pi$] photodimerization reaction (coumarin groups in the UVA and cinnamate groups in the UVB), which was utilized to crosslink and chain-extend macromolecules. Coumarin dimers possess the additional ability to photocleave and thus reverse when irradiated at 254 nm.

The coumarin reversible photodimerization reaction was utilized to reversibly increase the molecular weight and molecular weight distribution of coumarin-functionalized PEG monols and diols. For example, the number average molecular weight of the coumarin-functionalized PEG diol doubled and the

molecular weight distribution increased from 1.08 to 2.75 when exposed to 110 J cm^{-2} of UVA irradiation. Subsequent photocleavage (UVC irradiation, 2 J cm^{-2}) of the chain-extended PEGs, cleaved coumarin dimers decreasing the molecular weight and molecular weight distribution to their original values.

A number of poly(alkyl acrylate) and poly(methyl acrylate) systems were functionalized with coumarin groups to study the effect of the glass transition temperature and alkyl ester side group composition on the photodimerization reaction and subsequent crosslinking. The glass transition temperature (T_g) acted as an on/off switch for the photodimerization reaction. While the absolute difference between T_g and irradiance temperature did not affect the rate or extent of photodimerization reaction, polymers with a T_g greater than the irradiance temperature displayed less reaction than those with a T_g lower than the irradiance temperature. The final extent of conversion was controlled by a complex combination of factors including alkyl ester side chain steric bulkiness. Coumarin-functionalized alkyl acrylates based on ethylhexyl acrylate were tested as detachable PSAs. A 98% decrease in the adhesive peel strength was observed after exposure to UVA irradiation.

Cinnamate groups were utilized in the design and synthesis of UV-curable hot melt pressure sensitive adhesives (PSAs). The cinnamate groups were attached to the PSAs to provide a method to increase molecular weight and add a small amount of crosslinking leading to an increase the adhesive strength of the PSAs. Broadband UV irradiation from a laboratory scale industrial lamp increased the peel strength of the adhesives. Postcure of the irradiated cinnamate-

functionalized UV-curable hot melt PSAs was reduced compared to photoinitiated free-radical photocurable UV-curable hot melt PSAs.

Acknowledgments

I would like to extend my thanks to Dr. Brian J. Love who has been an excellent advisor since the first day I walked on campus and Dr. Timothy E. Long who has been an excellent guide and advisor over the last two and a half years. I would also like to thank the members of my committee: Dr. David A. Dillard, Dr. Judy S. Riffle, Dr. Thomas C. Ward, and the late Dr. Allan R. Shultz for their time and valuable instruction during my time at Virginia Tech.

I would also like to thank the Center for Adhesive and Sealant Science (CASS) at Virginia Tech, the Adhesive and Sealant Council (ASC) Education Foundation, Procter and Gamble, and the Avery Dennison for their constant financial support and introduction to the adhesive technologies field. The experiences during these interactions have greatly enhanced my overall experience in graduate school. I feel very fortunate to have experienced lectures and conferences with the extraordinary faculty associated with CASS. I would especially like to thank Tammy Jo Hiner and Ester Brann who made our trips to and from the CASS sponsored events smooth and comfortable. It was always a pleasure to sit and chat with the two of them between talks. In addition, I would like to give additional thanks to Dr. Dillard for providing students with the excellent opportunities to travel and learn at Adhesion Society and ASC meetings.

I would like to thank Dr. Cheryl Heisey for spending her time to read through and edit the majority of this work. You have made the publication and dissertation writing process so much easier for myself and the other students in the group.

I need to expressly thank Millie Ryan, Laurie Good, Angie Flynn and Susette Sowers for all of their continued help. When all of my efforts had failed, a quick trip to any of these ladies would get the job done in a minute. Ms. Jan McGinty is acknowledged for her repeated help with the chemistry stockroom. She was always able to find that "lost" package whether or not it had already arrived. I also want to thank Tom Glass, Geno Iannaconne and Steve McCartney who aided me with analytical equipment during my time here.

The bulk of my thanks go to those who I spent many hours with in the lab, beginning with those in the Hancock labs and ending with those in the Davidson. In the beginning, Mitch, Julie and Sumitra greatly helped me ease into graduate school. Then there was Emmett and Sandra in the Ward lab, both of whom I met during my first Adhesion Society conference and made every conference/bike ride/NASCAR race a wide-open experience. I also want to thank those whom I met during the last couple of years working in Davidson. There was Vlad, who "I don't know" what to say about him other than he taught me a form of chemistry, that I will never forget, "Maybe good, maybe bad, I don't know." Then there were the ones who really made lab life and outside life truly enjoyable. I would like to

thank the lunch group of Ann, Matt and Jeremy for all the great times in and out of the lab and for everything that I have learned from them. Jeremy, thanks for keeping me from falling asleep during the tremendously exciting time in north-central PA. Matt and Ann, thanks for all of the good times that we spent out of the lab and for the help getting home from some of those good times.

I would like to thank Rebecca and Erin whom have both helped me tremendously in the lab and I wish the best for both of you.

Many thanks go to all of my colleagues in the Long group Hahn Hall labs who also made my experience here memorable.

I would like to thank my parents for their guidance and support throughout my life. They guided me through the winding path of life, while giving me enough room to let me make my own mistakes (and hopefully learn from them).

I would like to thank Killian, my dog. No matter how badly things were going in the lab or just in general, he was always there wagging his tail and happy to see me.

Finally, where would I be without my wife, Julie. She has helped me in so many ways that I could not find the right way to start to thank her.

Table of Contents

List of Figures

List of Tables

List of Schemes

CHAPTER 1 INTRODUCTION AND RESEARCH SIGNIFICANCE

The primary focus of this work involves the use of coumarins and cinnamates in polymers as a method to modulate the crosslink density or molecular weight of the photoreactive polymers. 7-Hydroxycoumarin (Figure 1-1(a)), and some derivatives undergo a ($2\pi + 2\pi$) photodimerization reaction when irradiated in the Ultraviolet-A (UVA) region of the electromagnetic spectrum. The newly formed dimer, linked by a cyclobutane ring, can be later cleaved when irradiated at wavelengths less than 290 nm. Similarly, various derivatives of *trans*-cinnaminic acid (Figure 1-1(b)) also undergo a ($2\pi + 2\pi$) photodimerization and a competing *trans* to *cis* or *cis* to *trans* isomerization when irradiated in the Ultraviolet-B (UVB) region of the electromagnetic spectrum. As with the coumarin dimers, some of the cinnamate dimers are cleavable when irradiated in the Ultraviolet-C (UVC), although the photocleavage reaction is less efficient than the coumarin dimer. An additional drawback to cinnamate dimer photocleavage is the asymmetric cyclobutane cleavage reaction.

Reversible crosslink points can be added to polymers by incorporating coumarin or cinnamate groups through the 7-hydroxy position or the ester linkage of the coumarin and cinnamate groups, respectively. Upon irradiation in the UVA region, the photoactive groups dimerize, and a crosslink or branch point is incorporated into the photoactive polymer. Similarly, irradiation of the

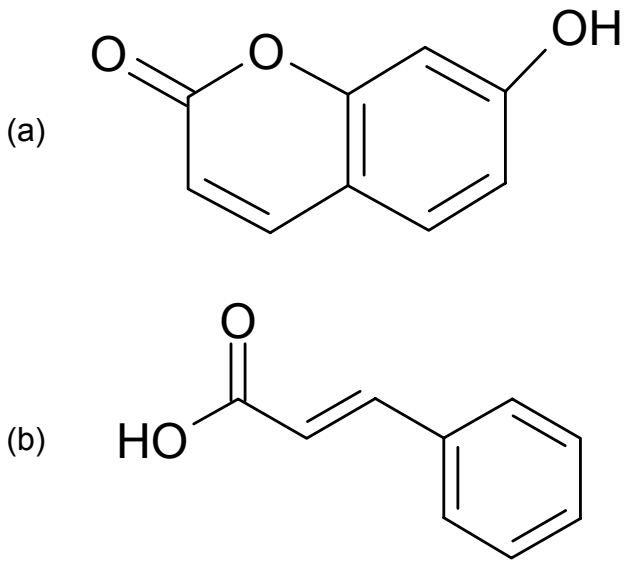

Figure 1-1. The chemical structure of 7-hydroxycoumarin (a) and *trans*-cinnaminic acid.

crosslinked/branched polymer below 290 nm cleaves the crosslink or branch point formed by the cyclobutane ring, and reverts the polymer structure to its initial structure.

This photodimerization/photocleavage is manipulated in a number of systems to achieve different goals (Figure 1-2). For example, changing the crosslink density in a pressure sensitive adhesive affords changes in the peel strength of the adhesive. Depending on the concentration of the photoactive groups, polymer composition, and polymer molecular weight, irradiation can increase, decrease or decrease then subsequently increase the adhesive peel strength.

This work will result in a better understanding of the photophysics of tailored polymer architectures containing coumarin or cinnamate groups incorporated as side chains within the polymer backbone or as chain ends. **Error! Reference source not found.**Figure 1-2 shows a summary of the work presented in this dissertation. Starting with $2\pi + 2\pi$ photodimerization as the core technology, reversible and nonreversible systems were designed using coumarin and cinnamate derivatives, respectively. Following the coumarin path (chapters four through seven), the photoreversible chain extension of PEG is studied, and subsequently the effect of chain- extension on its crystallization kinetics. The photocrosslinking of alkyl acrylates and alkyl methacrylates was also studied to determine the effect of chain mobility and glass transition temperature (T_g) on the extent of the photodimerization reaction. This understanding of coumarin dimerization reaction rates allowed for the use of either cinnamate or coumarin groups in a number of novel systems.

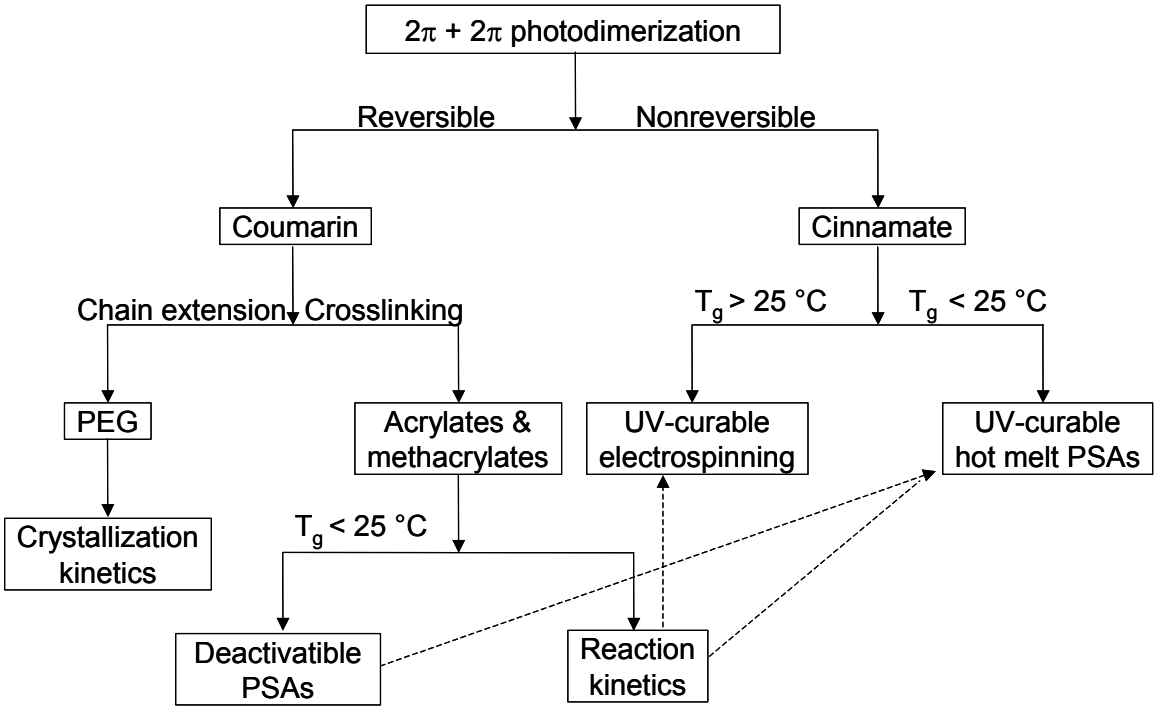

Figure 1-2. Roadmap of original scientific contributions. Dashed lines indicate transfer of results to a new system.

The low T_g acrylates were subsequently employed as deactivatable and reactivatable pressure sensitive adhesives. Following the cinnamate route (chapters eight through ten), two very different systems were studied. Both systems were designed utilizing what was learned from the coumarin-functionalized poly(alkyl acrylates) and poly (alkyl methacrylates). The first combines the photodimerization reaction of the cinnamate groups, with the electrospinning processing technique. Crosslinked, nonwoven fibers were made via the *in situ* UV-curing of electrospun fibers. The second system is a cinnamate functionalized multicomponent alkyl acrylate polymer for use as UV-curable acrylic hot melt adhesives.

CHAPTER 2 LITERATURE REVIEW

2.1 PRESSURE SENSITIVE ADHESIVES

2.1.1 Introduction.

Pressure sensitive adhesives (PSA) represent a major class of adhesive materials currently of industrial and scientific interest. The Pressure Sensitive Tape Council defines a PSA as a material that possesses the following five material properties:[1]

1. Aggressive and permanently tacky
2. Adheres without the need of more than finger or hand pressure
3. Requires no activation by water, heat or solvent
4. Exerts a strong holding force
5. Has sufficient cohesiveness and elasticity that it can be removed from smooth surfaces without leaving a residue.

These five requirements seem simple enough to achieve, although in practice, they are comprised of contradictory properties. For example, for a PSA to adhere with the application of a small amount of pressure, it must possess a low enough viscosity (liquid-like) to flow over the time scale of the application.[1-6] However, in order to exert a strong holding force, there must be sufficient resistance to flow (entanglements and crosslinks) to provide the desired mechanical strength. While the following sections will provide some insight into the factors influencing bond formation, rupture and the mechanical properties of PSAs, it is important to note that the processes governing the behavior of PSAs are far from understood.[7]

2.1.2 **Bond Formation.**

There are two major aspects governing the formation of a bond between a PSA and a substrate. The first is the surface chemistry of the substrate and the adhesive, and the second is the rheological properties of the adhesive in the bonding time scale. The work required to peel (Equation 2-1) is a combination of the thermodynamic factors (interaction between the substrate and the adhesive, W_A) and a term which describes the energy dissipated during peeling ($f(\nu,T)$).[1]

Equation 2-1. $$Work = W_A \times f(\nu, T)$$

The thermodynamic work of adhesion (Dupré equation, Equation 2-2) plays an important role in the formation of an adhesive bond. W_A describes the work per unit area required to separate the interface between the substrate (solid, S) and the adhesive (liquid, L) in a fluid medium (m, typically assumed to be air). Thus, in Equation 2-2, γ_L^m is the surface tension of the adhesive, γ_S^m interfacial free energy of the adherend and γ_{SL} is the interfacial free energy of the adhesive/substrate interface. Therefore, W_A is the free energy of the newly created surfaces minus the free energy of the surfaces destroyed during the bonding event.[7,8]

Equation 2-2. $$W_A = \gamma_S^m + \gamma_L^m - \gamma_{SL}$$

While γ_L term in the Dupré equation is easily measurable, the other terms are not directly measurable. However, measurement of the contact angle of the adhesive on the substrate leads to a relationship between the free energies of

the interfaces (Equation 2-3). Substitution of Equation 2-3 into Equation 2-2 gives the Young-Dupré equation (Equation 2-4), which allows one to calculate the thermodynamic work of adhesion from experimentally available quantities.

Equation 2-3. $$\cos\theta = \frac{\gamma_S - \gamma_{SL}}{\gamma_L}$$

Equation 2-4. $$W_A = \gamma_L(1+\cos\theta)$$

While the use of the Young-Dupré equation provides some insight regarding the bonding mechanism, it assumes only molecular interactions. In reality, other mechanism may greatly influence the formation of an adhesive bond including: adsorption of the adhesive across the interface, diffusion of the adhesive across the interphase, mechanical interlocking of the adhesive onto a "rough" surface, and electrostatic interactions across the interface.[7] Although the interactions do not occur with every adhesive bond, the interactions can individually increase the bond strength.

According to the Young-Dupré equation, it is apparent that wetting is important to adhesive formation. The degree of wetting (measured from the contact angle) should be as high as possible (i.e., the contact angle should be as low as possible) to maximize bond strength. The equation indicates that if the adhesive does not wet a surface, then formation of an adhesive bond is not possible. This is an obvious shortcoming of the equation, since PSAs that do not wet Teflon substrates have been employed as adhesives for Teflon.[1]

This contradiction leads into the other prerequisite for adhesive bond formation: rheological properties of the adhesive. Dahlquist first studied the adhesive creep compliance necessary for adhesive bond formation in the late 1960s.[3,9,10] He determined that a 1 s creep compliance greater than 10^{-5} Pa^{-1} (at the use temperature) was necessary for an adhesive to conform to the substrate. As the compliance increases above that value, the adhesive is less viscous and can flow and properly wet the substrate. On the other hand, if the compressive modulus is too low, the adhesive can flow out of the bond region and no bond is formed. A time scale of 1 s was chosen since it was the typical application time for PSAs. However, an adhesive with a compressive modulus > 10^5 Pa can still be used if the time scale is lengthened or the temperature is changed.

Chang and coworkers further developed this relationship with the viscoelastic windows (VW) concept.[4-6] The VW relationship describes various ranges of material properties such as the dynamic storage and loss moduli (G' and G'', respectively) appropriate for a typical range of applications (Figure 2-1). The combination of the values of the G' and G'', as measured from the rheological master curves of the PSA, are divided into four regions plus a general purpose region each describing the PSA properties.[4] For example, an adhesive with $8x10^4$ Pa < G' < $1x10^6$ Pa and $7x10^3$ Pa < G" < $1x10^6$ Pa (at the use temperature) is classified as a general purpose PSA because the viscoelastic properties of the adhesive place it in the transition flow region (medium modulus and medium energy dissipation during peel). If the desire was to produce a high

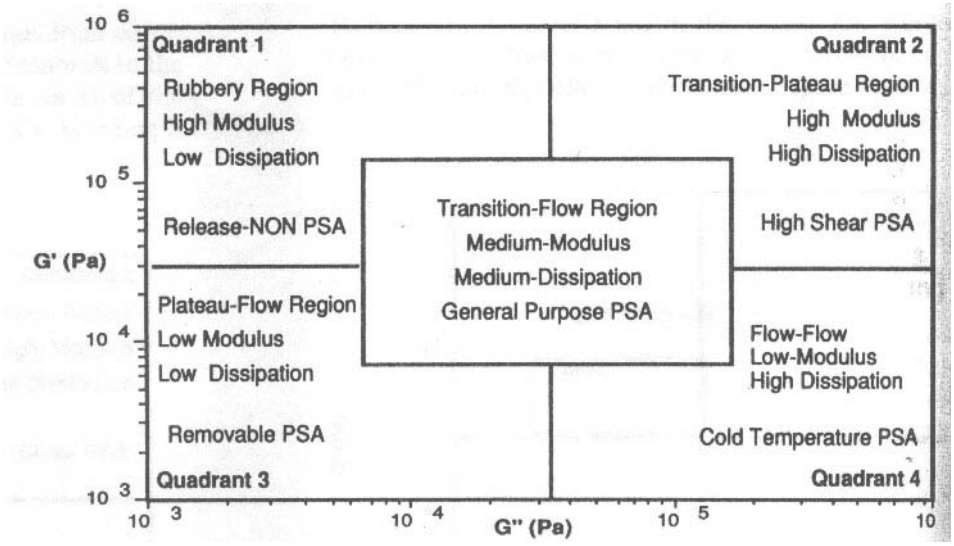

Figure 2-1. Chang's concept of viscoelastic windows of PSAs related to the rheological characteristics of the adhesive. Reprinted from [4] with permission of Taylor & Francis, Inc.

shear strength PSA, the desired G' and G'' values would be higher, leading to an adhesive that dissipates larger amounts of energy.

Chang later combined the effect of bond formation with the debonding process (180° peel test) into a single simplified correlation (Equation 2-5):[6,10]

Equation 2-5.
$$P \propto I \times \frac{G''(\omega_1)}{G'(\omega_2)}$$

Where P is the peel strength, *I* is related to the intrinsic surface energy, G' is measured at the bonding frequency (1 rad sec^{-1}) and G" at the debonding frequency (435 rad sec^{-1}). Chang's relationship used the debond frequency mathematically derived by Tse under the assumptions that a 37 μm adhesive was peeled at an angle of 180° at a rate of 30.48 cm min^{-1}.[11] Whereas, the bonding frequency was chosen as the approximate time for bond formation.

Tobing and Klein recently compared the adhesive and rheological properties of poly(EHA-*co*-AA) and poly(*n*BA-*co*-AA) to study Chang's relationship (Equation 2-5).[10] The authors discovered that the relationship did in fact hold true for the poly(EHA-*co*-AA) and poly(*n*BA-*co*-AA) systems. Although the polymers had equivalent molecular weights, the ratio of G":G' an order of magnitude higher in the poly(EHA-*co*-AA) than the poly(*n*BA -*co*-AA) and consequently exhibited significantly higher peel strength.

2.1.3 Effect of Polymer Parameters on PSA Mechanical Properties.

2.1.3.1 *Chemical Composition.* The adhesive composition plays an important role in the peel strength of the adhesive. *n*BA and EHA make up the highest

volume of monomers used in acrylic PSAs. While *n*BA and EHA both form polymers with T_gs less than -30 °C, the resulting adhesives have strikingly different properties. For example, if all other parameters are held constant, EHA based adhesives display higher peel strengths than the *n*BA based adhesives. The difference in properties results from the entanglement molecular weight (M_e) of each polymer (M_e for poly(EHA) = 37,400 and M_e for poly(nBA) = 20,700 as calculated from rubbery plateau measurements).[10,12] Tobing and Klein studied the difference in PSA properties between nBA and EHA based adhesives (each polymer had 2.5 wt% acrylic acid).[10] Since the M_e of poly(EHA) is approximately twice that of poly(nBA), the EHA adhesive dissipates a higher amount of viscoelastic energy during the peel test, thus increasing the peel strength relative to the poly(nBA). However, selecting the poly(EHA) adhesive reduces the shear strength of the adhesive, which is inversely proportional to M_e.

Zosel and coworkers studied the possible causes of fibrilation (elongation of cavities during tack testing) and its effect on tack strength.[13] Since the storage modulus is inversely proportional to M_e, it was proposed that adhesives with high M_e will separate by fibrilation and thus have higher tack energy. Zosel tested the hypothesis; of the polymers tested in the study, those with high M_e failed with the formation of fibrils and had higher tack energies. If Zosel's results were applied to Tobing's polymers, the poly(EHA) would form fibrils and thus have a higher tack than the poly(*n*BA). While the failure mechanisms were not discussed in Tobing's report, the poly(EHA) adhesives did have higher tack strengths than the poly(*n*BA).[10]

Many of the factors that affect peel strength of a PSA also influence the shear strength. Tobing's study included acrylic acid in order to increase the cohesive strength of the adhesives; this in turn increases shear strength.[1-3,10,14-16] Shull and coworkers studied the effect of adding small amounts of methyl acrylate or acrylic acid into poly(*n*BA) on PSA tack. While both comonomers increased tack and the cohesive strength of adhesives, the acrylic acid also has the ability to hydrogen bond either to other acrylic acid groups in the polymer or to hydrophilic substrates, further increasing the peel strength of the adhesive.[1-3,10,15] Shull reported that when polymers of equal molecular weight were compared, the polymer with a small fraction of methyl groups disentangled 10,000 times faster than the polymer with a small fraction of acrylic acid groups.[16-19] While the authors found this fact surprising because the relaxation time of the acrylic acid containing polymers was only 8 times lower, Shull may not have considered potential hydrogen bonding by the acrylic acid groups. Essentially, these researchers had unknowingly added hydrogen bonding to their system, which further increased the cohesive strength.

2.1.3.2 Adhesive Molecular Weights and Molecular Weight Distributions. Since the M_e of an adhesive is so important, it follows that molecular weights and molecular weight distributions also play an important role in adhesives.[20] PSAs typically exhibit a broad molecular weight distribution. In fact, a delicate balance of high and low molecular weights is necessary to achieve the desired properties: low molecular weights allow for short-term mobility (Dahlquist criteria) and high molecular weights are necessary for bonding and shear strength. Increasing an

adhesive's molecular weight can either increase or decrease the polymer peel strength. Since increasing molecular weight increases the modulus of elasticity, the peel will force increase, in the case of cohesive failure but will decrease if the adhesive fails adhesively.[8,15,20] Increases in molecular weight also decrease chain mobility, which can reduce the volume of adhesive deformed during the peel test, further reducing the peel force.

Although a PSA must to conform to the Dahlquist criteria to form the bond, adherence to the Dahlquist criteria is no longer necessary once the bond is formed. At this point, the M_e and gel fraction partially dictate the viscoelastic properties of the peel strength.[10,15,21] As with tack, the higher the M_e the easier the adhesive forms fibrils during peeling, thus increasing the peel strength (assuming the M_n of the polymer is significantly above M_e) until the high molecular weights decrease the mobility and tack begins to decrease. Figure 2-2 illustrates this behavior with an increase and subsequent decrease in the loop tack of an uncrosslinked acrylic based PSA as the ratio of M_w to M_e increases.[10]

Shull and coworkers have recently investigated the influence of "molecular features" on the tack of acrylic polymers.[16] In order to have good tack strength an adhesive needs to be viscous enough to flow around the substrate in compression, but also have enough entanglements (whether physical or chemical) to restrict chains and force them to slide past one another when pulled apart. Shull studied six polymers based on *n*BA with different acrylic acid contents and narrow molecular weight distributions. Even though the glass

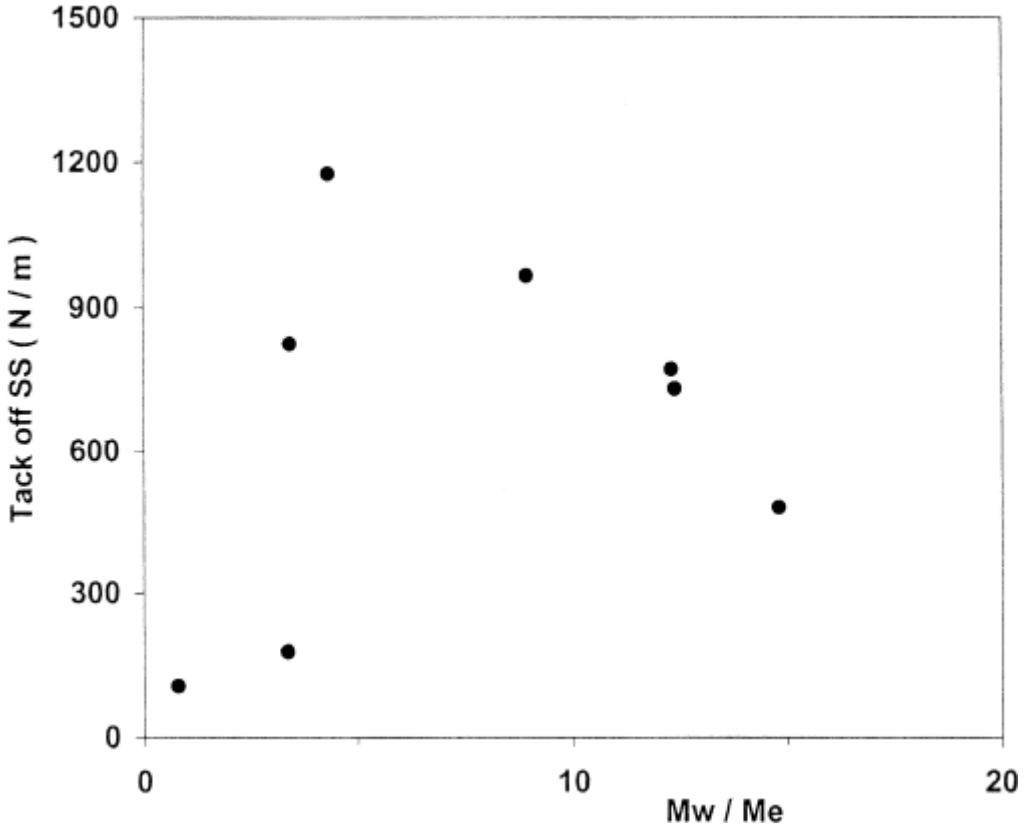

Figure 2-2. The effect of M_w/M_e on the loop tack strength of an acrylic PSA. Reprinted from ref. 10 with permission of John Wiley & Sons, Inc.

transition temperatures of the six polymers ranged from -47 to -57 °C, the range in molecular weights provided a larger range in relaxation times from 6.2 s to 3,100 s at 20 °C. Their findings indicate that cavitation is an elastic process and controlled by higher molecular weight molecules (longer relaxation times). A combination of the viscous and elastic properties of the adhesive dictated the final cavity size with a decrease in average size of the cavities with increasing molecular weight.[16] The final extension and adhesive bond breakage was not separable in the narrow molecular weight polymers but was determined to be governed by chain disentanglement from studies conducted on other PSAs.[16,19] Shull's research also concluded that due to the wide range of viscoelastic properties needed to provide the desired peel, shear, and tack properties, monodisperse polymer does not perform well as PSAs.[16] While short relaxation times are necessary for flow of the adhesive around the substrate, the longer relaxation times are necessary to increase the tack, peel and shear strength. Other researchers have reported similar results to Shull's work.[1-3,15,22]

2.1.3.3 Crosslinking. While a small amount of crosslinking is desirable in acrylic PSAs, extensive amounts of crosslinking PSAs typically increases the shear strength, while decreasing peel and tack strength.[2,3,8,15,22] Zosel reported that the UV-crosslinking of model PSAs with high M_es decreased its tack.[13,23] These results are partly due to the difference between the M_e and molecular weight between crosslinks (M_c) of the PSA. When $M_e < M_c$, the PSA can entangle into the gel. However, when $M_e > M_c$, the gel fraction acts as a filler in the PSA since the crosslinks are too close together for the loose chains to entangle.[10] Webster

and coworkers used what is typically a detrimental reaction, extensive crosslinking leading to a decrease in peel strength as an advantage.[24-26] Webster's group utilized photoinitiated polymerization of pendant acrylate groups to crosslink a medical grade pressure sensitive adhesive. The increase in the crosslink density decreased chain mobility and decreased the PSA peel strength.

While crosslinking is detrimental to peel and tack, it is advantageous to PSA shear strength. Shear strength is directly proportional to the zero-shear viscosity (whereas peel strength is not), which is influenced by the entanglement and crosslinking. Thus, decreasing the M_e (which increases entanglements) or increasing the crosslink density of the PSA increases the shear holding power while decreasing the peel strength.[1,2,9,21]

2.1.4 **Effect of Sample Preparation and Testing Parameters.**

While there are too many individual testing parameters influencing PSA properties to list them all, this section will describe a few of the more common effects. The first of these effects is the adhesive thickness. Similar to a number of the polymer parameters, adhesive thickness has opposite effects for peel and shear strengths. Gent and Kinloch have reported that peel strength increases with increasing adhesive thickness, reaching a maxima before decreasing. The position of the maxima relative to thickness depends on the contribution of plastic yielding in the backing material.[27,28] As for shear strength, Charmeau and others have reported that the shear holding time is inversely proportional to the bond thickness.[3,10,15,29]

The choice of backing materials, backing material thickness and peel angle all affect the peel strength. For example, increasing the thickness of the backing material increases the peel strength since the peel strength is directly proportional to the amount of adhesive under deformation and energy required to deform the backing material.[15,27] As the backing material becomes thicker, more energy is required to deform the backing and more PSA is deformed at the crack tip leading to higher peel strengths, with a maxima occurring at a specific thickness depending on the substrates.[27,30] The peel strength is also dependent on the peel angle and differs depending on the backing material. Kaelble reported peel strength displaying two maxima, the first between 60 - 70° and the second near 180° for glass cloth tape.[15] Kinloch reported that while the peel strength increases with increasing peel angle for polyethylene/aluminum laminates, the adhesive fracture energy remained constant.[30] Gent reported that 180° peel testing gave higher peel strengths than 90° peels for Mylar-backed adhesives(Figure 2-3).[27] This was due a combination of increased plastic deformation in the backing material and causing a larger deformation in the adhesive resulting in greater energy losses. The testing rate also influences the measures peel strength and tack. As the testing rate increases, the material acts more elastic and a transition from cohesive to adhesive failure occurs corresponding to the transition from rubbery to flow behavior. Once adhesive failure occurs, the peel strength increases with increasing peel rate until stick/slip failure becomes prominent and the peel strength begins to decrease.[8,15,17,19,31]

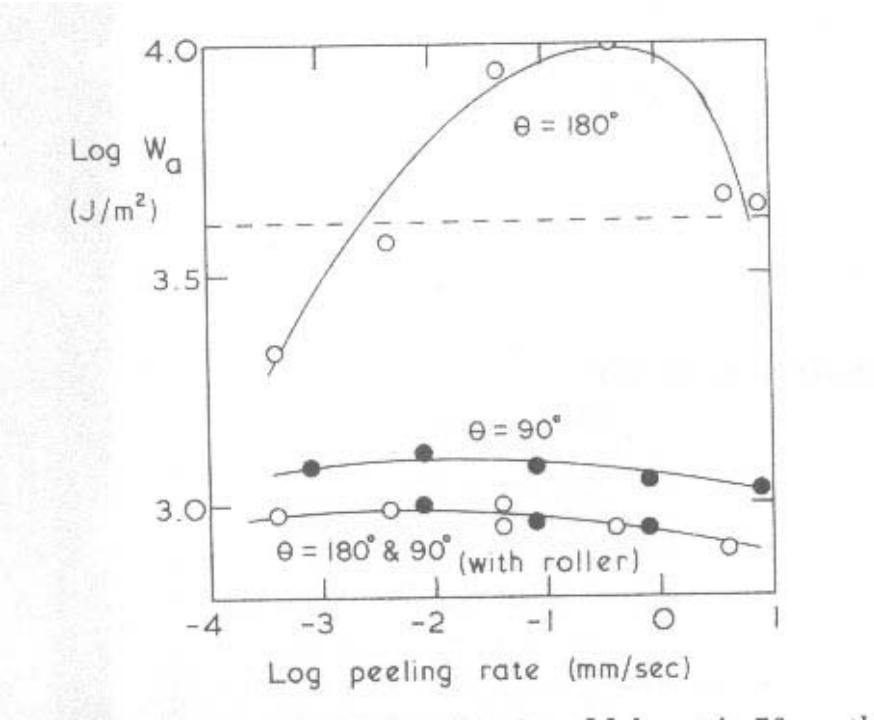

Figure 2-3. Effect of peel angle and peel rate on the work of adhesion for a Mylar-backed adhesive. The samples designated “with roller” employed a rolling device to remove effect of plastic deformation of the backing material. Reprinted from ref. 27 with permission of John Wiley & Sons, Inc.

2.1.5 Development of Hot Melt PSAs.

There are currently three predominant classes of PSAs available today: solvent based acrylics, emulsions (aqueous based) and hot melt adhesives (SIS and SBS materials).[1,2,32-40] Since the reduction in the use of solvents is environmentally desirable, emulsion and particularly hot melt adhesives are growing in popularity. Hot melt adhesives have experienced particular growth compared to emulsion systems because of increased water absorption of the emulsion polymers due to the surfactants incorporated during polymerization and lower shear holding power due to a heterogeneous network morphology.[10,21]

Hot melt adhesives are quite attractive due to their ease of use, high production speeds and lack of solvents. Since tackifiers and plasticizers are necessary to make the hot melts usable as PSAs, a single hot melt base polymer can be formulated to provide an almost limitless range properties. For these reasons, hot melt PSAs constitute that largest volume of the PSA market.[1] That said, traditional hot melts do have a few drawbacks. For example, unless the isoprene or butadiene blocks are hydrogenated, residual unsaturations in the polymer backbone are susceptible to oxidation that can lead to discoloration and embrittlement.

The introduction of radial polymers into the PSA market has addressed some of these difficulties. For example, Kraton™ G-6919 is a four-armed star with two styrene-ethylene/butylenes arms and two isoprene arms. The isoprene arms plasticize the system while the unsaturated ethylene/butylene arms increase the oxidative stability. A second possible disadvantage to hot melts is inherently built

into the polymer system, poor high temperature resistance is more difficult to overcome. Since the adhesives are melt processed, high temperature could soften the poly(styrene) hard segments thus reducing the cohesive strength of the PSA.[32,34,41] Researchers have crosslinked the block copolymers to increase the high temperature shear, but the crosslinking decreased the peel strength of the PSAs.[33,42-44]

Acrylate-based polymers are also utilized in a number of PSA applications and are the only PSAs that are inherently possess high tack (due to their low T_gs), but low mechanical strength.[1,2,10,21,45] Since high molecular weights are required of acrylic-based PSAs in order to achieve good adhesive properties, these materials typically have high viscosities in the processing temperature regime. As a result, acrylic PSAs are usually applied from an organic solvent rather than from the melt, which adds the additional processing step of solvent removal, and decreases line speed. In order to reduce the use of solvents, a recent goal in the PSA field is to synthesize acrylic-based adhesives that are applicable as a hot melt adhesive. In order to reach this goal, some type of molecular weight increase must occur between the processing of the acrylic PSA, (low molecular weight) and the application of the adhesive to form a bond. With development of UV curable hot melt PSAs and warm melt PSAs, researchers are attempting to formulate a melt processable acrylic adhesive.

While there are few references of UV curable adhesives in the technical literature, there are a number of publications in the trade and patent literature. Various companies are developing two types of UV curable acrylic PSAs: hot

melt and warm melt PSAs. Warm melt PSAs typically consist of a low molecular weight polyurethane acrylate, a mixture on acrylic monomers, tackifiers, antioxidants and a photoinitiator.[35,37,46,47] The mixtures are coated near or slightly above room temperature, then photopolymerized/crosslinked with UV irradiation. While these system show some promise, they have a number of shortcomings including high material costs, residual monomer after curing, low heat resistance, and low shear resistance.[32-41] Researchers have attempted to increase the shear resistance via increasing the UV dose, however those attempts led to decreased peel strengths.

One of the more promising UV-curable acrylic PSA was developed by Schumacher and coworkers at BASF.[32-34,41,48-53] The line of PSAs (acResin™) have melt viscosities as low as 10 Pa s at 140 °C, however use at over 150 °C is not recommended.[54] Schumacher incorporated vinyl derivatives of a common photoinitiator (benzophenone) into the polymer composition. When irradiated in between 220 and 280 nm, the benzophenone decomposes, forming a radical which then reacts with a tertiary carbon in the polymer to form a crosslink.[34,53,55,56] This reaction increases molecular weight of the adhesive and begins to form a lightly crosslinked gel. These researchers reported an increase in the gel fraction and cohesive strength with increasing UV dose, while the adhesive and tack decrease with UV dose.[41]

Mehnert and coworkers further studied the photocrosslinking of the Schumacher UV-curable PSA with real-time FTIR.[55,56] The authors found that while the reaction stopped as soon as the light was removed, the system was

easily overcured. Figure 2-4 illustrates the effect of UV dose on the peel strength and shear failure temperature of the adhesive. As the adhesive is irradiated, the peel strength increases to a maximum of ~13 N cm^{-1} (65 g m^{-2} at 200 mJ cm^{-2}), before decreasing to less than 6 N cm^{-1} with continued irradiation due to increased crosslink density. Conversely, the increased crosslink density increases the shear failure temperature of the PSA (inset of Figure 2-4). In addition, the reaction rate and extent of reaction was significantly dependent on temperature.

2.2 Current Topics in Polymer Photochemistry

2.2.1 Photopolymerization

The formation of polymers by photoinitiated polymerization is the basis for the majority of the commercial applications of photopolymer technology.[57] Photoinitiated polymerization can result in a number of different reaction schemes including free radical, cationic, and living polymerizations. Reiser and Fouassier have published comprehensive reviews of photopolymerization.[58,59]

2.2.1.1 *Photoinitiated Free Radical Polymerizations.* The most common type of photoinitiated polymerization is free radical polymerization. The basic components of this reaction usually include acrylate or methacrylic monomers or oligomers, along with a free-radical generating photoinitiator.[58,59] The polymerization begins with the formation of a free-radical species through the absorption of light by the photoinitiators, then proceeds by a typical chain-growth mechanism or crosslinking.[59-61]

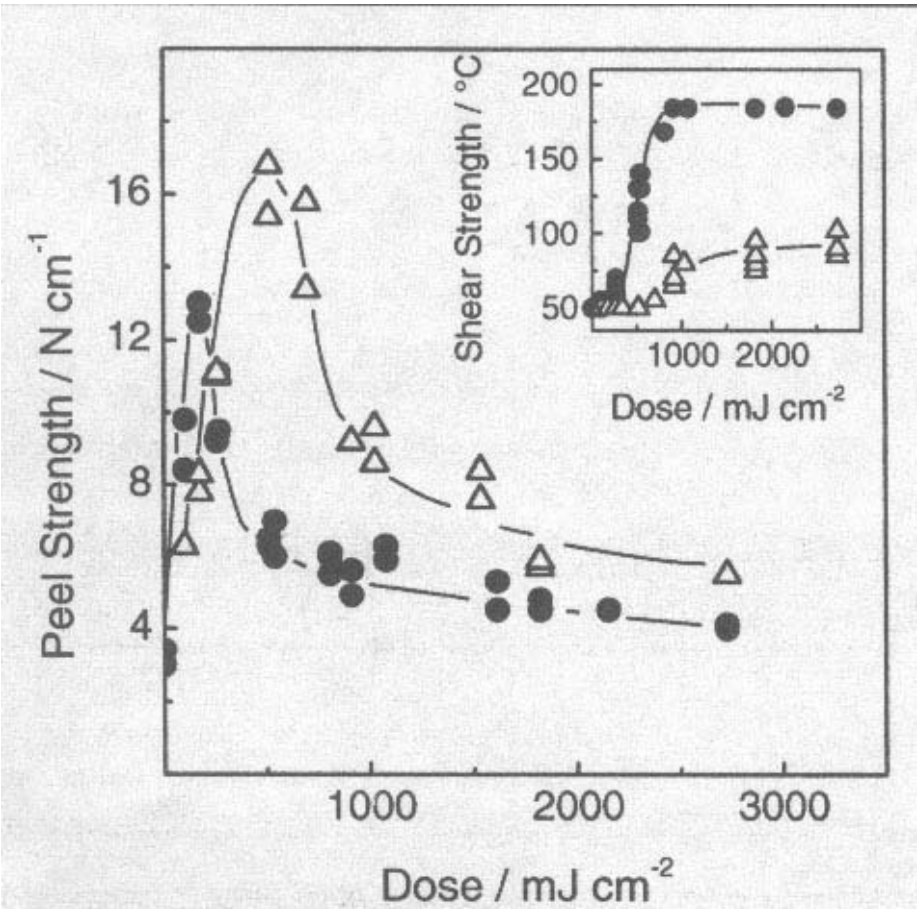

Figure 2-4. The effect of adhesive thickness and UV dose on the peel strength and shear failure temperature of the Schumacher UV-curable PSA. Circles are a coat weight of 65 g m^{-2} and triangles represent 130 g m^{-2}. Reprinted from ref. 56 with permission of Federation of Societies for Coatings Technology.

A combination of laser induced photoacoustic calorimetry and molecular modeling has allowed Fouassier *et al.* to characterize the photocleavage reaction of eight acetophenone derivatives.[62] Laser induced photoacoustic calorimetry uses a piezoelectric crystal to measure the acoustic wave formed after laser excitation of a sample.[63] Fouassier was able to measure then compare the quantum yield of dissociation to the computed bond dissociation energy. The authors reported that there was no correlation between quantum yield of dissociation to the photoinitiators bond dissociation energy. Another interesting finding was that while the photoinitiators studied were known to be highly efficient, the quantum yields of dissociation Fouassier's group measured were notably less than unity.

Due to the speed of these reactions, much work has gone into discovering methods to better understand and characterize them. Purvis and coworkers utilized differential scanning photocalorimetry (DPC) to study the photoinitiated polymerization of vinyl acetate and the phenomena of "stumbling polymerization."[64] The "stumbling" was observed as a splitting in the DPC curves and was thought to be indicative of a temporary cessation in the reaction. Other new methods utilized for reaction characterization include real-time infrared spectroscopy (RTIR) and nuclear magnetic resonance (NMR).[65,66] Combining DPC and solid state C^{13} NMR, the heat of polymerization and the number or remaining double bonds were determined for the 2,2-dimethoxy-2-phenyl-acetophenone photoinitiated polymerization of 1,1,1-trimethylolpropane triacrylate.[66] Decker has developed a novel RTIR method which allows for the

simultaneous measurement of both conversion and temperature changes during the photopolymerization of hexanediol diacrylate and a polyurethane-diacrylate photoinitiated with bis-acylphosphine oxide.[65] In this work, the monomers and photoinitiator were sandwiched between two polypropylene films, which permitted for the measurement of temperature due to an increase in its absorbance at 842 cm^{-1} with increasing temperature. Decker's work showed that increasing the light intensity increased the reaction rate and temperature of this system; the higher temperature subsequently allowed for a faster conversion and a higher ultimate degree of conversion.

Lovell *et al*. also utilized near-IR spectroscopy to correlate the double bond conversion during the photopolymerization of a model dental material to the cured adhesive's flexural strength.[67] Lovell *et al*. measured the near-IR spectra of the formulation immediately before and after the irradiation as well as 5 days after the irradiation to determine the extent of postcure in the system. The conversion of the double bonds continued to occur after irradiation had ceased. On average, the final conversion (5 days after irradiation) was 5% higher than the conversion measured immediately following the irradiation of the adhesives. The flexural strength of the adhesives tracked well with the double bond conversion and displayed a similar increase with time following the initial light exposure. Over 75% conversion of the double bonds was needed to provide a sample with a flexural strength over 80 MPa.

In order to gain a better understanding of the effect of chain-length-dependent termination and chain transfer agents in photoinitiated polymerizations, Bowman

and coworkers have studied the photoinitiated polymerizations of 2-hydroxyethyl methacrylate (HEMA) lightly crosslinked with diethylene glycol dimethacrylate (DEGDMA).[68] Bowman monitored the kinetics of the polymerization at various concentrations of chain transfer agents and initiation rates, i.e. different concentrations of initiator. Bowman's group discovered a deviation from the accepted relationship (proposed by Pravednikov in the 1950's) between the polymerization (R_p) and initiation rates (R_i), finding that the initiation rate had less of an effect on the polymerization rate than predicted. Figure 2-5 shows a plot of Bowman's data. The conversion is shown as a function of polymerization time multiplied by the initiation rate to the 0.38 power, a power function that is considerably less than the classically predicted value of 0.5 ($R_p \alpha R_i^{0.5}$). The addition of the chain transfer agent lessened the deviation from the predicted power function (0.5 power) and delayed the onset of diffusion-controlled termination. The deviation indicated that it may not be desirable to use high intensity irradiations in an attempt to minimize processing times, especially in biomedical applications. The use of high intensity irradiation can cause the formation of low molecular weight species that could be soluble and thus diffuse out of the construct, plasticize the system or affect the swelling behavior of the construct.[68]

Coussens *et al.* recently reported an increase in the reactivity of acrylic monomers with an increase in the hydrogen bonding in the monomer.[69] Coussens *et al.* synthesized an array of monomers capable of hydrogen bonding

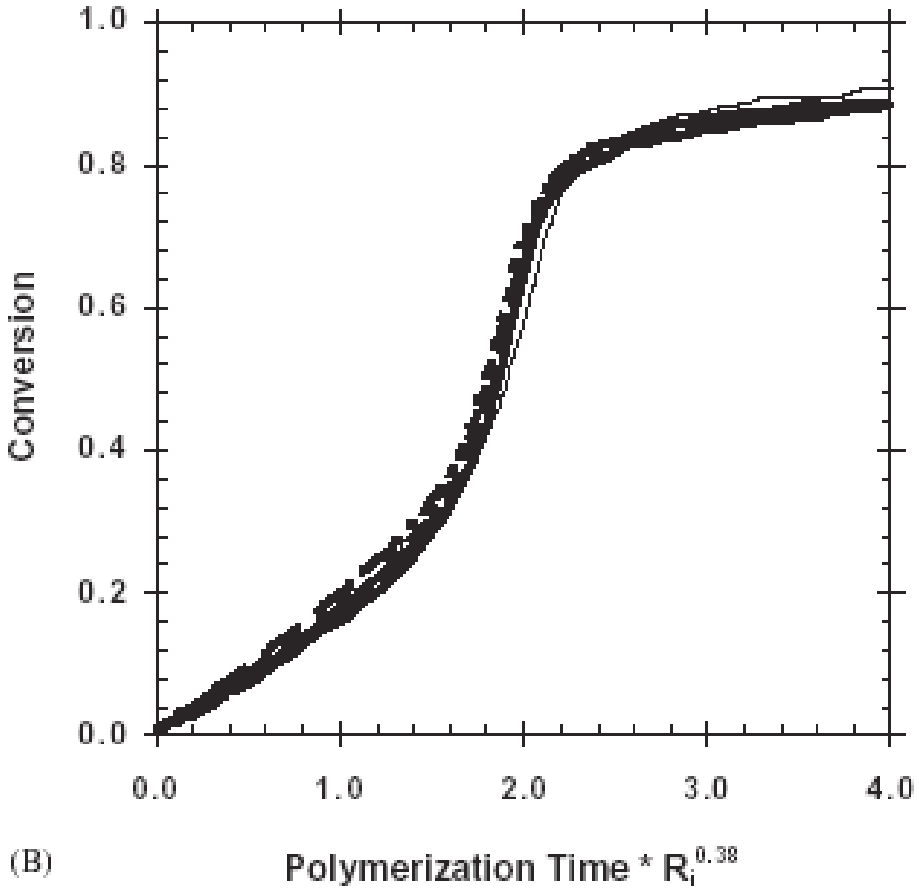

Figure 2-5. Conversion versus time data for the photoinitiated polymerization of HEMA and DEDGMA (99:1) with 1 wt% photoinitiator, scaled using $R_p \alpha R_i^{0.38}$.[68]

along with their non-hydrogen bonding controls. In all cases, the monomers capable of hydrogen bonding displayed a higher R_p than those without the hydrogen-bonding capability. The length of the alkyl ester spacer between the unreacted double bond and the hydrogen-bonding group also affected the polymerization rate, with longer spacing leading to decreases in R_p.

A number of new systems have also been recently synthesized. In an attempt to reduce polymer photodegradation, Decker and coworkers combined a photopolymerized polyurethane-acrylate telechelic oligomer with a HALS radical scavenger and a phenyltriazine UV absorber to produce additives as UV-resistant coatings.[70] Once the coating was cured by 3 seconds of UV-radiation (80 W/cm^2), it greatly increased the weathering resistance of a number of polymeric materials. The coating was also used to recover photodegraded polymer and made the recovered polymer resistant to weathering.[70] In another study on the formation of a different protective coating, Decker used sunlight to cure a mixture of acrylate monomers and an acyl-phosphine oxide photoinitiator in a PMMA (M_w = 126,000) or a styrene-butadiene matrix.[71,72] Due to the consumption of free radicals by O_2, sunlight induced free radical polymerizations are typically inefficient. In Decker's study, the addition of the PMMA and the styrene-butadiene matrix reduced the effect of oxygen inhibition and allowed for the formation of polymer films.

Free-radical photopolymerizations have also allowed for the use of adhesives in harsh environments such as cold seawater. With a slight modification to a traditional dental composite restorative formulation, Love and coworkers

prepared an underwater adhesive suitable for use at temperatures as low as 1°C.[73,74] Lap shear adhesive bond strengths as high as 2.5 MPa were measured with 30 seconds of irradiation (2.5 mW/cm^2 at λ = 470 nm) on PMMA substrates at 1°C. Lap shear strengths increased to a maximum of 4.5 MPa at 40°C and 10 minutes of irradiation. A modified version of the underwater adhesive was studied for use as bone cement for total hip arthroplasties.[75]

Photoinitiated polymerizations have also found a use in manufacturing microfluidic devices. Fréchet and coworkers have successfully used the photoinitiated polymerization to make monolithic porous polymers.[76,77] While porous polymers are typically produced by suspension polymerization, photoinitiated polymerization affords the preparation of the porous polymers within capillaries or channels of the device. This advance allows for the preparation of monolithic materials with a wide variety of chemistries and porosities in a single step.

Photoinitiated polymerizations have found acceptance in medical applications due to their rapid polymerization rates, spatial and temporal control, chemical versatility and solvent-free processing.[78-81] Anseth and coworkers have studied photopolymerized methacrylated anhydrides (shown in Figure 2-6) for uses as degradable orthopedic materials. The degradation of the orthopedic materials was controlled with the hydrophobicity of the core of the material and the rapid cleavage of the anhydride linkages. Since water cannot diffuse into the hydrophobic, highly crosslinked core, only the surface degrades and the

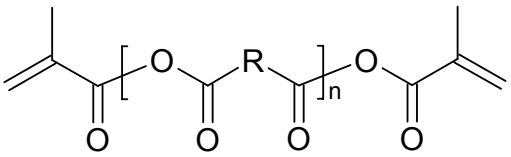

R = $(CH_2)_8$ or

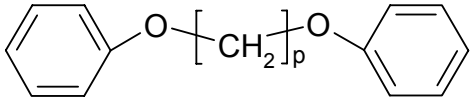

P= 3 or 8

Figure 2-6. Chemical structure of methacrylated polyanhydrides [79].

materials retain greater than 70% of their tensile modulus with more than 50% mass degradation.[82] These polyanhydrides have also shown no adverse effect to local tissue when photopolymerized in 3 mm holes drilled into rat tibias and analyzed three days postimplantation.[79]

In another biomaterial application, photoinitiated free-radical polymerization was used to create an adhesive and an insulating material for autonomic nerve activity recording.[83] Currently, liquid paraffins and mineral oil are used to attach and insulate the metallic electrodes to nerve bundles. However, the paraffins do not provide strong adhesion between the electrodes and the nerves, and therefore detachment of the electrodes can occur. Electrodes were bonded with a photopolymerized 1,12-dodecanediol diacrylate with camphorquinone in Vaseline® (utilized as a viscosity modifier), onto the aortic depressor nerve of a rabbit and nerve activity was measured. The major advantage to a photopolymerized adhesive over the currently used methods is that the material can be photocured in small amounts and does not require the formation of a cavity around the recording site.

2.2.1.2 *Photoinitiated Cationic Polymerizations.* As previously mentioned, airborne free radical polymerizations can be inhibited by the presence of oxygen. The use of cationic mechanisms circumvent this problem since cationic photopolymerizations are insensitive to oxygen.[71] Crivello and coworkers have sunlight cured fiberglass-epoxy matrices up to 2 mm thick in 25 min.[84] This was accomplished by cationic photopolymerization of epoxidized vegetable oils and synthetic epoxy resins, which were initiated with diaryliodonium and

triarylsulfonium salts. More recently, Crivello has reduced diaryliodonium and triarylsulfonium salts by free radicals produced by the hydrogen abstraction reaction of photoexcited ketones to photopolymerize vinyl and epoxide monomers with long-wavelength and visible light.[85]

2.2.1.3 Photoinitiated "Living" Polymerizations. Bowman and coworkers have experimented with the living photopolymerization of methacrylates.[86-88] By using an iniferter such as 2,2-dimethoxy-2-phenylacetophonone in combination with tetraethylthiuram disulfide, this group synthesized polymers with narrow molecular weight distributions and no trapped radicals. An iniferter is a compound that can initiate, chain transfer and terminate radical polymerizations. The polymerization proceeds in a stepwise fashion with reversible radical termination by tetraethylthiuram disulfide. Bowman has photopolymerized 2-hydroxyethyl methacrylate (HEMA), diethylene glycol dimethacrylate, and triethyleneglycol dimethacrylate using this or a similar method. Bowman's group has also performed living polymerizations to graft acrylic acid onto polypropylene (PP) membranes.[89] This was done by photografting benzophenone on the surface of PP films, after which the monomer solution was added and the system was polymerized using UV irradiation. Using this two-step method, the grafting density and the graft chain length can be controlled independently since the initiator formation and graft polymerization occur independently. Figure 2-7 illustrates the growth of the graft chains as a function of irradiation time.

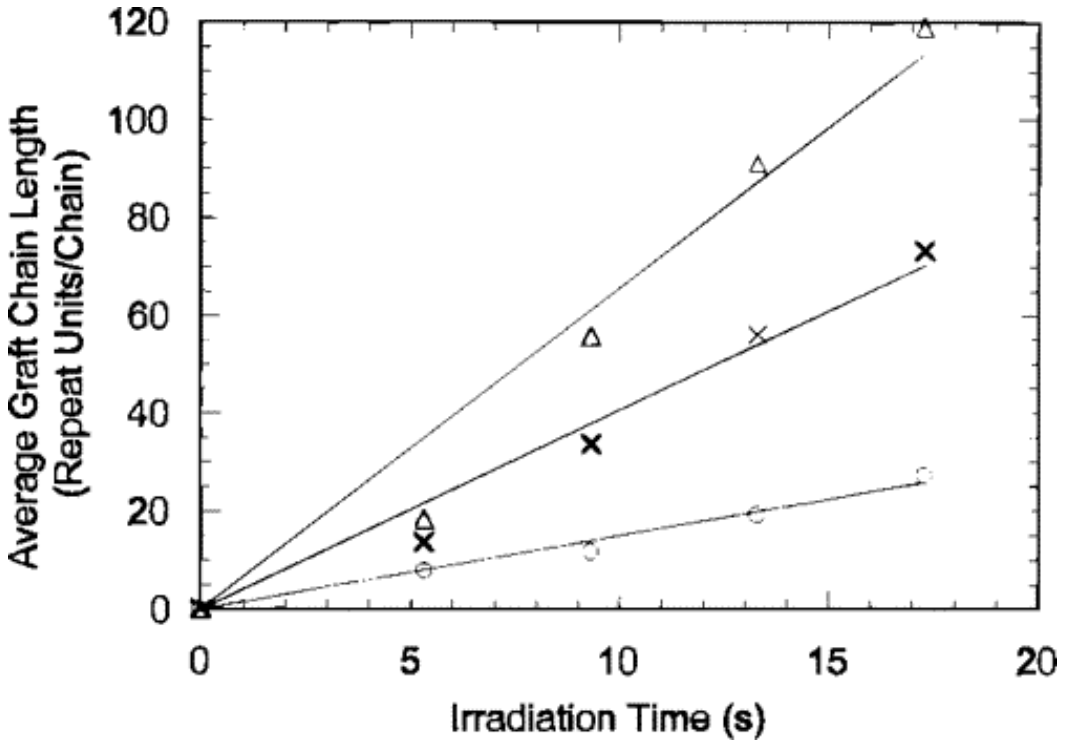

Figure 2-7. Average graft chain length versus irradiation at: o = 5 wt%, x = 10 wt% and ∆= 10 wt% acrylic acid. Reprinted with permission from [89]. Copyright 2000 American Chemical Society.

2.2.2 Photocrosslinking.

Photocrosslinking causes the formation of insoluble and infusible polymer networks and offers a number of advantages over thermal crosslinking such as speed, low cost of materials and energy, the ability to selectively cure systems as well as solvent-free formulations.[59,90-102] Photocrosslinked materials have found uses in photoresists, printing plates, inks, coatings, adhesives, biological and biomedical applications.

2.2.2.1 *Photoresists.* In reducing the environmental impact of current photoresists, researchers have studied water-soluble resists. Fréchet has studied the photocrosslinking of sugar containing PMMA in an attempt to make environmentally friendly or "green" photoresists.[99] The polymer crosslinks through the formation of glycosidic linkages and is able to resolve features on the order of 0.200 μm. While these materials appear promising, they exhibit pooretch resistance with etch rates of 2,519 Å min^{-1} compared to 702 Å min^{-1} for commercial systems. Another water-soluble photoresist was developed based on the photocrosslinking of poly(vinyl alcohol) with hexamethoxymethylmelamine.[100,103] This system had the same difficulties with a high etch rate, as did the sugar functionalized PMMA.

2.2.2.2 Adhesives. Photocrosslinking is also utilized in the adhesives industry, both for hot melt and pressure sensitive adhesives (PSAs). In one study, a hot melt adhesive based on Kraton D (poly(styrene-b-butadiene-b-styrene)) was crosslinked using Irgacure 651 (2,2-dimethoxy-1,2-diphenylethan-1-one).[43] The

crosslinking of the poly(butadiene) phase resulted in reduced peel strength and tack while having little effect on the surface energy of the system.

A desirable property for a medical grade PSA is to adhere strongly when desired and release when desired with little or no trauma to the user [104]. Webster and coworkers have developed a methacrylate functionalized PSA which can photocrosslink.[24-26,105-107] This adhesive was synthesized by polymerizing itaconic anhydride, 2-ethylhexyl acrylate and *n*-butyl acrylate. The resulting terpolymer was then further reacted with HEMA to provide the functionalized PSA, and the photoinitiator, Irgacure 784, was added. The chemical structure of the resulting PSA is shown in Figure 2-8. Peel strength reduction was achieved via photoinitiated crosslinking of the pendent acrylate groups using irradiation with a halogen lamp and using sunlight. The crosslinking decreased the energy dissipation during peel testing and thus reduced the peel strength. Peel strengths were reduced by as much as 79% with 2 min of irradiation with higher light intensities having a greater effect on peel strength reductions as a function of time.

2.2.2.3 *Biomedical Applications.* Another new area of research for photocrosslinking includes the fields of tissue engineering and drug delivery. Researchers have recognized that hydrogels possess the desired structure and mechanical properties of tissue engineered scaffolds.[78] By combining poly(ethylene oxide) with a number average molecular weight (M_n) of 100,000 g/mole, poly(ethylene oxide)-dimethacrylate with M_n = 3,400 g/mole, a

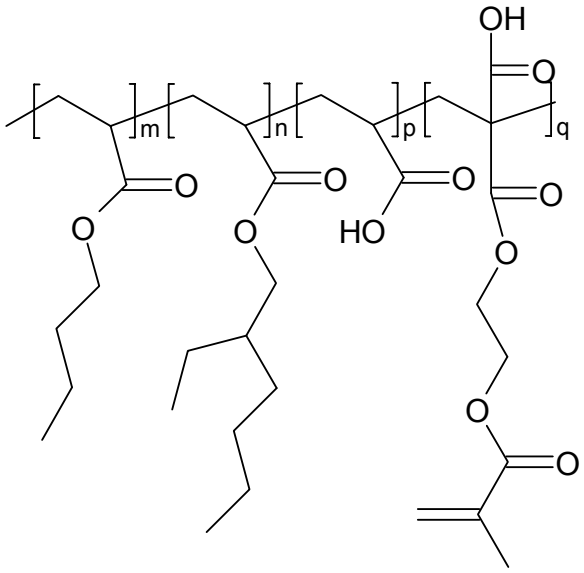

Figure 2-8. The structure of the photocrosslinkable PSA.[24,26,105-107]

photoinitiator and chondrocytes harvested from a calf femoropatellar groove, Langer and coworkers have produced an injectable tissue engineered cartilage system.[108] A schematic for the procedure of harvesting the cells, injecting the hydrogel into the mouse subcutaneously and transdermal photopolymerizing is shown in Figure 2-9. By exposing the skin to 20 mW/cm^2 of UV light (broadband source), the effective intensity of the light available to initiate the photoreaction is approximately 0.3 mW/cm^2, an intensity sufficient for crosslinking in three minutes.[79] At six weeks post-implantation, the hydrogels were removed and the construct's glycosaminoglycan and collagen content were similar to other tissue engineered cartilage constructs.

A photoreactive tissue engineered drug delivery system was produced by Anseth and coworkers based on triblock copolymers of poly(lactide)-b-poly(ethylene glycol)-b-poly(lactide) and a graft copolymer of poly(lactide)-g-poly(vinyl alcohol), both of which were endcapped with methacrylate moieties.[109] Photocrosslinking was initiated with a number of photoinitiators at 365 nm. The degradation of the networks and the release of bovine serum albumin were monitored as a function of time in phosphate buffered saline solution. Experimental results found that the compressive modulus of the networks decreased exponentially, while the swelling ratio increased exponentially with time during the degradation studies, indicative of network degradation.

Trudel and Massia have recently studied the photocrosslinking of dextran and hyaluronan based hydrogels with the aim of using the hydrogels to aid in the

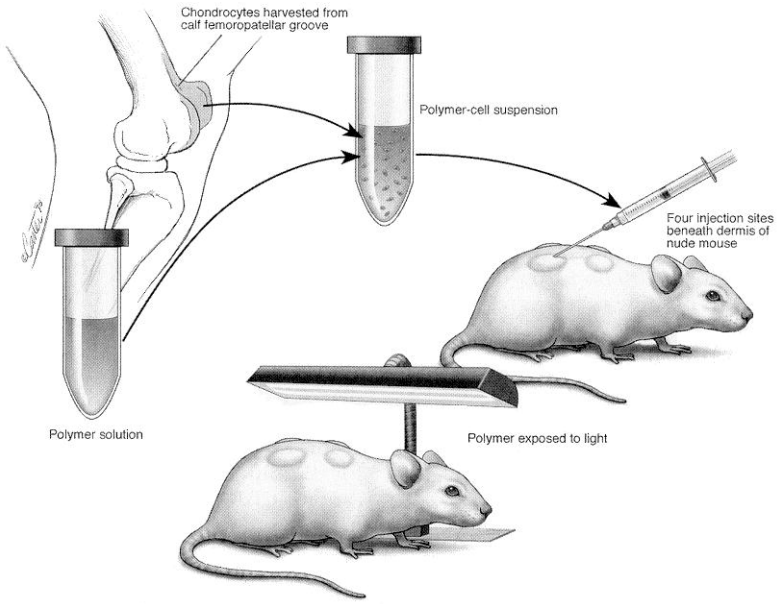

Figure 2-9. Schematic of the procedure for transdermal photopolymerization. Reprinted from ref. 108 with permission of Lippincott Williams & Wilkins.

acceptance of cardiovascular implants. [110] Hyaluronan is an extracellular matrix polysaccharide consisting of repeat units of D-glucuronate and N-acetyl-D-glucosamine with a molecular weight on the order of several million grams per mole. Hydrogels were fabricated by dextran and/or hyaluronan derivatized with glycidyl methacrylate and mixed with a photoinitiating package of 2,2-dimethoxy-2-phenylacetophenone and 1-vinyl-2-pyrrolidinone and crosslinked with UV light. The hydrogels were tested for cytotoxicity using vascular smooth muscle cells. Hyaluronan based hydrogels were found to be cytotoxic and caused cell migration from the hydrogels. However, the hydrogels made from dextran or mixtures of dextran and hyaluronan were highly compatible with the smooth muscle cells *in vitro* and thus are possible candidates for cardiovascular drug delivery appliances.

In a study undertaken to create a photocurable drug delivering tissue adhesive, Matsuda and coworkers first functionalized gelatin with styrenic groups containing pendent double bond moieties.[111,112] The double bonds were photopolymerized with visible light using carboxylated camphorquinone as the photoinitiator. The gelatin-based hydrogels were tested as both transdermal and *in vivo* drug delivery systems using a dye-conjugated protein as a deliverable. Figure 2-10 shows: (a) the fixation of the gel onto rat liver tissue, (b) the crosslinked gel three days post-implantation, (c) the stained cross-section of the liver showing drug penetration, and (d) drug delivery profile from the gel into phosphate buffered saline. This study successfully produced an *in situ* photocrosslinkable tissue-adhesive that can provide localized drug delivery.

(a)

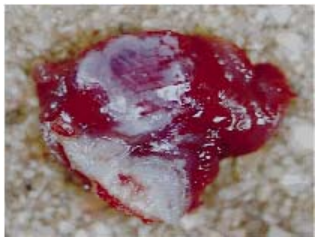

(b)

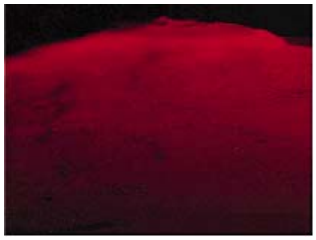

(c)

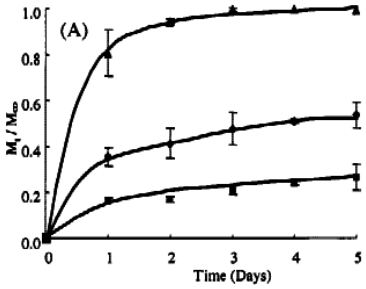

(d)

Figure 2-10. (a) Visible light irradiation for hydrogel fixation to rat liver (b) the cured gel three days post-implantation (c) liver specimen cross-section showing dye penetration into the tissue and (d) drug release profile from gel to PBS solution. Reprinted from ref 111 with permission of John Wiley & Sons, Inc.

Matsuda and coworkers have also studied a number of other systems for use as tissue engineering scaffolds.[113-116] In one such study, Matsuda used carboxylated camphorquinone as the photoinitiator to investigate the photocrosslinking of styrene-derivatized heparin and albumin. The styrene-derivatized heparin and albumin were photocrosslinked into an acrylic acid matrix grafted onto a polyurethane substrate. Matsuda and coworkers found reduced platelet adhesion and an increased endothelial cell adhesion and proliferation to the constructs with the albumin and heparin layers versus the bulk polyurethane. The increased adhesion of the endothelial cells may allow for better incorporation of the construct into the body if implanted and thus a more successful scaffold.[116]

By attaching acrylic and styrenic groups to low molecular weight poly(ε-caprolactone-co-trimethylene carbonate) (M_n=2,200 g/mol; also see 2.4.4.1) or polysaccharides, Matsuda has photofabricated constructs in various geometries.[113-115] Figure 2-11 shows SEM micrographs of the tubular constructs prepared by irradiating polysaccharide mixtures containing 30 wt% styrene-derivatized gelatin and 5 wt% methacrylated heparin. Stereolithography was used to produce various geometrical constructs using acrylated-endcapped poly(ε-caprolactone-co-trimethylene carbonate) in the presence of either camphorquinone or benzophenone and visible or UV irradiation (50 mW/cm^2) as shown in Figure 2-12. The geometries formed include microbanks (Figure 2-12a), microwells (Figure 2-12b), tubes (Figure 2-12c) and microneedles (Figure 2-12d).[114,115]

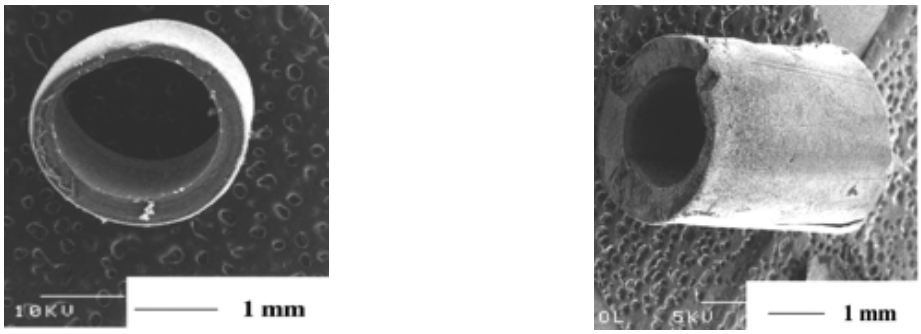

(a) (b)

Figure 2-11. SEM micrographs of the cross sections ((a) top view and (b) side view) of photofabricated tubular constructs fabricated by Matsuda and coworkers. Reprinted in part with permission from ref 113. Copyright 2002 American Chemical Society.

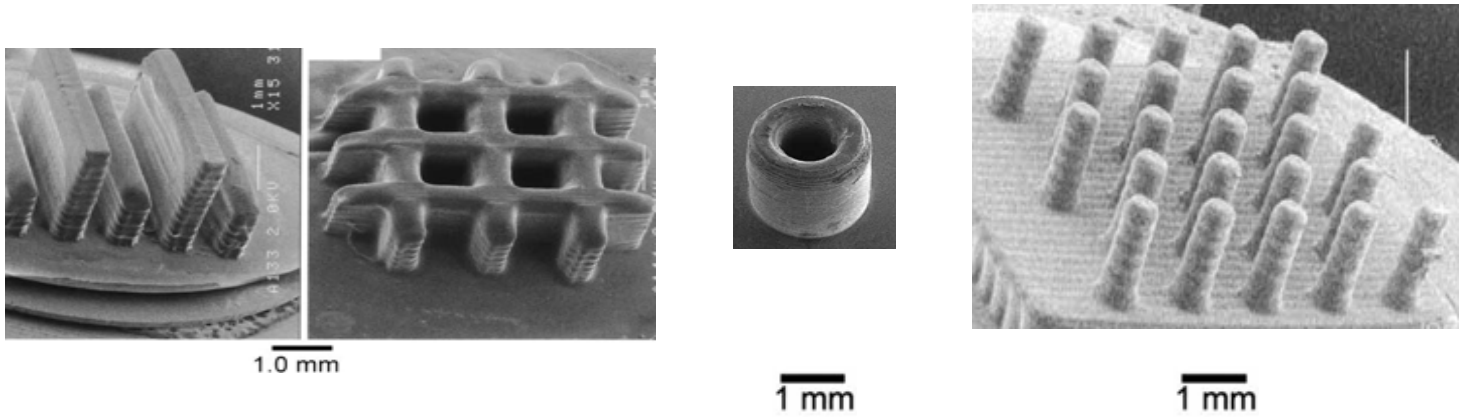

Figure 2-12. (a) microbanks, (b) microwells, (c) microcylinder and (d) microneedles photofabricated by Matsuda and coworkers using computer-aided stereolithographic irradiation of poly(ε-caprolactone-co-trimethylene carbonate) at 488 nm. Reproduced from refs. 114,115 with permission of John Wiley & Sons, Inc.

In another study, Anseth's group increased cell attachment for tissue engineered heart valves using a photocrosslinkable mixture of poly(lactide)-*g*-poly(vinyl alcohol) endcapped with methacrylate groups and heart valve interstitial cells.[79,117] The mixture was crosslinked at 365nm for 10 min (5.0 mW/cm^2). Varying the number of lactide repeat units per side chain, macromer concentration and crosslink density controlled *in situ* degradation times.

John and Morita have recently photocrosslinked terpolymers of poly(L-lactic acid-*co*-glycolic acid-*co*-L-serine) to produce biodegradable polymer scaffolds for tissue engineering. The terpolymer was first acrylated (structure is shown in Figure 2-13a) then photocrosslinked by three different methods.

Photocrosslinking using solution and bulk methods resulted in a crosslinked network and a hydrophilic crosslinked network, respectively. Morita also photocrosslinked the terpolymer in suspension with ethylene glycol dimethacrylate, which formed crosslinked beads. An optical micrograph of the beads swollen in DMSO is shown in Figure 2-13b.[118]

2.2.2.4 *Reversible Structures.* Taking photocrosslinking a step further, Shirai *et al.* have designed a photocrosslinkable polymer, which can be thermally degraded at reasonable temperatures ($T < 200^{\circ}C$).[119,120] In order to crosslink the polymer, the polymers included epoxy units, which can photocrosslink when initiated by photochemically generated acids. The desired degradation occurs through tertiary epoxy linkages, which break down into carboxylic acids and alkenes upon heating above 180°C. The polymer

(a)

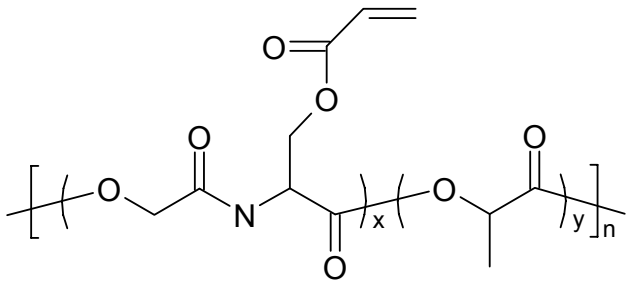

(b)

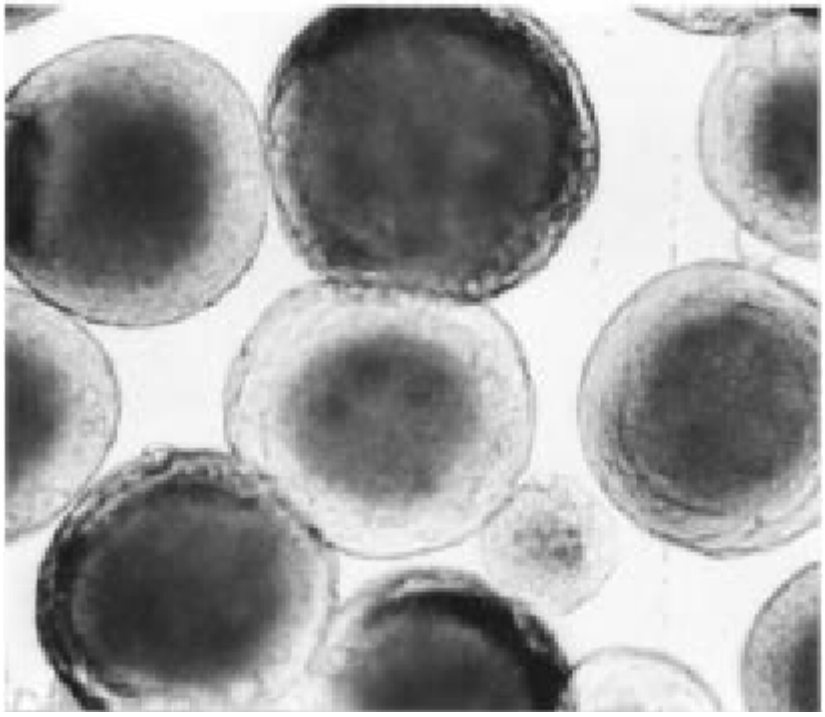

Figure 2-13. (a) acrylated terpolymer poly(L-lactic acid-co-glycolic acid-co-L-serine) and (b) optical micrograph of the crosslinked beads swollen in DMSO, magnification approximately 50x. Reprinted in part with permission from ref. 118. Copyright 1999 American Chemical Society.

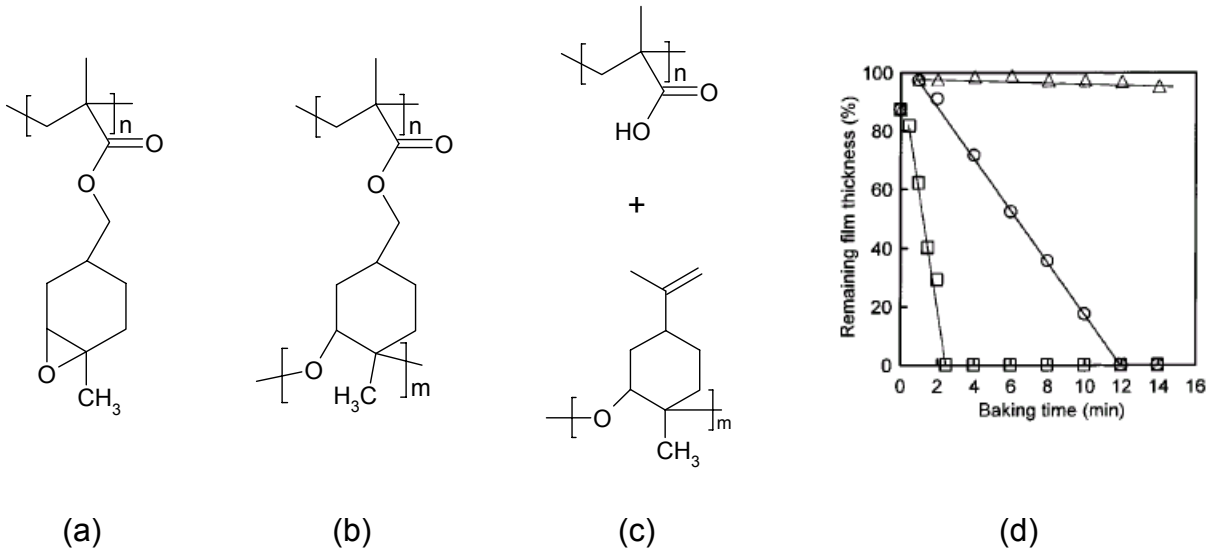

(a) (b) (c) (d)

Figure 2-14. (a) Structure of a photocrosslinkable and thermally degradable polymer, (b) the crosslinked polymer, (c) the degradation products of polymer shown in (b) and (d) degradation of film (b) with heating at (Δ) 140°C, (o) 160°C and (□) 180°C after development in methanol. Reprinted in part with permission from ref. 119. Copyright 2002 American Chemical Society.

(Figure 2-14(a)) was photocrosslinked (structure shown in Figure 2-14(b)) in the presence of 3.6 mol% of the photoacid generator 9-fluorenilideneimino *p*-toluenesulfonate and was insoluble in tetrahydrofuran (THF). The crosslinked polymer was then heated to between 140 and 180°C, the crosslinked polymer degraded resulting in the polymer shown in Figure 2-14(c). Figure 2-14(d) shows the resulting crosslinked film thickness after baking the film and removing the soluble fraction in methanol.

In a similar study, the same group synthesized photocrosslinkable, thermally degradable polymers from the repeat unit shown in Figure 2-14(a) and various sulfonated styrene derivatives. Shirai *et al.* were able to photocrosslink the polymer with UV light and a photoacid generator. The crosslinked polymers then degraded to water-soluble polymers after baking between 120 and 200 °C, depending on the structure of the sulfonate styrene monomer used.

Recently, synthetic methods that enable the reversible tuning of molecular weights and crosslink densities of polymers via multiple hydrogen bonding have generated significant interest.[121-128] Meijer has also reported photo-induced depolymerization of multiple hydrogen bonding polymers.[124] Meijer first synthesized a multiple hydrogen bonding oligomers, which grow linearly via the 2-ureido-4-pyrimidone chain ends. A sterically hindered chain stopper, i.e. a small molecule that hydrogen bonds to the chain ends, was then added to the chain-extended polymer. Photocleavage of the o-nitrobenzyl ether protecting group, allowed for the formation of the neat chain stopper and resulted in the

endcapping of the hydrogen bonded polymer and a reduction in apparent molecular weight.

2.2.3 Radical Termination in Photoinitiated Free Radical Polymerizations.

Bowman's groups has thoroughly studied postcure, specifically the termination mechanisms which affects postcure for highly crosslinked systems over the last 15 years.[67,68,86,129-136] For highly-crosslinked photoinitiated polymerization reactions, there are typically three mechanisms of termination. The first is the traditional diffusion controlled termination method, while the second method is the unimolecular trapping of radicals. However, the third method, bimolecular termination through reaction diffusion, is the dominant mechanism.[136] In this case, the radical propagates through unreacted double bonds. Bowman's group applied Russell's theory based on termination of poly(methyl methacrylate) at high conversions to highly crosslinked systems.[136-138] Russell proposed that the termination kinetics follow Equation 2-6:

Equation 2-6.
$$k_t(res) = \frac{4\pi}{3} p k_p [M] a^2 r_a$$

where, k_t(res) is the reaction diffusion controlled termination constant, *p* is the probability for two radical to come in close enough proximity to react, *a* is the root-mean-square end-to-end distance per square root of the number of monomer units and r_a is the radical radius of interaction.[136-138] The size of the radius of interaction (r_a) was further defined to be limited by two extremes (R_{min}, Equation 2-7 and R_{max}, Equation 2-8).[137,138] The minimum value of r_a occurs when the chain end cannot move on the same time scale as propagation due to

chain rigidity. For this case, the r_a is limited to the half-life of the Lennard-Jones diameter of the monomer ($\sigma/2$), which leads to the R_{min} (Equation 2-7) value. In the second case (Equation 2-8), that of a flexible chain, r_a depends on the $a(j_c)^{½}$, where a (defined above) and j_c is the distance between entanglements. This R_{max} value is used due to the increased mobility of the radical at the chain-as the last entanglement point of the polymer chains is its only limitation.

Equation 2-7. $$R_{\min} = \frac{2\pi}{3} p a^2 \sigma$$

Equation 2-8. $$R_{\max} = \frac{4\pi}{3} p a^3 j_c^{1/2}$$

Bowman's group has reported that the experimentally measured termination constant typically falls between the two calculated k_t values using R_{max} and R_{min}.[68,136] Typical values for R are 2 L mol^{-1} for methacrylates and 3-5 L mol^{-1} for acrylates as methacrylates typically have stiffer chains. These models only pertain to heavily crosslinked systems, not to polymers with low levels of crosslinking. For lightly crosslinked systems, there is sufficient mobility for the for R to reach or exceed R_{max} especially for crosslinking reactions performed above the polymer T_g.[136] Thus, the degree of postcure reported in the literature, is dependent on a number of factors including those cited above.

2.2.4 Hydrogen Bonding and Photoreactions

Recently, synthetic methods that enable the reversible tuning of molecular weights and crosslink densities of polymers have generated significant interest.

For example, the research groups of Meijer, Whitesides, Rotello, Long and others have pioneered the use of multiple-hydrogen bonding moieties and the introduction of the various moieties into polymers providing for reversible apparent molecular weights.[122,124-126,139-142] In addition, Long and coworkers have recently studied thermally reversible multiple hydrogen bonding in telechelic poly(styrene), poly(isoprene), poly(styrene)-*b*-poly(isoprene), and randomly functionalized poly(acrylates).[121,127,128] Although multiple hydrogen bonding in a telechelic and random fashion offers great promise, these supramolecular structures are typically exposed to higher application temperatures, which result in hydrogen bond dissociation and subsequent loss in apparent molecular weight and/or mechanical strength.

Meijer reported photo-induced depolymerization of multiple hydrogen bonding polymers (Scheme 2-1). Photodegradation of a sterically hindered multiple hydrogen bonding additive resulted in the endcapping of the hydrogen bonded polymer and a reduction in apparent molecular weight.[124] Another interesting possibility is to combine the effects of hydrogen bonding and photoreactions to possibly construct a desired structure via hydrogen bonging and use photoreactions to lock the structure. For example, Jeon *et al.* recently described the synthesis and photostabilization of self-assembled dendrimers.[143] Meijer first synthesized the diacetylene-endcapped amide-urethane dendrons via the convergent methodology. The dendrimers self-assembled in water forming lamellar or columnar structures depending on the dendrimer generation.

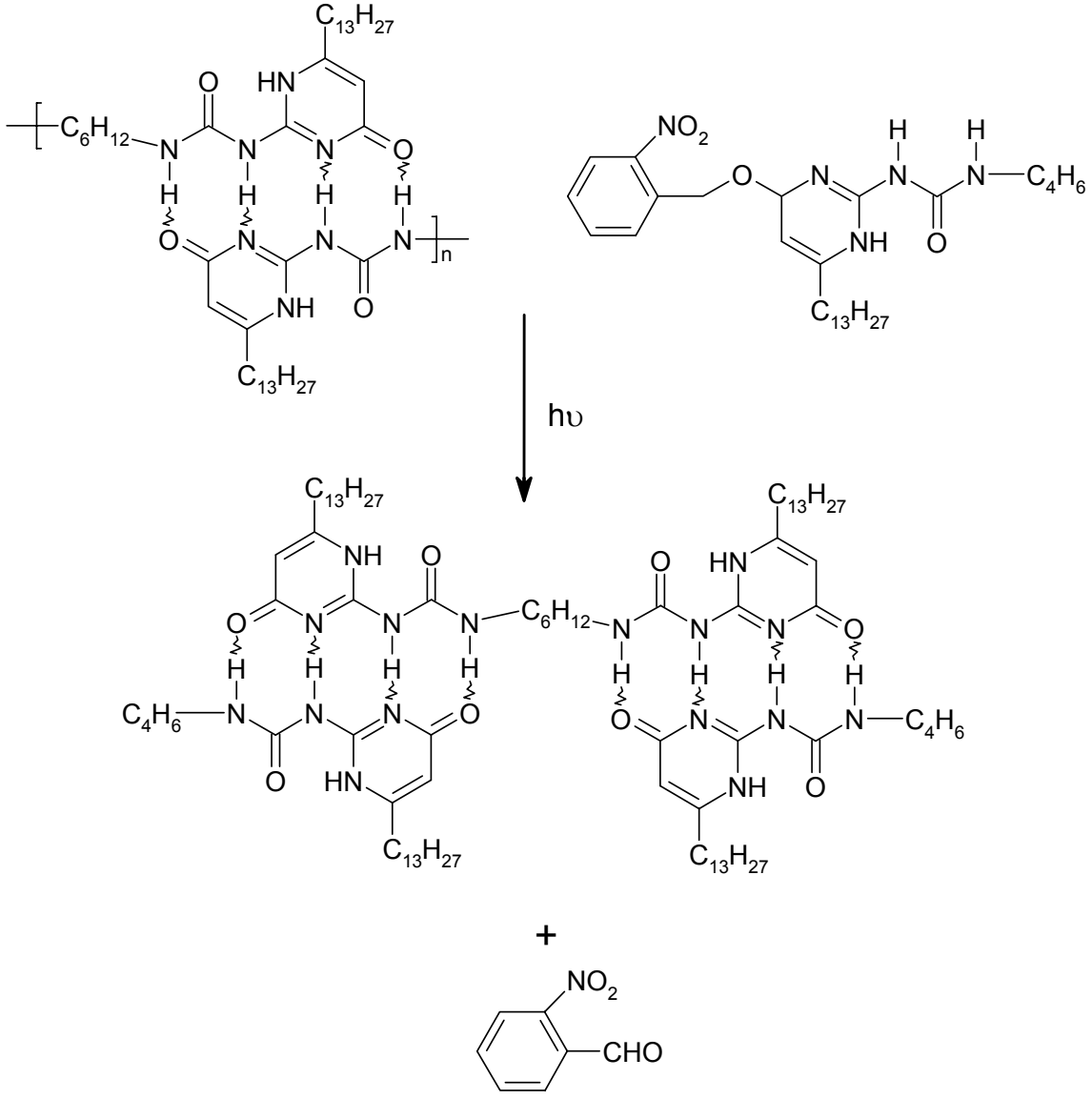

Scheme 2-1. The photo-induced depolymerization of multiple hydrogen bonding polymers via the photocleavage of the *o*-nitrobenzyl ether group.[124]

UV irradiation of the structures crosslinked and stabilized the structures so they were no longer soluble in chloroform. Similarly, Cao and coworkers utilized a layer-by-layer technique to construct self-assembled ultra-thin films of hydroxyphenol-containing polymers with diazoresin-containing polymers.[144,145] Films, as thick as 50 bilayers, were assembled via alternating layers of the hydroxyphenol-containing polymers (proton donor) with diazoresin-containing polymers (proton acceptor) in nonpolar solvents. The films quickly dissociated in polar solvents. However, the films crosslinked and thus became insoluble in the polar solvents upon irradiation with UV light or X-ray energy. The proposed mechanism is shown in (Figure 2-15). While the self-assembled films were initially insoluble in polar solvents, the photoreaction stabilized the films.

2.2.5 Photoactive Groups.

Matsuda and coworkers have studied the use of photoactive groups to crosslink liquid polymers to make 3-dimensional biopolymer constructs.[111,112,146-153] While their earlier work has focused on the use of coumarins, they have recently studied the use of phenylazides to crosslink ε-caprolactone and trimethylene linear, tri- and tetra-armed star copolymers.[149] The reactions that phenylazides undergo, when irradiated with UV radiation, are shown in Figure 2-16(a). After endcapping the copolymers with phenylazide groups, the authors tested the photocuring characteristics, prepared 3-D constructs and tested the surface wettability and cell attachment and proliferation. SEM micrographs of a honeycomb structure built by surface layering and photocuring individual layers

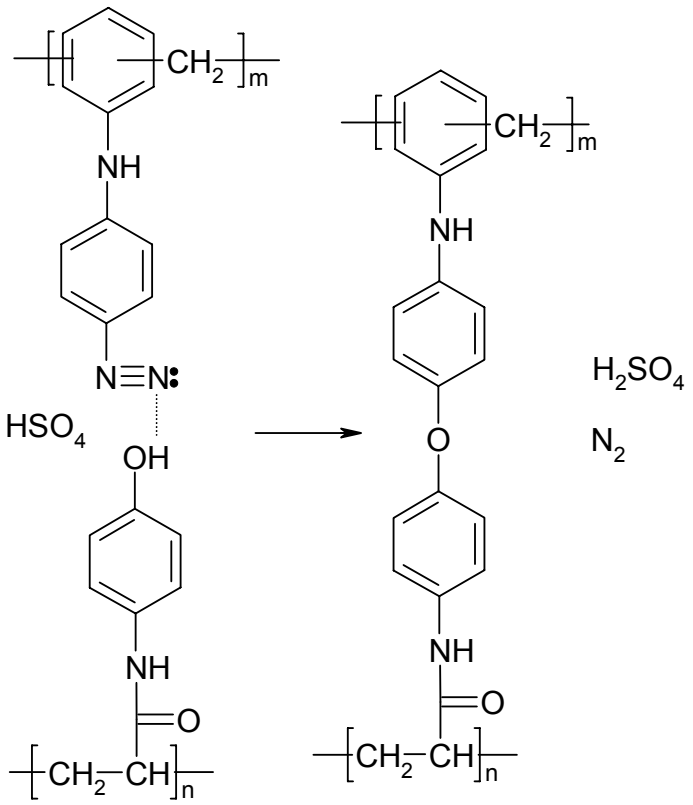

Figure 2-15. Crosslinking mechanism leading to the crosslinking of the layer-by-layer self-assembled films.[145]

(a)

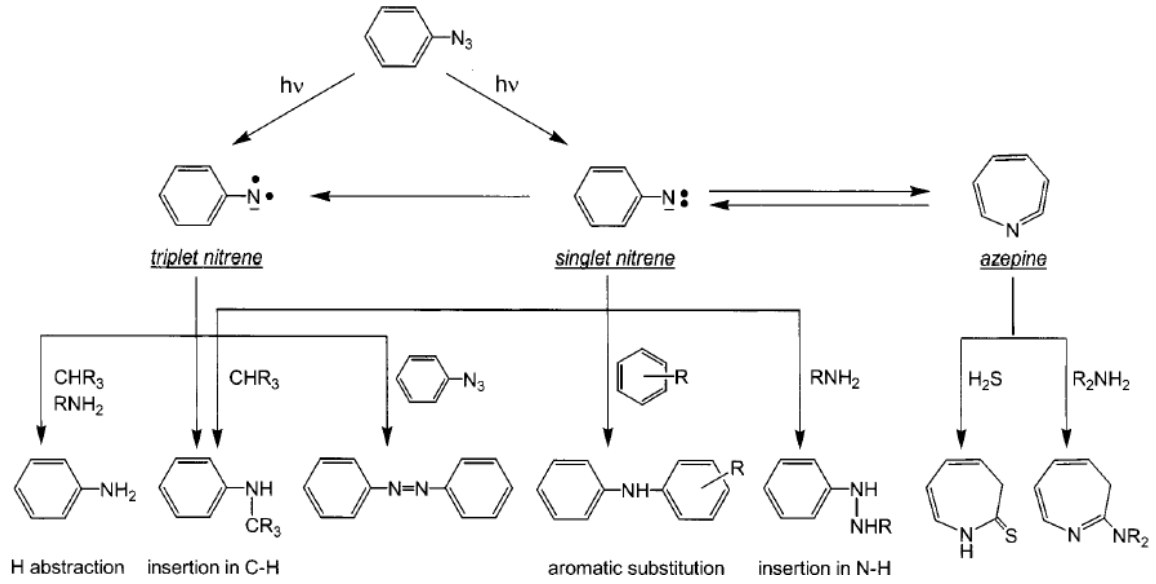

(b)

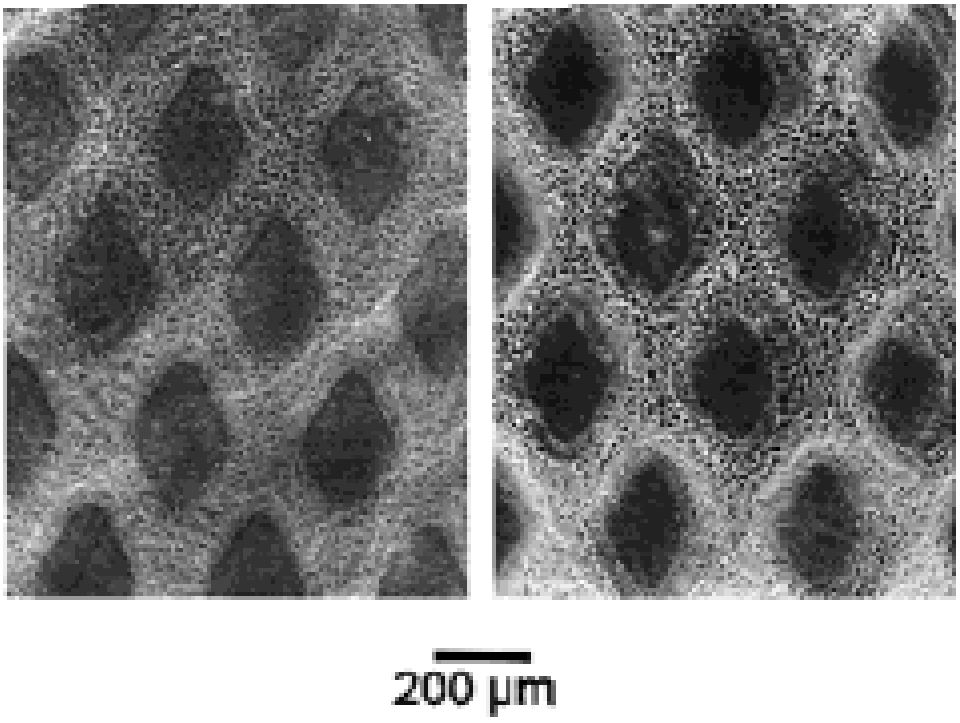

Figure 2-16. (a) the chain extension, crosslinking and surface fixation photoreactions of phenylazide when irradiated with UV irradiation and (b) SEM micrographs of photocured honeycomb patterned layered surfaces. Reprinted with permission from ref. 149. Copyright 2002 American Chemical Society.

of the 4-armed star and polylactide films are shown in Figure 2-16(b). Photocuring the constructs proved beneficial to the water wettability and the adherence and growth of cells. This is attributed to the increase in the ratio of nitrogen:carbon at the surface of the construct as demonstrated utilizing X-ray photoelectron spectroscopy. When compared to coumarin endcapped copolymers, the phenylazide endcapped copolymers were less dependent on crosslinking rate as a function of light intensity and reacted faster than the coumarins. Both advantages are afforded by the free-radical nature of the crosslinking with the phenylazide groups versus the [2π+2π] cycloaddition reaction utilized by the coumarin groups.

Minsk and coworkers first reported polymer crosslinking through the photodimerization of cinnamate groups of poly(vinyl cinnamate) in the 1950's.[154-158] Since then, photocrosslinking via photodimerization has been well studied for maleimides,[159] furans,[160-162] cinnamates,[58,91,92,158,163-187] chalcones,[188-190] anthracene,[58,180,191,192] acridizinium,[58,193] stilbazolium salts,[93,94] and coumarins [58,146-148,150,170,171,194-236]. With the exception of the anthracene groups that dimerize via a [4π+4π] cycloaddition, the photodimerization of the other photodimerizable groups listed proceed by a [2π+2π] cycloaddition of ethylenic groups above 300nm.[58,180] While this discussion only focuses on current photowork on maleimides, furans, chalcones, anthracene, acridizinium, and stilbazolium salts[93,94], cinnamate and coumarins will be described later in this text.

One unique photoactive system, that does not dimerize, has contributed to the development of optomechanical machines. This group has utilized azobenzene chromophores in the backbone of a polymer to develop a polymer that can reversibly contract and expand upon irradiation at 365 and 420 nm, respectively.[237] The contraction and expansion of the polymer is due to the cis/trans isomerization that azobenzene undergoes with irradiation. The configurational change of a single polymer chain was shown to exert up to 500 pN of force on AFM tips.

Photoreversible hydrogels were recently synthesized in the form of a random terpolymer composed of *n*-isopropyl acrylamide, acrylic acid and acridizinium functionalized acrylic acid.[193] The acridizinium group was chosen over the stilbazolium salts used in the same group's previous hydrogel formulations due to increased dimerization speed and better photoreversibility.[93,94,193] The authors were able to slightly, but reversibly, change the cloud point temperature and the lower critical solution temperature of a solution containing the terpolymer and water, which is important for microsystems that cannot be thermostated.

Shimoboji and coworkers have recently synthesized novel photoresponsive Streptavidin proteins.[238] The photoactivity was added to the proteins via a thiol coupling reaction with the addition of azobenzene-containing polymers near the Streptavidin's recognition site. Figure 2-17 shows the photoactive polymer along with a schematic of how the photoresponsive polymer modulates the activity of a protein. When the protein-polymer conjugate was irradiated with visible light, the

(a)

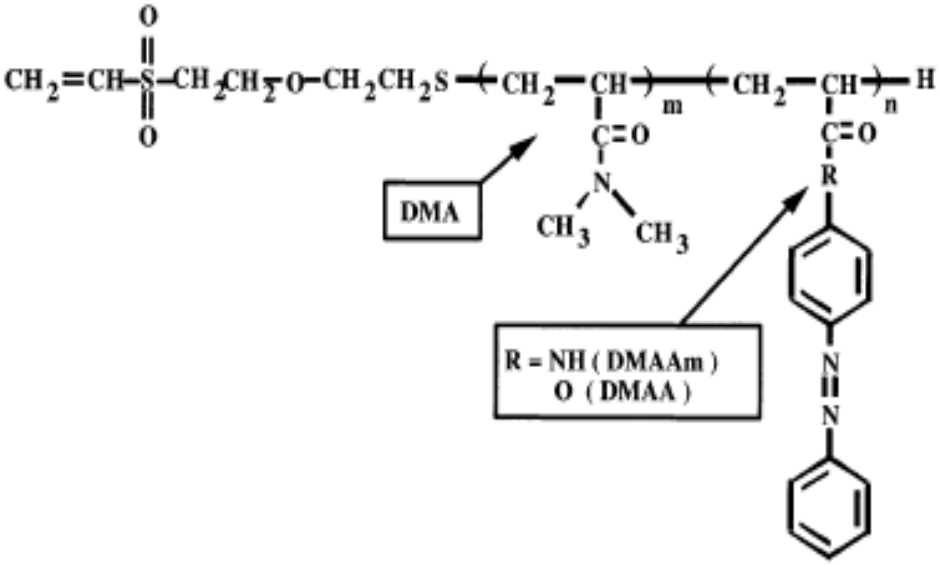

(b)

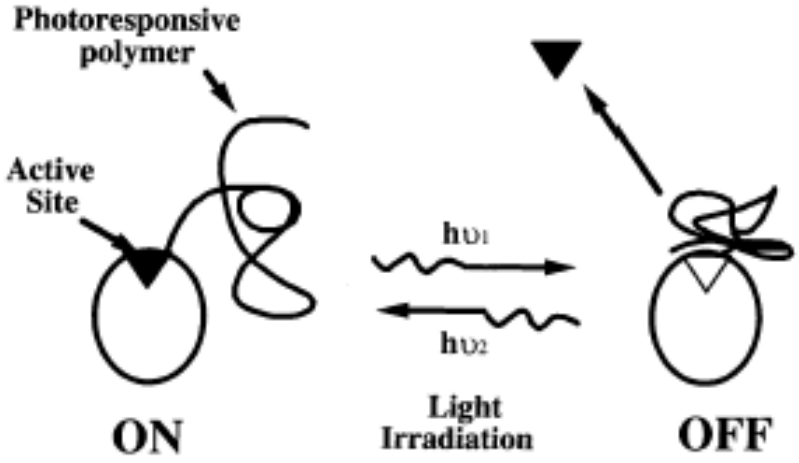

Figure 2-17. (a) the photoresponsive polymer used to modify the Streptavidin protein and (b) a schematic showing the use of light to modulate the activity of the Streptavidin. Reprinted with permission from ref 238. Copyright 2002 American Chemical Society.

photoactive azobenzene group caused the polymer to collapse, thus sterically hindering the binding of free biotin. When the protein-polymer conjugate was irradiated with UV light, the polymer relaxed, allowing the binding of the free biotin.

Gandini's group has focused on the use of furans in polymers and have penned a recent review on the topic.[160-162] In their most recent study, they attached a number of furan derivatives to poly(vinyl alcohol) via a terminal aldehyde functionality on the furan derivatives. They were able to photodimerize up to 46% of the pendant furan groups polymers with 25 h of exposure from a 500 W medium-pressure mercury lamp filtered to remove wavelengths below 300 nm. It is important to note that the furans (like the cinnamates) undergo a *trans-cis* isomerization, which competes with the dimerization reaction during irradiation.[173,239-241]

In addition to photoinitiated reactions previously mentioned, Decker et al. has also studied polymer photocrosslinking via the dimerization and free radical methodologies utilizing maleimides functionalized poly(methyl methacrylate).[159] Maleimides can undergo three different types of photoreactions when irradiated. The first of which is the [2π+2π] cycloaddition leading to the formation of a cyclobutane ring. They also can homopolymerize via a free radical mechanism when exposed to UV irradiation in the presence of a photoinitiator or form a perfectly alternating copolymer when they are irradiated in the presence of a electron donating monomers such as vinyl ethers. Decker concluded that the type of reaction that resulted greatly depended on the system. For a copolymer

of methyl methacrylate and maleimides, UV irradiation led only to inter and intramolecular cyclodimerization. This was realized since the addition of a photoinitiator had no effect on the reaction rate. In the case of mixtures of the maleimides and divinyl ether, UV irradiation formed a crosslinked alternating copolymer of the two monomers.

2.3 CINNAMATES IN POLYMERS

As previously mentioned, Minsk and coworkers reported the first synthetic photoreactive polymers via the photodimerization of poly(vinyl cinnamate).[158,163,165-167] Since the initial studies, cinnamates many researchers have studied the use of cinnamates in polymers.[91,152,153,168,169,172,176,181,182,184,185,242-258]

Andreopoulos and coworkers have reported most of the recent published research on crosslinking through cinnamate dimerization, synthesizing reversible poly(ethylene glycol) (PEG) hydrogels.[92,177-179,181,211] The hydrogels are synthesized by the reaction of cinnamylidene acetyl chloride and the termini of 4-armed PEG (MW=20,000) results in hydrogel formation. The structure of the product along with a schematic of the reversible photodimerization is shown in Figure 2-18. The reversible degree of swelling of the hydrogel caused by the reversible photodimerization/crosslinking in water is shown in Figure 2-19. The data show that alternating the wavelength of irradiation can reversibly change the degree of swelling exhibited by the hydrogel.

Andreopoulos has also studied the biocompatibility of these hydrogels and the photoimmobilization of organophosphorus hydrolase, an enzyme that

(a)

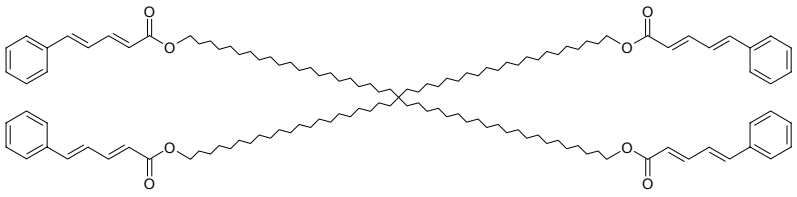

(b)

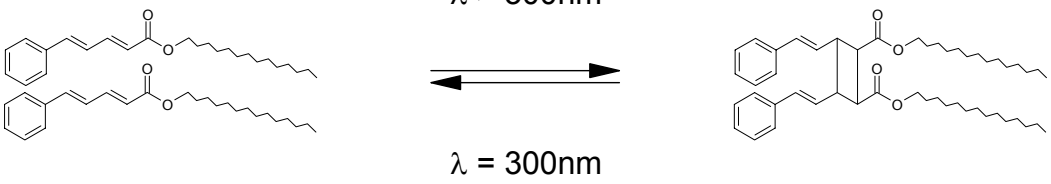

Figure 2-18. (a) the cinnamate modified PEG hydrogel and (b) schematic of the reversible dimerization.[92,177,178]

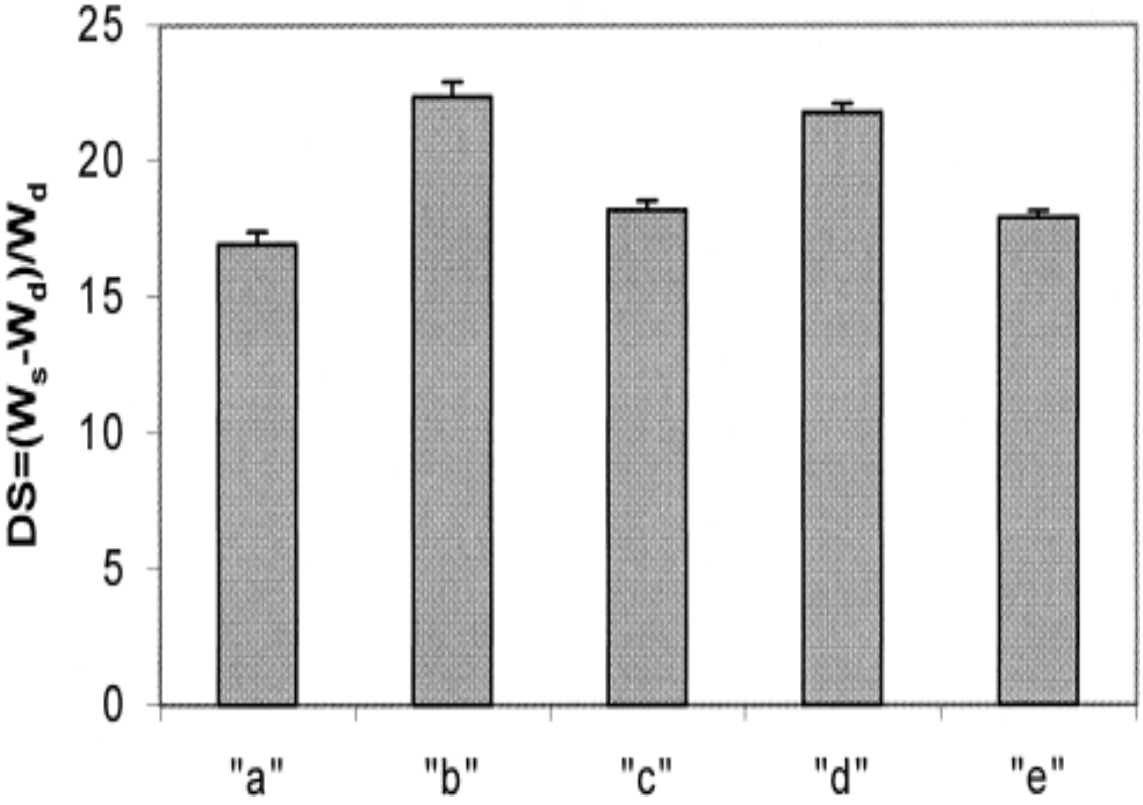

Figure 2-19. Degree of swelling of cinnamate PEG hydrogels as a function of irradiation wavelength; (a) 2 h of >300 nm irradiation; (b) 2 h of >300 nm + 2 min of 254 nm irradiation; (c) 1 h of >300 nm + 2 min of 254 nm + 1 h of >300 nm; (d) sample “c” + 2 min of 254 nm. (e) sample ”d” + 1 h of >300 nm. Reprinted from ref. 177 with permission from John Wiley & Sons.

degrades pesticides.[92,178] In similar studies, Andreopoulos used nitrocinnamate or anthracene groups attached to an eight-arm PEG hydrogel in an attempt to increase the sensitivity of the reversible photoreaction. Environmental scanning electron microscopy (ESEM) of the hydrogels containing nitrocinnamate groups optically demonstrated changes in the surface of the hydrogels upon irradiating the system.[181] Figure 2-20 contains the ESEM micrographs of the PEG hydrogel. Examination of the micrographs reveals that the surface of the as prepared hydrogel is rough (Figure 2-20(a)) then becomes smooth with large pores upon photodimerization of the cinnamate groups. Finally, the hydrogel reverts to its initial rough topology upon photocleavage of the cinnamate groups. Both of the materials demonstrated photosensitivity slightly better than the cinnamate modified PEG hydrogel as measured using UV-Vis spectroscopy.[180,181]

Nanjundan et al. studied the synthesis and photocrosslinking of polymers containing bromo-substituted cinnamate derivatives.[255] They synthesized a methacrylated cinnamate monomer which was then polymerized free radically yielding polymers of high molecular weights (M_n = 20,800 and M_w = 40,300) and yields of up to 45%. The polymers were then crosslinked in a variety of solvents to test their applicability as negative photoresists.

In an effort to synthesize thermosetting polymers from renewable resources, Esen *et al.* reacted epoxidized soybean oil with cinnamic acid yielding photocrosslinkable soy-based polymers.[256] The reaction between the epoxidized

(a)

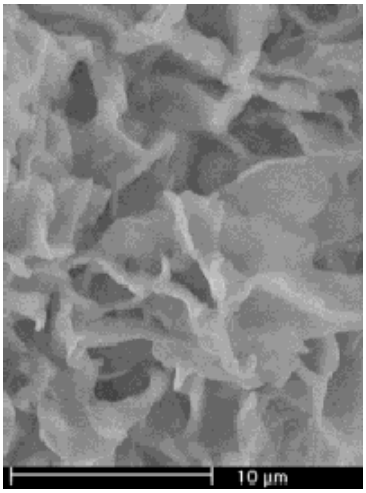

(b)

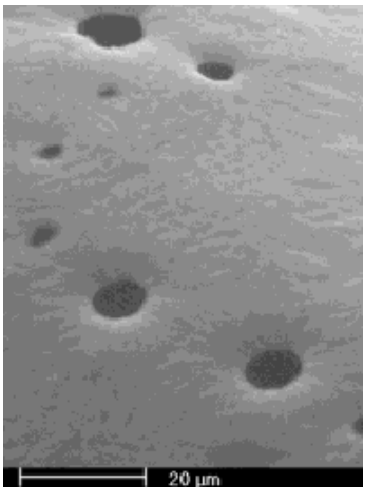

(c)

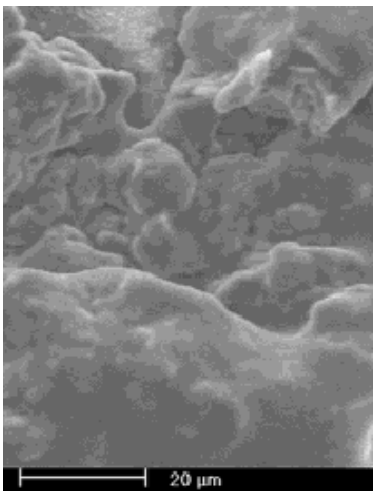

Figure 2-20. ESEM micrographs of nitrocinnamate modified PEG hydrogels (a) as cast, (b) after photodimerization and (c) after photocleavage. Reprinted from ref. 181 with permission from John Wiley & Sons.

soybean oil and cinnamic acid was highly successful; averaging over three cinnamate groups per triglyceride molecule. The macromer was then reacted via a number of methodologies including and UV crosslinking via photodimerization and free radical homopolymerization or copolymerization initiated with an epoxide initiator. Esen successfully copolymerized the macromer with vinyl acetate, styrene and methyl methacrylate. The styrene-containing copolymer (25 wt% styrene) was the most promising displaying two T_g at 54 °C and a small shoulder from the triglyceride at 0 °C (DSC). The insoluble and infusible polymer had good mechanical properties with a storage modulus of 3 $x10^9$ Pa at room temperature.

Mashiko *et al.* recently used direct irradiation and triplet energy transfer to crosslink cinnamate endcapped dendrimers.[252] They synthesized first, third and fifth generation poly(propylene imine) dendrimers, which were subsequently endcapped with cinnamoyl chloride. Irradiation of the dendrimers at 313 nm predominately isomerized the cinnamates (*trans* to *cis*) on the first generation dendrimer, while it promoted photodimerization of the cinnamates on the third and fifth generations. Steric hindrance of the cinnamate groups was the proposed explanation of this effect. The addition of Michler's ketone to the 3rd and 5th generation allowed for dimerization of the cinnamate groups with irradiation at 365 nm. The Michler's ketone absorbs the 365 nm energy and transfers the energy through the dendrimer via a double electron exchange of both the HOMO and LUMO from the donor (Michler's ketone) to the acceptor (cinnamate).

Scanning tunneling microscopy (STM) is an important tool to study a number of different self-assembled monolayers at the graphite/liquid interface.[182,259-261] A self-assembled monolayer of oligomeric cinnamates (see Figure 2-21(a) for structure) and its [2+2] photodimerization were studied by STM. An STM image of the dimerized cinnamate, irradiated for at least 10 min. (λ=300 nm), is shown in Figure 2-21(b). Although cinnamate dimerization was not expected to occur due to the theoretical packing structure, the cinnamates dimerized due to fluctuations in the packing of the molecules.[182]

2.4 Coumarins in Polymers: From Light Harvesting to Photocrosslinkable Tissue Engineering Scaffolds

Scott R. Trenor, Allan R. Shultz, Brian J. Love, and Timothy E. Long

2.4.1 Introduction.

The use of polymer photoreactions dates back some 4,000 years to when ancient Egyptians and Babylonians used sunlight to photocrosslink linens during mummification and to waterproof papyrus boats via the photopolymerization of an asphalt oil.[71,208,262] The first synthetic photoreactive polymers resulted from work done by Minsk and coworkers on the photodimerization of poly(vinyl cinnamate).[158,163,165-167] Soon afterwards, Plambeck developed and patented the photoinitiated free-radical polymerization of acrylates.[263]

(a)

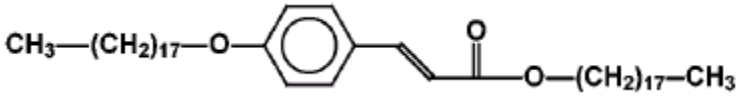

(b)

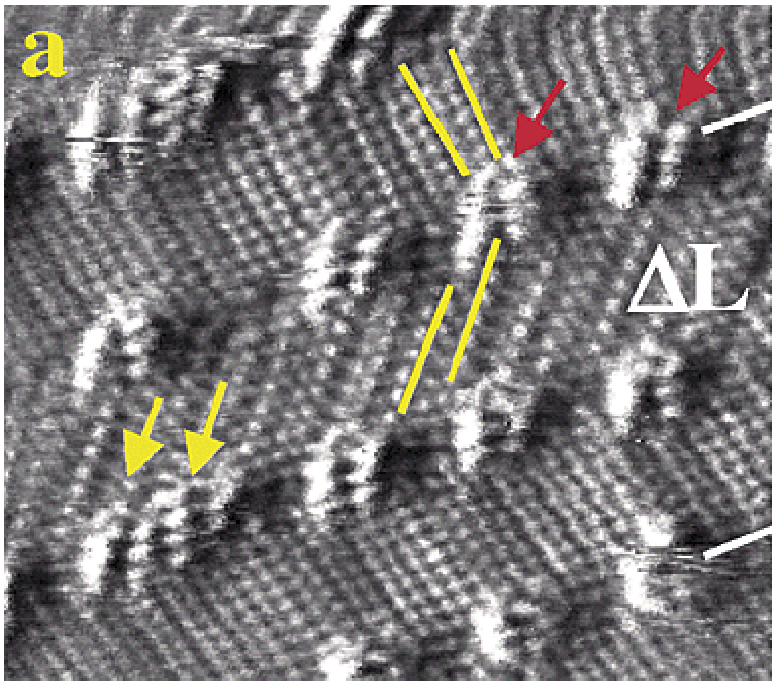

Figure 2-21. (a) Structure of the oligomeric cinnamate studied and (b) STM image (10.7 x 10.7 nm^2) of the dimmer. Yellow lines are alkyl chains and red arrows point towards the dimer core. Reprinted with permission from ref. 182. Copyright 2001 American Chemical Society.

The uses for coumarins are as diverse as the structures of the 800 different derivatives in the coumarin family. Coumarins are used in the fields of biology, medicine and polymer science. They are also present or used in perfumes, sunscreens, sweeteners, cigarettes, alcoholic beverages, laser dyes and were linked to a number of cases of homicide and suicide in Korea.[207,264-283]

This review will focus on the use of coumarin and coumarin derivatives in polymers. First, an overview of coumarin and coumarin derivatives is presented, followed by a discussion of the use of coumarin containing polymers in electro-optical studies, the development of photoreversible polymer systems, the use of coumarin in biopolymer studies, and the use of coumarins in other systems.

2.4.1.1 *Coumarin, Coumarin Derivatives, and Properties.* Coumarin (Figure 2-22a), was first reported and isolated in the 1820's, recognized as the hay-like sweet aroma of the tonka bean.[264,269] Since then, more than 1000 derivatives have been investigated with naturally occurring coumarin derivatives isolated from over 800 species of plant life. Most of the coumarin derivatives have at least one additional oxygen atom at one or more of the six other available positions (i.e. positions 3 - 8 in Figure 2-22(a)), with all except for approximately 35 derivatives being oxygenated at the seventh position.[269,284] For this reason, 7-hydroxycoumarin, shown in Figure 2-22(b), also known as umbelliferone, is often considered the "parent" of the more complex coumarins. For earlier reviews on individual coumarin derivatives, their biological action, and occurrences, the reader is referred to reviews by Murray et al., Nielsen, and O'Kennedy et al.[266,268,269,284]

(a)

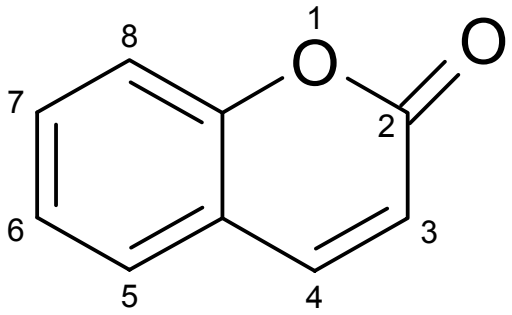

(b)

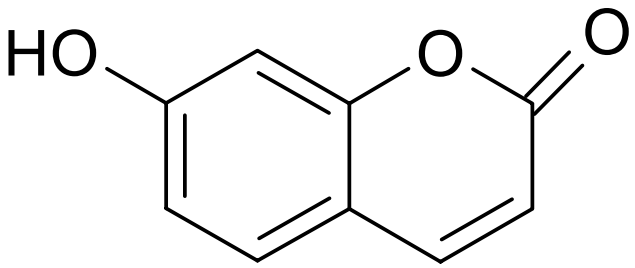

Figure 2-22. Structure and numbering scheme of (a) coumarin and (b) 7-hydroxycoumarin.

The uses for coumarins are as diverse as the structures of the over 1000 different derivatives in the coumarin family. In addition to the previously mentioned uses, coumarins are well documented as therapeutic agents and have been used as medicines in ancient Egypt and in aboriginal cultures.[266,267,284-292] One example, warfarin, is the most prescribed anticoagulant on the market.[293-295] Recent medicinal research has focused on the use of coumarin derivatives as Anti-HIV agents. A recent review by Yu and coworkers described the study of over 150 coumarin derivatives and their efficacy in fighting HIV. Some of the derivatives have effective concentrations (EC_{50}) 180,000 times less than that of AZT, though poor water solubilities have hampered further testing and development.[296]

The ability of coumarin to reversibly photodimerize and subsequently photocleave (to be described in section 2.4.1.4) was studied as a possible controlled drug release mechanism.[297,298] Tanaka and coworkers synthesized mesoporous silica substrates with coumarin groups attached to the pores. A model drug, cholestane, was impregnated into the coumarin functionalized silica substrates and was released when the silica substrates were washed without irradiation. If the impregnated substrates were irradiated above 300 nm and then washed, the substrate failed to release the cholestane since the photodimerized coumarin now blocked the pores. With subsequent re-irradiation at 250 nm, the coumarin dimers were photocleaved and the cholestane was released with washing. This model system worked well, but other systems may fail if the drug, pore, and coumarin dimer size are not matched.

2.4.1.2 Synthesis of Coumarin and Coumarin Derivatives. Simple coumarin derivatives are naturally derived as a derivative of cinnamic acid via the shikimate-chorismate biosynthetic pathway.[284] Briefly, trans-cinnamic acid is hydroxylated, glucosylated and isomerized to the cis-2'-glucosyloxycinnamic acid, resulting in the bound form of coumarin (coumarinyl glucoside). Coumarin derivatives were first synthesized via the Perkin reaction in 1868 and many simple coumarins are still derived from this method. In the early 1900's, the Knoevenagel reaction emerged as an important synthetic method to synthesize coumarin derivatives with carboxylic acids at the 3 position.[299,300] Later, researchers condensed ethyl cyanoacetate and various o-hydroxyacetophenones to synthesize 4-methylcoumarin derivatives.[301,302]

Recently, the Pechmann reaction was utilized in conjunction with Nafion®/silica nanocomposites as catalysts to synthesize 7-hydroxycoumarin derivatives.[303] Via a reaction of resorcinol and ethyl acetoacetate, 7-hydroxy-4-methylcoumarin was synthesized at yields of 81-96% with high recyclability of the Nafion®/silica nanocomposite catalysts. A more recent scheme that was utilized to synthesize coumarin derivatives is ring-closing metathesis using the Grubb's catalyst.[304] De Kimpe and coworkers synthesized six coumarin derivatives starting with phenolic compounds which then underwent *O*-allylation followed by an *o*-Claisen rearrangement, base-induced isomerization, acylation with acryloyl chloride and finally ring-closing metathesis. The yields of the five-step reaction ranged from 70 to 90%.

While coumarin derivatives are readily synthesized by the aforementioned reactions, most require harsh reaction conditions and non-environmentally friendly solvents. Sartori *et al.* have reported "greener" reaction schemes utilizing recyclable catalysts and water as the solvent.[305-307] Sartori modified the Knoevenagel reaction, using montmorillonite clays as catalysts, to synthesize coumarin-3-carboxylic acids with yields ranging from 50 to over 90%. Their research indicated that the clays serve as a ditopic catalyst with both acidic and basic sites. They proposed that the basic sites activated the Knoevenagel reaction, while the acidic sites promoted α-pyrone ring formation via transesterification. Sartori's group has also studied the use of water as a solvent to synthesize 3-carboxy coumarins via a reaction between Meldrum's acid and salicylaldehydes. The reactants were refluxed in water for 10 h with yields above 78%. Their proposed mechanism included nucleophilic attack of the active methylene (on Meldrum's acid) to the carbonyl group of the salicylaldehyde followed with dehydration leading to the coumarin derivative.

2.4.1.3 *Photophysics and Fluorescence.* Coumarin and its derivatives show sufficient fluorescence in the visible light range to be used in laser dyes and organic LEDs.[271,274-278,280,308] Figure 2-23(a) shows the fluorescence, phosphorescence, and polarized phosphorescence spectra of coumarin in ethanol when irradiated at 320 nm. Researchers have studied the photophysics of coumarin compounds since the 1940s due in part to the tunability of their absorbance and fluorescence.[207,274-276,279-282,309-317]

(a)

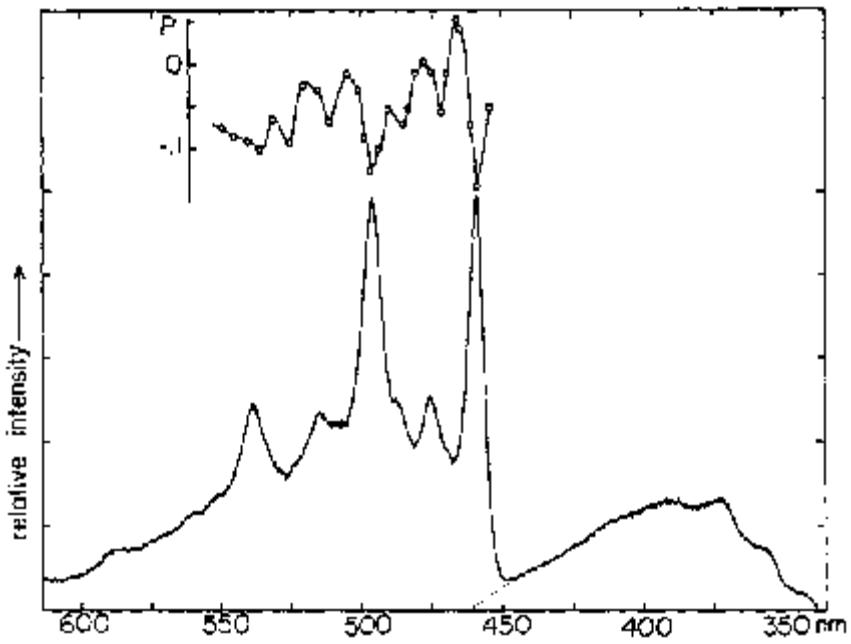

(b)

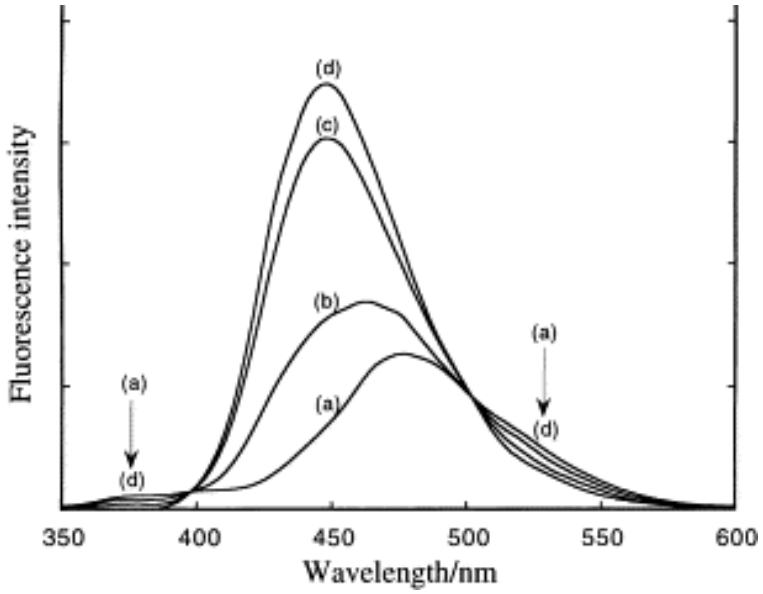

Figure 2-23. (a) the phosphorescence (left of 450 nm), fluorescence (right of 450 nm) and polarized phosphorescence (inset) of coumarin in ethanol when excited with irradiation at 320 nm. Reprinted with permission from [311]. Copyright 1973 American Chemical Society. (b) the effect of pH on the fluorescence spectra of 7-hydroxy-4-methylcoumarin in MeOH-H_2O solution with KCl and HCl as pH increases from 1 (curve (a)) to 10.5 (curve (d)). Reprinted from ref. [282] with permission from Elsevier.

In the late 1950s, Wheelock showed substitutions on the coumarin structure shifted the fluorescence band.[310] For instance, adding a methyl group to the 4-position of 7-hydroxy- or 7-methoxycoumarin red shifts (i.e., shifts to longer wavelengths) the fluorescence spectra. Wheelock's results showed that the addition of electron-repelling groups in the 4, 6, or 7 position or electron-attracting groups in the 3 position all shift the fluorescence band to longer wavelengths. When the carbonyl is substituted with a thione, the absorbance was red shifted and the fluorescence was quenched.[207,281]

Changing the solvent or the solution pH also affected the fluorescence spectra. The effect of solution pH on 7-hydroxy-4-methylcoumarin is shown in Figure 2-23(b), illustrating that increasing the solution pH raised the fluorescence intensity.[282] As for the solvent, Jones and coworkers studied the effect of changing the solvent polarity on 13 coumarin derivatives. They found that increasing solvent polarity red-shifted the absorbance as well as red-shifted and broadened the emission of the coumarins due to increased hydrogen bonding.[275] In a similar study, Sharma *et al.* studied the excited-state properties of 4- and 7-substituted coumarin derivatives. They also observed that solvent polarity shifts both the emission and absorption peaks, with a greater shift observed in the emission spectra. This indicated that the excited state dipole moment of the solute molecule was greater than the ground state dipole moment.[318]

2.4.1.4 *Photodimerization and Photocleavage.* The photodimerization of coumarin was discovered by Ciamician and Silber in 1902, when they used sunlight to irradiate coumarin dissolved in alcohol for over 2 years.[195] The

dimerized product exhibited a melting point of 262 °C, much higher than the original coumarin melting temperature of 68 – 70 °C.[195,220] In 1904, Ström reported a dimer with a melting point above 320 °C.[220,319] Since the first two studies reported two different melting points, it was not resolved until Schenck and coworkers observed that both structures were in fact dimers of coumarin.[220] Schenck used ^{1}H NMR spectroscopy to determine the structure of the four possible dimers that were produced from the irradiation of coumarin at different reaction conditions. Figure 2-24 shows the structure of the four possible dimers formed from the UV irradiation of coumarin.

The actual coumarin dimer formed on irradiation depends on the combination of dose, solvent, and coumarin concentration. The structure of the dimer resulting from irradiation was contested in the late 1960s and early 1970s by the research groups of Schenck, Morrison Anet, and Hammond.[212,214,220,224,320,321] They concluded that the dimer formed via the [2πs+2πs] cycloaddition formation of a cyclobutane ring. The combined results of their studies indicated that coumarin irradiation yielded mainly three products: the syn head-to-head dimer (Figure 2-24(a)), the anti head-to-head dimer (Figure 2-24(b)), and the syn head-to-tail dimer (Figure 2-24(c)). At high concentrations, the coumarin singlet reacts with a ground-state coumarin and forms the syn head-to-head dimer, while at low concentrations, inefficient intersystem crossing produces the triplet coumarin and the anti head-to-head dimer is formed.[221]

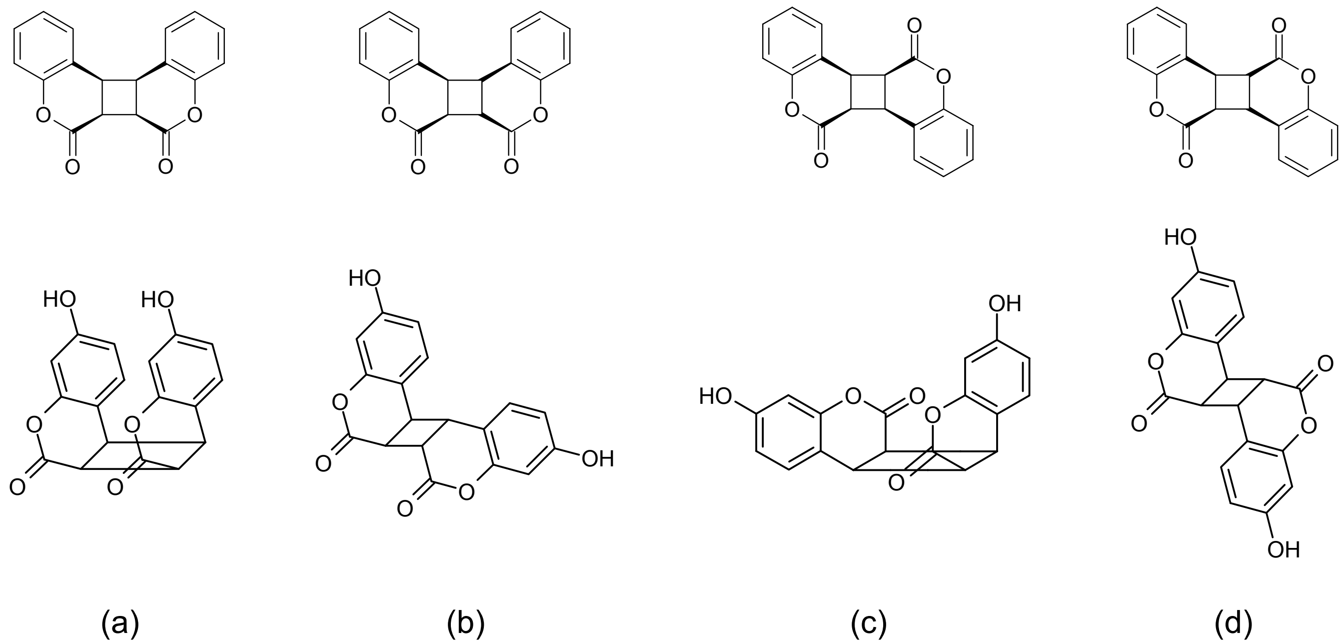

Figure 2-24. The four isomers resulting from the photodimerization of coumarins (coumarin top and 7-hydroxycoumarin below) using different conditions. (a) syn head-to-head dimer, (b) anti head-to-head dimer, (c) syn head-to-tail dimer and (d) anti head-to-tail dimer.[212,214,220,221,224,322]

The reaction scheme in Figure 2-25 summarizes the UV radiation induced formation of the coumarin photodimers. In polar solvents, the singlet state is favored, resulting in the formation of mostly syn photodimers, while nonpolar solvents or the addition of photosensitizers such as benzophenone lead to mostly anti photodimers.[200,212,214,219,221,224,322,323] The heavy-atom effect becomes important with chlorinated solvents. It reduces the concentration of the excited singlet state coumarins by reducing the lifetime of the excited singlet. The shorter lifetime is due to a shift in the equilibrium of molecular spin and orbital motions, making the spin change more desirable and thus reducing the lifetime of the singlet excited states. The smaller singlet concentration increases the relative concentration of excited triplet state coumarins, thus pushing the dimer equilibrium toward the anti products.[200,214,224] Belfield and coworkers have recently studied the two-photon dimerization of 5,7-di-methoxycoumarin as a model for psoralen enone photochemistry.[324] They found that ratios of the dimer formed, via two-photon excitation at 650 nm, were similar to the ratios achieved with the traditional single-photon UV exposure.

Researchers have also studied the solid-state dimerization of coumarin compounds both in the bulk and in inclusion complexes. [218,222,223,322] In one such study, Brett and coworkers studied the photodimerization of 7-hydroxy-4-methylcoumarin in a β-cyclodextrin complex. The host β-cyclodextrin materials allowed for the positioning of the reactive double bonds on the coumarin to be

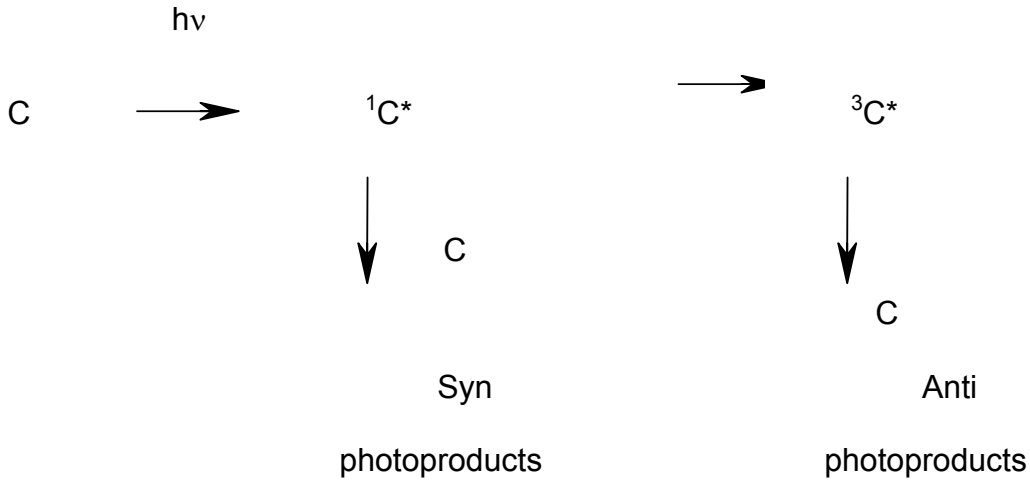

Figure 2-25. Reaction scheme leading to the dimerization of coumarin.[200,212,214,221,224]

3.5-3.7 Å apart and aligned parallel to adjacent coumarin groups. Upon UV irradiation for 7 days, the coumarins dimerized forming the anti-head to tail dimer as observed using X-ray crystallography.[322]

Ramamurthy *et al.* studied the solid-state dimerization of 28 coumarin derivatives.[218] Figure 2-26 shows their results in the form of dimer yield as a function of irradiation time. Of the 28 coumarin derivatives studied, 12 formed dimers in the solid state. From their measurement using ^{1}H NMR spectroscopy, thin-layer chromatography, and X-ray analysis, they resolved several conditions for promoting solid-state dimerization, such as close proximity of the double bonds. Ramamurthy found that a double-bond separation of less than 4.2 Å was necessary for most coumarin derivatives. The exception proved to be 7-chlorocoumarin, which dimerized with separations up to 4.5 Å. Chloro and acetoxy groups also enhanced dimer formation by "steering" the double bonds into the correct position, but no explanation on how this is accomplished was provided.[218]

Delzenne and Laridon first studied the photodimerization of coumarin groups attached to polymers in the mid 1960s.[208] This group studied copolymers of ethyl acrylate and 7-acryloxycoumarin, poly(hydroxyethers) with coumarin derivatives, and partially hydrolyzed poly(vinylbutyral) modified with 6-coumarin sulfonyl. They were able to photocrosslink the polymers through the coumarin moiety to form insoluble networks where the light sensitivity of the polymer was directly proportional to the degree of coumarin substitution.

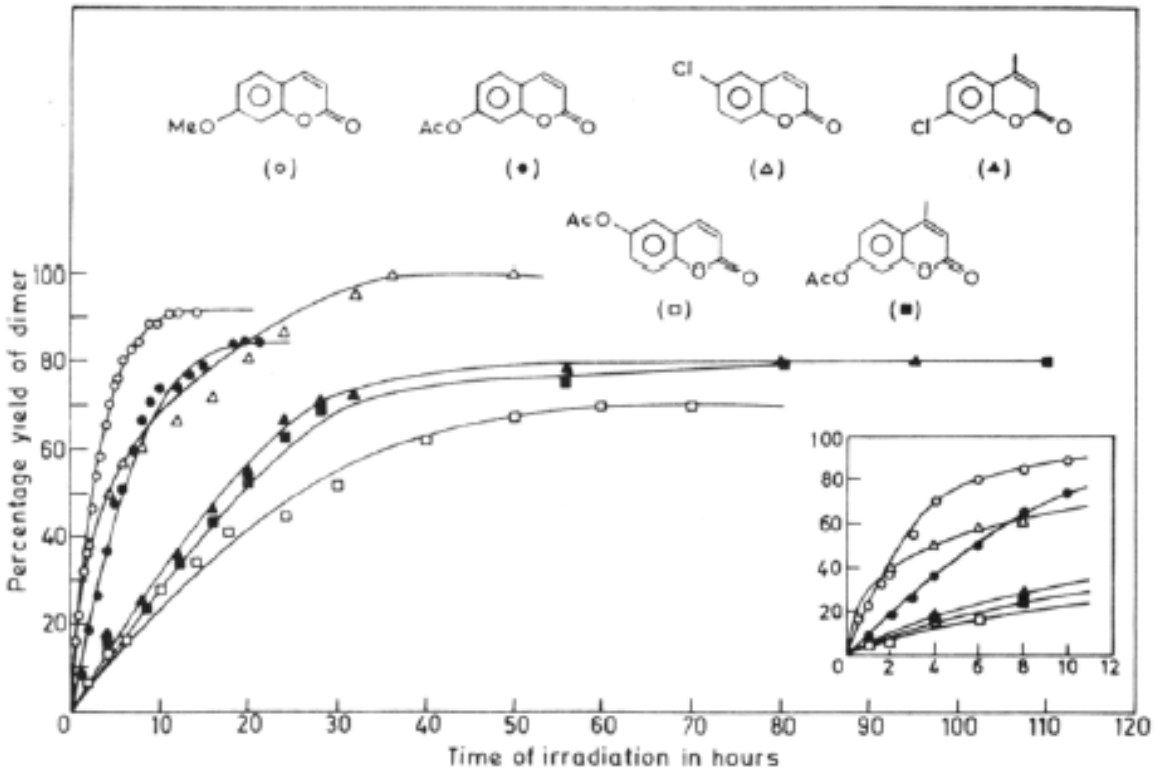

Figure 2-26. Dimer yield for various coumarins as a function of irradiation time using a 450 W medium pressure Hg arc lamp, as measured using ^{1}H NMR. Reprinted with permission from ref. 218. Copyright 1985 American Chemical Society.

Schenck and coworkers first discovered the photocleavage of a coumarin dimer during their research on the dimerization of coumarin.[198,202,220] However, the photoscission reaction has not been studied as extensively as the dimerization reaction. Most of the references in the literature on the photocleavage of cyclobutane dimers points toward work by Lamola on the photocleavage of thymine dimers.[235,325]

Cyclobutane photocleavage has been studied to some extent by Hasegawa and coworkers.[235,326,327] The generic photocleavage reaction scheme is shown in Figure 2-27. Cyclobutane rings that are formed from coumarin dimerization undergo symmetric cleavage. Several interesting trends emerged from their studies. All of the compounds that have stable 5- or 6- membered rings attached to the cyclobutane ring cleaved, preserving the more stable ring. For the dimers without stable rings, the symmetric or asymmetric cleavage that resulted was due to either steric repulsions or other repulsions between neighboring groups.[235] Coumarin photodimers have also been cleaved via a two-photon excitation to circumvent difficulties encountered when attempting to irradiate at 254 nm, i.e., composite layers with high UV absorptions. Kim and coworkers utilized a Nd:YAG laser at 532 nm to cleave the coumarin dimers. While they were able to quantitatively cleave the dimers, the dose necessary for the reaction was approximately 9.0 kJ at 532 nm, whereas for the same unit area less than 500 mJ was necessary to cleave the dimer at 266 nm.[328]

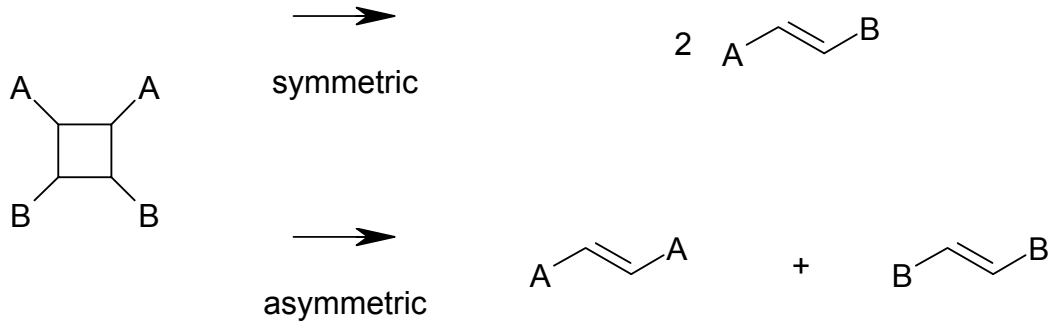

Figure 2-27. Symmetric and asymmetric cleavage of cyclobutane compounds formed via photodimerization.[235,326,327]

2.4.2 Coumarins in Electro-optical Studies.

2.4.2.1 *Liquid Crystalline Polymers.* A number of researchers have reviewed polymeric liquid crystals, and the liquid crystals have recently attracted considerable attention due to the combination of polymer-specific properties and the unique anisotropic behavior of liquid crystalline (LC) molecules.[131,329-336] The introduction of polymers into LC systems can increase the mechanical strength and may considerably change the LC phase behavior. Photoinduced alignment control has also been the focus of recent research activity due to the ability to induce structural and orientational alterations of the macromolecules that are localized at the surface of the construct.[225]

Most of the polyimide films currently used as LC substrates necessitate mechanical rubbing/buffing to induce the desired orientation and thus LC alignment. The use of photoalignment techniques eliminates the need for the mechanical buffing of the films used as LC substrates, which can damage the construct.[217] Photocrosslinkable liquid crystalline polymers (LCP) have the added advantage of containing both photoactive groups and mesogens in their structures.[336] In particular, photocrosslinkable side chain liquid crystalline polymers (SCLCP) are useful in manufacturing information storage devices, nonlinear optical devices, aligned membranes for permeation of drugs and gases, and flat television and computer displays.[336,337]

Work on coumarin SCLCPs began with the work of Schadt and coworkers who studied LC alignment patterns with bias tilt angles.[337] Using the polymer and photoalignment reaction shown in Figure 2-28, they bypassed the abrasion

process and produced a film, which was optically and thermally stable to 200 °C. When coumarin side chains were used, the tilt angle changed from perpendicular to the electric field vector (**Ê**), as with the use of cinnamate side groups, to **n** (shown in Figure 2-28) which is a function of **Ê** and **k**, the angle of the incident UV radiation.[337-339] The tilt angle of the coumarin SCLCP was adjustable from 0° to 90° by changing the polarization of the light. Coumarin SCLCPs performed better than cinnamate SCLCPs as the cinnamate SCLCPs undergo a competing cis/trans isomerization in addition to the [2+2] photodimerization, which leads to added complications.[171,225,242]

Schadt's publication spawned a number of other coumarin SCLCPs studies.[171,216,217,225,233,242] Obi and coworkers studied the factors that affected the alignment of coumarin SCLCPs using a polymer similar to the one used by Schadt.[225] Obi's study defined the R group in the side chain as $(CH_2)_n$ with n = 0, 2, or 6. The results of their study on the polymer with n = 2 is shown in Figure 2-29. Figure 2-29(a) is a plot of UV absorption versus wavelength, and shows the decrease in absorbance at 320 nm resulting from the dimerization of the coumarin group. As the coumarin dimerizes, the level of unsaturation decreased due to the formation of crosslinks between cyclobutane rings. Figure 2-29(b) illustrates the influence of irradiation on the azimuthal orientation of a LC cell. With an irradiation of 10 mJ/cm^2, the LC cell shows homogeneous alignment. The results from this study indicated that the coumarins photodimerized without any side reaction (such as the isomerization observed with the use of

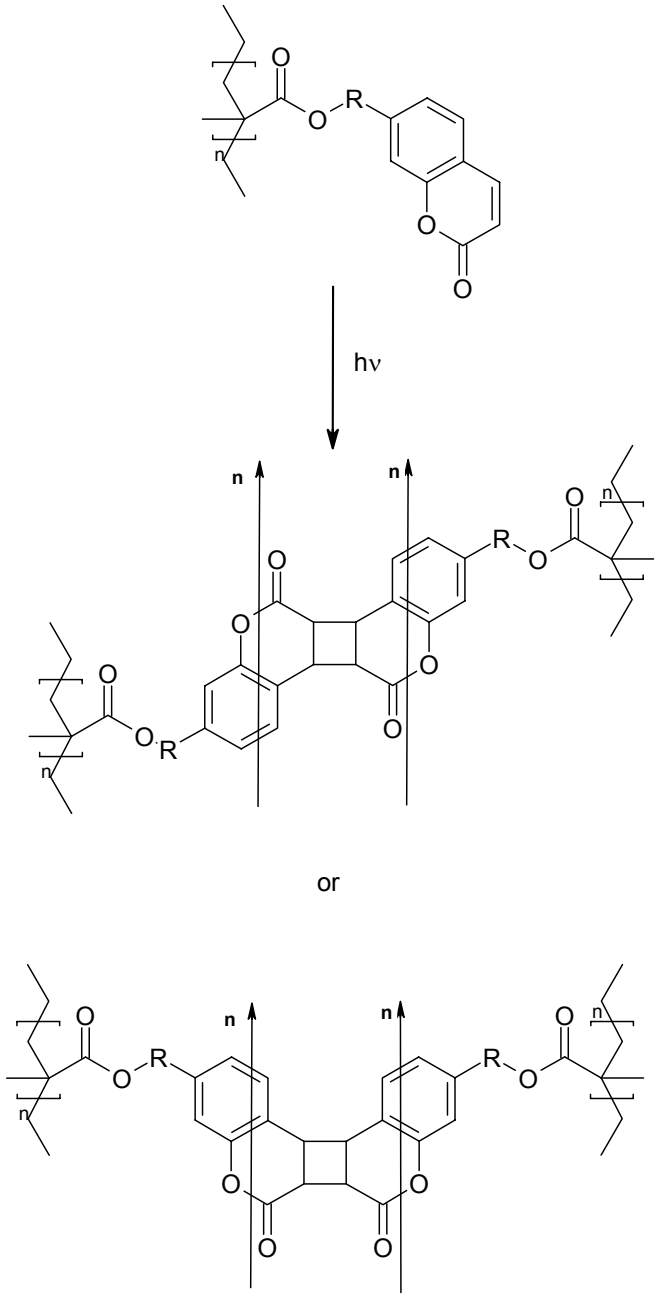

Figure 2-28. Side chain LCP used by Schadt and coworkers where n = director direction and R = unspecified side chain spacer.[337]

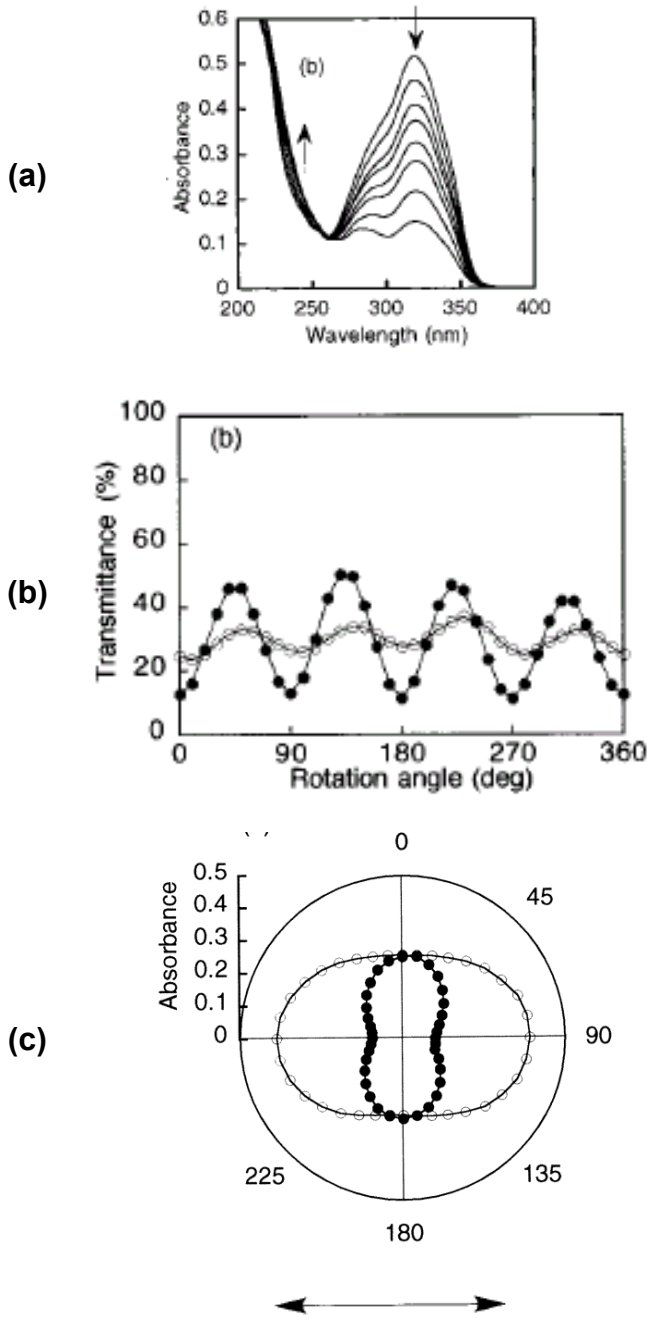

Figure 2-29. Coumarin SCLCP (n=2). (a) UV absorbance change with irradiation at 313 nm (arrows indicate trends with increasing irradiation time). (b) Percent transmittance of linearly polarized light as a function of LC cell rotation angle after exposure doses of (o) 5 mJ/cm^2 and (•) 10 mJ/cm^2. (c) The circular diagram absorbance of a dichroic dye in an LC cell (coumarin SCLCP with n=0) after exposure doses of (o) 1 J/cm^2 and (•) 10 J/cm^2. Reprinted in part with permission from ref. 225. Copyright 1999 American Chemical Society.

cinnamates). Additionally, an increase in dimerization speed was observed with increasing spacer length, a result attributed to increased molecular mobility.

Obi's study revealed that the alignment direction of the coumarin SCLCP without a methylene spacer (n = 0) changed on prolonged polarized irradiation. With short irradiation times, the film's orientational alignment was parallel to the polarization direction (**P**). With further irradiation, the alignment degraded prior to adopting an alignment perpendicular to **P**. Figure 2-29(c) shows the circular diagram of absorbances of a dichroic dye in a LC cell fabricated from the SCLCP polymer with n = 0 and the direction of the electric vector of the incident light. The change in the shape of the plot indicated a reorientation of the LC from one that was parallel to the vector to one that was perpendicular. The polymers which were synthesized with two and six methylene spacers, displayed no change in orientation and remained aligned parallel to **P**.[217,225]

Jackson and coworkers further studied orientation changes using the coumarin SCLCP shown in Figure 2-30(a).[216,217,244,340] These researchers found that the alignment direction of the polymer was aligned parallel to **P** at small exposure doses (<0.72 J/cm^2), while the alignment switched to one perpendicular to **P** at a higher dose of 0.72 J/cm^2. This jump from parallel to perpendicular is plotted Figure 2-30(b) as the change in Φ, the angle between the LC alignment direction at the photoaligned surface and the polarization direction of the incident beam. Based on birefringence, FTIR spectra, and anchoring data as a function of UV exposure, Jackson hypothesized that the parallel alignment was due to the

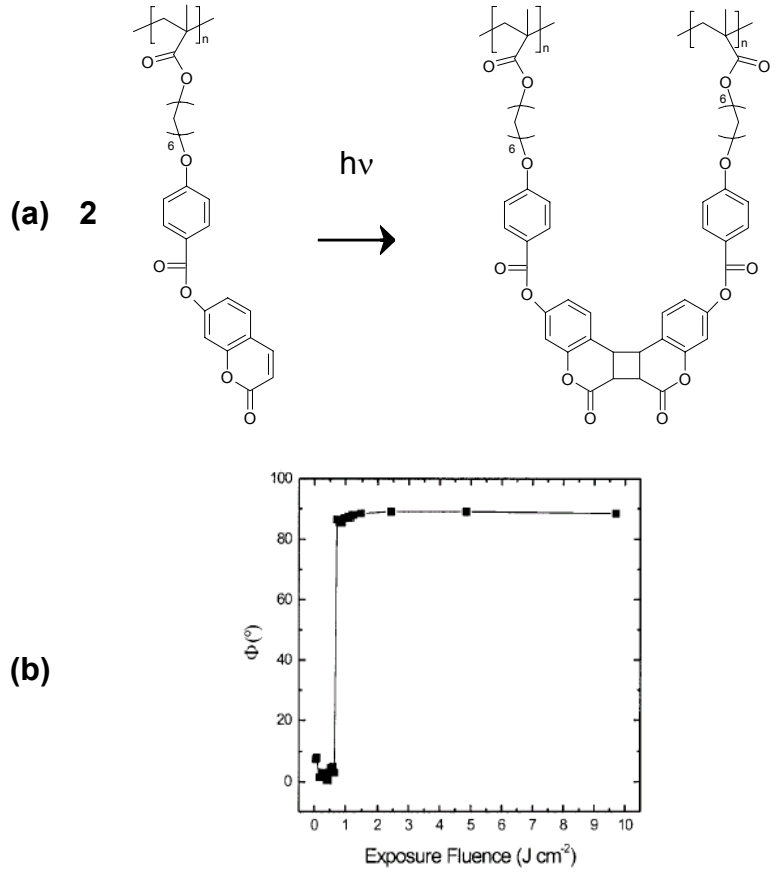

Figure 2-30. (a) Polymer and reaction studied by Jackson and coworkers and (b) LC alignment direction measured with respect to P as a function of UV irradiation at λ = 300.5nm. Reprinted with permission from ref. 217. Copyright 2001 American Chemical Society.

initial photocrosslinking of the dimers. Changes in the FTIR spectra coupled with the low birefringence of the system led to the conclusion that photocrosslinking saturated after approximately 40% of the side chains had dimerized. As the polymer was exposed to more energy, the birefringence and anchoring energy increased. In addition, the alignment switched to one perpendicular to **P,** due to possible photodegradation of the nondimerized and photodimerized side chains. The photodegradation of the dimerized side chains entails the breaking of the cyclobutane rings, which lead to a decrease in the LC dispersive interaction parallel to **P**.

Degradation of the polymers was further studied using grazing angle X-ray reflectivity.[216] X-ray data showed an increase in the surface roughness of irradiated coumarin SCLCPs spun-cast on silicon wafers, confirming polymer degradation. While degradation is usually undesirable in LC systems, Jackson and coworkers noticed no deterioration in the performance of their coumarin SCLCP after 2 years, once the alignment switched to perpendicular alignment to **P**.[217]

Using the same acrylate backbone, Tian and coworkers also studied the liquid crystalline properties of two series of coumarin side chain polymers and coumarin-containing block copolymers.[233,341] Figure 2-31 shows examples of each polymer series studied and optical micrographs of the smectic A phase of the polymers at 190 °C. This group found that the chemical composition of the side groups at the 3 and 4 positions of the coumarin ring (Figure 2-22(a) for

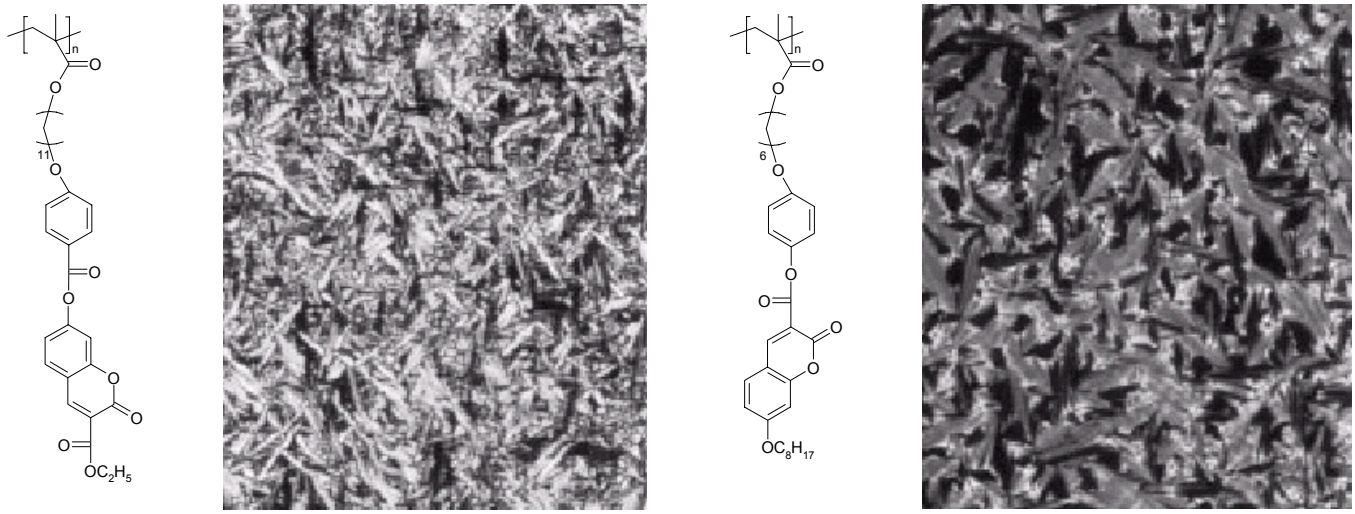

(a) (b) (c) (d)

Figure 2-31. (a) structure of a series 1 polymer, (b) optical polarizing micrograph of smectic A phase of (a), (c) structure of a series 2 polymer, (d) optical polarizing micrograph of smectic A phase of (c). Reprinted from ref. 233 with permission of John Wiley & Sons, Inc.

the numbering scheme) greatly affected the LC phase. For example, when a polymer had a substituent in the third position such as the polymer shown in Figure 2-31(a), the polymer exhibited a mesophase. When the fourth position had a substituent, the polymer had no mesophase. As for crystallinity, polymers in series 1 (Figure 2-31(a)) were amorphous, while the polymers in series 2 (Figure 2-31(c)) exhibited a crystalline state.

Tian's group also synthesized di- and tri-block copolymers of both the polymer in Figure 2-31(a) and polystyrene by atom transfer radical polymerization from a polystyrene macroinitiator.[341] GPC traces showed a distinct shift in the peak, which indicated quantitative initiation from the polystyrene macroinitiator. Irradiation of the homopolymers and copolymers led to coumarin dimerization and insolubility of the polymers. One difficulty with the study was encountered when the DSC curves were compared to the TEM micrographs of the diblock copolymers. The DSC thermograms showed only a single T_g (between 20 and 24 °C), which indicated phase mixing, and a high-temperature isotropic transition. The TEM micrographs indicated microphase separation, which should lead to two glass transition temperatures; one for the coumarin (between 10 and 20 °C) containing block and one for the polystyrene block (near 100 °C). This contradiction was not described in their report. One interesting finding was the disappearance of the isotropic transition upon photocrosslinking of the coumarin blocks.

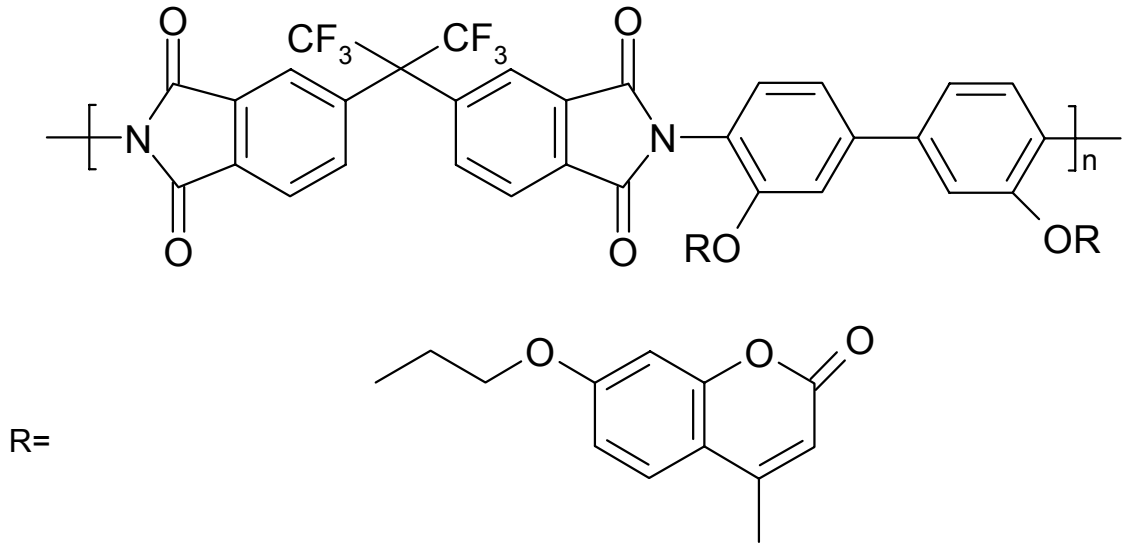

Figure 2-32. Structure of the coumarin SCLCP polymer studied by Ree and coworkers.[227]

Ree and coworkers have recently studied the alignment behavior of photosensitive polyimides with coumarin and cinnamoyl side groups.[227] The polymer, shown in Figure 2-32, has an absorption maximum at 306 nm. An exposure dose of 7.5 J/cm^2 was sufficient to complete the coumarin groups in the polymer. As with the other coumarin SCLCPs, the photosensitive groups that aligned with the electric vector of the incident polarized light dimerized sooner than those with other alignments. [216,217,225,227,244,337,340] Dimerization of the coumarin groups reoriented the polymers with the new preferred alignment at the polymer surface.[227]

2.4.2.2 Photoactive Surfaces. Coumarins, in oligomeric as well as polymeric form, have been the focus of recent research. Oligomeric coumarins have been studied for possible photomemory and photoactive surface applications.[210,342,343] Fox's group studied the photodimerization of 7-(10-mercaptodecyloxy)coumarin) monolayers on gold using grazing angle FTIR, contact angle measurements, and surface fluorescence measurements. The structure of the coumarin molecule and the FTIR data are shown in Figure 2-33.

The FTIR spectra tracked the dimerization reaction through changes in the peaks at 1745 and 1626 cm^{-1} due to the C=O stretch and the C=C ring stretch, respectively. As the dimerization reaction proceeded, the carbonyl stretch splits into two peaks due to the emergence of the new nonconjugated carbonyl. Simultaneously, the peak at 1626 cm^{-1} decreased in size and the peaks due to the C=C bond (1200, 1161, and 1129 cm^{-1}) decreased in size and shifted as the

(a)

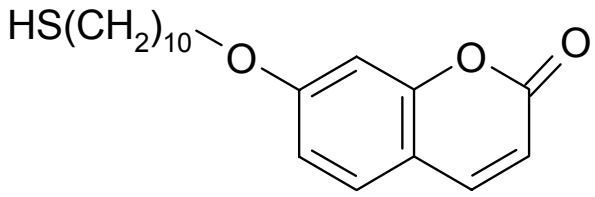

(b)

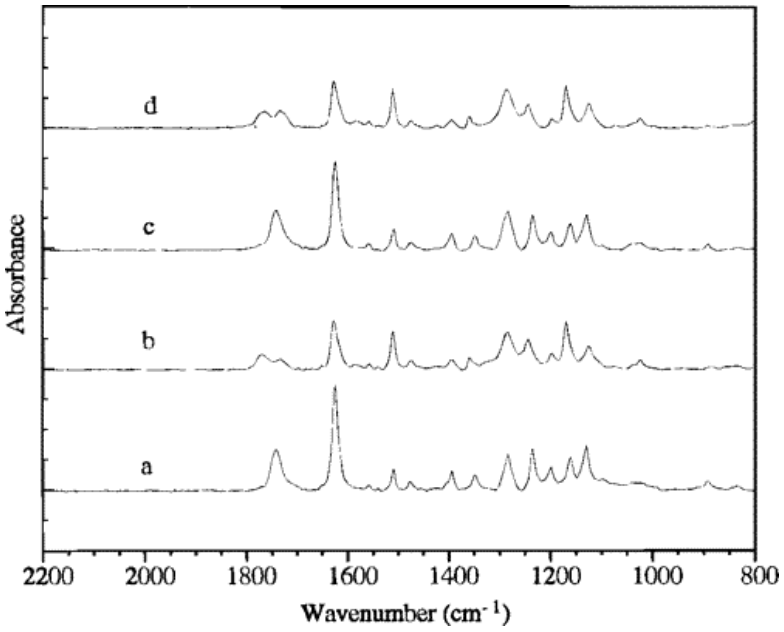

Figure 2-33. Structure of 7-(10-mercaptodecyloxy)coumarin and grazing angle FTIR spectra of a monolayer of 7-(10-mercaptodecyloxy)coumarin: (a) before dimerization, (b) after photodimerization, (c) after photocleavage and (d) after a second dimerization. Reprinted with permission from ref. [343]. Copyright 1997 American Chemical Society.

double bond was broken to form the cyclobutane ring. With photocleavage, the two C=O peaks merge and the double bond peaks increase in size and shift back to their original positions. The authors found quantitative recovery of the monomer upon photocleavage of the dimer. The water contact angle on the monomer was also reversibly changed from 58 to 63° for the monomer and dimer, respectively.[343] In a similar study, Fang examined the photodimerization of self-assembled monolayers of 7-(8-trimethoxysilyoctyloxy)coumarin on silicon and quartz. Their research also demonstrated that the coumarin dimerization induced homogeneous alignment of the liquid crystal coumarin monomers.[210]

Tian and coworkers have also studied oligomeric coumarin derivatives by attaching coumarins to cyclic tetramethyltetrasiloxanes.[342] The attachment was accomplished via the hydrosilylation of vinyl-terminated coumarin derivatives with 2,4,6,8-tetramethylcyclotetrasiloxane. Each of the cyclic coumarin containing molecules with substitution at the 3 position of the coumarin group displayed mesomorphic properties. The length of the tail group (substituted at the 3 position) influenced the crystallizability of the molecules, i.e., longer tail groups displayed no melting transition, while those with shorter tails melted. UVA irradiation of the films crosslinked the molecules, although high-temperature irradiations were not performed to determine if the liquid crystalline phases could be locked in.

2.4.2.3 *Electroluminescence Studies.* Polymeric electroluminescent materials have distinct advantages over their inorganic counterparts, including ease of film preparation and color tunability throughout the visible spectrum.[344] Polymers

garnering their electroluminescent properties from coumarin moieties have received some interest in both published and patent literature. [211,344-351] Uchida and coworkers have patented a series of acrylate-based polymers consisting of a coumarin derivative and N-vinylcarbazole used in the production of an electroluminescent device.[346] They fabricated electroluminescent devices with colors ranging from red to violet by changing the coumarin derivative and the ratio of the number of coumarin groups to the number of N-vinylcarbazole groups in the polymer.

Fomine and coworkers have studied the use of coumarin-containing polymers for electroluminescent devices and have synthesized a wide range of polymers. By employing techniques such as ring-opening metathesis polymerization, free radical polymerization, and step-growth polymerization, they synthesized polyamides, polyesters, hyperbranched, comblike and fully aromatic polymers containing coumarin groups.[344,345,347,348,350] Examples of some of the polymers synthesized are shown in Figure 2-34. All of their formulations displayed electroluminescence in the blue-green range. These polymers exhibited turn-on voltages of 3-6 V, which depended on the specific polymer structure.

2.4.2.4 Light and Energy Harvesting. The harvesting of solar energy has been a topic of interest for quite some time. Recently, coumarins have been incorporated into polymers in an attempt to harvest and transfer solar radiation energy.[102,352-355] These studies began in the early 1990s with the work of Lang and Drickamer on the energy transfer between cyclopenta[c][1]benzopyran-

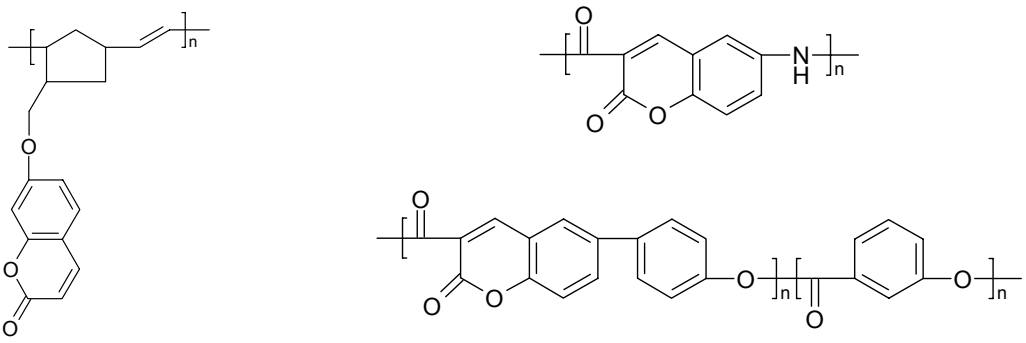

Figure 2-34. Examples of electroluminescent polymers synthesized by Fomine and coworkers.[344,345,348]

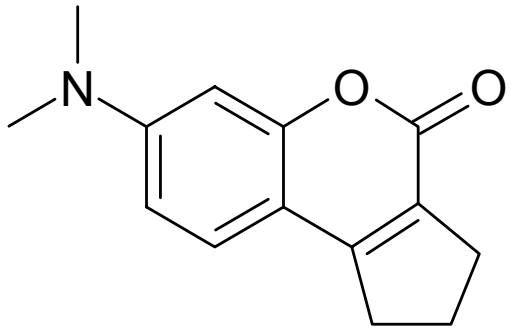

Figure 2-35. The structure of coumarin 138.

4(1H)-one, 7-(dimethylamino)-2,3-dihydro- (9CI) (coumarin 138, Figure 2-35) and rhodamine B in a poly(acrylic acid) matrix.[352] The work on energy harvesting using coumarin groups was continued by Palmans and coworkers when they attached coumarin side groups to a poly(p-phenylene ethynylene) backbone resulting in the polymer shown in Figure 2-36.[353] The existence of energy transfer in the polymer was evidenced by the absence of donor emission (i.e., the emission of the coumarin group) and a large increase in the emission of the polymer when the polymer was irradiated at the excitation wavelength of the coumarin (λ_{ex} = 320 nm). Palmans and coworkers measured energy-transfer efficiencies of approximately 80%.

Fréchet and coworkers have also studied energy transfer in coumarin-containing polymers.[101,102,354-357] Their first effort was the synthesis of coumarin-labeled poly(aryl ether) dendrimers. The dendrimers were envisioned as antennae with coumarin 2 (H-1-benzopyran-2-one, 7-(ethylamino)-4,6-dimethyl-(9CI)) groups at the periphery and a coumarin 343 (1H,5H,11H-[1]benzopyrano[6,7,8-ij]quinolizine-10-carboxylic acid, 2,3,6,7-tetrahydro-11-oxo-(9CI)) moiety as the core. The structure of the coumarins used and the fourth-generation (G-4) dendrimer are shown in Figure 2-37.[101,354]

The dendrimers were synthesized using a typical convergent strategy with the exception that the terminal and focal functionalities were reversed. Coumarin 2 (donor molecule) has an absorption in the range of 310 – 380 nm and emits between 400 and 480 nm in the range of absorption for coumarin 343 (acceptor

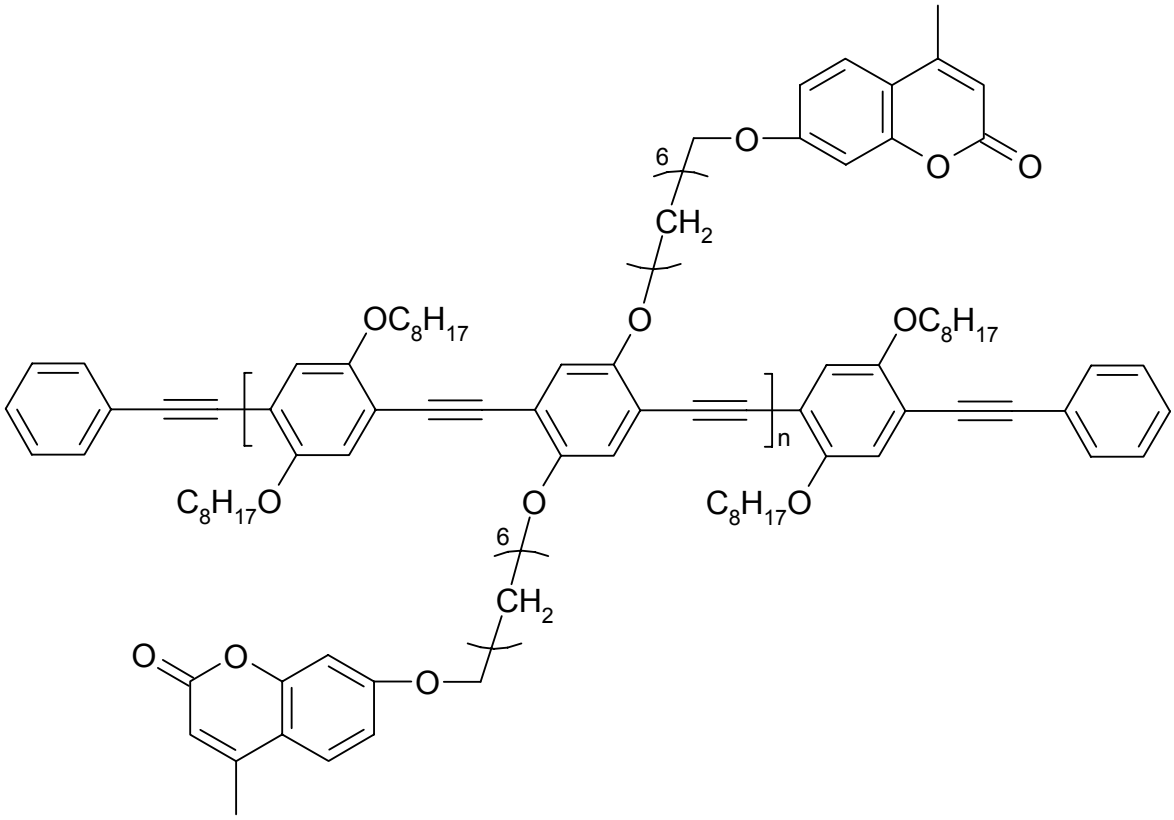

Figure 2-36. Coumarin modified poly(p-phenyleneethynylene) studied for energy harvesting and transfer.[353]

Coumarin 2

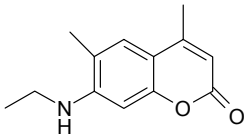

Coumarin 343

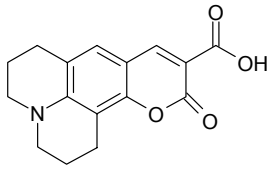

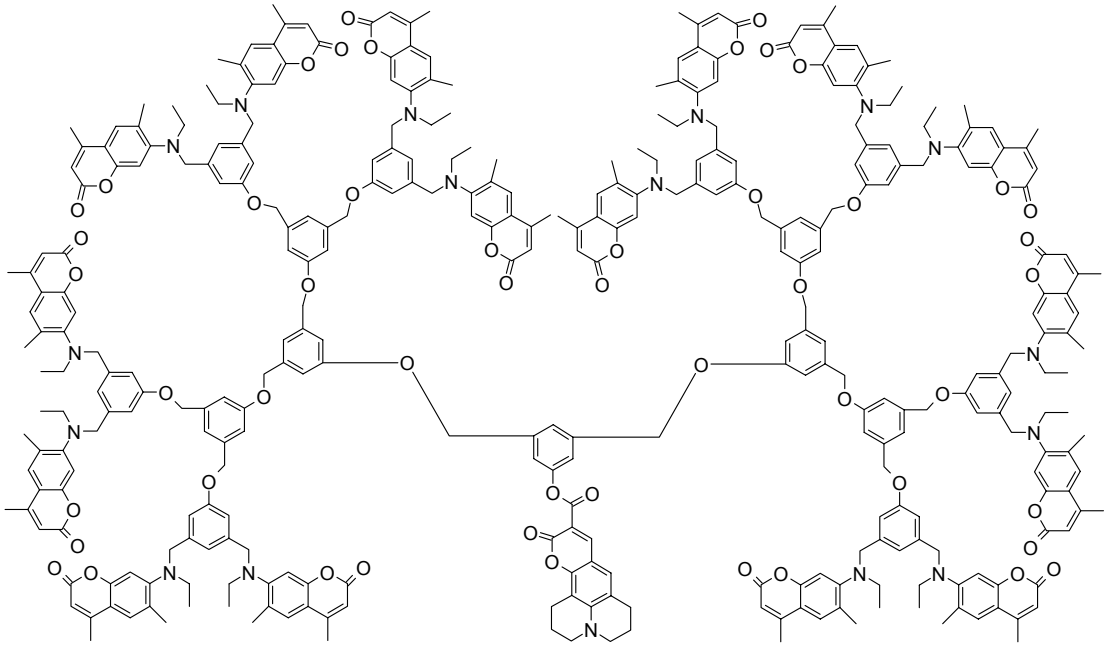

Figure 2-37. The structure of coumarin 2, coumarin 343 and the coumarin labeled G-4 poly(aryl ether dendrimer).[101,354,357]

molecule). Thus, coumarin 343 absorbs the emission from the coumarin 2 antennas and emits light with a maximum near 480 nm. As the dendrimer increases in generation, the number of coumarin 2 groups present in the dendrimer doubles, and the dendrimer is able to absorb more light. The intensity of the emission of the dendrimer's core (the coumarin 343 molecule) also nearly doubles with each increase in generation, which indicated that the energy transfer from the antenna to the core was extremely efficient.

Also notable was a significant blue-shifting of the photoluminescence spectra as the generation increased from G1 to G4. The blue-shift indicated film inhomogeneities in the lower generation polymers, which were later detected utilizing photoluminescence near-field scanning optical microscopy.[357] Utilizing steady-state and time-resolved fluorescence spectroscopy, Fréchet measured the energy-transfer efficiency of each generation of the dendrimers, which ranged from a low of 92.0 to a high of 98.9%.[101,354]

Although Fréchet's dendrimers harvested and transferred energy, they proved to be difficult to synthesize.[355] To circumvent the difficult synthetic methods, linear polymers with chemical compositions mimicking the first five generations of the dendrimers were synthesized.[102,355] Coumarin 2- and coumarin 343-functionalized monomers were synthesized by reacting the respective coumarin with vinyl benzyl chloride. Coumarin 2- and coumarin 343-functionalized polymers were synthesized by polymerizing the vinyl benzyl-functionalized coumarins with styrene. The general structure and emission spectra of the resulting polymers are shown in Figure 2-38. The coumarin-labeled polymers

had comparable energy-transfer efficiencies to the model dendrimers. Unfortunately, the coumarin-labeled polymers also had some undesirable properties not present in the dendrimers such as low fluorescent quantum yields and low solubilities in nonchlorinated and nonpolar solvents.

Fréchet and coworkers also studied the vinyl benzyl coumarin 2 and ruthenium complexes shown in Figure 2-38.[102] The metallopolymer shown in Figure 2-39(a) exhibited an energy-transfer efficiency of 70%. It also exhibited a 5-fold increase in the fluorescence of the ruthenium complex when irradiated at wavelengths that excite the coumarin groups, versus irradiation at the wavelength, which excites the ruthenium complex. Similarly, the polymer shown in Figure 2-39(b) had an energy-transfer efficiency of 95% and a 3.6-fold increase in the fluorescence of the ruthenium complex. When a second coumarin chromophore was added (coumarin 343), a terpolymer was formed, and the absorption and luminescence properties of the metallopolymers were improved compared to the single-coumarin-containing polymer. The metallopolymers are under continuing research for use in photonic and photovoltaic devices.

2.4.3 Polymer Photoreversibility.

The ultraviolet light-triggered photodimerization of cinnamates,[58,91,92,158,163-179,181-183,185,186,358] chalcones,[188,189] anthracenes,[58,180,191] acridiziniums,[58,193] stilbazolium salts,[93,94] and coumarins [58,146-148,150,170,171,194-235,359] has been well studied since it was first utilized in the photocrosslinking of poly(vinyl cinnamate)

(a)

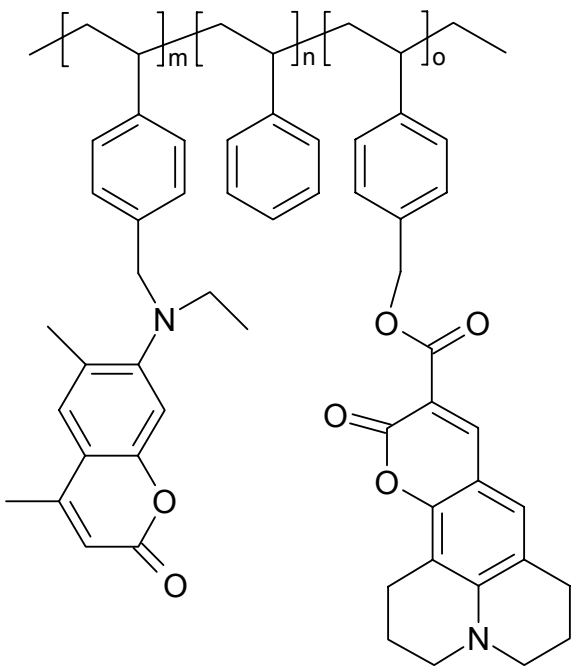

(b)

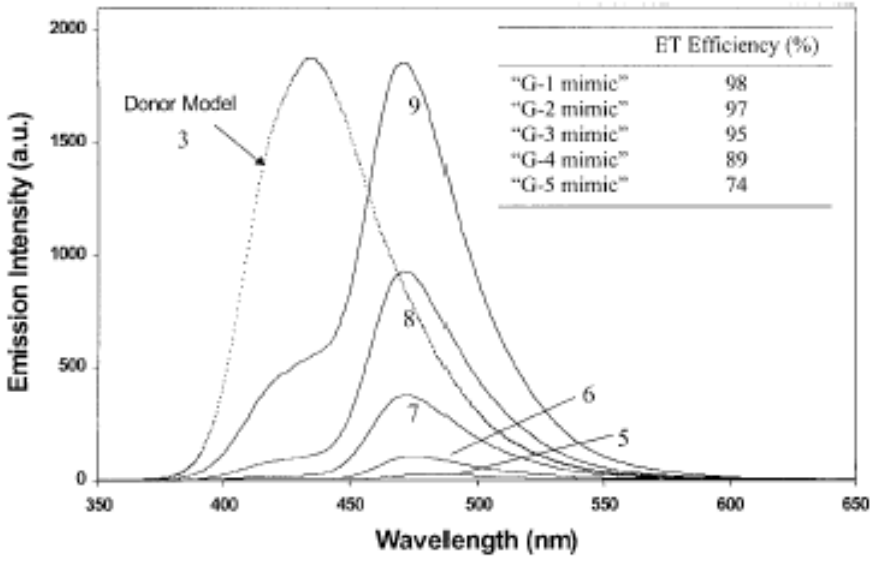

Figure 2-38. (a) Structure of the coumarin-labeled polymers and (b) emission spectra and energy-transfer efficiencies of the polymers with 3 = no acceptor moieties, 5 = G-1 mimic, 6 = G-2 mimic, 7 = G-3 mimic, 8 = G-4 mimic and, 9 = G-5 mimic. Reprinted from ref. 102 with permission of John Wiley & Sons, Inc.

(a)

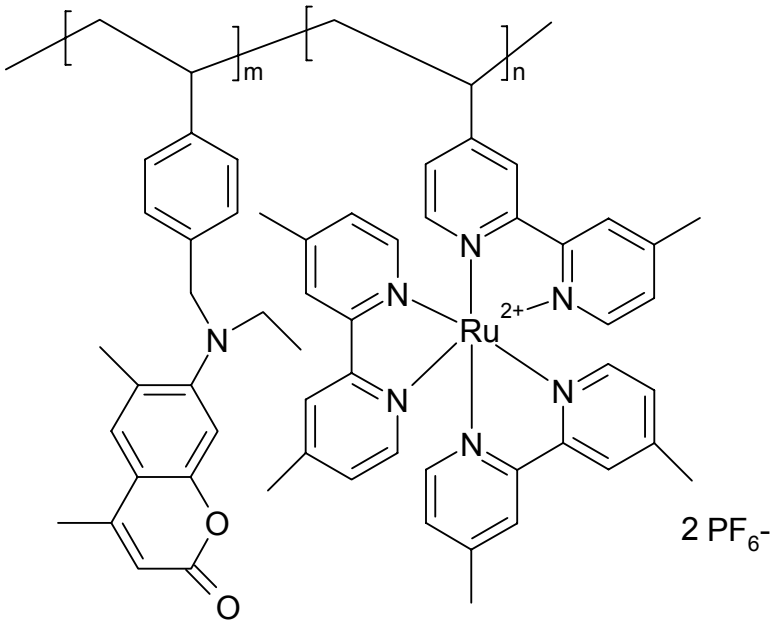

(b)

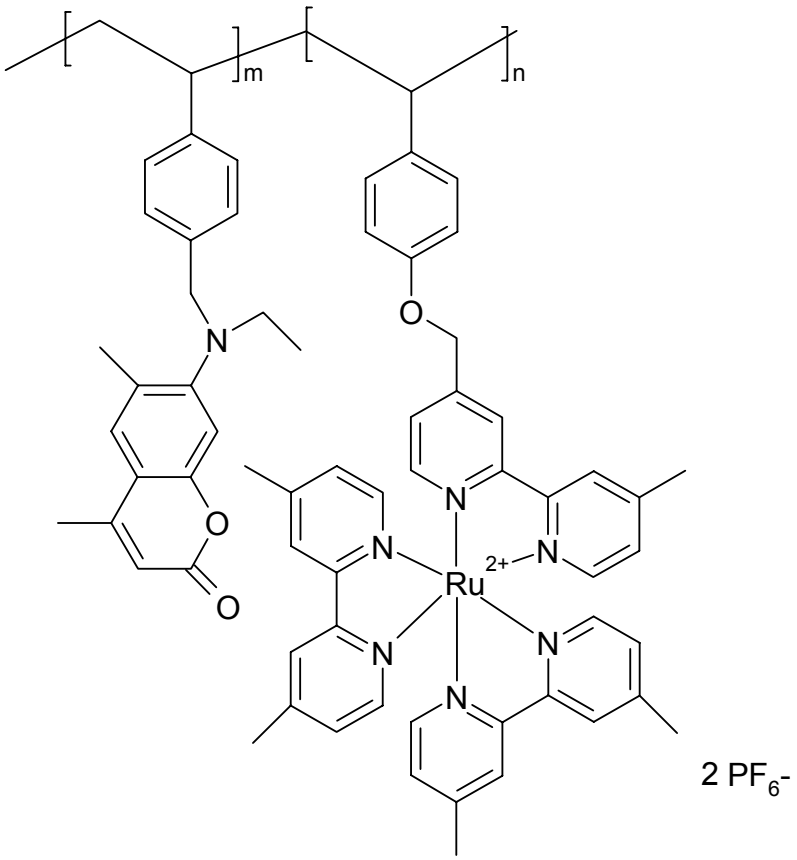

Figure 2-39. Coumarin labeled ruthenium containing metallopolymers.[355]

by Minsk and coworkers in the 1950s. With the exception of the anthracene groups that dimerize via a [4+4] cycloaddition, the photodimerization proceeds by the [2+2] cycloaddition of the ethylenic groups above 300 nm.[58,180] In addition to the cycloaddition reaction, photocleavage allows some dimers to revert to their original structure.[196-202,206,359,360] For example, cyclobutane rings that are derived from α-truxxilate, β- or δ- truxinates, and the coumarin and thymine dimers reverse upon irradiation near 250 nm.[164] When the cyclobutane rings formed by coumarin dimers are used as crosslinks or branch points in polymers, the crosslink is breakable, thus reducing the crosslink density of the light-modified polymer.

Reversible Photocrosslinking and Photocleavage. While coumarin groups were first incorporated into polymers in the mid 1960s, they were not utilized for their reversibility until the late 1980s.[208,359,360] Saegusa and coworkers studied the gelation and reversible gelation of polyoxazolines. Saegusa synthesized polyoxazolines via the ring-opening polymerization of 2-methyl-2-oxazoline, and then modified the polymer by hydrolyzing the pendent methyl group and reacting it with 7-coumaryloxy acetic acid (shown in Scheme 2-2). The resulting polymer had degrees of coumarin substitution between 1.2% and 30.4%. The photodimerization of the polymer was performed with a 450 W high-pressure Hg lamp for up to 3 h, while the photocleavage reaction was accomplished with 253 nm irradiation for 2 h (reaction shown schematically in Figure 2-40). After 30 min of irradiation, an insoluble gel with a swelling ratio of 14:1 (w/w H2O/gel) formed.

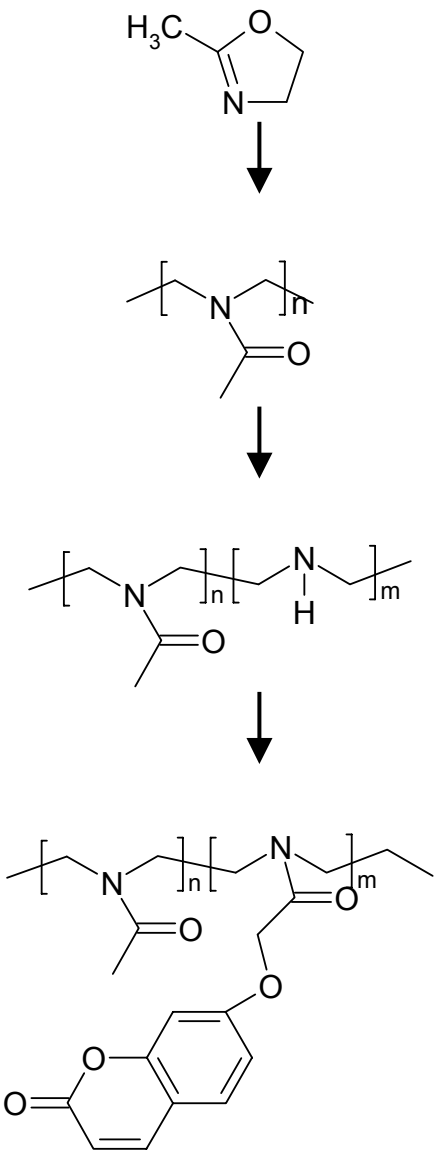

Scheme 2-2. Synthesis of Saegusa's coumarin modified polyoxazoline.[359]

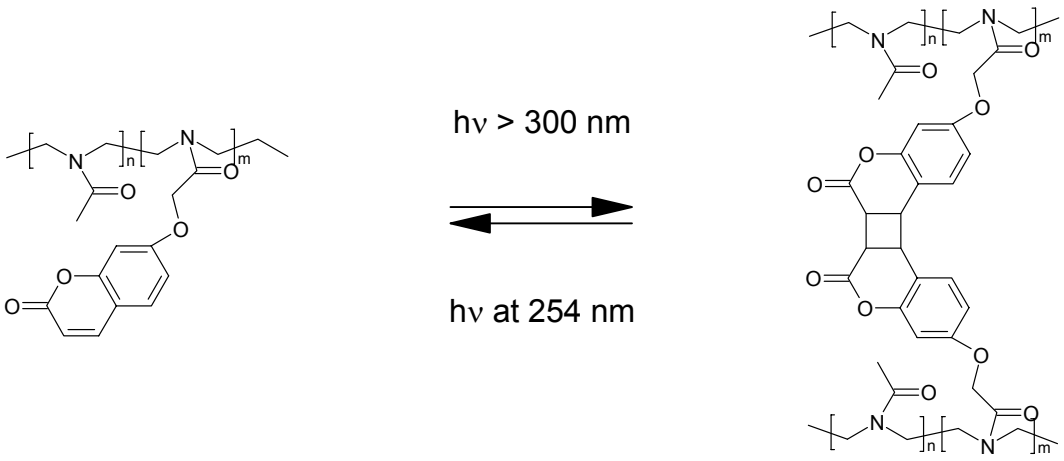

Figure 2-40. Reversible photocrosslinking of the coumarin modified polyoxazoline.[359]

Further irradiation increased both the gel yield (to 69%) and the crosslink density. UV–vis spectroscopy indicated that 95% of the coumarin groups had dimerized with 350 min of irradiation.

UV-Vis spectroscopy and swelling experiments verified the photocleavage of the coumarin polymer showing that 55-60% of the dimer reverted to the starting material. Crosslinked polymer films irradiated for long times were not soluble after irradiation at 253 nm. Films that were photocrosslinked for shorter times and rendered insoluble in methanol, however, dissolved after irradiation at 253 nm (Figure 2-40). This study was the first to demonstrate the photoreversibility of crosslinks using coumarin groups.

Little work utilizing the reversible dimerization of coumarin in polymers was published until Chen and coworkers studied the reversible photodimerization of coumarin derivatives in poly(vinyl acetate) (PVAc).[197] Previous studies from Chen's group dealing with optically active polymers containing coumarin moieties will be described in Section 2.4.5.2. In their photoreversible polymer studies, Chen attached alkyl chains to 7-hydroxycoumarin and 7-hydroxy-4-methylcoumarin resulting in the structures shown in Figure 2-41. The photodimerization (at 300 and 350 nm) and photoscission reactions of the coumarin derivatives were followed using UV-Vis spectroscopy. They demonstrated that their coumarin derivatives underwent dimerization at 300 and 350 nm, with the dimerization occurring more rapidly for the derivatives with the longer alkyl chains. Chen's work also found that the coumarin derivatives with

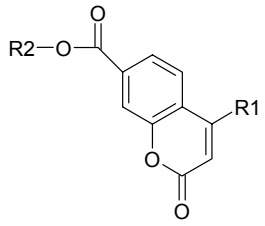

R1	R2
CH_3	CH_3-CH_2
CH_3	CH_3-$(CH_2)_{13}$-CH_2-
H	CH_3-CH_2
H	CH_3-$(CH_2)_{13}CH_2$-

Figure 2-41. Structure of the coumarin derivatives synthesized by Chen and coworkers for dispersion in PVAc.[197]

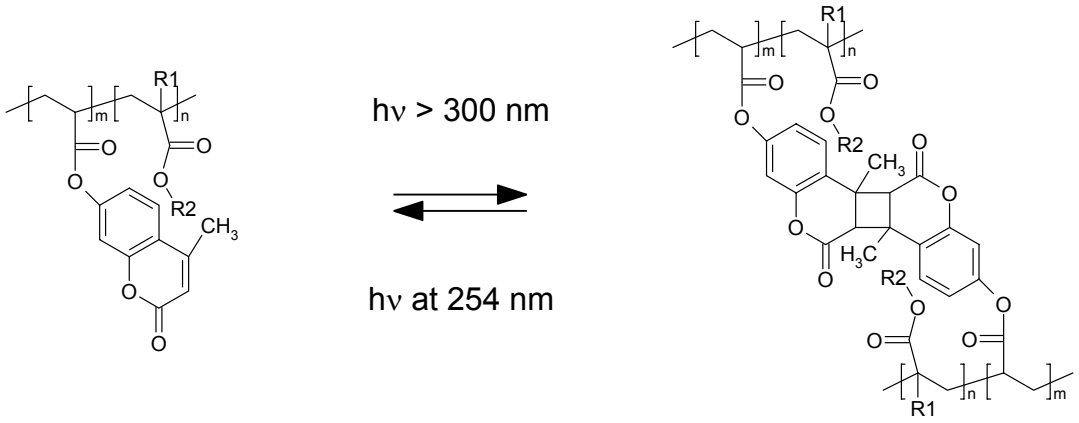

Figure 2-42. (a) general structure and (b) dimerized (crosslinked) structure of coumarin functionalized acrylic polymers. R1 and R2 are various alkyl groups.[198,199]

the methyl group at the 4 position dimerized at a rate 200 times quicker at 350 nm and two times faster at 300 nm than those without the methyl group.

Building on their work with coumarin derivatives in PVAc, Chen and coworkers synthesized a number of polymers containing coumarin derivatives. They studied the photocrosslinking and photoscission of polyacrylates and polyamides as well as the chain extension of polyethers, polyurethanes, and polyesters.[196,198-202,206] Chen copolymerized various acrylates with 7-acryloyloxy-4-methylcoumarin, resulting in the polymers shown in Figure 2-42 and the corresponding to the crosslinked polymer structure. Photocrosslinking was performed in chloroform with irradiation at 300 nm, and the photoscission of the acrylate was conducted at 254 nm. The photoreactions were monitored using UV-Vis spectroscopy (shown in Figure 2-43). Figure 2-43(a) shows the reduction in the absorbance of the acrylate polymer at 310 nm on crosslinking. As the cyclobutane crosslinks form, the coumarin double bond, which absorbs at 310 nm, disappears. The change in absorbance due to the photocrosslinking and photoscission reactions is shown in Figure 2-43(b). The increase in the absorbance at 310 nm is indicative of scission of the cyclobutane ring and reversion to the starting material. The amount of photoscission at 254 nm was found to be the result of a dynamic equilibrium, with both crosslinking and scission occurring at 254 nm. These researchers performed a similar study with copolymers synthesized from n-(1-phenylethyl)acrylamide and 7-acryloyloxy-4-methylcoumarin.[206] Similar to the acrylate study, polymers that were reversibly crosslinkable in solution were also obtained.

(a)

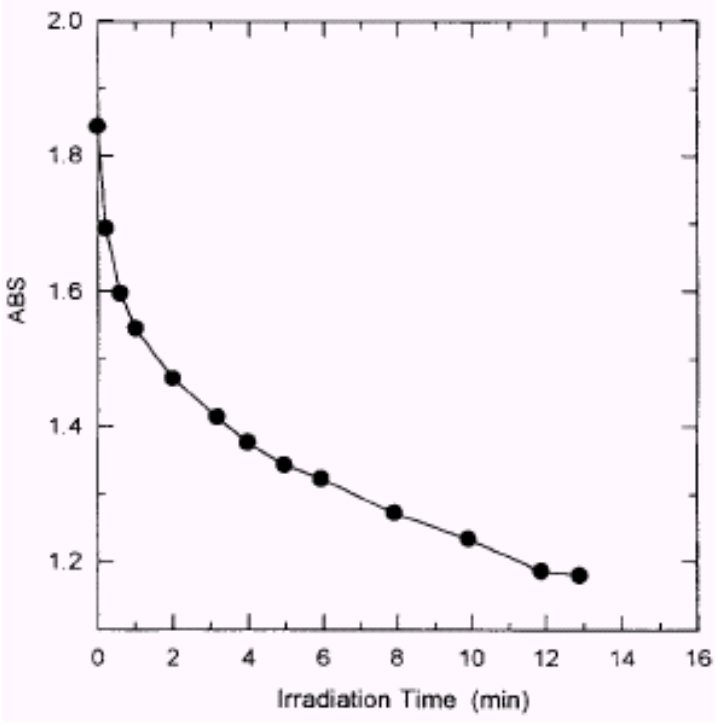

(b)

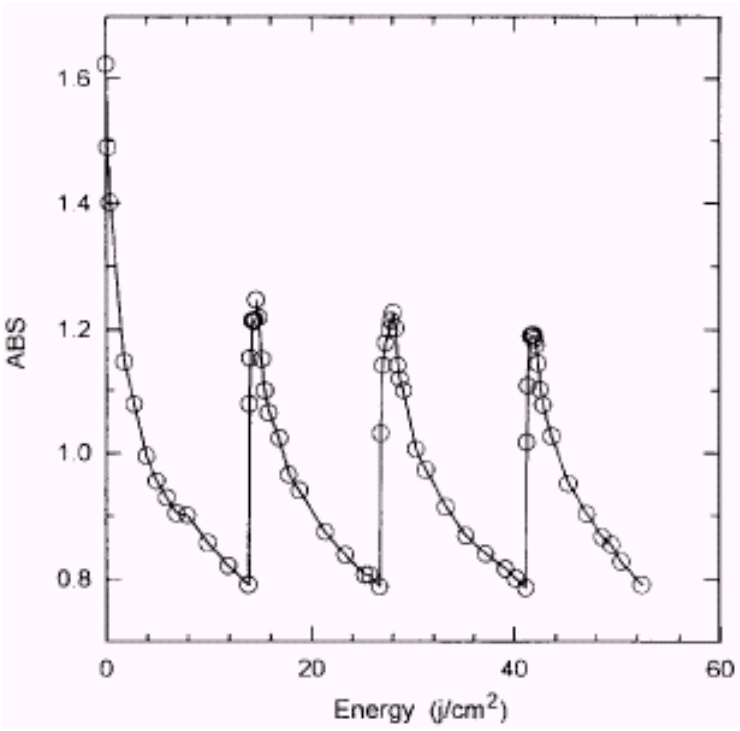

Figure 2-43. (a) Absorbance of polymer shown in Figure 2-42(a) at 310 nm as a function of irradiation time and (b) change in absorbance due to irradiation at 300 nm (decrease in absorbance) and 254 nm (increase in absorbance). Reprinted from ref. 199 with permission from Elsevier.

2.4.3.1 *Reversible Photoextension and Photocleavage.* In our labs, we have studied the reversible chain extension of coumarin functionalized poly(ethylene glycol) methyl ether and telechelic PEG oligomers.[361] PEG monols were quantitatively functionalized with 7-hydroxycoumarin acid chlorides (Scheme 2-3) then solvent cast from chloroform onto glass microscope slides. UVA irradiation of the films dimerized and chain-extended the PEG molecules as observed with UV-Vis spectroscopy (Figure 2-44(a)). Subsequent irradiation at 254 nm cleaved and reverted the dimers to their initial state (Figure 2-44(b)).

Chen and coworkers also studied the reversible chain extension of a series of polymers in solution, including polyesters (Figure 2-45(a)), polyethers (Figure 2-45(b)) and polyurethanes (Figure 2-45(c)) endcapped with coumarin groups.[196,200-202] The reversible photoextension and photocleavage reactions of the polyurethanes and polyethers were monitored using UV-Vis spectroscopy. The results of the absorbance measurements as a function of irradiation time and wavelength resemble those shown in Figure 2-43(a) and Figure 2-43(b), which indicated the dimerization and cleavage of the coumarin group. They also studied the effect of the presence of a methyl group at the coumarin 4 position. While the major photoproduct of the chain extended polymers without the methyl group was the head-to-head form of the dimer, the presence of the methyl groups produced the head-to-tail form of the dimer (see Section 2.4.1.4 for description of head-to-head versus head-to-tail).

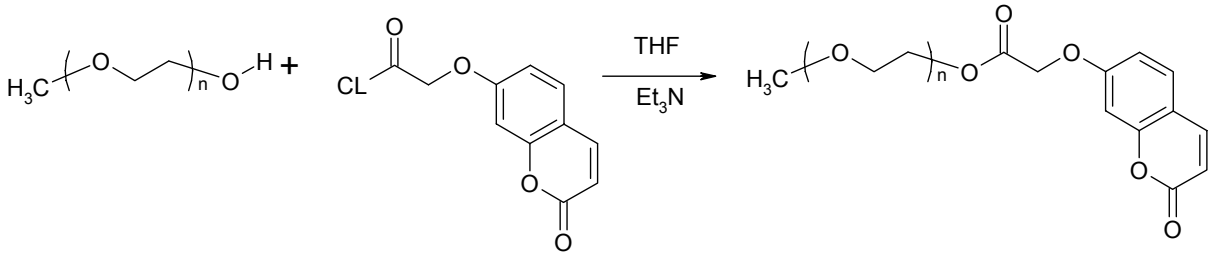

Scheme 2-3. PEG methyl ether modification reaction scheme.

(a)

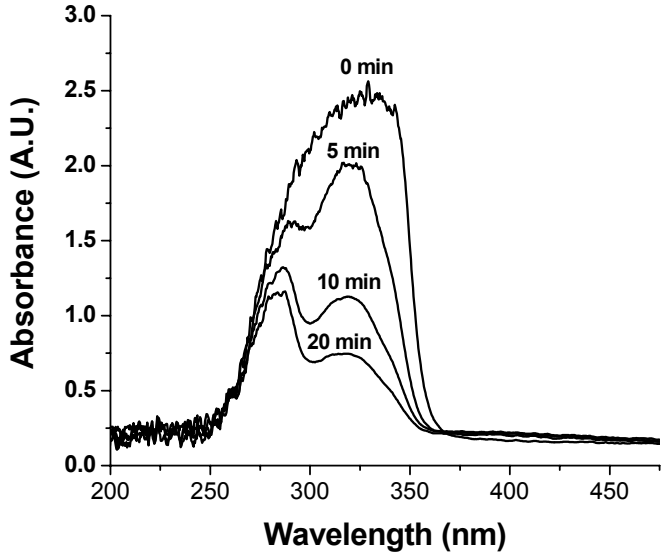

(b)

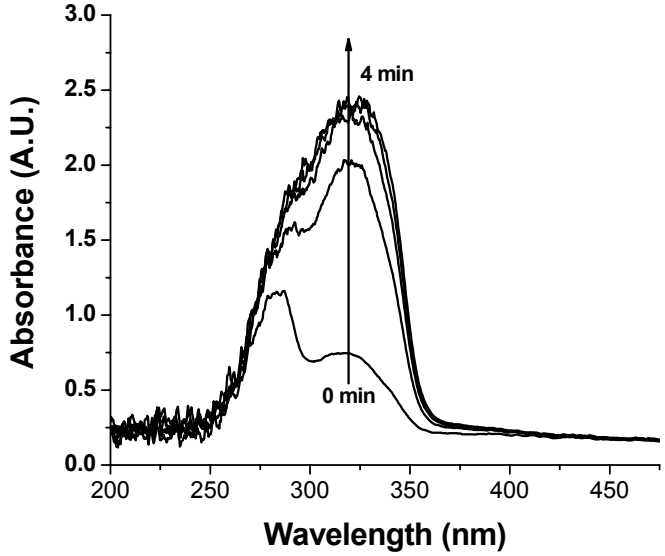

Figure 2-44. (a) Decrease in UV absorbance of coumarin-modified PEG with UVA irradiation and (b) the increase in UV absorbance of chain-extended, coumarin-modified PEG with 254 nm irradiation.

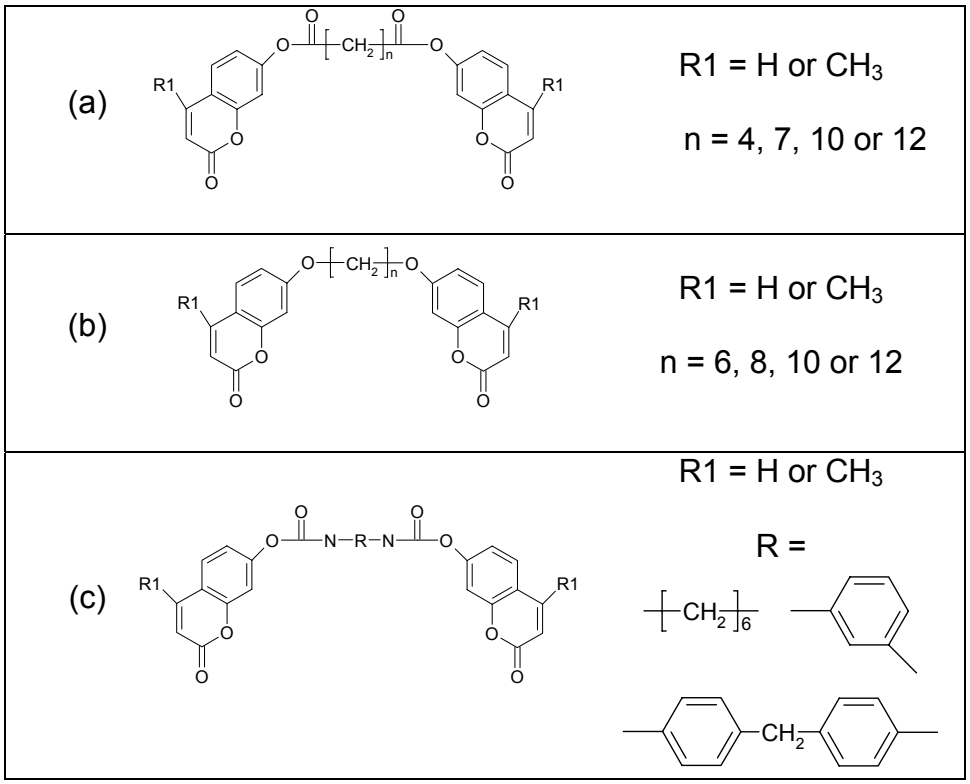

Figure 2-45. Coumarin endcapped (a) polyesters, (b) polyethers and (c) polyurethanes studied by Chen and coworkers.[196,200-202]

Chen and coworkers also discovered differences in the photocleavage reaction between the methyl-substituted coumarin and the non-methyl substituted coumarin; the methyl-substituted polymer was more reversible than the other polymer. In both studies, the photodimerization reaction proceeded more rapidly when irradiated at 300 nm versus 350 nm, due to a better match of the coumarin absorbance using the 300 nm light. Photocleavage at 254 nm proceeded more rapidly than the photodimerization at both 350 and 300 nm. In addition to the effect of wavelength on photodimerization rate, the addition of benzophenone (which is a triplet photosensitizer, see section 2.4.1.4) also increased the dimerization rate without changing the photocleavage rate.[196,201,202]

Chen's utilized fluorescence spectroscopy, solution viscosity and absorbance measurements to characterize the photoreactions of coumarin endcapped polyesters (Figure 2-45(a)).[200] The results indicated similar trends to those established in their studies on polyethers and polyurethanes with regard to 4-methyl substitution, polarity of the solvent and the addition of benzophenone. Fluorescence spectroscopy results of the unsubstituted polyester dissolved in DMSO after 2 hours of irradiation at 350 nm revealed a second broad peak centered at 510 nm. This peak was indicative of the emission of the singlet excimer. The second peak was not present when either the polyester was dissolved in dichloromethane or when the 4-methyl-substituted polyester was studied. The lack of the second emission band in dichloromethane was due to the heavy-atom effect described in Section 2.4.1.4.

Chen and coworkers concluded that the polymers (when dissolved in DMSO) undergo the same singlet reaction scheme as monomeric coumarin (shown in Figure 2-25). In dichloromethane, alternatively, dimerization proceeded through the triplet state (also shown in Figure 2-25). The reversibility of the photodimerization was observed with absorbance and viscosity measurements shown in Figure 2-46. The measured absorbance increased at 312 nm that was due to the formation of the double bonds (Figure 2-46(a)). The intrinsic viscosity decreased from 0.42 to 0.008 dL/g with 4 hours of irradiation, which is also indicative of a decrease in molecular weight (Figure 2-46(b)).

2.4.4 Coumarins in Biomaterials.

2.4.4.1 Biomaterials. Photoreactive biopolymers have recently received increased attention in biological materials and processes. [226,234] Since the early 1980s, Yamamoto and coworkers have studied photoresponsive peptides and polypeptides, initially focusing on the optical activities of phenylazobenzyl modified poly(L-lysine).[226,234,362-372] Recent work has shifted to the photocrosslinking of polypeptides containing coumarins for the preparation of biodegradable crosslinked materials. The two polypeptides studied were based on L-ornithine (Orn, $C_5H_{12}N_2O_2$) and L-lysine (lys, $C_6H_{14}N_2O_2$) and coumarinated versions of the peptides as shown in Figure 2-47. Both polymers were synthesized containing 0 - 100 mol% of the coumarinated peptide. Both studies found that the rate of biodegradation of both polymers by enzymes (trypsin or protease type XXIII) or by soil fungi was controlled by the ratio of coumarinated

(a)

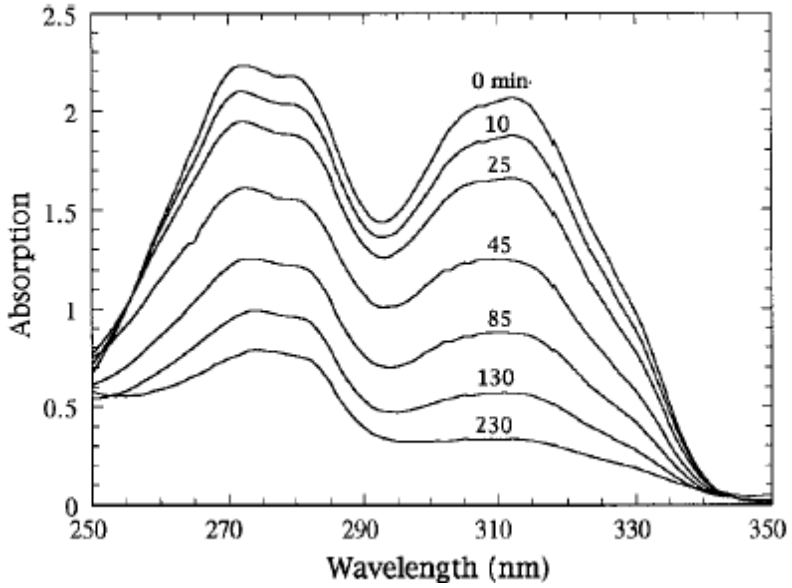

(b)

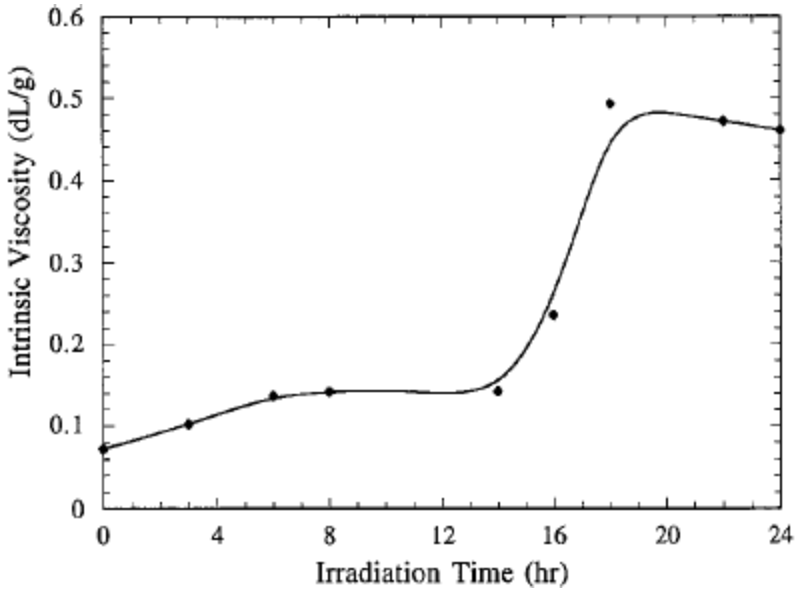

Figure 2-46. The change in (a) absorbance and (b) intrinsic viscosity of the polymer shown in Figure 5-6(a) (n = 10) as a function of irradiation time. Reprinted from ref. 200 with permission from John Wiley & Sons, Inc.

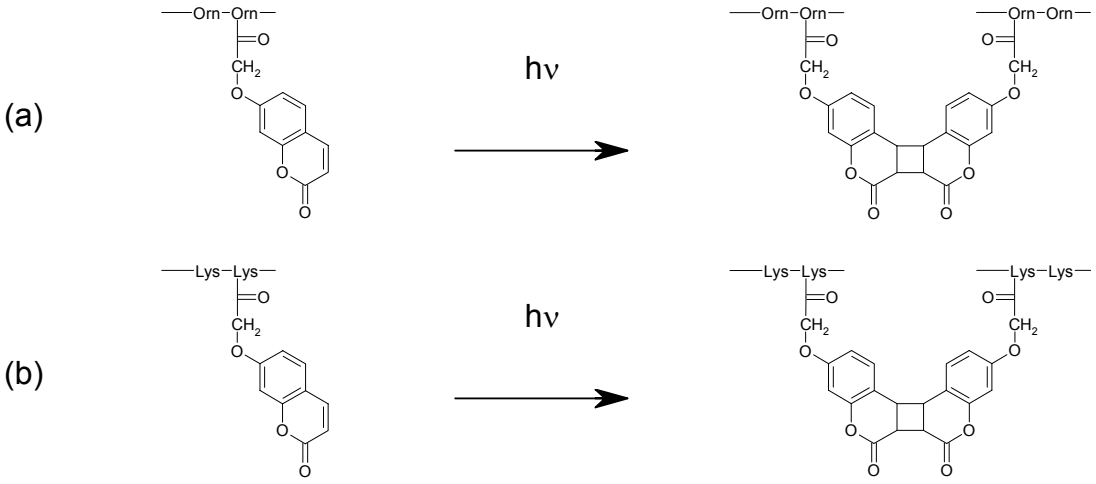

Figure 2-47. General structure and photocrosslinked structure of (a) ornithine and (b) lysine polymers. [226,234]

to native protein and by the crosslink density of the polypeptides.[226,234]

Matsuda and coworkers synthesized 4-arm stars based on random copolymers of ε-caprolactone (CL) and trimethylene carbonate (TMC), and subsequently endcapped the arms at the hydroxyl terminus with coumarin groups (poly(CL/TMC)).[146-148,150,373] The chemical structure of the stars is shown in Figure 2-48. The goal of these studies was to design liquid photocurable precursors that were amenable to photocrosslinking into desired geometries for the microfabrication of medical devices and drug encapsulation. The authors utilized stereolithography to photocrosslink the stars, build three-dimensional structures, and study the degradation of the crosslinked stars both *in vitro* and *in vivo* (subcutaneously). Scanning electron photomicrographs of the three-dimensional photocrosslinked (60 min at 10 mW/cm^2) constructs are shown in Figure 2-49. The labels on the images refer to the chemical composition of the construct. Sample “e” was prepared from b-PEG with a ratio of 0.49 CL : 0.51 TMC. Samples “b” and “d” were prepared from the pentaerithritol with ratios of 0.49 CL : 0.51 TMC and 0.00 CL : 1.00 TMC, respectively. As implantation time increased, the disappearance of the materials due to surface erosion was evident (with the sample “b” degrading at the slowest rate). They were able to manufacture tailor-made and precision-shaped templates, *in vitro* degradation tests of the films were good indicators for the *in vivo* degradation, and surface erosion proceeded without causing any significant tissue damage.[146]

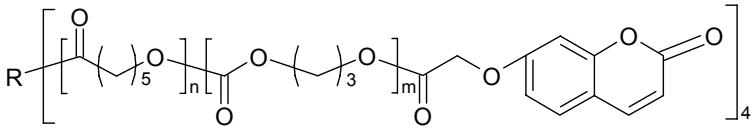

R =

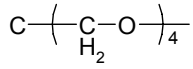

or

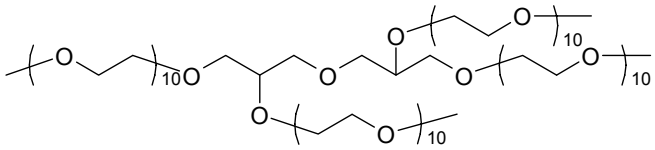

pentaerithritol b-PEG

Figure 2-48. Structure of poly(CL/TMC).[146,148,150]

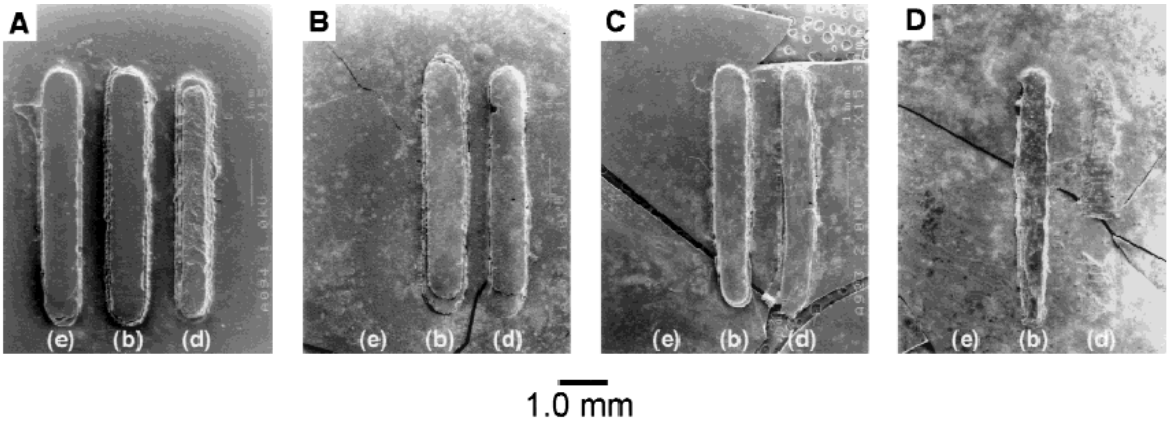

Figure 2-49. Scanning electron photomicrographs of films (A) before implantation, (B) after 1 month of implantation, (C) after 3 months of implantation, (D) after 5 months of implantation. Reprinted from ref. 146 with permission of John Wiley & Sons, Inc.

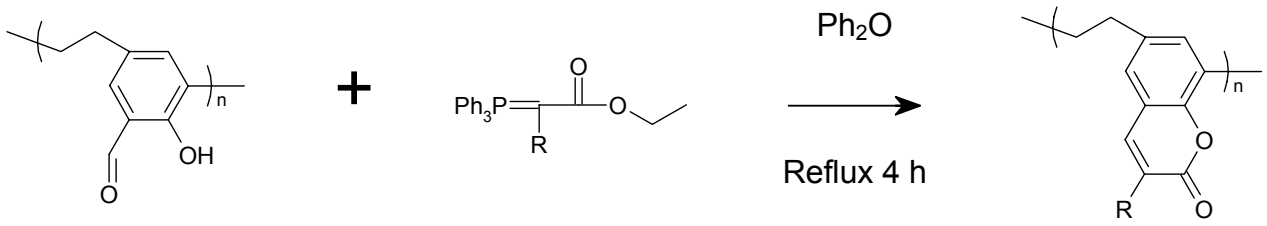

Scheme 2-4. Synthesis of poly(3-substituted coumarin ethylene) under Witting reaction conditions.[194]

The biological activity of poly(coumarin ethylene)s has been recently studied by Patel and coworkers. The authors synthesized poly(3-substituted coumarin ethylene) by reacting salicylaldehyde-1,2-dichloroethane resin (M_n = 1530 g/mol) with various carbethoxytriphenyl alkylidine phosphoranes under Wittig, Knoevenagel, and Perkin reaction conditions, as shown in Scheme 2-4.[194] They also reacted a polymer synthesized from salicylaldehyde and 1,2-dichloroethane with carbethoxytriphenyl alkylidine phosphoranes under Perkin and Knoevenagel reaction conditions with N-acetyl glycine and ethyl acetoacetate, respectively. The polymers were tested for their toxicity using fungal growth measurements. All of the polymers exhibited less than 50% inhibition on the growth of *Aspergillus Niger* and insignificant inhibition on the growth of *Antrodiella* leading to the conclusion that the polymers display no considerable toxic effect on fungal growth.

2.4.5 Coumarins in Other Studies.

2.4.5.1 Fluorescent Tags and Fluoroprobes. As previously mentioned in section 2.4.1.3, coumarins exhibit fluorescence, and this feature was exploited to monitor the kinetics of activation/deactivation in the living free-radical polymerization of a TEMPO-capped polystyrene.[191,374] The nitroxide switch, shown in Figure 2-50, fluoresces when it traps macroradicals. When the coumarin-modified nitroxide is added in excess to a TEMPO mediated reaction, the trapping of the macroradical by the modified nitroxide is favored over trapping by TEMPO. The propensity of the modified nitroxide to trap the radical allowed the authors to determine the

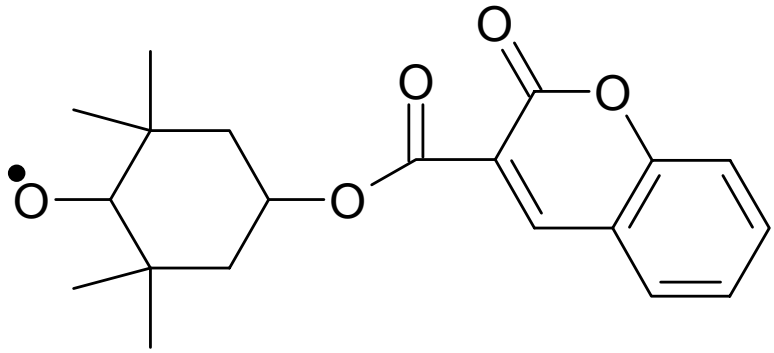

Figure 2-50. Coumarin modified nitroxide switch.[374]

rates of radical formation by measuring fluorescence, and, in turn, to determine bond dissociation energy (30.2 kcal/mol) for the C-O bond cleavage in the polystyrene-TEMPO system.

Coumarin fluoroprobes have also been studied for use in fluorescent ligand displacement assays for herbicide detection, in domain forming polymers, and as an aid in measuring diffusion.[375-377] By binding 7-carboxymethoxy-4-methylcoumarin to a molecularly imprinted crosslinked polymer of 4-vinylpyridine and ethylene glycol dimethacrylate, researchers have manufactured a competitive assay. As the herbicide enters the polymer and the imprinted regions, the coumarin probe is displaced and the fluorescence of the imprinted polymer decreases. The sensitivity of the system was determined to be approximately 100 nM.[376,378] A review of the utility of imprinted polymers for immunoassays is provided by Bruggemann *et al.*[379]

Similarly, coupling coumarin 343 to poly(organosiloxane) microgels (radius ≈ 10 nm), the particles can be used as tracers in diffusion studies using fluorescence correlation spectroscopy.[377] Schmidt and coworkers attached the coumarin to the core of the particle, which prevented it from interfering with the diffusion behavior of the particle under investigation. Although there have been further studies on the formation of poly(organosiloxane) microgels for use as MSO cocatalysts, no further work has been published on the coumarin-derivatized microgels.[379-383]

The fluorescent properties of the 7-aminocoumarins (coumarin 7, coumarin 30 and coumarin 6) have also been utilized as probes to study domain-forming

polymers and to study polysaccharides.[274,375,384] As a result of solubilizing the dyes in the polyelectrolyte poly(methacrylic acid), researchers correlated changes in the fluorescence wavelength, quantum yields, lifetimes, and polarization of the coumarins in water to changes in the identity of the bound dye due to pH and the conformational details of the macromolecule. These changes led to the production of a monitoring system for macromolecular properties in solution by fluorescence measurements. Similarly, initial research by Carré and coworkers indicated that coumarin-functionalized dextrans were suitable for use as fluoroprobes to characterize the cell-carbohydrate interactions.[384]

2.4.5.2 Chiral Stationary Phases for HPLC. Because many drug and pharmaceutical compounds show different activities between their optical isomers, optical resolution of enantiomers has become an important research topic.[205] To design a chiral stationary phase packing material for HPLC columns, Hasegawa and coworkers have synthesized optically active polymers containing coumarin dimer components.[203-205,213,229-231,235] The reaction scheme used for the synthesis of the optically active polymers is based on ring-opening step-growth polymerization and is shown in Scheme 2-5.

From this scheme, the authors synthesized a number of chiral stationary phases by varying the methylene spacer (m = 2-10) and tested the effectiveness on over 20 different racemates with varying degrees of success. The polymer in Scheme 2-5 displayed an even-odd discrimination: polyamides with an even methylene number (m is even) showed chiral recognition ability, whereas those

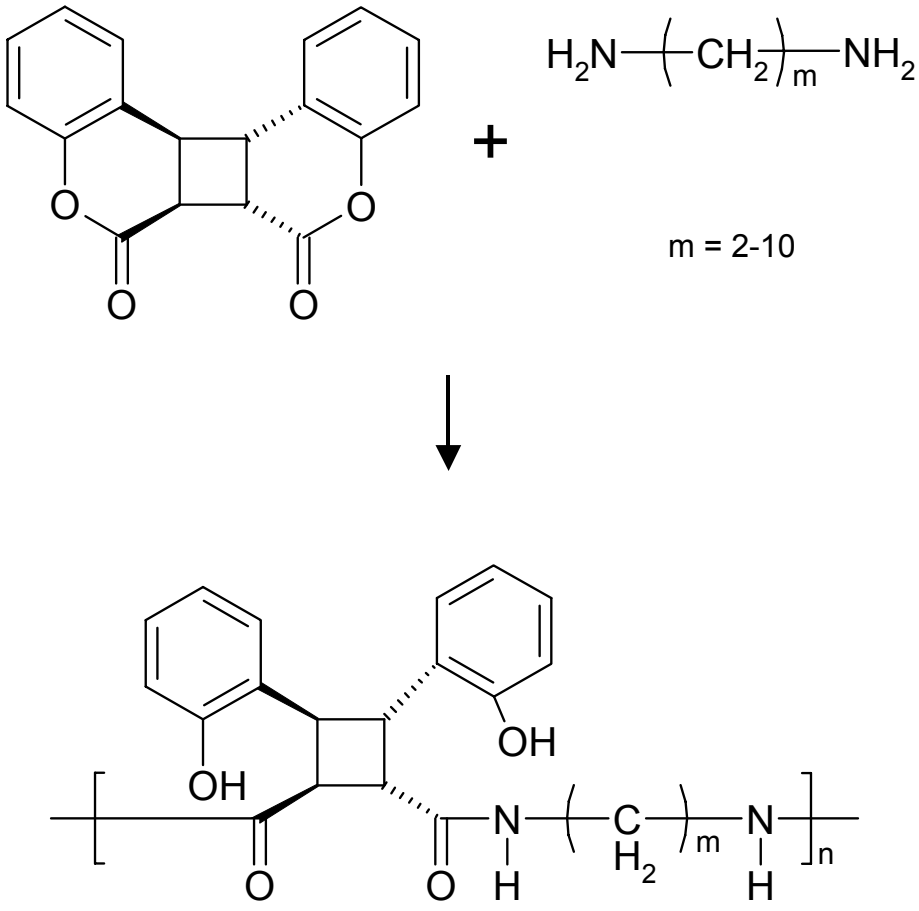

Scheme 2-5. General reaction scheme used to synthesize optically active polymers [230].

with an odd methylene number showed no chiral recognition.[228,230] Chen, who was Hasegawa's coworker, continued the work on optically active polymers with the synthesis of optically active polyurethanes by a polyaddition reaction of the ring-opened dicoumarin and 4,4'-diphenylmethane isocyanate.[203,205] The polyurethanes displayed satisfactory resolution ability to some of the aromatic racemates tested.

2.4.5.3 Polymerizations. Coumarin derivatives have recently been utilized as initiators in free radical and two-photon polymerizations.[59,385-388] Mixtures of various coumarin derivatives were used as sensitizers in photoinitiating systems for acrylic monomers.[385] The coumarins were chosen due partially to their absorbance in the UV and visible regions, as shown in Figure 2-51(a), which allows for the initiation of polymerization using visible light. Figure 2-51(b) illustrates that the presence of coumarin derivatives enabled an increase in conversion and polymerization rate for photopolymerization initiated at 405 nm.

Singh and coworkers investigated the use of 4-hydroxycoumarin in the enzyme-mediated free radical polymerization of styrene with the aim of finding a more environmentally friendly method to produce polystyrene.[387] The reaction mixture included styrene, horseradish peroxidase, hydrogen peroxide, and the initiator dissolved in a 7:3 mixture of water and THF. Of the initiators used, 4-hydroxycoumarin generated polystyrene at a 14.5% yield with a molecular weight of 57 200 g/mole and a polydispersity of 1.64, the lowest polydispersity of the initiators studied.

(a)

(b)

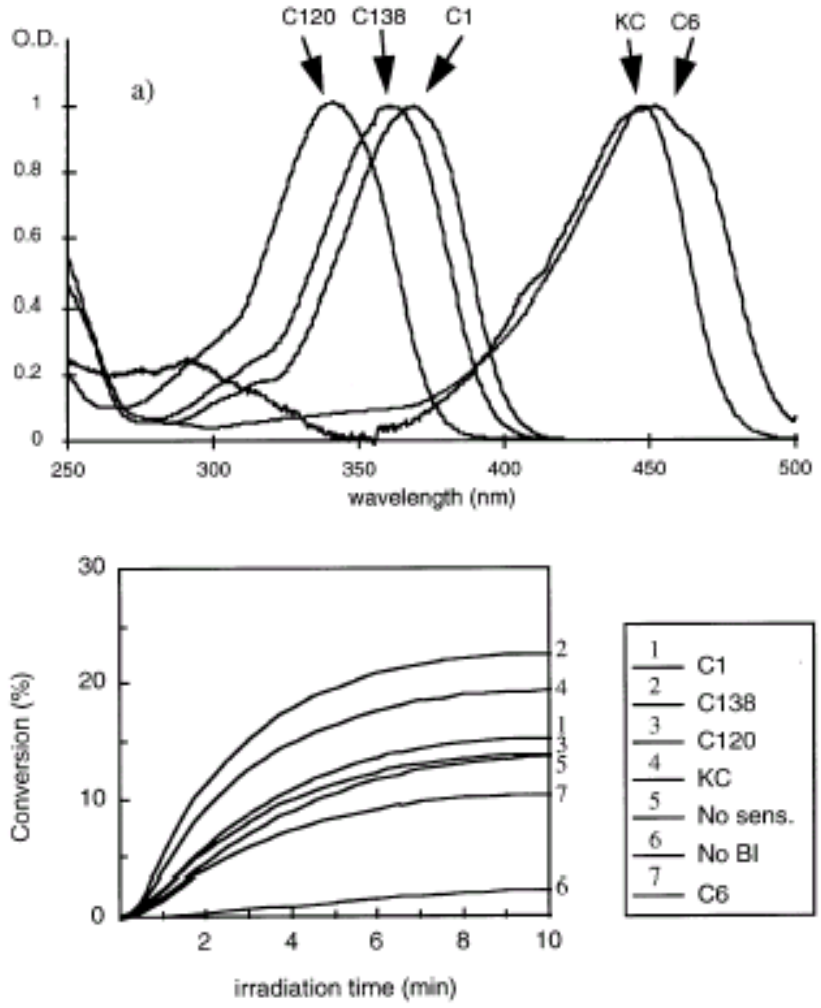

Figure 2-51. (a) Absorbance of the coumarin derivatives used as photosensitizers in the photopolymerization of styrene and (b) conversion as a function of irradiation time at 405 nm. No sens. = no sensitizer, No BI = no chlorohexaaryl-bisimidazole radical initiator. Reprinted from ref. [385] with permission from Elsevier.

Two-photon polymerization affords the ability to achieve higher spatial resolution than conventional photoinitiated polymerizations.[388] Qihuang copolymerized 2-hydroxyethyl acrylate and dipentaerythrital using a three-part initiating system consisting of N-phenylglycine, titanocene, and 7-diethylamino-3-(2'-benzimidazyl) coumarin. It was proposed that the coumarin derivative absorbed light from an 800 nm laser and excited the coumarin derivative to the triplet state. The excited coumarin then transferred an electron to the N-phenylglycine, which initiated the copolymerization. Using this method, Qihuang's group was able to cure lines as narrow as 1.8 μm.

Walshe et al. utilized 7-hydoxycoumarin during the copolymerization of methacrylic acid and ethylene glycol dimethacrylate to form a molecularly imprinted polymer for solid-phase extraction.[389] Once the crosslinked polymer was isolated and pulverized, the 7-hydoxycoumarin was extracted, yielding the molecularly imprinted polymer. A column prepared with the polymer was utilized to selectively retain 7-hydoxycoumarin from various urine samples with 90% recovery.

CHAPTER 3 DESCRIPTION AND DESIGN OF UV PHOTOREACTOR SYSTEMS

3.1 SUMMARY

Polymer photoreactions have recently garnered significant attention due to the environmentally benign nature of the process and the ability these reactions afford in manipulating both the molecular and mechanical properties of many polymer systems. This chapter provides a brief review of some of the important factors in UV studies and a description of the UV equipment used in the open literature and in our laboratories.

3.2 INTRODUCTION

Photoreactions on polymers and small molecules are published throughout the current literature. Factors influencing their popularity include the overall ease of experimentation and the overall low cost of the equipment. In fact, for less than a $100 investment, research groups can purchase UV lamps from various commercial sources. Wide spread use has often lead to sloppy reporting of the type and specifications of the UV lamps utilized in published studies; often these facts are overlooked or just reported as a “mercury lamp”. Due to the different spectral distribution and intensities of the individual lamps from individual manufacturers, the proper specifications are imperative to reproduce cited work. To properly cite UV research, researchers should list a number of specifications including: the make and model of the lamp, the intensity of the lamp at the

desired wavelength(s) and the make and model of the radiometer utilized to measure the lamp intensities. Specifying the radiometer used is important since radiometers from various manufacturers utilize different wavelengths ranges and have varied sensitivities to the individual wavelength ranges measured. The three spectral bands are known as UVA (320 – 390 nm), UVB (280 – 320 nm), UVC (250 –260 nm). While most lamps are broadband sources, some have built in filters and are available with a spectral output in one of the aforementioned spectral bands. Typical intensities are also grouped into ranges with "low" = 5 – 10, "high" 100 – 1000 and "very high" > 1000 mW cm^{-2} and differ from the indicated wattage for the bulbs used.[390]

Most of the UV studies in the literature use some type of pressured mercury gas arc lamp. As the pressure in the bulb increases, both the light intensity and the irradiation wavelengths increase. The transition for low to medium pressure lamps occurs at a pressure of approximately seven atmospheres of pressure. The spectral emission for low pressure bulbs includes the UVC range and intensity spikes in the following wavelength ranges: 360 - 370, 400 - 410, 430 - 440, 540 - 550, and 570 - 580 nm. Further increases in pressure increases the intensity of the individual spikes and fills in the wavelengths between the individual spikes. Since most lamps emit over the multiple bands listed, individual research groups sometimes utilize various filters to isolate smaller wavelength regions. This work will provide a short review on current irradiation equipment as well as a description of the equipment in our laboratories.

3.3 UV Sources in Small molecule Studies

Lasers are more commonly employed in small molecule photochemistry than in polymer photochemistry. For example, Fouassier used Nd:Yag (neodymium:yttrium aluminum garnet) lasers to study photoinitiators decomposition.[59,62,385] Fouassier's pulsed lasers provide a dose of 15 mJ cm^{-2} (9 ns pulse) at various wavelengths chosen to coincide with the absorbance of the each photoinitiator. Similarly, Wolff *et al.* utilized a Nd:Yag laser at 354 nm and an eximer laser (wavelengths of 308 and 248) to study coumarin dimerization.[391] Hampp *et al.*coupled a Nd:Yag laser with a Shimadzu spectrofluorimeter to study two-photon absorption of coumarin photodimers.[328]

In addition to the Nd:Yag laser, Wolff's groups utilized 100 W Hg lamps coupled to a high pass filter to remove wavelengths below 305 nm when they studied the effect of photodimerization on the viscosity of 6-alkylcoumarin (alkyl group length varying from C1 to C16) micellar solutions. [392,393] DeSchryver employed a small tabletop UV lamp with two 8 W bulbs emitting at 300 nm to study photodimerization of cinnamate derivatives with scanning tunneling microscopy.[182]

3.4 Polymer Curing

3.4.1 **High, Medium and Low Pressure Hg Lamps.**

Since most of the current published studies utilize tabletop or hand-held Hg lamps, this section will cover some of the current literature before discussing the state-of-the-art systems. The use of non-descript light sources is more the rule than the exception in the open literature. For example, Fréchet used a VWR

lamp with two 365 nm 8 W UV bulbs for photoinitiated *in situ* polymerization within a microfluidic device.[76] Benson reviewed the use of radiation in biomaterials science, reporting that authors of individual studies used various nonspecified UV and vacuum UV lamps to alter surface properties of biocompatible materials.[78] Decker also uses a variety of light sources, most recently a 200 W medium pressure Hg lamp to study photoreactions in methacrylates and maleimides.[159]

Bowman *et al.* utilized lamps originally manufactured for the dental industry to study the effect of light intensity and spectral distribution on various dental materials.[67] This group used two broadband sources emitting between 400 and 500 nm (actually in the visible spectrum): a VIP light (Variable Intensity Polarizer) by Bisco Inc. with varied intensity from 100 - 600 mW cm^{-2} at increments of 100 mW cm^{-2} and an Apollo 95E PAC light source from Dental/Medical Diagnostics with an intensity of 2,000 mW cm^{-2}.

The Southern New England Ultraviolet company makes one of the more popular UV irradiation systems, the Rayonet line of reactors. These consist of a ring of UV lamps of selected wavelengths that surround a sample chamber. The interior of the reactor can include a rotating disk or magnetic stir plates to homogenize dose. Chen and coworkers used a Rayonet RPR-100 with 16 bulbs emitting at 350 nm providing a total intensity of 400 W in their studies on photocrosslinking of coumarin-containing polymers.[196-202,206,394] Esen *et al.* also used a Rayonet photochemical reactor with 16 bulbs emitting at 250 nm to photocrosslink cinnamate functionalized epoxidized soybean oil.[256]

While manufacturers and specifications are not specifically mentioned, most of the literature from industrial sources references a UV lamp (or series of lamps) positioned above a conveyor belt system.[32,34-38,41,51-53] Decker recently utilized a Fusion UV Minicure IST system coupled to a conveyor. Similarly, Mehnert and coworkers used a medium pressure Hg arc lamp with a conveyor system to study the curing of a UV-curable pressure sensitive adhesive.[55,56]

3.4.2 **Filtered and Polarized Hg Lamp Systems.**

Because most illumination systems described use broadband sources, filters are sometimes needed to isolate or remove specific wavelengths. A variety of band pass, long pass and short pass filters are available commercially through companies such as ThermoOriel, Reynard, Edmund Optics, etc. The most common filter is a glass or Pyrex filter. Glass filters absorb majority of wavelengths below 300 nm, without filtering light in the UVA or visible spectrum. Similarly, polarizers are sometimes utilized to selectively remove light waves without the preferred orientation for the individual study.

Obi and coworkers used a high-pressure Hg lamp combined with a glass filter and solution filter to isolate 313 nm. They also used a Glan-Taylor type polarizer to yield linearly polarized light when they studied photoalignment in liquid crystals with coumarin side chains.[225,242] For their study on photocrosslinkable coumarin-endcapped poly(lactides), Matsuda used a 250 W Hg-Xe lamp filtered through a Pyrex filter.[113-115,149-151,373]

Some studies employ polarizers to selectively utilize the preferred orientation of light. Jackson and coworkers used an Ar laser with linearly polarized light

(300.5 nm) to study photoalignment of side-chain coumarin polymer liquid crystals.[216,217,244,340,395] Ree also used a polarizer and an optical filter, in series, to yield linearly polarized light at various wavelengths from a high-pressure Hg lamp when they studied cinnamate functionalized polyimide liquid crytals.[143,227,243,250,254,304,396]

3.4.3 Lamps Coupled to Other Equipment.

Some of the most innovative irradiation systems have a UV lamp or laser coupled to other analytical equipment. One well-known combination of light and analytical equipment is the photoDSC. Purvis utilized a DSC coupled to an Osram 200 W Hg lamp which had the capability to vary the light intensity from 1 - 55 mW cm^{-2} to study photopolymerization of vinyl acrylate.[64]

One of the most popular combinations of irradiation equipment and spectroscopy is the combination of irradiation and IR spectroscopy. Crivello typically uses a Hg arc lamp connected to a flexible liquid light guide which is fed into a Midac M-1300 FTIR spectrometer to study photoinitiated cationic polymerization.[84,85,397] Similarly, Catalina and coworkers couple a 400 W Hg lamp to a Nicolet 520 IR spectrometer to study the real-time photocuring of acrylics.[398-401]

Mehnert and coworkers have assembled novel systems to study photocuring consisting of an Osram HBO 103 W Hg arc lamp attached to an Biorad FTS 6000 ATR-IR spectrometer. After passing through a with a water filter to block IR, the light intensity on the ATR crystal is 1300 mW cm^{-2}. An electronic shutter controlled by the spectrometer computer enables synchronization between the

UV irradiation and spectra recording. The shutter allows for continuous, multiple or flash-like irradiations simultaneously taking IR measurements.[55,56]

3.5 PHOTOREACTOR CAPABILITIES IN OUR LABORATORIES

3.5.1 **254 nm Lamp.**

The UVC irradiations in our laboratories are performed with a UV Products UVGL-55 handheld lamp (Figure 3-1). The lamp consists of a dual-band source that emits at 254 and 365 nm and is manufactured for use in fluorescence and chemical analysis and anti-germicidal applications. The undesired wavelength is blocked with a metal faceplate. The lamp intensity at 254 nm is ~ 1 mW cm^{-2} and is typically used for thin layer chromatography and photocleavage studies in our laboratories.

3.5.2 **Oriel Lamp System.**

The Oriel lamp system is a custom assembled broadband lamp system (Figure 3-2) equipped with a 350 W Hg Arc lamp. The emission spectrum of the lamp is shown in Figure 3-3. The light from the lamp is focused and directed through a light condenser and water-cooled housing before reaching a remote controlled shutter. When the shutter opens, the light exits the light guide and travels through a filter housing, which can hold various 2 inch diameter filters depending on the specific wavelength(s) desired. An optional liquid light guide is attachable to the filter holder for spot irradiation experiments. The typical UVA intensity with a short wave UV filter is ~ 75 mW cm^{-2}, which decreases to 10 – 20 mW cm^{-2} as the bulb ages. Light intensity and wavelengths are controlled via a number or filters. Varying the irradiation time controls the total dose.

Figure 3-1. UVGL-55 UV lamp.

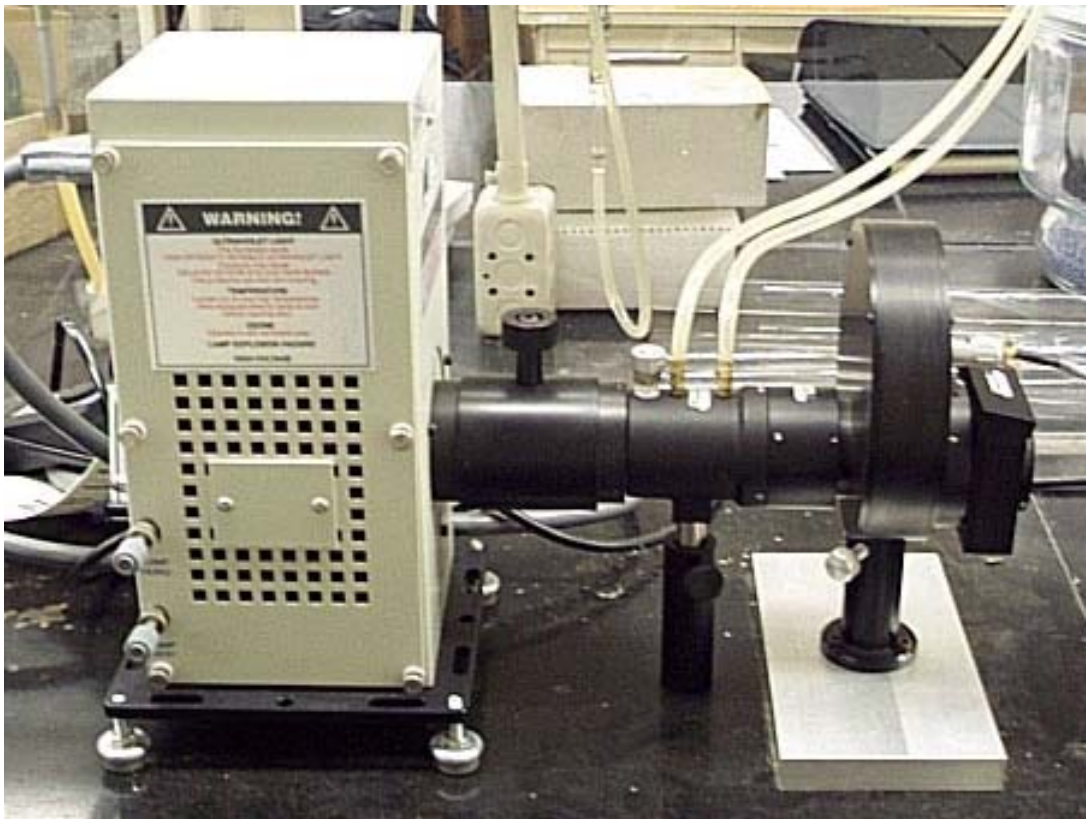

Figure 3-2. Oriel lamp system housing.

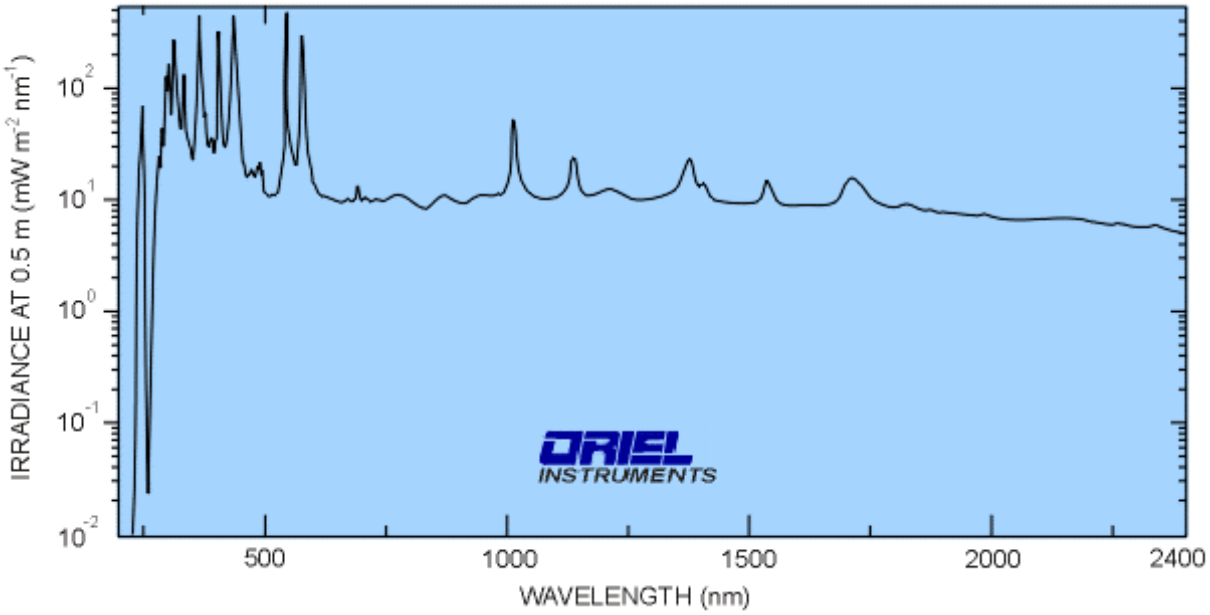

Figure 3-3. UV spectrum of the 350 W Hg arc lamp in the Oriel lamp system.

3.5.3 Fusion UV System.

The lamp system most often used in our laboratories is the Fusion UV conveyor system (Figure 3-4), which is a laboratory scale version of a typical industrial conveyor irradiation system.[34,37,51,53,56,159] A Fusion P300MT power supply provides power to the 118 W cm^{-1} (300 watt $inch^{-1}$) microwave powered electrodeless lamp. The 15.2 cm (6 inch) electrodeless lamp provides constant power throughout the estimated 8,000 hour lifetime. The light from the lamp is focused on the sample with an elliptical mirror, which also absorbs infrared energy to minimize sample heating. The lamp is positioned on a turntable that increases the distance from the lamp to the sample approximately 2.5 cm (1 inch) per rotation, thus controlling the intensity of the light to the sample. Dose is controlled with the conveyor system, which varies in speed from 3 – 150 cm s^{-1} (6 - 290 feet min^{-1}), resulting in irradiation time ranging from 0.33 to $6.8x10^{-3}$ s.

In contrast to the Oriel system, the wavelengths are controlled with interchangeable bulbs (H, D and V bulbs) that represent the typical wavelengths used in industrial processes. The spectrum for the H bulb is shown in Figure 3-5 and is similar to that of a typical high pressure Hg arc lamp. The spectrum for the D bulb is shown in

Figure 3-6. The output of the D bulb is shifted more towards the UVA region than the H bulb with maximum intensities between 350 and 390 nm. Finally, the spectrum for the V bulb is shown in Figure 3-7. The output of the V bulb is shifted more towards the visible wavelengths than the H or D bulbs with

Figure 3-4. The Fusion UV lamp system.

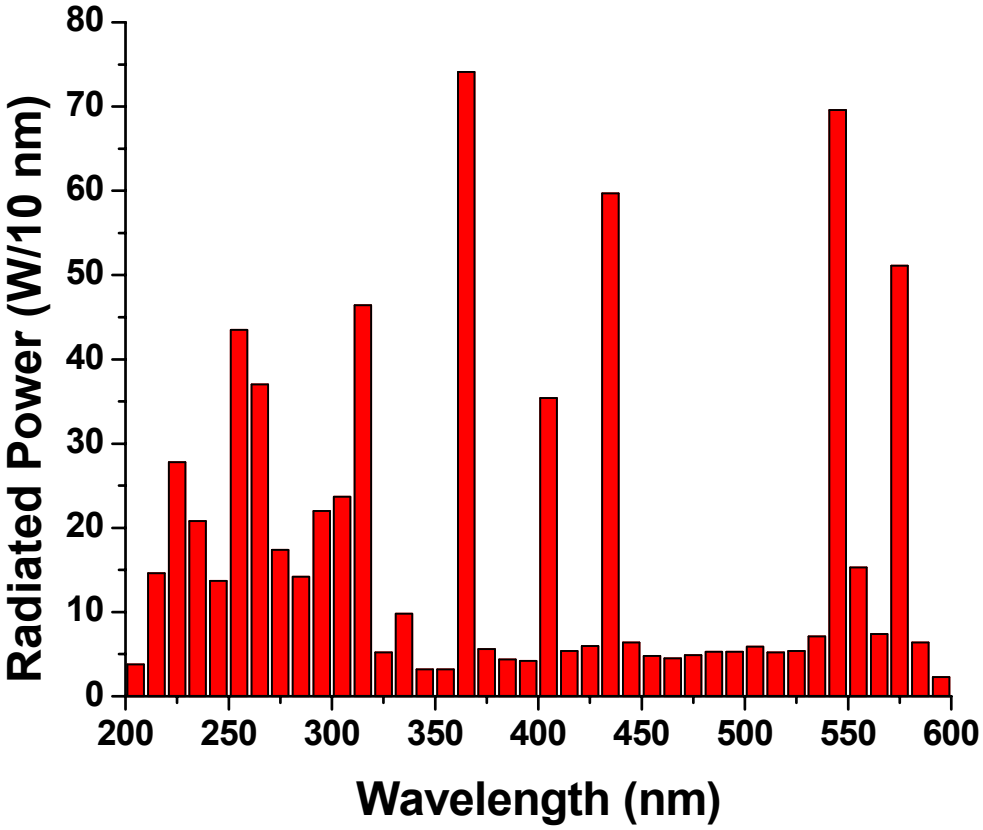

Figure 3-5. Spectral output of the H bulb.

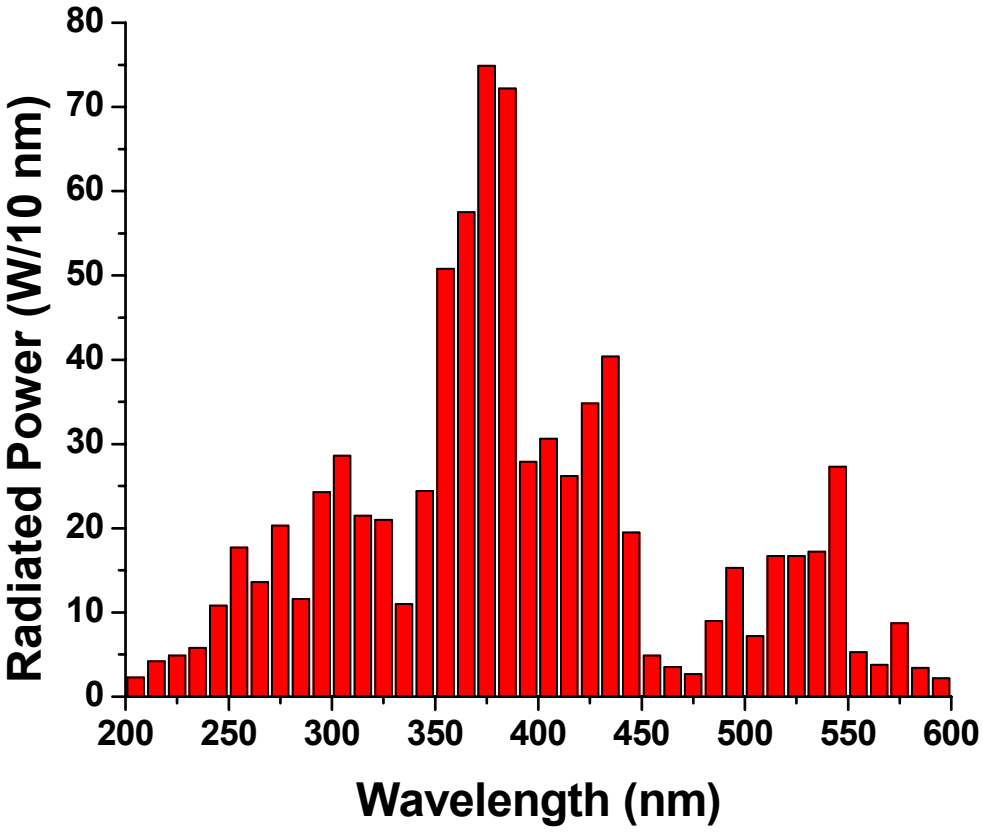

Figure 3-6. Spectral output of the D bulb.

maximum intensities between 400 and 430 nm. Fusion UV also offers various other bulbs with different spectral outputs. In addition to varying the bulb, filters are also utilized as masks to select the wavelength(s) during sample irradiation.

3.5.4 **Neutral Density Filters.**

Our laboratories make use of neutral density filters (NDF) to control the intensity of light reaching the samples. The filters (shown in Figure 3-8) are used as masks during sample irradiation. Figure 3-8(a) is a picture of the fused silica stepped NDF (Edmund Industrial Optics) employed in our labs. The linear step filter varies in transmission from an optical density of 0 (100% transmittance) to an optical density of 2 (1% transmittance) in 11 steps. Figure 3-9 shows the filter transmission at 325 nm as a function of filter step. This allows us to examine the effect of light intensity on the extent of conversion for up to 11 different intensities with a single irradiation.

The fused silica circular variable NDF (Figure 3-8(b), Reynard Optics Inc.) is similar to one used in Zumbrum's graduate work studying the effect of light intensity on epoxy curing at Virginia Tech.[402] As with the neutral density step filter, the circular variable NDF also blocks light from reaching the sample. However, the filter varies from an optical density of 0 to 3 (0.1% transmittance) as the filter is rotated about its center. While the continuously variable filter provides a nearly infinite number of transmittances, it is considerably more difficult to use than the step filter since the change in transmittance is continuous.

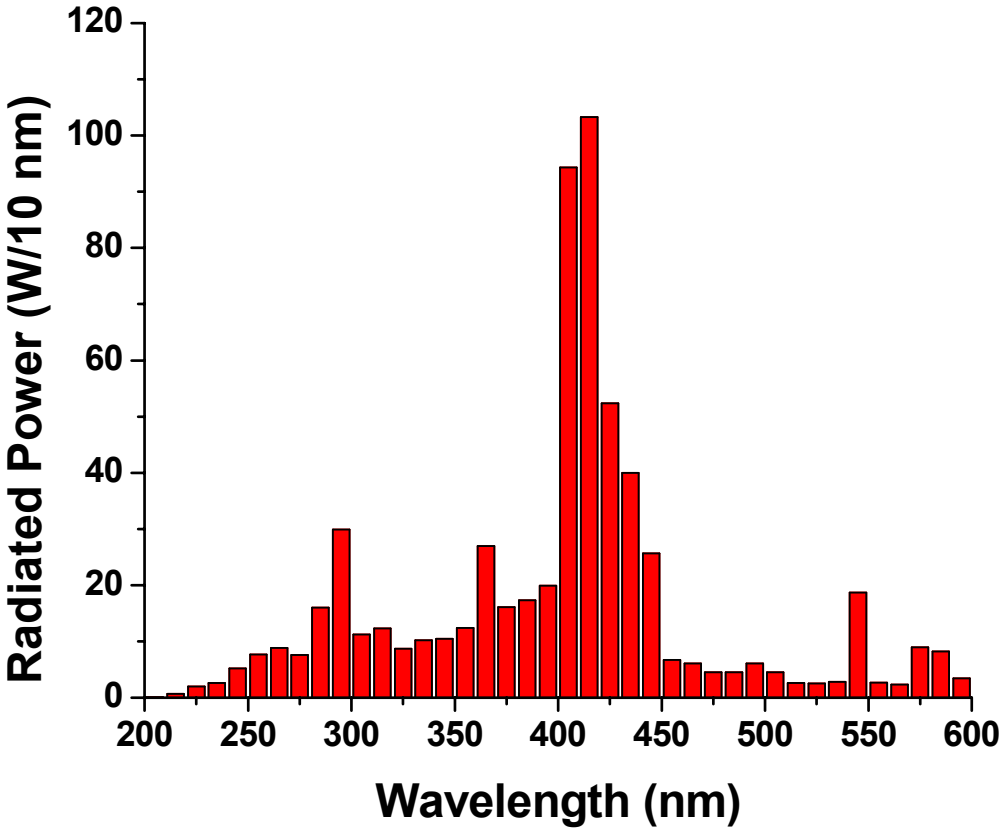

Figure 3-7. Spectral output of the V bulb.

(a)

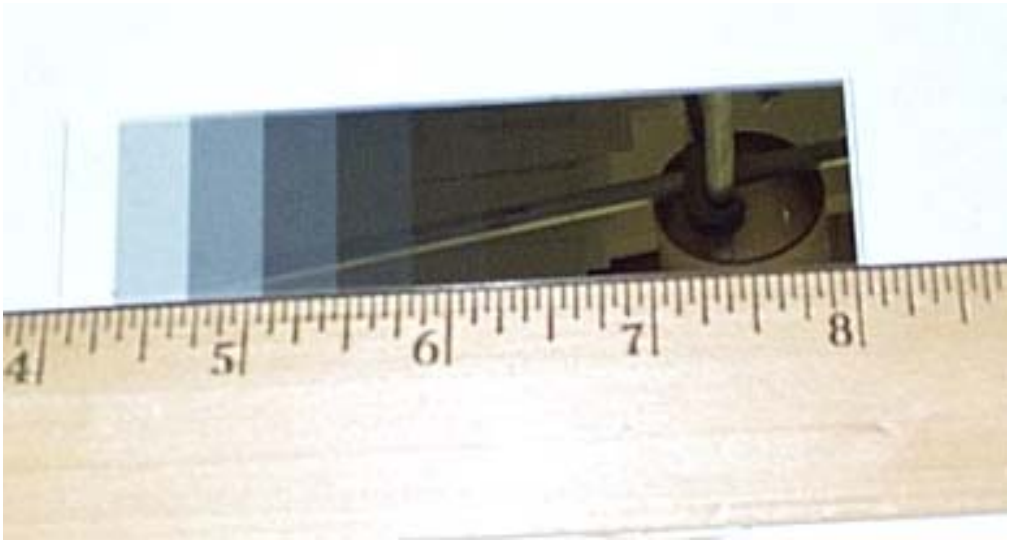

(b)

Figure 3-8. (a) Neutral density step filter and (b) circular variable neutral density filter.

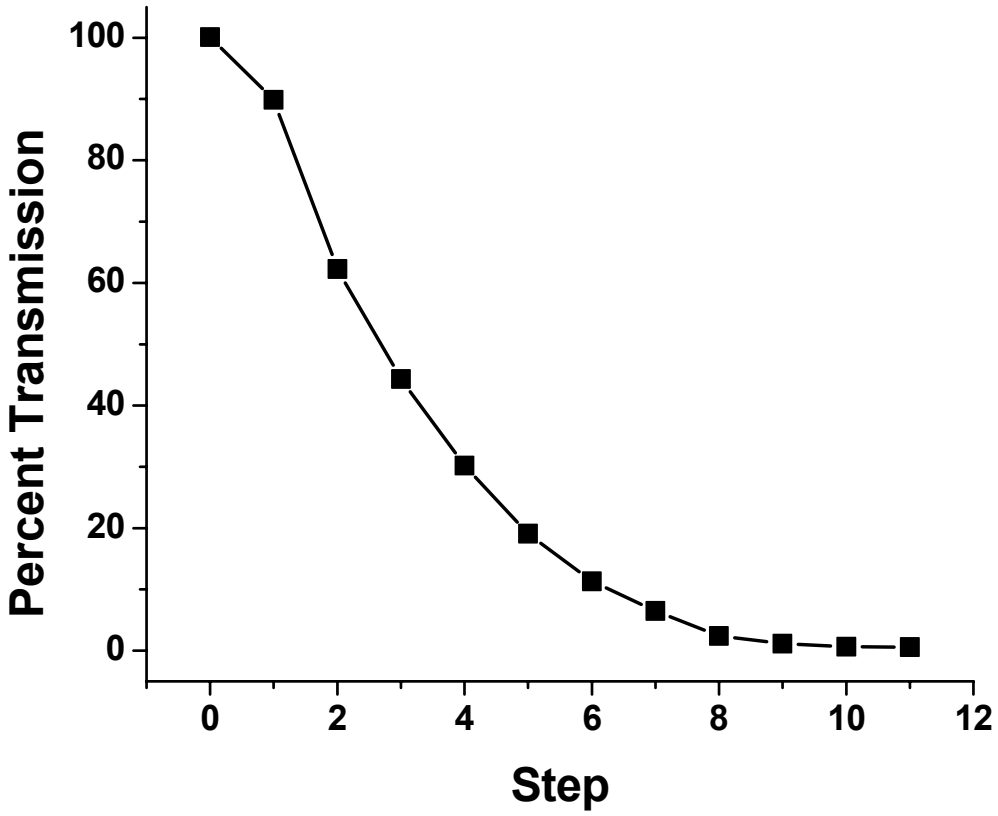

Figure 3-9. Percent transmission versus filter step for the neutral density linear step filter.

CHAPTER 4 PHOTOREVERSIBLE CHAIN EXTENSION OF POLY(ETHYLENE GLYCOL)

Scott R. Trenor, Timothy E. Long [1*] and Brian J. Love [2]
[1] Department of Chemistry
[2] Department of Materials Science and Engineering
Virginia Polytechnic Institute and State University
Blacksburg, VA 24061

Reprinted from: Trenor, S. R.; Long, T. E.; Love, B. J. *Macromolecular Chemistry and Physics* **2004**, *205*, 715.

4.1 SUMMARY

Coumarin containing poly(ethylene glycol) monols and diols were prepared in a telechelic fashion using quantitative end group esterification. The coumarin modified poly(ethylene glycol) monols and diols were solution cast into films (1 to 15 μm) and chain extended via the dimerization of the coumarin derivatives with UVA (> 300 nm) light irradiation. The coumarin-modified PEG diol doubled in molecular weight, and the molecular weight distribution increased from 1.17 to 2.75 upon exposure to 110 J cm^{-2} of UVA light. The chain extended poly(ethylene glycol)s were subsequently converted to their original molecular weight via the photocleavage reaction of the coumarin dimer at 254 nm with less than 2 J cm^{-2}. The photoreversible chain length modulation was monitored utilizing GPC, DSC and UV-Vis spectroscopy.

Keywords: photochemistry, coumarin, telechelics, reversible chain-extension

4.2 INTRODUCTION

Recently, synthetic methods that enable the reversible tuning of molecular weights and crosslink densities of polymers have generated significant interest. For example, Meijer and coworkers have pioneered the use of quadruple-hydrogen bonding and others have advanced the introduction of various tailored hydrogen bonding sites and reversible apparent molecular weights.[122,124-126,139-142] Meijer also reported photo-induced depolymerization of multiple hydrogen bonding polymers. Photodegradation of a sterically hindered multiple hydrogen bonding additive resulted in the endcapping of the hydrogen bonded polymer and a reduction in apparent molecular weight.[124] In addition, Long and coworkers have recently studied thermally reversible multiple hydrogen bonding in telechelic poly(styrene), poly(isoprene), poly(styrene)-*b*-poly(isoprene), and randomly functionalized poly(acrylates).[121,127,128] Although multiple hydrogen bonding in a telechelic and random fashion offers great promise, these supramolecular structures are typically exposed to higher application temperatures, which result in hydrogen bond dissociation and subsequent loss in apparent molecular weight and/or mechanical strength. An attractive alternative to a thermoreversible system is a tunable photoreversible system. Moreover, if a photoreversible system is designed such that the photocleavage wavelength is not commonly observed at ambient conditions, the undesired dissociation reactions are avoided.

7-Hydroxycoumarin (Figure 4-1), and various derivatives photodimere ($2\pi+2\pi$ cycloaddition) when irradiated in the ultraviolet-A (UVA) region of the

electromagnetic spectrum. The cyclobutane ring dimer is cleaved when irradiated at wavelengths shorter than 290 nm (Figure 4-1). The dimers are thermally stable and exhibit melting temperatures as high as 320 °C, although most coumarin dimers melt between 170 and 200 °C depending on configuration.[195,214,220,224,319] Although Ciamician and Silber first discovered photodimerization reactions involving coumarin in 1902, the photocleavage reaction was not discovered until the 1960's when Schenck and coworkers further studied the photodimerization reaction.[195,220] It is important to note that neither the photodimerization nor the photocleavage reactions are thermally allowed. Delzenne and Laridon first utilized coumarin groups to photocrosslink polymers in the mid-1960's, approximately 10 years after cinnamate dimerization was initially demonstrated to photocrosslink poly(vinyl cinnamate).[157,167,403] Delzenne and Laridon photocrosslinked coumarin-functionalized polyhydroxyethers and hydrolyzed poly(vinyl butyral) to form insoluble networks. Moreover, it was demonstrated that the light sensitivity of the polymer was directly proportional to the degree of coumarin substitution.

Recent efforts have demonstrated the photoreversible crosslinking and chain extension of oligomers using coumarin and various other photoactive groups. For example, Saegusa et al. studied the photoreversible crosslinking of polyoxazolines, and insoluble gels were formed upon irradiation above 300 nm, and the gel was partially solubilized with subsequent irradiation at 254 nm.[359,360] Chen and coworkers have studied the reversible photocrosslinking of randomly

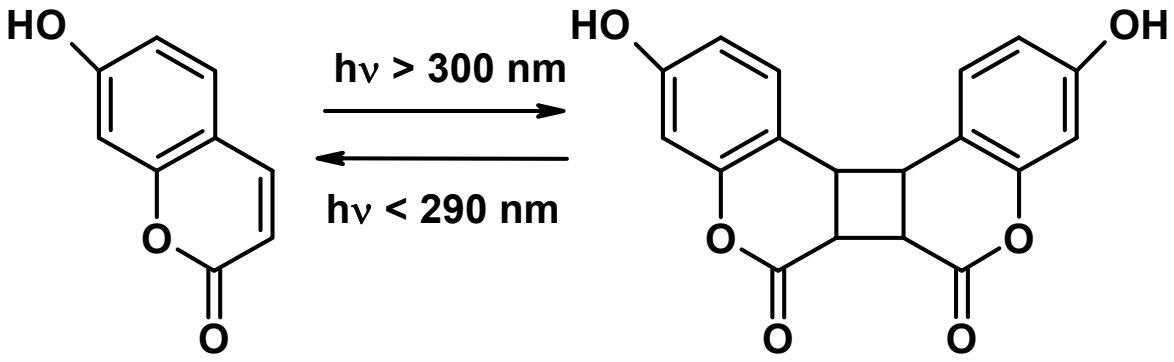

Figure 4-1. The photoreversible dimerization reaction of 7-hydroxycoumarin.

substituted coumarin-containing acrylates and the chain extension of low molecular weight (MW < 500) telechelic polyesters, polyethers, and polyurethanes; however, the polymer precursors were often synthesized in low yields and exhibited poor yields (< 60%) of reversibility.[196,198-202] These earlier investigations have clearly demonstrated that reversible photoreactions are properly characterized using both UV-Vis spectroscopy and gel fraction measurements. Chen and Jean also utilized dilute solution viscosity measurements to monitor the photoreversible chain extension of polyethers.[201,202] Irradiation at 350 nm (56 h) of various telechelic polyethers in CH_2Cl_2 increased the reduced viscosity from 0.022 dL g^{-1} to a maximum of approximately 0.21 dL g^{-1}. Ngai and Wu recently used laser light scattering to study the molecular dynamics of coumarin-containing acrylates that were crosslinked in solution.[404] It was observed that irradiation in concentrated solutions (> 5 wt% polymer) led to the formation of homogenous gels, whereas only finite clusters of crosslinked polymer were formed in more dilute systems.

Andreopoulos and coworkers have described telechelic crosslinking using cinnamate photodimerization, leading to reversible poly(ethylene glycol) (PEG) hydrogels for use as drug delivery vehicles.[92,177-179,181] The crosslinked hydrogels were synthesized via a reaction between either cinnamylidene acetyl chloride or 9-anthracenecarbonyl chloride and the terminal hydroxyl units of a 4-armed PEG (MW = 20 000 g mol^{-1}) star-shaped polymer. Andreopoulos and coworkers reversibly controlled the degree of swelling (between 10 and 20%) of the hydrogels in water. This was accomplished via the reversible

photodimerization/crosslinking of either the telechelic cinnamate or anthracene groups, and alternating the wavelength of irradiation reversibly changed the degree of swelling. The reversible dimerization of the cinnamate containing star-shaped PEGs was also monitored via environmental scanning electron microscopy. The hydrogel films initially displayed a rough surface, which became smooth with irradiation above 300 nm (crosslinking) and rough again following the photoscission reaction.[181,249] The authors attribute the change in the surface roughness to thermal effects and non-uniform crosslinking leading to a process similar to soft annealing.

One of the obvious shortcomings of the previous photoreversible systems is the inherent difficulty with the analysis of crosslinked systems. Both photodimerization and photocleavage in the solid state and photoreversible chain extension of coumarin-modified poly(ethylene glycol) (PEG) are described herein. Coumarin groups were quantitatively coupled to PEG monols and diols via the terminal hydroxyl functionality. The modified PEGs were photodimerized upon irradiation in the UVA region and were photocleaved upon irradiation at 254 nm (UVC). UV-Vis spectroscopy, FTIR spectroscopy, and gel permeation chromatography were employed to monitor changes in the chemical structure and molecular weight of the soluble coumarin-modified PEGs.

4.3 Experimental Section

4.3.1 **Reagents.**

7-Hydroxycoumarin, PEG monol and diol (Table 1), ethyl bromoacetate, and thionyl chloride were purchased from Sigma Aldrich Chemical Co. and used as

received unless otherwise noted. All other solvents and reagents were purchased from commercial sources and were used without any further purification unless otherwise noted. THF was distilled from sodium/benzophenone under a nitrogen atmosphere prior to PEG/acid chloride reactions.

4.3.2 Instrumentation.

^{1}H NMR spectra were recorded using either a Varian Unity 400 MHz or a Varian Inova 400 MHz spectrometer at 25 °C in $CDCl_3$ at ambient temperature. UV-Vis spectroscopy was performed using an Analytical Instrument Systems Inc. spectrometer equipped with fiber optic light guides, a DT1000CE light source, and an Ocean Optics USB2000 UV-Vis detector. FTIR-ATR spectroscopy was accomplished with an Olympus Bx51 microscope modified with a SensIR IlluminatIR ATR objective and stage. Molecular weights were determined at 40 °C in chloroform or THF (HPLC grade) at 1 mL min^{-1} using polystyrene standards on a Waters GPC equipped with 3 in-line PLgel 5 μm MIXED-C columns with an autosampler, and a 410 RI detector. DRI peak deconvolution was performed using Origin® 7.0 SR2 software. The data was represented as a series of Gaussian distributions.[405] Thermal gravimetric analysis was performed using a TA Instruments Hi-RES TGA 2950, with a temperature ramp from 25 °C to 600 °C at 10 °C min^{-1} under a nitrogen atmosphere. Differential scanning calorimetry (DSC) was performed with a Perkin Elmer Pyris 1 at a heating rate of 20 °C min^{-1} after quenching from 120 °C at 80 °C min^{-1} under nitrogen. UVA irradiation was accomplished using an Oriel UV reactor equipped with a glass filter, which

efficiently blocked wavelengths below 300 nm. Irradiation at 254 nm (UVC irradiation) was accomplished using a UVP model UVGL lamp. Irradiance and effective energy density were measured at time intervals no longer than 5 minutes with an EIT UV Power Puck radiometer. PEG films were solvent cast from chloroform or THF onto quartz or glass microscope slides and drawn in a controlled manner using a doctor blade. Film thickness was measured using microcalipers and confirmed with UV-Vis spectroscopy utilizing the molar absorptivity of coumarin groups and the Beer-Lambert Law. Homogenous films of less than 3 μm thickness were prepared for UV-Vis spectroscopy and 10 – 15 μm thick films were prepared for GPC sample preparation.

4.3.3 **Synthesis of Coumarin Precursors.**

The related synthesis of the 7-hydroxycoumarin derivatives is published elsewhere, however, Scheme 4-2 summarizes the synthetic methodology.[147,148] Briefly, 7-hydroxycoumarin (10.0 g, 61.6 mmol) was combined with ethyl bromoacetate (12.4 g, 73.9 mmol), potassium carbonate (12.5 g, 90 mmol), and acetone (450 mL) and refluxed for three hours. After salt filtration, the product was recrystallized from ethanol with an isolated yield of 90%. The product (7-ethoxycarbonylmethoxycoumarin) (7.05 g, 28.2 mmol) was subsequently hydrolyzed for 18 hours in a mixture of 1,4-dioxane (280 mL), water (400 mL) and sodium hydroxide (15.8 g, 395 mmol).

The resulting product (7-carboxymethoxycoumarin) was extracted with a 3:1 chloroform/methanol mixture and recrystallized from ethanol with an isolated

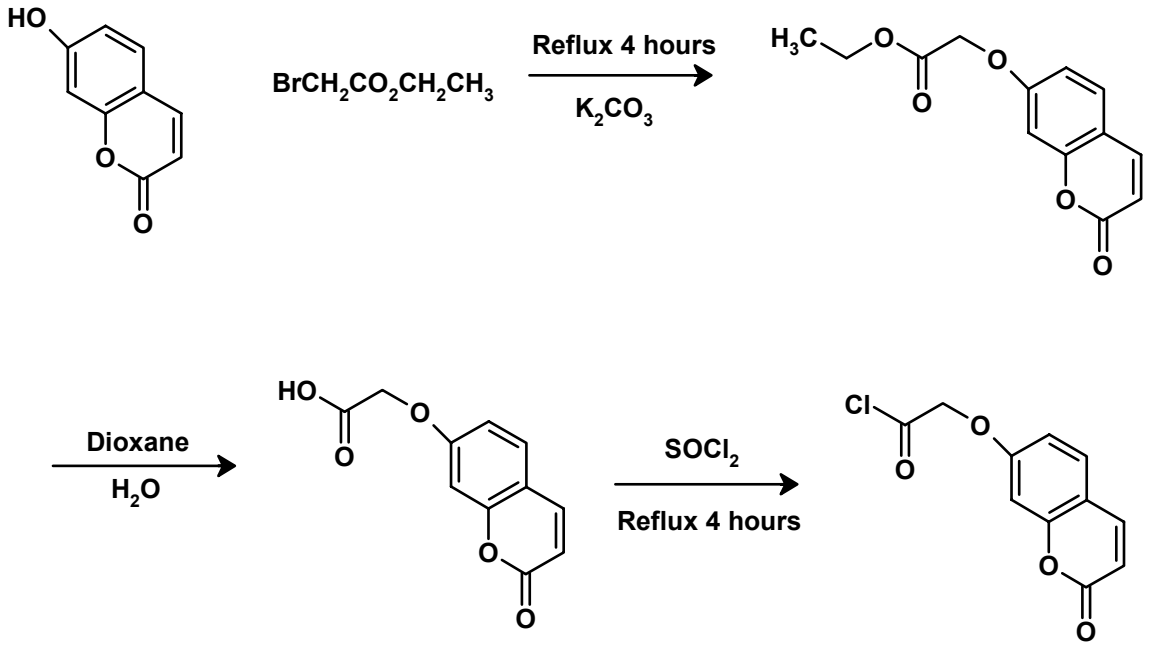

Scheme 4-1. Synthetic methodology for the synthesis of coumarin acid-chloride derivative.

yield of 85%. The 7-carboxymethoxycoumarin (2.44 g, 11 mmol) was refluxed for three hours in thionyl chloride (20.0 mL 277 mmol) providing 7-chlorocarbonylmethoxycoumarin at a yield greater than 98%. Unreacted thionyl chloride was quantitatively removed under reduced pressure. ^{1}H NMR (400 MHz, $CDCl_3$, ppm): 7.65 (d, 1H, CH), 7.43 (d, 1H, Ar H), 6.86 (d, 1H, Ar H), 6.80 (s, 1H, Ar H), 6.31 (d, 1H, CH), 5.02 (s, 2H, CH_2).

4.3.4 Poly(ethylene glycol) Diol Modification with 7-Chlorocarbonylmethoxycoumarin (COU-PEG-COU).

PEG diol (^{1}H NMR M_n = 2020, GPC RI M_n = 3370, M_w/ M_n = 1.04 versus polystyrene standards) was dried overnight under vacuum at 80 °C. PEG (5.0 g, 2.5 mmol) was dissolved in 50 mL distilled THF then combined with triethylamine (1.18 g, 11.7 mmol) and stirred in a nitrogen atmosphere. 7-Chlorocarbonylmethoxycoumarin (2.63 g, 11.0 mmol) was dissolved in 20 mL distilled THF and added dropwise to the PEG and triethylamine mixture. The reaction mixture was stirred at 0 °C overnight under a nitrogen blanket. After filtration of the salt, the resulting polymer was purified with a silica column and the solvent was removed under reduced pressure. The purified yield was 74%. ^{1}H NMR (400 MHz, $CDCl_3$, δ): 7.64 (d, 1H, CH), 7.39 (d, 1H, Ar H), 6.88 (d, 1H, Ar H), 6.78 (s, 1H,Ar H), 6.27 (d, 1H, CH), 4.72 (s, 2H, CH_2), 4.37 (m, 2H, CH_2), 3.63 (br, m, 120H, O-CH_2-CH_2-O). GPC RI (versus polystyrene standards) bimodal, 1st M_n = 3750, M_w/ M_n = 1.03, 2nd peak M_n = 8300, M_w/ M_n = 1.03 (Table 4-1 and Figure 4-2(a)).

Oligomer	Molecular Weights (g mol^{-1})		
	^{1}H NMR	GPC (DRI Vs. PS)	
		M_n	M_w
PEG Monol	2010	3205	3350
PEG Diol	2020	3370	3500
PEG-COU	2210	3650	4030
COU-PEG-COU	2420	4110	4810

Table 4-1. Molecular weights of the PEG oligomers before and after functionalization.

(a)

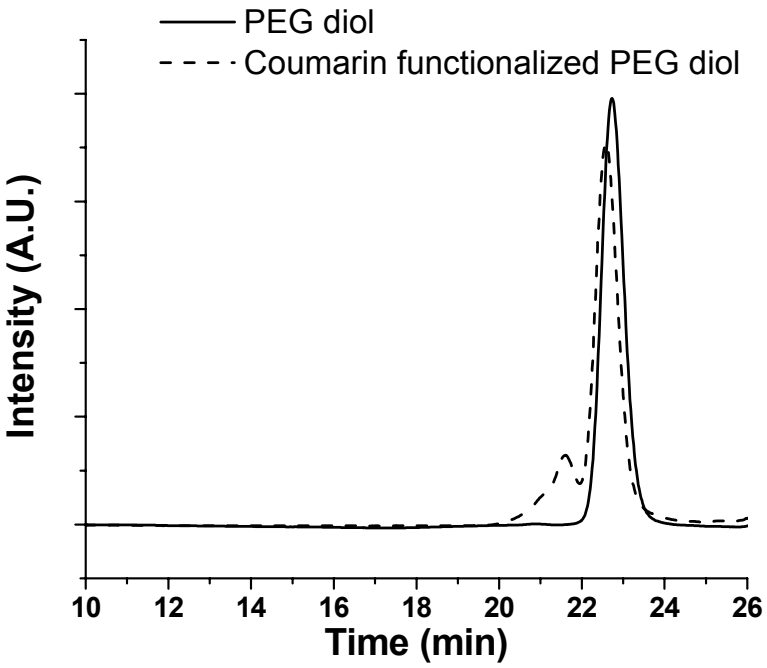

(b)

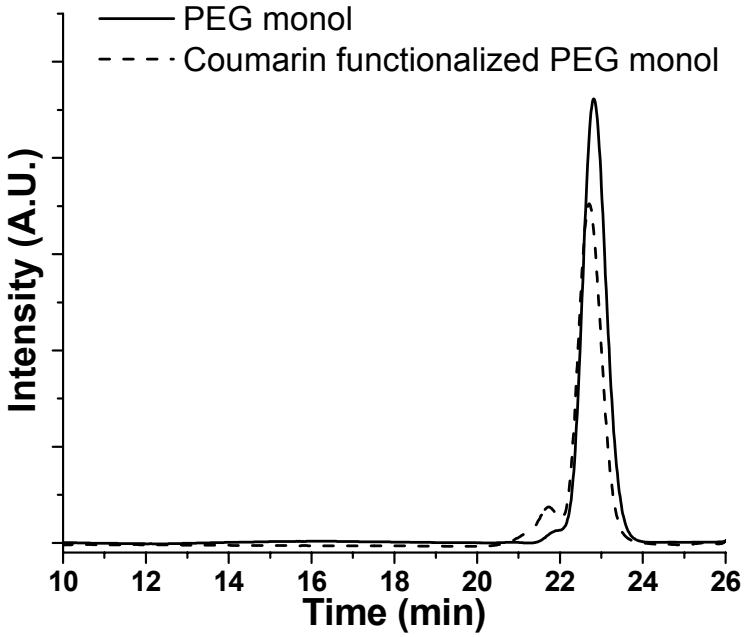

Figure 4-2. (a) GPC traces of PEG diol and coumarin functionalized PEG diol and (b) GPC traces of PEG monol and coumarin functionalized PEG monol.

4.3.5 Poly(ethylene glycol) Monol Modification with 7-Chlorocarbonylmethoxycoumarin (PEG-COU).

Poly(ethylene glycol) monol (^{1}H NMR M_n = 2010, GPC RI M_n = 3205, M_w/M_n = 1.04 versus polystyrene standards) was dried overnight under vacuum at 80 °C. PEG (5.0 g, 2.5 mmol) was dissolved in 50 mL distilled THF and then combined with triethylamine (0.557 g, 5.50 mmol) and stirred under nitrogen. 7-Chlorocarbonylmethoxycoumarin (1.31 g, 5.49 mmol) was dissolved in 20 mL distilled THF and added dropwise to the PEG and triethylamine mixture. The reaction mixture was stirred at 0 °C overnight under a nitrogen blanket. After filtration of the salt, the resulting polymer was purified with a silica column and the solvent was removed under reduced pressure. The purified yield was 87%. ^{1}H NMR (400 MHz, $CDCl_3$, δ): 7.64 (d, 1H, CH), 7.39 (d, 1H, Ar H), 6.88 (d, 1H, Ar H), 6.78 (s, 1H, Ar H), 6.27 (d, 1H, CH), 4.72 (s, 2H, CH_2), 4.37 (m, 2H, CH_2), 3.63 (br, m, 176H, O-CH_2-CH_2-O), 3.36 (s, 3H, CH_3). GPC RI (versus polystyrene standards) bimodal, 1st M_n = 3440, M_w/M_n = 1.03, 2nd peak M_n = 7390, M_w/M_n = 1.01 (Table 4-1 and Figure 4-2(b)).

4.4 Results and Discussion

4.4.1 Coumarin modified PEG diol (COU-PEG-COU).

PEG diols were functionalized with the 7-hydroxycoumarin acid chloride derivative (Table 4-1 and Scheme 4-2). ^{1}H NMR spectroscopy analysis indicated that greater than 97% of the hydroxyl terminal groups were converted to coumarin groups. The resulting polymer product exhibited a slight shift to higher molecular weight (GPC), which was proportional to the addition of the coumarin

unit, and a small (less than 3 mol%) peak due to premature dimerization from ambient light (Figure 4-2(a)). The thermal stability of COU-PEG-COU under nitrogen exhibited a slight decrease (within experimental error) in the 5 wt% loss temperature from 333 to 320 °C (Figure 4-3). The addition of the coumarin end groups disrupted the thermal transitions of the PEG oligomers as depicted in Figure 4-4. Figure 4-4 shows the DSC traces of unmodified PEG, COU-PEG-COU, and COU-PEG-COU irradiated with 110 J cm^{-2} of UVA light. Both the COU-PEG-COU and the irradiated COU-PEG-COU samples exhibit T_g values at -48 and -49 °C, respectively, while the unmodified PEG does not exhibit a T_g. The maximum in the melting endotherm (T_m) for both the COU-PEG-COU and the irradiated samples was shifted down approximately 15 °C from the melting temperature of the unmodified PEG (T_m = 52 °C). The decrease in the melt temperature was attributed to steric hindrance of the coumarin end groups, which act as defects in the PEG crystal structure.

UVA light chain-extended the COU-PEG-COU oligomers in bulk. The λ_{Max} absorbance near 325 nm of COU-PEG-COU is typical of 7-hydroxycoumarin containing polymers (Figure 4-5).[147,148,201,202] The decrease in the intensity of the coumarin double bond absorbance at 325 nm was utilized to measure the extent of dimerization. As the double bond was converted to the cyclobutane dimer (Figure 4-1), the extent of conjugation of the coumarin endgroup was decreased, resulting in a lower absorbance at 325 nm and an increase at 248 nm.[196,197,199,202,212]

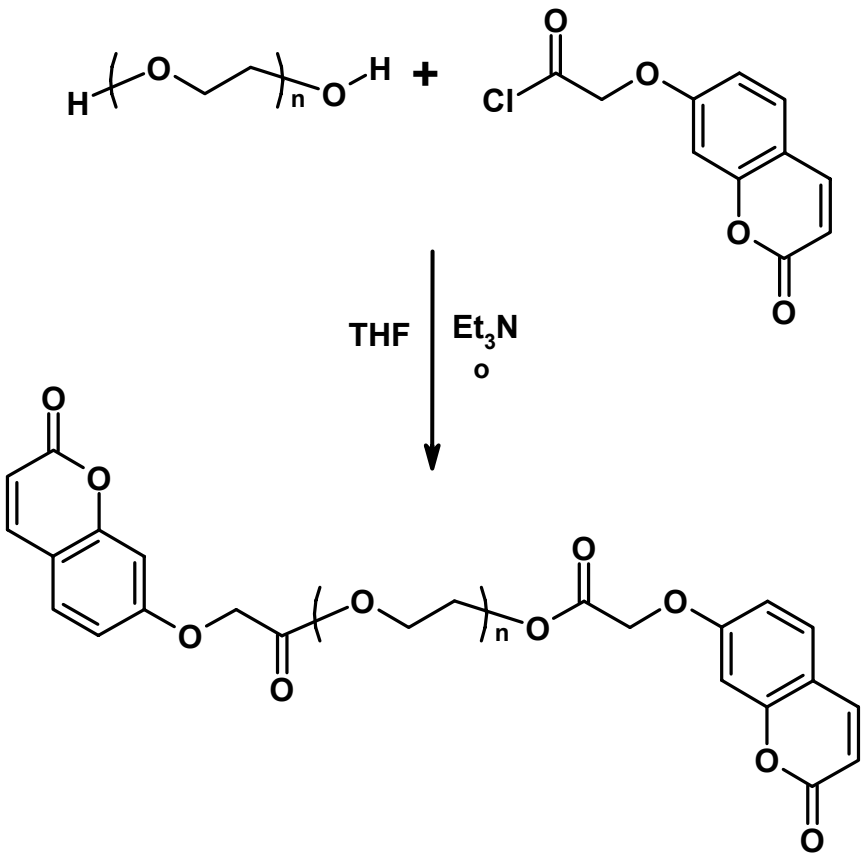

Scheme 4-2. Typical PEG modification reaction scheme.

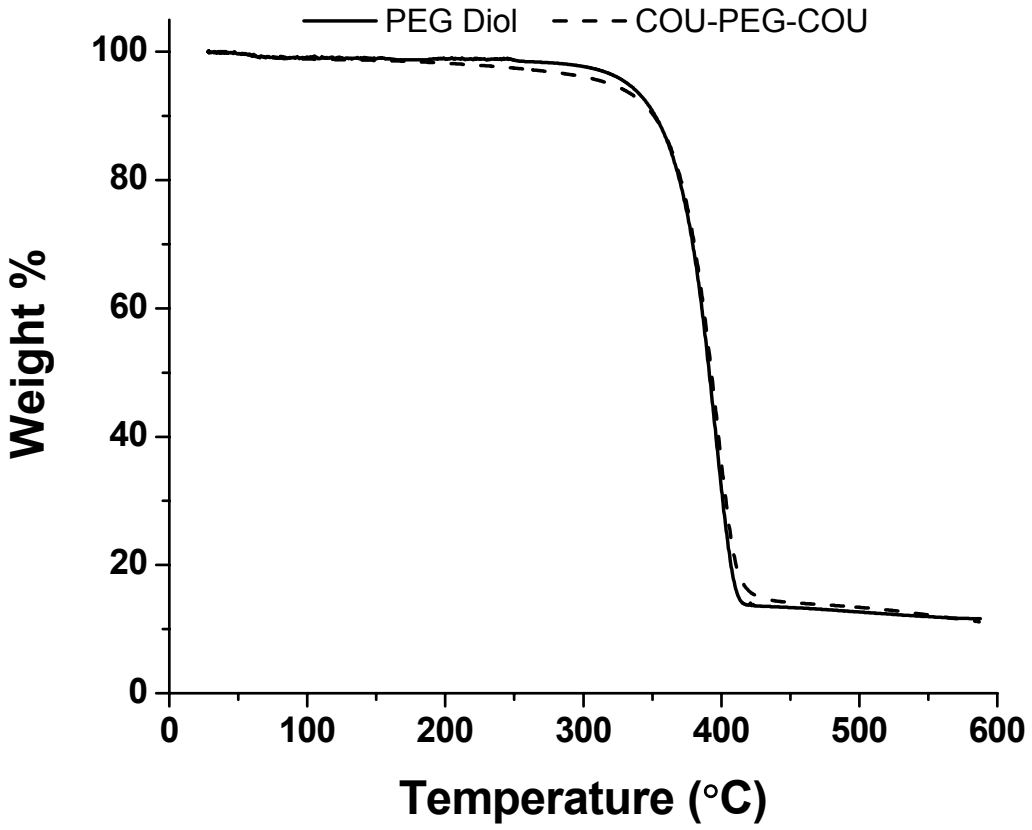

Figure 4-3. TGA trace of percent weight loss versus temperature for the PEG diol and COU-PEG-COU.

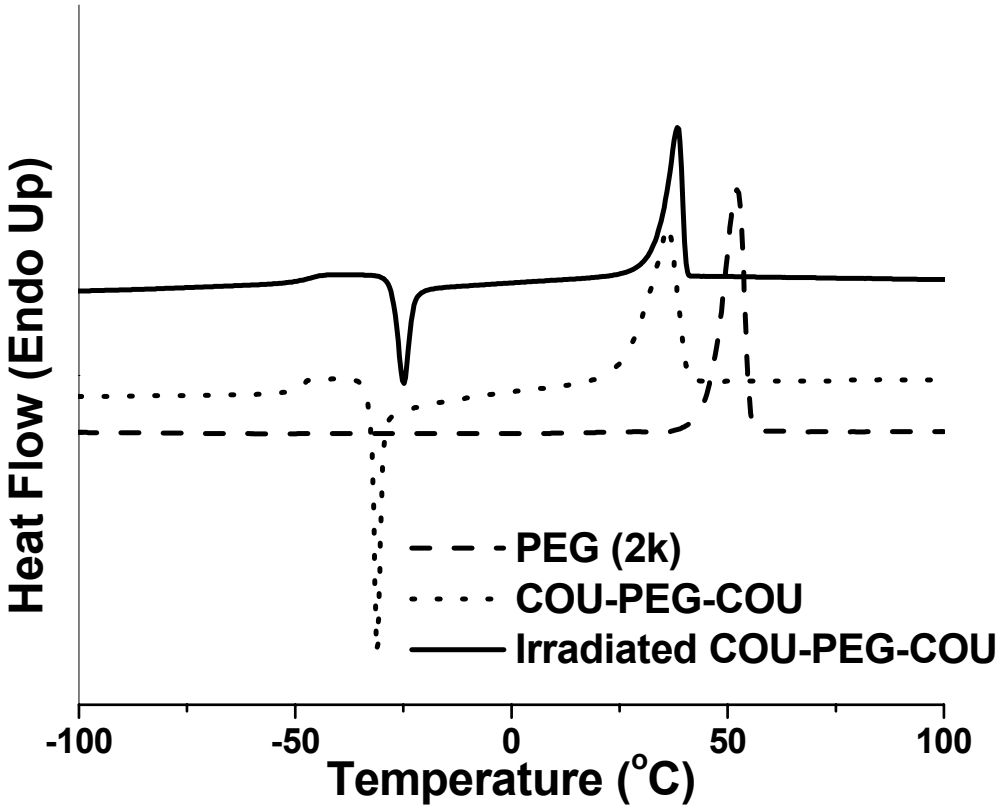

Figure 4-4. DSC traces of unmodified PEG, COU-PEG-COU, and irradiated COU-PEG-COU (110 J cm^{-2}).

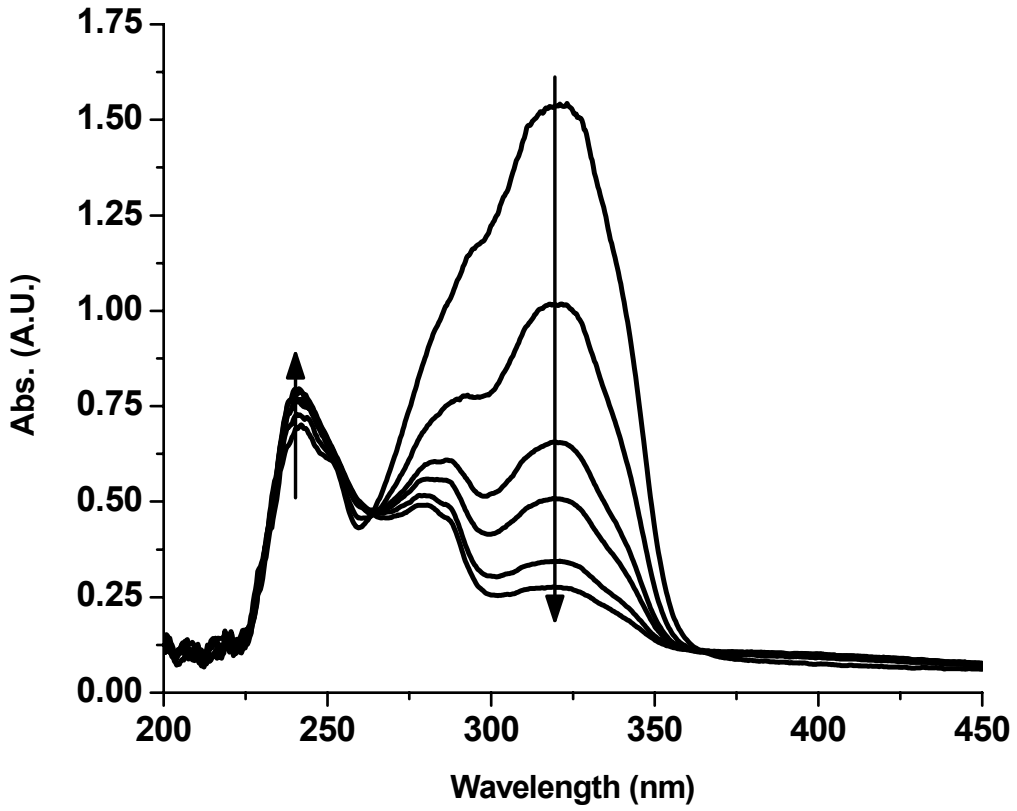

Figure 4-5. Decrease in absorbance at 325 nm due to dimerization of coumarin endgroups in COU-PEG-COU upon irradiation above 300 nm.

The intensity decrease was proportional to the consumption of the 3,4-olefin in the coumarin derivative, while an increase in the absorbance is indicative of cleavage of the cyclobutane rings and reversal to the original lactone structure. Figure 4-5 shows the typical decrease in absorbance (chain extension of COU-PEG-COU) upon irradiation above 300 nm (UVA intensity ~ 2.2 J cm^{-2} min^{-1}). The subsequent change in absorbance due to photocleavage upon irradiation at 254 nm was observed as an increase in the absorbance at 325 nm. Figure 4-6 shows the reversibility of the photodimerization/photocleavage of the COU-PEG-COU utilizing UV-Vis spectroscopy. The squares correspond to the dimerization/chain extension reaction due to UVA irradiation, and the circles represent the photocleavage reaction (UVC irradiation) and reversal to the original COU-PEG-COU. The photodimerization/photocleavage cycle was repeated three times with approximately 90% reversion and comparable changes in absorbance with each cycle. The absorbance did not revert quantitatively due to a well-documented equilibrium between the dimer and cleaved coumarin at 254 nm.[199,206]

It was also observed that heat from the light source melted and redistributed the semi-crystalline COU-PEG-COU films during UVC irradiation. Thus, an analysis of the melting behavior of the coumarin modified PEGs (Figure 4-4) was performed. The melting and redistribution during UVC irradiation of the COU-PEG-COU and chain-extended COU-PEG-COU and PEG-COU films was due to the significantly lower T_m onset (near 27 °C) compared to the unmodified PEG (near 40 °C).

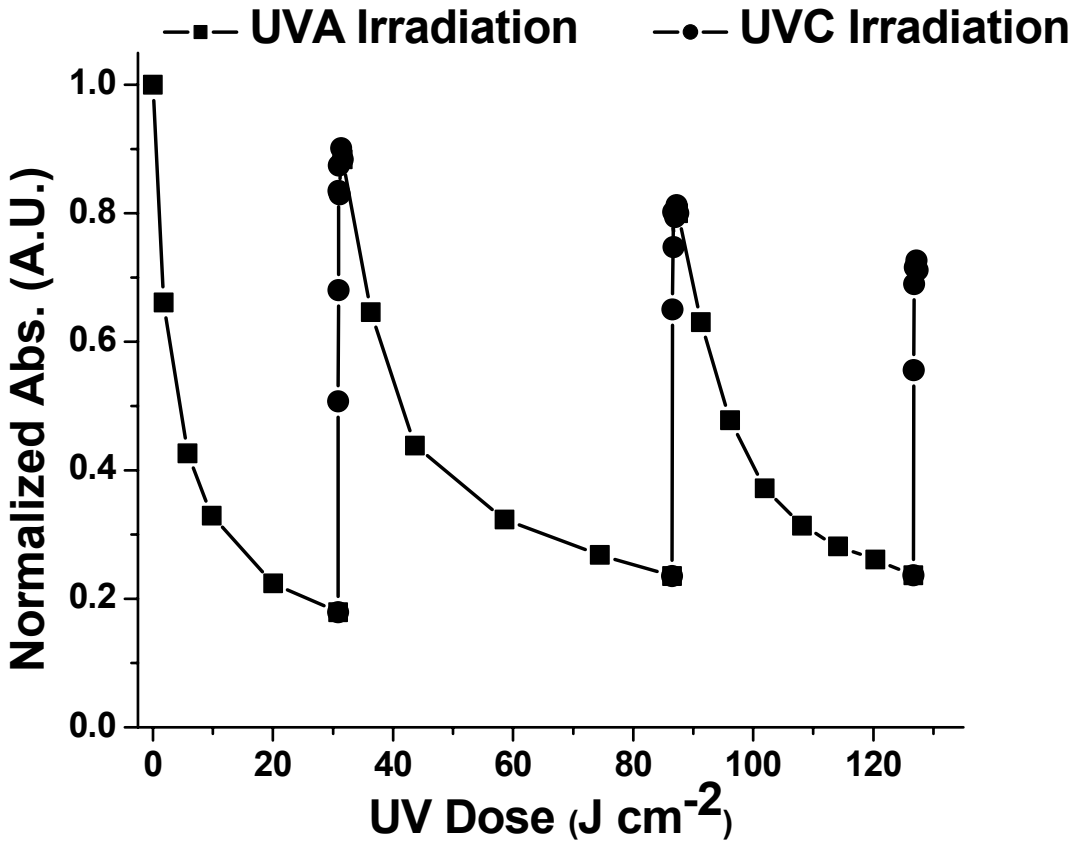

Figure 4-6. Cyclic chain extension (UVA irradiation, squares) and reversion (UVC irradiation, circles) of COU-PEG-COU.

The dimerization reaction was also monitored using both ^{1}H NMR spectroscopy and FTIR-ATR spectroscopy (Figure 4-7(a) and (b)). The top ^{1}H NMR spectrum represents the COU-PEG-COU, and the lower spectrum represents an irradiated COU-PEG-COU (approximately 110 J cm^{-2}). The new resonances at 3.8 - 4.8 and 6.1 – 7.0 ppm, were attributed to the newly formed cyclobutane protons as well as a shift in the original resonances for the dimerized coumarin moiety as described earlier.[201,202] Figure 4-7(b) shows the change in the FTIR-ATR spectra upon COU-PEG-COU irradiation. After UVA irradiation, the absorbance at 1616 cm^{-1} (C=C ring stretch) decreased and the C=O stretch shifted from 1730 to 1757 cm^{-1} as a new carbonyl (α to a cyclobutane ring) formed.[343] Figure 4-8 shows the correlation between the ^{1}H NMR data (▲) and the UV-Vis data (●) for a single dimerization/cleavage cycle. An average of the change in the peak integrals at 7.7, 7.4, 6.8, 6.7 and 6.3 ppm was used to determine the extent of reaction. ^{1}H NMR spectroscopy indicated approximately 90% reversion of the coumarin dimers (Figure 4-8).

Figure 4-9 shows the changes in the molecular weight of the COU-PEG-COU samples upon UVA (squares) and UVC (circles) irradiation. Thicker samples (10 – 15 μm films) were utilized for the molecular weight study in order to obtain sufficient sample for GPC analysis, whereas thinner samples (2 – 3 μm films) were utilized for the UV-Vis experiments to adhere to the Beer-Lambert Law. The efficacy of the photodimerization was not affected over this range of sample thicknesses. The M_n (versus polystyrene standards) of the irradiated COU-PEG-

(a)

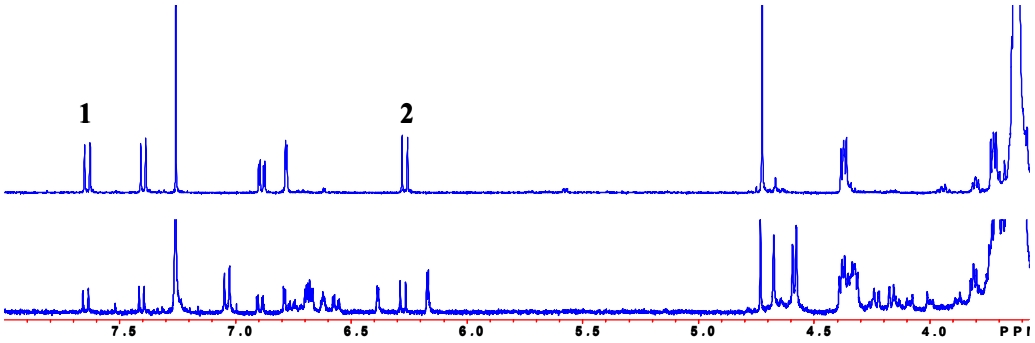

(b)

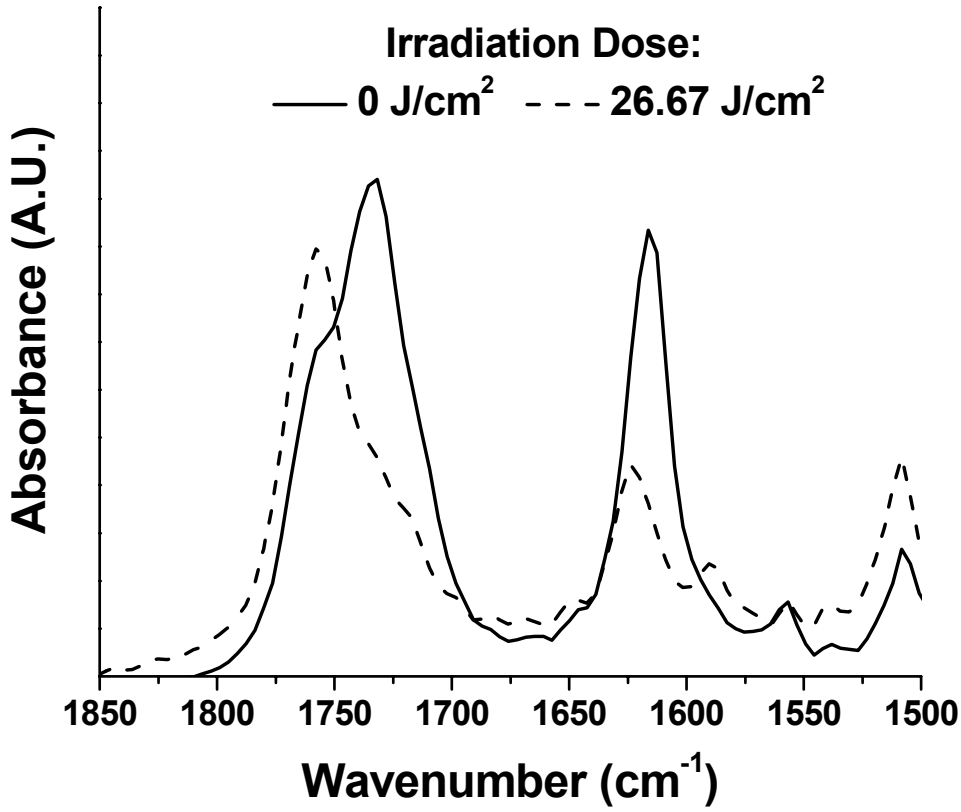

Figure 4-7. (a) ^{1}H NMR spectra before (above) and after (below) irradiation. Resonances labeled (1) and (2) are those of the double bond on the lactone ring. (b) The change in the FTIR spectra before (solid line) and after (dashed line) irradiation.

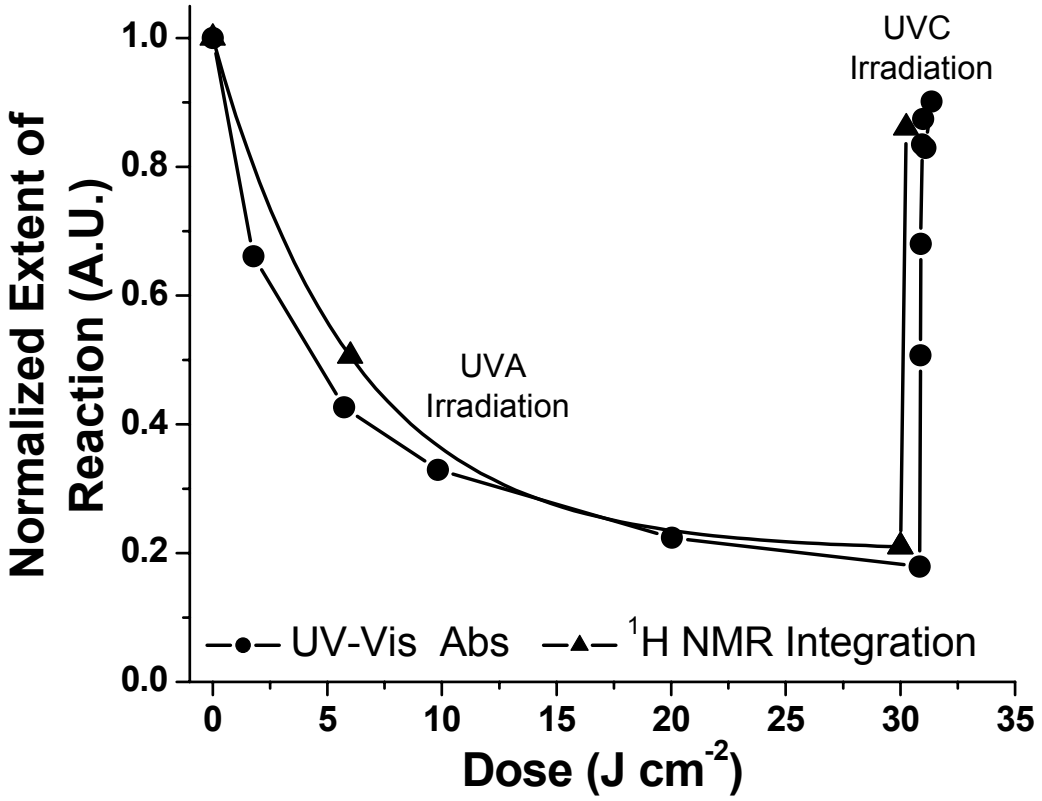

Figure 4-8. Comparison of absorbance changes of irradiated COU-PEG-COU as measured with ^{1}H NMR peak integration and UV-Vis absorbance maxima.

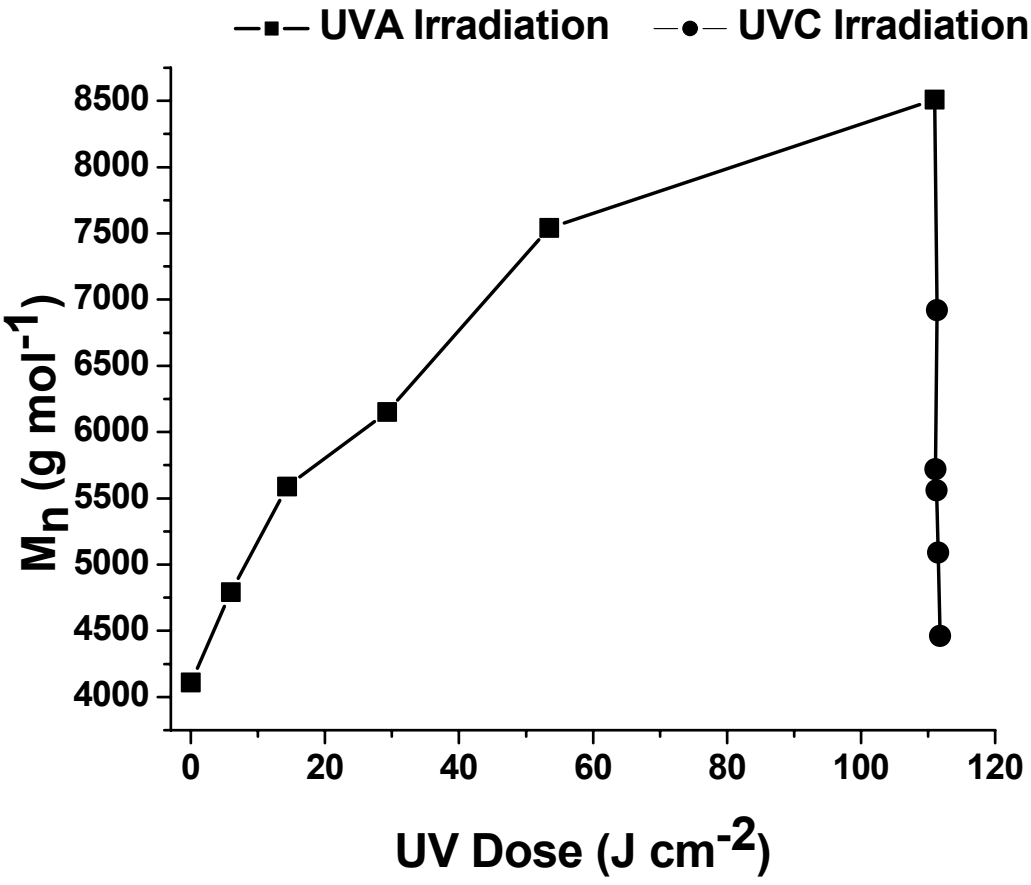

Figure 4-9. Increase and subsequent decrease in M_n of COU-PEG-COU upon of UVA and UVC irradiation, respectively.

COU increased from 4100 g mol^{-1} (M_n of the non-irradiated COU-PEG-COU versus polystyrene standards) to over 8500 g mol^{-1} with 110 J cm^{-2} of UVA light, then decreased to 4400 g mol^{-1} with 1.1 J cm^{-2} of UVC light. As expected, the polydispersity increased from 1.17 to 2.75 then decreased to 1.24 with UVA and UVC irradiation, respectively. The increase in molecular weight and broadening of the polydispersity were indicative of the chain-extension of the COU-PEG-COU oligomers when irradiated above 300 nm. The decrease in molecular weight and narrowing of the polydispersity were indicative of the photocleavage of the chain-extended COU-PEG-COU oligomers with UVC irradiation. Unfunctionalized PEG monols and diols were also exposed to UVA and UVC irradiation and exhibited no change in molecular weight or molecular weight distribution, indicating that the changes in molecular weight measured were due to the photoreversible dimerization of the telechelic coumarin groups.

The DRI GPC data was further deconvoluted to illustrate the concentration of unreacted COU-PEG-COU, dimers, trimers, tetramers, pentamers, and hexamers that were present in the UVA irradiated samples (Figure 4-10). As COU-PEG-COU was initially irradiated above 300 nm, the concentration of dimers and longer units increased while the concentration of un-reacted COU-PEG-COU decreased. At higher doses (longer irradiation times), the concentration of dimers and trimers decreased as the dimers and trimers were converted to tetramers, pentamers, and hexamers. Photocleavage upon UVC irradiation was evident from the decrease in the concentration of longer units, an

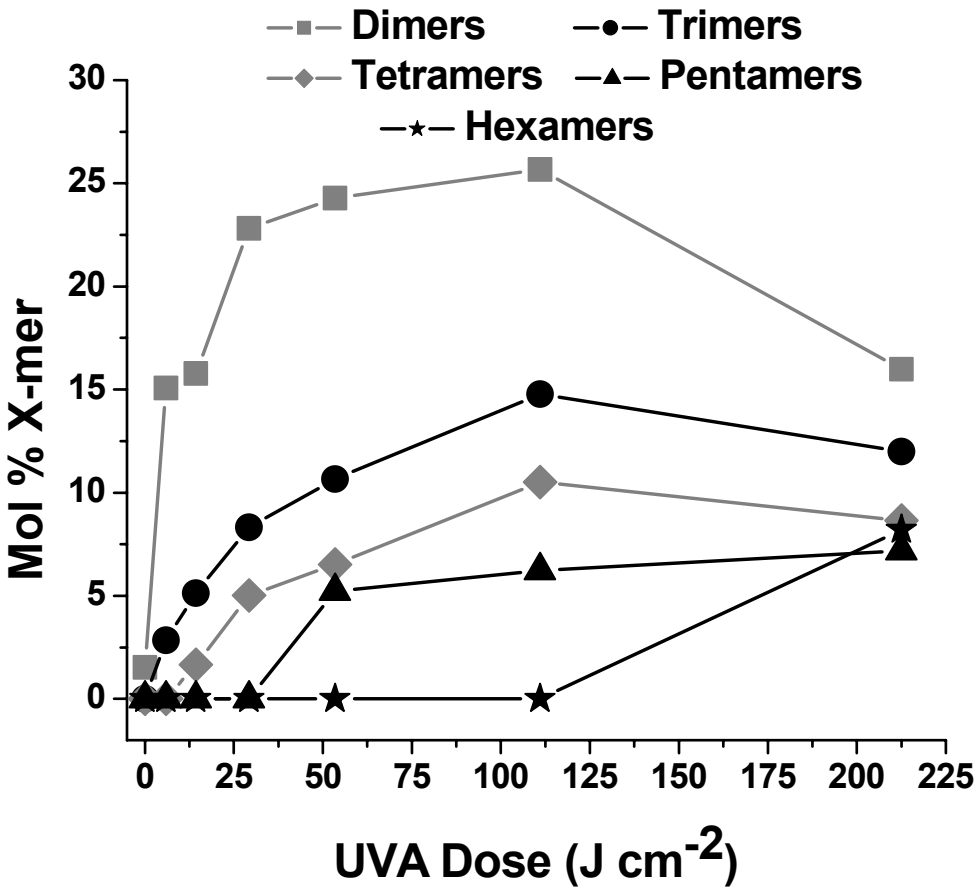

Figure 4-10. Increase in higher molecular weight species of COU-PEG-COU upon irradiation above 300 nm.

increase in the concentration of COU-PEG-COU oligomer, and a decrease in M_n (Figure 4-9). This increase and subsequent decrease in the molecular weight provides the clearest evidence of photoreversible chain extension reactions observed to date.

4.4.2 **Coumarin modified PEG monol (PEG-COU).**

PEG monols were also quantitatively functionalized with the 7-hydroxycoumarin acid chloride similar to the functionalized diols (Scheme 4-2). ^{1}H NMR spectroscopy analysis indicated that 98% of the hydroxyl terminal groups were converted to coumarin groups. GPC analysis indicated a slight shift to higher molecular weight, which was consistent with the addition of the coumarin unit, and a small (less than 1.5 mol%) peak due to premature dimerization from ambient light (Table 4-1 and Figure 4-2(b)). The UV-Vis absorbance spectrum of PEG-COU was nearly identical to COU-PEG-COU as shown in Figure 4-5.

The cyclic photoreversibility of the PEG-COU was also monitored using UV-Vis spectroscopy (Figure 4-11). The squares correspond to the dimerization/chain extension due to UVA irradiation, and the circles represent the photocleavage reaction (UVC irradiation) back to the original PEG-COU oligomer. The photodimerization/photocleavage cycle was repeated three times with a similar extent of reversion as the COU-PEG-COU. UV-Vis spectroscopy indicated incomplete reversal due to the equilibrium between the dimer and the cleaved coumarin at 254 nm and the melting and

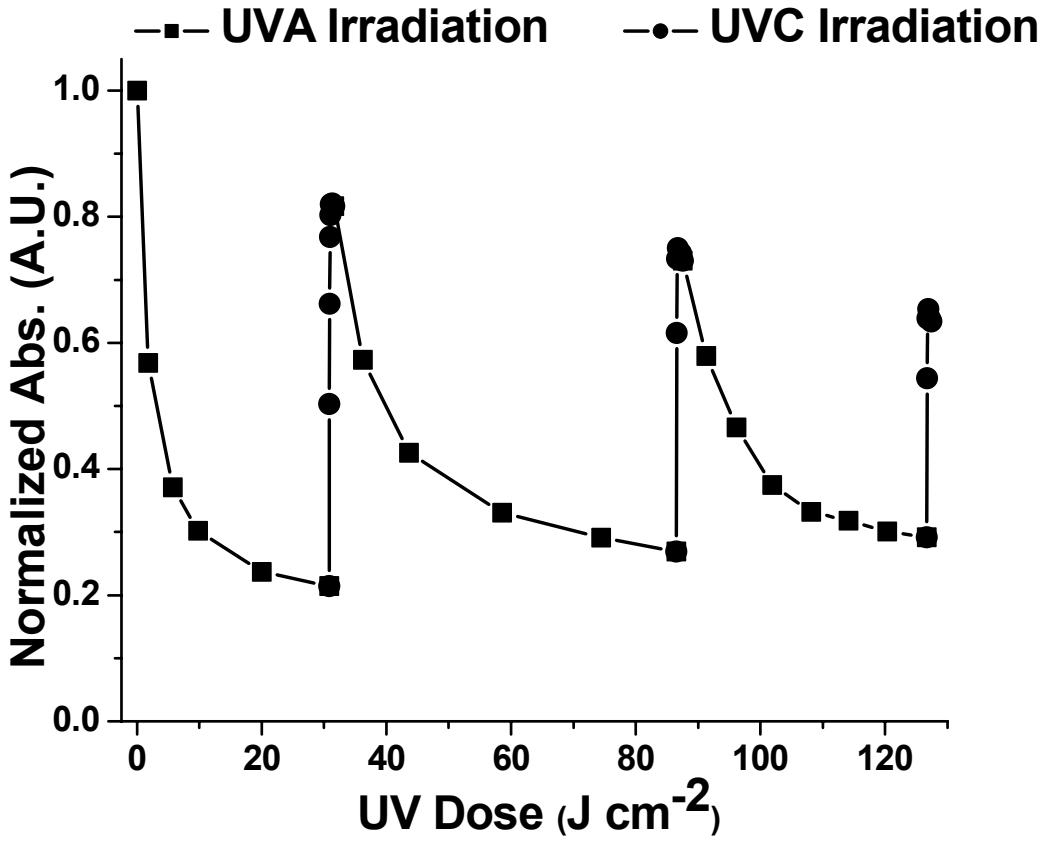

Figure 4-11. Cyclic chain extension (UVA irradiation, squares) and chain cleavage (UVC irradiation, circles) of PEG-COU.

redistribution of the PEG crystallites during the UVC irradiation process, as discussed before for COU-PEG-COU.

The changes in absorbance also correlated well with an increase in the molecular weight and concentration of dimers (4K chains) as measured using GPC (Figure 4-12 and Figure 4-13(a), respectively). As PEG-COU was irradiated above 300 nm (squares in Figure 14), the M_n (versus polystyrene standards) increased from approximately 3400 g mol^{-1} to 5300 g mol^{-1}, while the polydispersity broadened from 1.06 to 1.31. The concentration of dimers increased from 3.0 to nearly 60 mol% with 220 J cm^{-2} of exposure. The decrease in both the M_n and the dimer concentration upon irradiation at 254 nm (circles in Figure 4-12 and Figure 4-13(b)) was indicative of photocleavage. The M_n decreased to 4300 g mol^{-1} and the mol% dimer decreased to approximately 25% with 1.1 J cm^{-2} of UVC irradiation. When the PEG-COU dimers with M_n = 4300 g mol^{-1} were redissolved, recast, and irradiated with an additional 1.1 J cm^{-2} of UVC irradiation, the M_n decreased to 3500 g mol^{-1} and the mol% dimer decreased to near 10 %. This limitation was due to the UVC absorbance of the PEG repeating unit, which prohibited sufficient UVC light from reaching the PEG-COU dimers, and further dimer cleavage in the thicker (10 –15 μm) GPC samples.

4.5 CONCLUSIONS

Photoreversible PEG oligomers were prepared from a quantitative reaction of PEG monols or PEG diols and an acid chloride derivatized 7-

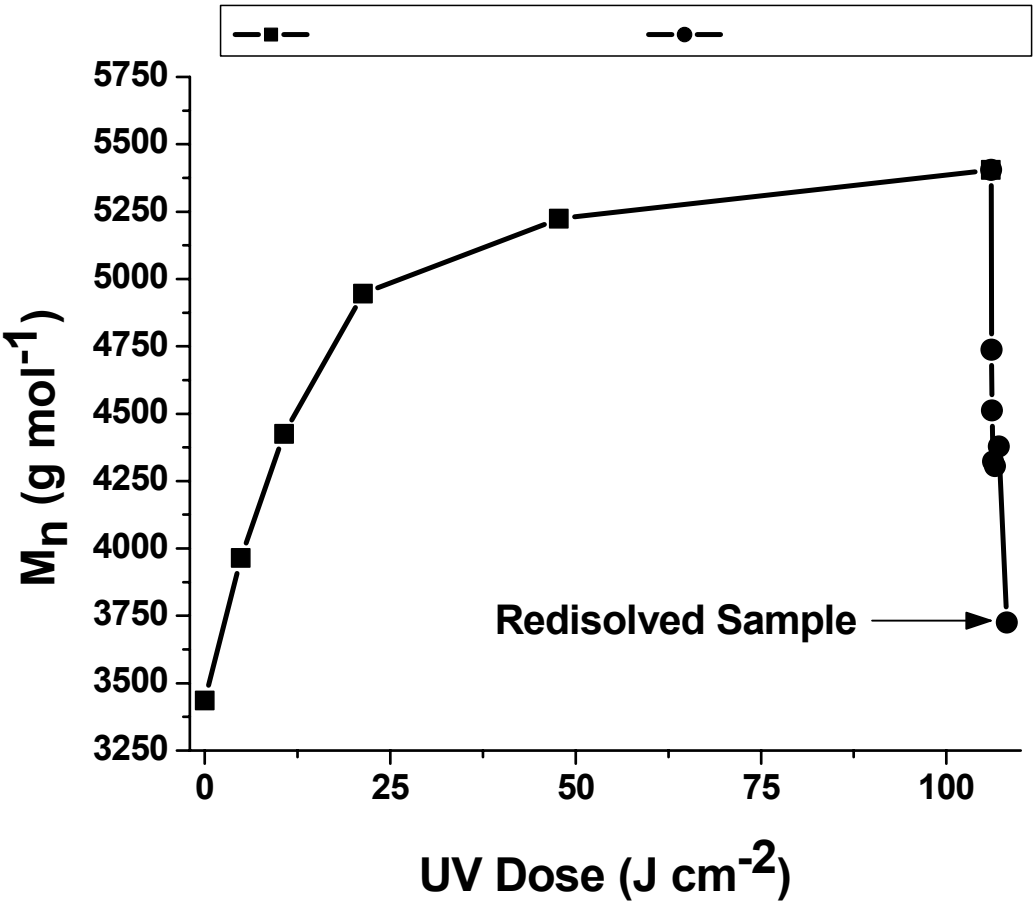

Figure 4-12. Increase and subsequent decrease in M_n of PEG-COU upon UVA and UVC irradiation, respectively.

(a)

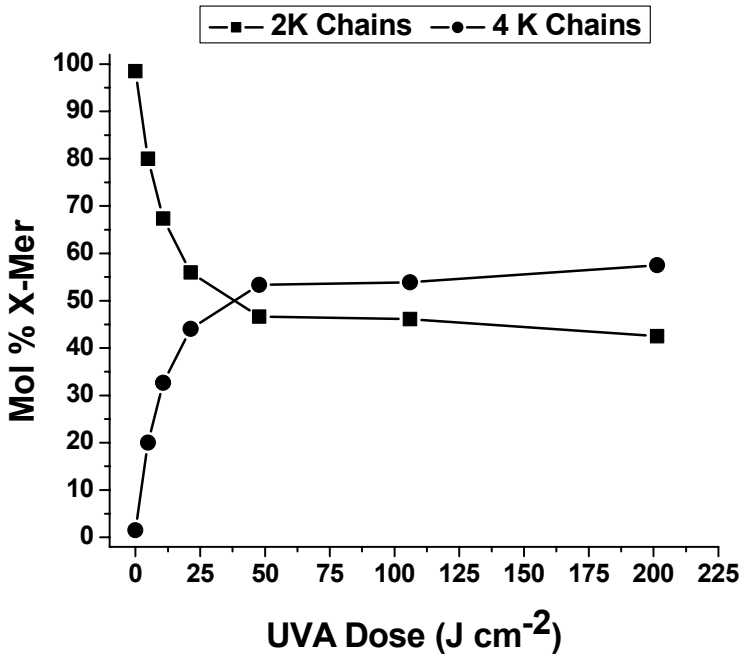

(b)

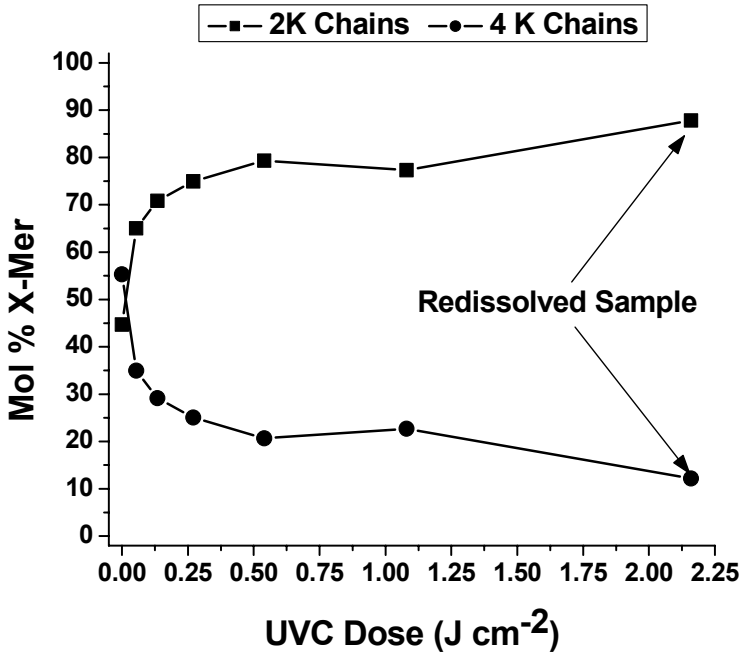

Figure 4-13. Change in coumarin-modified PEG-COU dimer concentration as a function of (a) UVA irradiation dose and (b) UVC irradiation dose.

hydroxycoumarin. The coumarin-modified PEGs chain extended upon irradiation above 300 nm and reverted to their original M_n upon irradiation at 254 nm. The photoreactions were monitored using GPC, UV-Vis, FTIR, and ^{1}H NMR spectroscopy. Photo-chain extension doubled the M_n of the COU-PEG-COU samples and broadened their polydispersity from 1.17 to 2.75. UVC irradiation of the chain-extended COU-PEG-COU decreased the M_n to within 200 g mol^{-1} of the starting material. Similarly, the molecular weight of the coumarin functionalized monols increased with UVA irradiation, then decreased to near the M_n of the unirradiated polymer. The major difference in the two systems is that irradiation of the PEG monols only leads to dimer formation due to monofunctionality, however, the irradiation of diols leads to the formation of a distribution of higher molecular weight. GPC analysis of the chain-extended PEG oligomers provided new insight into the photoreactions of coumarin functionalized polymers. Earlier published photocrosslinked systems and Chen's chain-extension study did not provide soluble products or a demonstration of reversibility.[201,202] The photoreversibility was quantitative and was not affected by excess irradiation as shown in earlier literature for other polymers containing coumarin functionality.[199,201,202]

4.6 Acknowledgments

The authors would like to thank the Center for Adhesive and Sealant Science at Virginia Tech and Procter and Gamble for graduate research fellowships. This material is based upon work supported in part by the U.S. Army

Research Laboratory and the U.S. Army Research Office under grant number DAAD19-02-1-0275 Macromolecular Architecture for Performance (MAP) MURI.

CHAPTER 5 CRYSTALLIZATION OF PHOTO-CHAIN EXTENDED POLY(ETHYLENE GLYCOL)

Scott R. Trenor, Timothy E. Long [1] and Brian J. Love [2*]
[1] Department of Chemistry
[2] Department of Materials Science and Engineering
Virginia Polytechnic Institute and State University
Blacksburg, VA 24061

5.1 SUMMARY

The crystallization of the coumarin-functionalized PEG oligomers synthesized and characterized in the previous chapter was studied. The coumarin-functionalized PEG monols and diols were isothermally crystallized before and after exposure to approximately 110 J cm^{-2} of UVA irradiation. Irradiation dimerized the coumarin groups and chain-extended the coumarin-functionalized PEG oligomers. The higher molecular weights crystallized slower than the non-irradiated coumarin-functionalized PEG oligomers. Hoffman's kinetic nucleation theory was utilized to evaluate the types of nucleation that occurred for the coumarin-functionalized PEG diols (COU-PEG-COU). Crystallization regimes II and III were observed for the coumarin-modified PEG oligomers before and after exposure to UVA light.

5.2 INTRODUCTION

Many research groups have thoroughly studied the crystallization of PEG and PEO via a number of methodologies including optical microscopy, DSC, in situ AFM and small angle X-ray scattering.[406-414] In the late 1970's and early 1980's Kovacs and coworkers published a number of reports on the melting and

crystallization behavior of low molecular weight PEO films. They reported that the crystallization rate of low molecular weight PEO (<10,000 g mol^{-1}) decreased with increasing molecular weight due to in part to increased melt viscosity.[406] Cheng and coworkers studied the effects of chain ends on 3,000 and 7,000 g mol^{-1} PEG.[409,410] For the 3,000 g mol^{-1} polymer, crystallization rate decreased with increasing endgroup size (-OH, $-OCH_3$, $-OC(CH_3)_3$ and $-OC_6H_5$). However, since the endgroups are a lower weight fraction of the 7,000 g mol^{-1} polymer, the endgroups had no pronounced effect on the crystallization rate. Goh and Huang also reported a similar endgroup effect during their study of C_{60} endcapped PEO (M_w = 3,000 g mol^{-1}).[412] The addition of a single C_{60} chain end only depressed the T_m from 54.6 °C (as received PEO) to 53.0 °C, while the second C_{60} chain end further depressed the T_m to 43.4 °C. A similar trend was observed for the crystallization rates with the bulky C_{60} chain ends greatly decreasing the rate of crystallization.

There are three growth regimes observed in the crystal growth rate of PEG and other polymers; each regime displays a distinct growth curve and nucleation constants.[214,406,408,412,414-418] In regime I, at small undercoolings, a single nucleation occurs and the substrate is completely covered by the crystallization growth layer from the single nuclei. Multiple nucleations occur at larger undercoolings where crystal growth and additional nucleation are competing factors (regime II). At even larger undercoolings (regime III), nucleation occurs at such a high rate that the distance between nucleation sites is approximately the same size as the width of a single chain (reptation tube) as it is incorporated

into the crystal.[412,414,415,417,419] Hoffman first reported and others have verified that the nucleation constants for regimes I and III are similar and are theoretically (and experimentally verified) twice that of regime II.[412,414,415,417,419]

The crystallization rates of coumarin-functionalized PEG monols and diols with and without exposure to UV light are described herein. Isothermal crystalline growth rates of the coumarin-functionalized PEGs were measured with optical microscopy. Kinetic data was calculated from the crystallization measurements and compared to those in the literature. The second and third crystallization regimes were separable by a transition region where more data would be needed to determine an exact transition point.

5.3 Experimental Section

5.3.1 **Reagents.**

7-Hydroxycoumarin, PEG monol and diol, ethyl bromoacetate, and thionyl chloride were purchased from Sigma Aldrich Chemical Co. and used as received unless otherwise noted. All other solvents and reagents were purchased from commercial sources and were used without any further purification unless otherwise noted. THF was distilled from sodium/benzophenone under a nitrogen atmosphere prior to PEG/acid chloride reactions.

5.3.2 Instrumentation.

^{1}H NMR spectra were recorded using either a Varian Unity 400 MHz or a Varian Inova 400 MHz spectrometer at 25 °C in $CDCl_3$ at ambient temperature. UV-Vis spectroscopy was performed using an Analytical Instrument Systems Inc. spectrometer equipped with fiber optic light guides, a DT1000CE light source,

and an Ocean Optics USB2000 UV-Vis detector. FTIR-ATR spectroscopy was accomplished with an Olympus Bx51 microscope modified with a SensIR IlluminatIR ATR objective and stage. Molecular weights were determined at 40 °C in chloroform or THF (HPLC grade) at 1 mL min^{-1} using polystyrene standards on a Waters GPC equipped with 3 in-line PLgel 5 μm MIXED-C columns with an autosampler, and a 410 RI detector. Differential scanning calorimetry (DSC) was performed with a Perkin Elmer Pyris 1 at a heating rate of 20 °C min^{-1} after quenching from 120 °C at 80 °C min^{-1} under nitrogen. UVA irradiation was accomplished using an Oriel UV reactor equipped with a glass filter, which efficiently blocked wavelengths below 300 nm. Irradiance and effective energy density were measured at time intervals no longer than 5 minutes with an EIT UV Power Puck radiometer. PEG films were solvent cast from chloroform or THF onto quartz and drawn in a controlled manner using a doctor blade. Film thickness was measured using. Homogenous films of less than 3 μm thickness were prepared for optical microscopy.

5.3.3 **Synthesis and Characterization of Coumarin-Functionalized PEGs.**

The related synthesis of the coumarin derivatives, functionalization of the coumarin-functionalized PEG monols (PEG-COU) and diols (COU-PEG-COU) and the effect of irradiation on molecular weight is described in Chapter 4.

5.3.4 **Isothermal Crystallization.**

Isothermal crystallization was monitored using an Olympus BX51 microscope equipped with polarizing filters and an Olympus CD12 camera linked to computer via Olympus MicroSuite software. A Linkam THMS 600 temperature controllable

stage and the corresponding Linkam TMS 94 temperature controller were used to modulate the crystallization temperature. Dry ice-cooled IPA was utilized to cool the temperature stage. All samples were heated to 70 °C and held for 5 minutes before cooling to the desired temperature at 30 °C min^{-1}. Images were recorded with the MicroSuite software at set time intervals. The crystal radii were measured with the MicroSuite software. All reported growth rates are the average of at least two experiments.

5.4 Results and Discussion

5.4.1 Effect of Coumarin Endgroups on Isothermal Crystallization.

The effect of coumarin end groups on the crystallization at T_m – 15 °C is shown in Figure 5-1. The addition of the single coumarin group on the PEG-COU sample decreased the radial growth rate from 3.8 μm s^{-1} to 3.4 μm s^{-1}. The double coumarin substitution further decreased the growth rate to 0.45 μm s^{-1}. This decrease was expected as others have reported that the addition of bulky endgroups retards PEG crystallization rate.[409,410,412] Table 5-1 summarizes the changes in the thermal transitions and the growth rates of the PEGs due to the coumarin end groups. Crystallization exotherm and glass transitions were not observed for the PEG and PEG-COU samples as the polymers fully crystallized during quenching.

UVA irradiation of the coumarin-functionalized PEG oligomers chain-extended the macromolecules via coumarin cycloaddition. For example, exposure to 110 J cm^{-2} increased the M_n of the PEG-COU and the COU-PEG-COU to 5,300 and

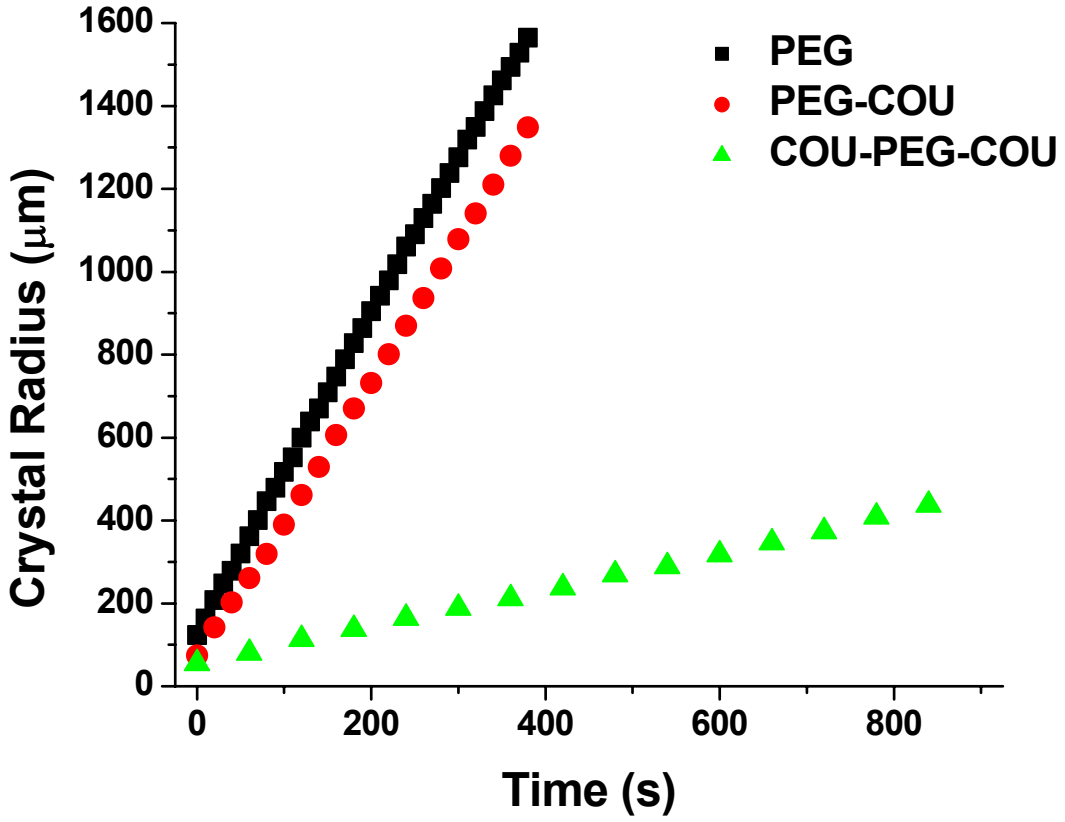

Figure 5-1. The effect of coumarin endgroups on the crystal growth of the PEG macromolecules (isothermal crystallization at T_m – 15 °C).

Sample	T_g (°C)	T_c (°C)	T_m (°C)	T_m (°C)[a]	Radial growth rate at T_m - 15 °C ($\mu m\ s^{-1}$)
PEG	N/D	N/D	52	55	3.8
PEG-COU	N/D	N/D	50	47	3.4
COU-PEG-COU	-48	-31	36	40	0.45

Table 5-1. Summary of the thermal transitions (DSC) and the crystalline radial growth rates (optical microscopy). a = measured via optical microscopy, N/D = not detected.

8,500 g mol^{-1} (versus polystyrene standards), respectively. The increase in the molecular weight, caused a 28% decrease the radial growth rate of PEG-COU and a 49% decrease in the radial growth rate of COU-PEG-COU (Figure 5-2). Kovacs and coworkers reported similar decreases in the growth rates of PEG and PEO with increasing molecular weights.[406-411]

5.4.2 Effect of Temperature on the Crystallization of COU-PEG-COU Before and After Exposure to UV Irradiation.

The effect of temperature on the growth rates of the COU-PEG-COU and the chain-extended COU-PEG-COU (110 J cm^{-2} of UVA irradiation) was also studied to gain insight into the molecular dynamics of the crystallization process. Figure 5-3 and Figure 5-4 show the effects of crystallization temperature on crystal growth with and without UVA irradiation, respectively. As the temperature is decreased (increase supercooling) the crystallization rate increases.

Figure 5-5 shows the Hoffman-Lauritzen plots for COU-PEG-COU before irradiation and after exposure to approximately 110 J cm^{-2} of UVA light. The lines on the graph are linear fits (R_2 > 0.985) for two regimes for each sample. The plot is based on the crystal growth rate for each regime ($G(i)$, Equation 5-1):

Equation 5-1.
$$G(i) = G_o(\Delta T)\exp\left(\frac{-U^*}{R(T_c - T_\infty)}\right)\exp\frac{-K_g(i)}{T_c \Delta T f}$$

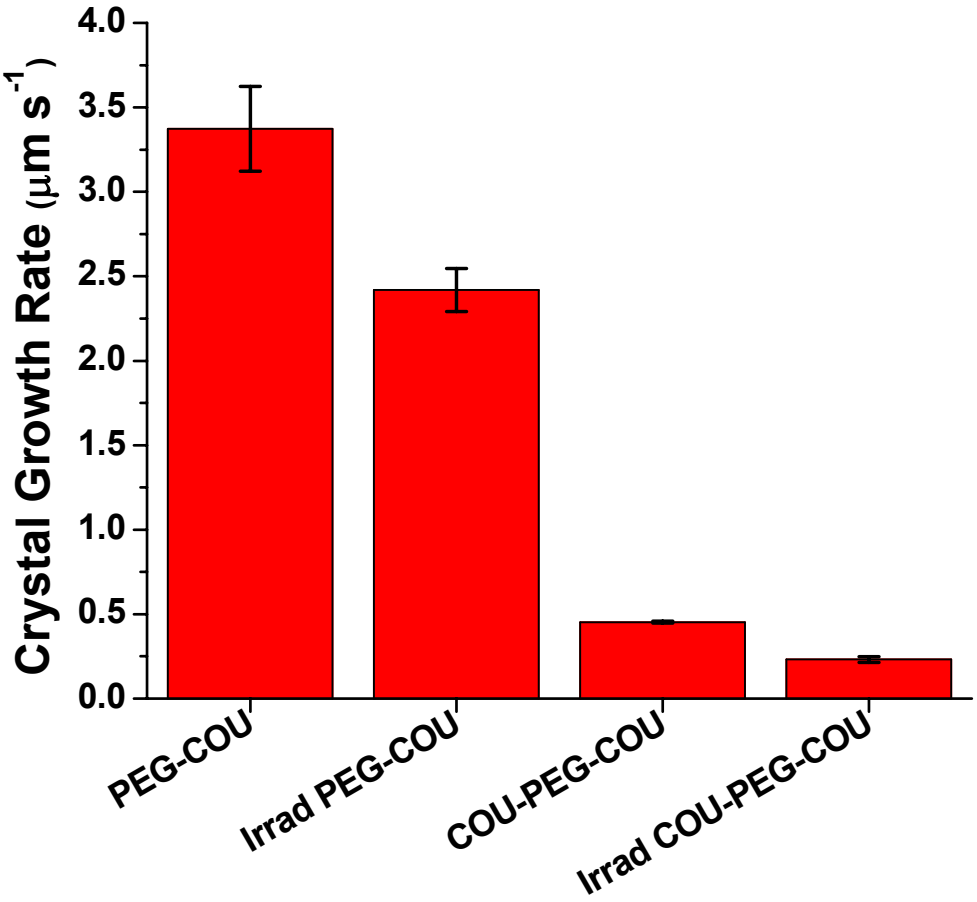

Figure 5-2. The effect of UVA irradiation exposure (110 J cm^{-2}) on the crystallization radial growth rates.

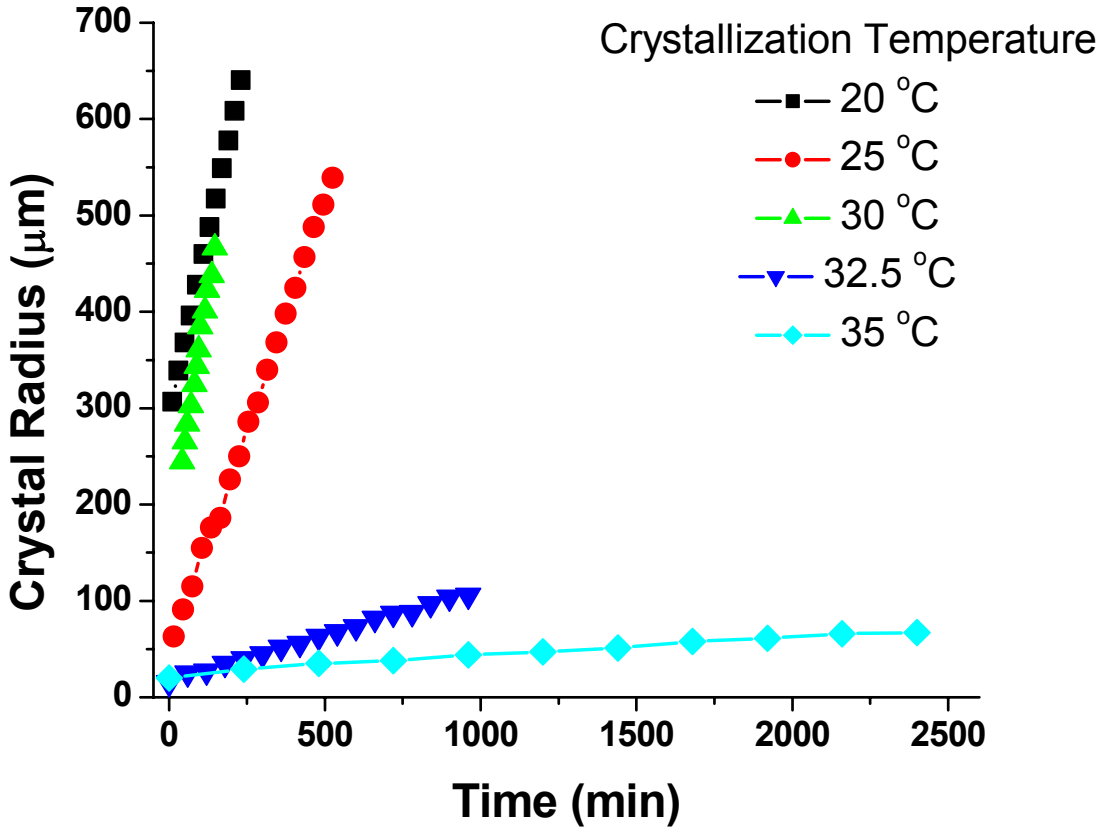

Figure 5-3. The effect of temperature on crystal radius as a function of time for the nonirradiated COU-PEG-COU.

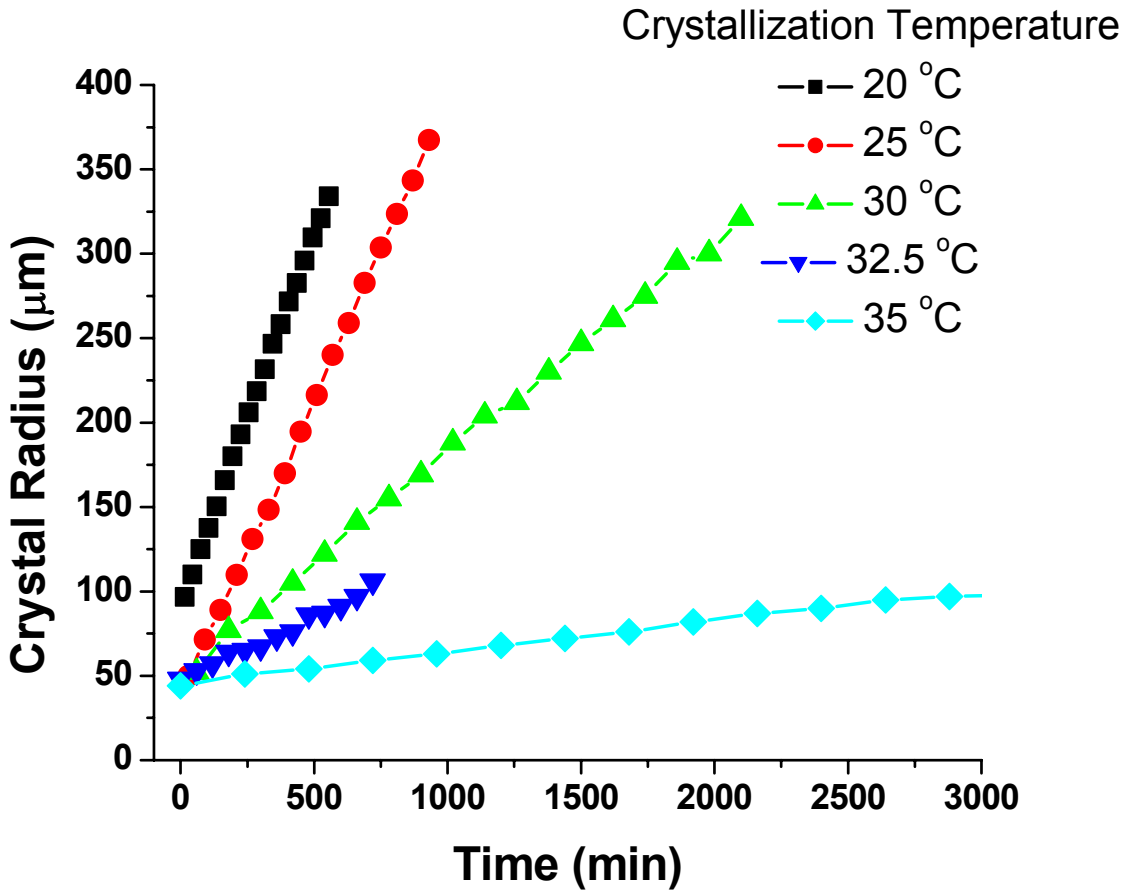

Figure 5-4. The effect of temperature on crystal radius as a function of time for the photo chain-extended COU-PEG-COU.

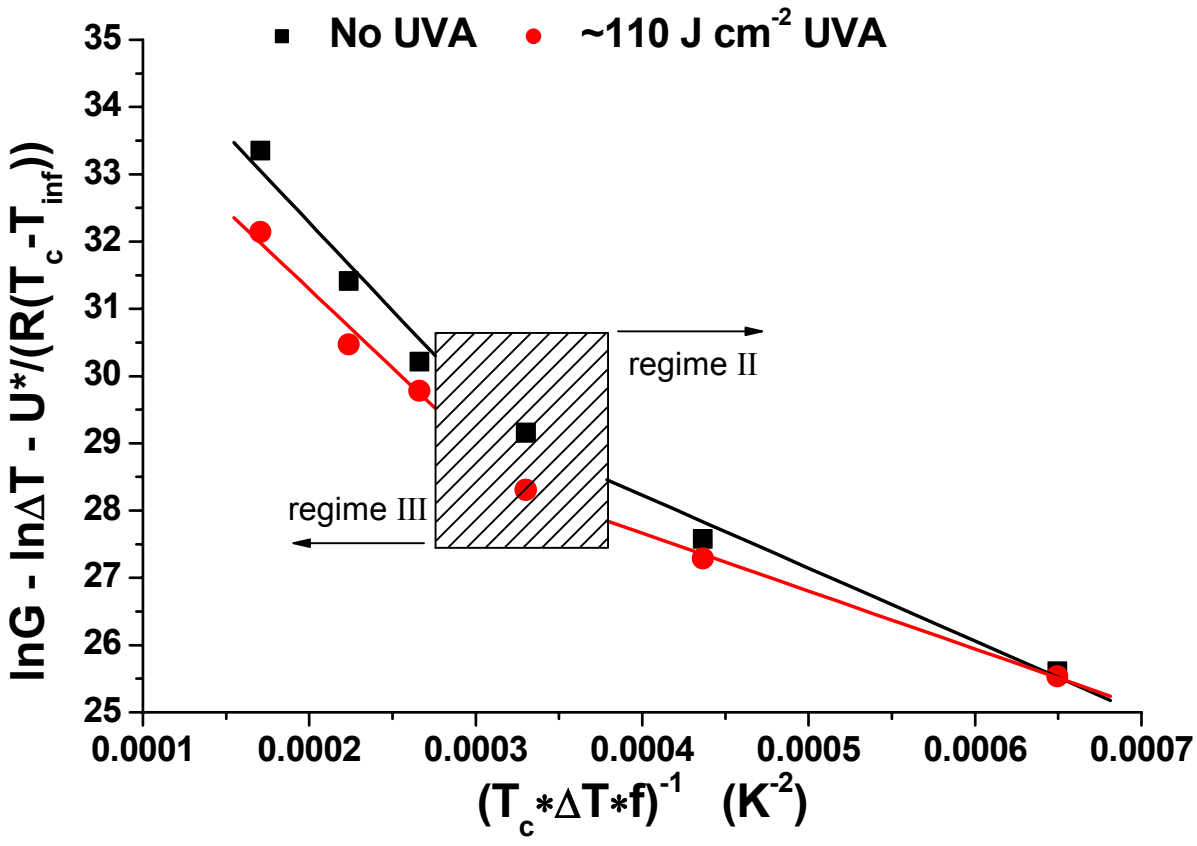

Figure 5-5. The Hoffman-Lauritzen plots for nonirradiated and irradiated COU-PEG-COU.

where *i* represents the crystallization regime, *R* is the gas constant, ΔT is the degree of supercooling (T_m – T), T_c is the crystallization temperature, U^* is the activation energy required for chain movement through its melt reptation tube, T_∞ is the temperature at which reptation ceases and *f* is a temperature correction factor (Table 5-2 lists literature values of the constants used in this analysis). Taking the log of both sides provides (Equation 5-2):

Equation 5-2. $$\ln G - \ln \Delta T + \frac{U^*}{R(T_c - T_\infty)} = \ln G_o - \frac{K_g}{fT_c \Delta T}$$

Once plotted, the data shows two crystallization regimes with a transition zone separating the regimes typical of PEO crystallization studies. A linear regression of the data provided insight to the nucleation rate and the surface and fold energies of the COU-PEG-COU. The nucleation constant for each crystallization regime is $K_g(i)$ (Equation 5-3):

Equation 5-3. $$K_g(i) = \frac{na_0 \sigma \sigma_e T_m^0}{\Delta H_f k}$$

where σ is the lateral surface energy, σ_e is the fold surface energy, *k* is Boltzmann's constant, *n* is a constant for each regime of crystallization (*n* = 4 for regime I and III and *n* = 2 for regime II), T_m^0 is the equilibrium melt temperature, a_0 is the molecular width, and ΔH_f is the heat of fusion per crystal unit volume.[214,414] It is important to note that the equilibrium melting temperature used in this analysis was measured via optical microscopy (40 °C). While this is

Constant	Value
U*	29.3 kJ mol^{-1}
T_∞	T_g - 30
ΔH_f	2.13×10^8 J m^{-3}
A	1.72×10^{-19} m^2
a_0	4.55 Å

Table 5-2. Values for constants used in crystallization growth rate analysis.[412,414]

not an equilibrium measurement, variations of +/- 5 °C had little effect on the results. The values for K_g, $\sigma\sigma_e$, q (the work of chain folding) and the ratio of K_g in the 3rd regime to K_g in the 2nd regime are listed in Table 5-3. The fold surface free energy (σ_e) was calculated by first solving for σ, where $\sigma = 0.1 * a_0 \Delta H_f$ then substituting the value for σ into Equation 5-3.[412,414] The energy per fold (q) was determined from $\sigma_e = q/2A$ where A is the cross-sectional area of the chain.

The calculated values of the thermodynamic parameters, listed in Table 5-3, are similar to those published in the literature.[409,410,412,415,419] This was somewhat surprising as the published research was conducted on ideal PEO or PEG fractions, i.e., narrow molecular weight distributions. In this study, even the non-irradiated sample had a small amount of chain-extended chains (M_w/M_n = 1.17), while the irradiated sample had a molecular weight distribution of 2.75. In addition, the coumarin dimers that link the chain-extended chains together were thought to greatly influence the molecular mobility of the chains as they pack into the crystals. These factors probably led to the ratios K_g (III): K_g (II) listed in Table 5-3, which vary from the theoretical and experimentally verified value of 2.0.[409,410,412,414,419] Another observation of note was the variation in the values of q. While, the values for q in regime III are greater than those for regime II, as is noted in the literature, the difference in the values for the irradiated and nonirradiated samples illustrated an interesting trend. The values of q for the irradiated samples are less than those for the nonirradiated samples. As q is a measure of the amount of energy required to fold a chain, the data suggests that the irradiated chains are easier to fold than the nonirradiated chains.

UVA Irradiation	Regime	K_g (K^{-2})	$\sigma\sigma_e$ (J^2 m^{-4})	σ_e (J m^{-2})	q (J $fold^{-1}$)	K_g(III)/ K_g(II)
None	III	26,000	1.4×10^{-4}	1.5×10^{-2}	5.3×10^{-21}	2.4
	II	11,000	1.1×10^{-4}	1.3×10^{-2}	4.4×10^{-21}	
110 J cm^{-2}	III	23,000	1.2×10^{-4}	1.4×10^{-2}	4.7×10^{-21}	2.7
	II	8,700	9.0×10^{-5}	1.0×10^{-2}	3.5×10^{-21}	

Table 5-3. Kinetic data for COU-PEG-COU before and after exposure to 110 J cm^{-2} UVA irradiation.

5.5 CONCLUSIONS

Optical microscopy was used to measure the growth of coumarin-functionalized PEG crystals. The addition of a single coumarin endgroup to the end of a PEG monol greatly affected the crystallization kinetics resulting in a reduction in the crystallization rate, with a second coumarin endgroup further decreasing the rate. Irradiation and subsequent chain-extension of the coumarin-functionalized PEGs also decreased the crystallization rate compared to the non-irradiated coumarin-functionalized PEGs. A Hoffman-Lauritzen treatment was performed on the coumarin-functionalized PEG diols before and after exposure to UVA light. Both, the irradiated and non-irradiated PEGs displayed two of the three crystallization regimes (regimes II and III). No crystallization was observed to occur in regime I; this was an expected result as researchers typically seed the nucleation experiments in order to observe regime I crystallization. The values of the kinetic data were similar to those published in the literature, with only the ratios of the nucleation constants varying greatly from the theoretical and published values. This was surprising as coumarin-functionalized PEG diol used in this study had a much broader molecular weight distribution than those used in other studies.

5.6 ACKNOWLEDGMENTS

The authors gratefully acknowledge financial support from the Avery Dennison Chemical Company, the Center for Adhesive and Sealant Science (CASS) at Virginia Tech, and the Adhesive and Sealant Council Education Foundation. This material is based upon work supported in part by the U.S.

Army Research Laboratory and the U.S. Army Research Office under grant number DAAD19-02-1-0275 Macromolecular Architecture for Performance (MAP) MURI.

CHAPTER 6 EFFECT OF GLASS TRANSITION TEMPERATURE AND ALKYL ESTER SIDE GROUP ON PHOTODIMERIZATION OF COUMARIN-FUNCTIONALIZED POLY(ALKYL ACRYLATES) AND POLY(ALKYL METHACRYLATES)

Scott R. Trenor, Rebecca H. Huyck, Brian J. Love[1] and Timothy E. Long[2]*

[1] Department of Materials Science and Engineering
[2] Department of Chemistry
Virginia Polytechnic Institute and State University
Blacksburg, VA 24061
*To whom all correspondence should be addressed:

telong@vt.edu

6.1 SUMMARY

Coumarin-containing poly(alkyl acrylates) and poly(alkyl methacrylates) were prepared via quantitative side group esterification of hydroxyl-containing acrylic copolymers. The coumarin-modified poly(alkyl acrylates) and poly(alkyl methacrylates) were solution cast into films (1 - 2 μm) and photocrosslinked via the dimerization of the coumarin derivatives with UVA (> 300 nm) light irradiation. The coumarin-modified poly(alkyl acrylates) and poly(alkyl methacrylates) crosslinked upon exposure to UVA light and exhibited a gel fraction between 74 and 99%. The effect of polymer glass transition temperature (T_g) on the photocrosslinking reaction was studied for coumarin-modified poly(alkyl acrylates) and poly(alkyl methacrylates). Although the absolute difference

between T_g and irradiance temperature did not affect the rate or extent of photodimerization reaction, polymers with a T_g greater than the irradiance temperature displayed less reaction than those with a T_g lower than the irradiance temperature. The alkyl ester side groups dictated the final extent of conversion for polymers with a T_g lower than the irradiation temperature. Coumarin-functionalized poly(2-ethylhexyl methacrylate-*co*-2-hydroxyethyl acrylate) was further examined to study the effect of light intensity and irradiation time (reciprocity law) on the photodimerization of the coumarin-containing polymers. For the intensities studied, the polymers followed the Bunsen-Roscoe reciprocity law.

Keywords: photoreactive effects, coumarin, UV-Vis spectroscopy, glass transition, reciprocity

6.2 INTRODUCTION

7-Hydroxycoumarin (Figure 4-1) and various derivatives are known to undergo a photodimerization ($2\pi+2\pi$ cycloaddition) reaction when irradiated in the ultraviolet-A (UVA) region of the electromagnetic spectrum.[195,212,320,321,420] The resulting photodimerized coumarin is cleavable when subsequently irradiated at wavelengths below 290 nm (Figure 4-1), but neither reaction is thermally allowed. The photodimerized entities are thermally stable above 300 °C, and have reported melting temperatures between 170 and 200 °C depending on their configuration.[195,214,220,224,319]

A number of researchers have studied the use of coumarin moieties in polymers, including the early efforts of Delzenne and Laridon, who first utilized

coumarin groups to photocrosslink polymers in the mid-1960's.[208,420] The photocrosslinking of coumarin-functionalized poly(hydroxyethers) and hydrolyzed poly(vinyl butyral) was evaluated for the formation of insoluble networks. Later, Ramamurthy et al. studied the dimerization of many coumarin derivatives and less than 0.5 nm separation of the 3,4-olefin in the coumarin derivative was necessary for two coumarin moieties to dimerize.[421] Thus, efficient coumarin dimerization required sufficient molecular mobility.

Since these initial studies, researchers have confirmed the use of coumarin groups to photoreversibly crosslink or chain extend a variety of polymers.[147,199,200,202,359,360] In addition to the photodimerization reaction, researchers have also utilized the photocleavage of coumarin dimers in the synthesis of photodegradable polyamides.[326,327] Recent efforts have demonstrated the efficacy of coumarin and other photoactive groups to photoreversibly crosslink and chain extend oligomers. For example, the photoreversible chain extension of coumarin-endcapped PEG monols and diols were recently investigated in our laboratories.[361] The coumarin modified poly(ethylene glycol) monols and diols were chain extended via the dimerization of the coumarin derivatives with UVA light irradiation. The coumarin-endcapped PEG diols doubled in molecular weight, and the molecular weight distribution increased from 1.17 to 2.75 upon exposure to UVA light at 110 J cm^{-2}. The chain extended PEG diols were subsequently converted to the original molecular weight via the photocleavage reaction of the coumarin dimer upon exposure to less than 2 J cm^{-2} of irradiation at 254 nm.

Ngai and Wu recently used laser light scattering to study the molecular dynamics of poly(methyl methacrylate-*co*-7-acryloyloxy-4-methylcoumarin) , which was crosslinked in solution.[404] Irradiation in concentrated solutions (> 5 wt% polymer) led to the formation of homogenous gels, whereas only finite clusters of crosslinked polymer were formed in more dilute systems. Furthermore, the molecular dynamics of the polymer in solution revealed that slow relaxation modes became slower during the transition from the semidilute regime to the fully crosslinked polymer.[422] This study was the first to suggest that the slow mode relaxation was attributed to thermally agitated density fluctuations.

A number of factors influence successful polymer modification reaction including polymer concentration in solution, steric effects, and others.[96] For example, bulkier alkyl ester side chains sterically hinder nucleophilic attack of the pendent esters on a polymer chain. Another critical factor is polymer concentration in solution and solvent choice. In poor solvents, the concentration of reactive centers is higher in the collapsed polymer coils compared to the bulk polymer solution.[96] Since there is a decreased concentration of polymer outside the collapsed coils, the reaction rate outside the coils is zero, leading to a slower than average reaction rate. Finally, since the compositional distribution is random, all chains are not compositionally equivalent. Therefore, individual polymer chains may lack the desired reactive groups prior to functionalization, and the functionalization reaction may not occur on a particular chain. Thus, after the attempted functionalization, both circumstances lead to polymer chains

that lack the desired functional group and are inseparable from the bulk of the functionalized polymer.

In the early 1860s, Bunsen and Roscoe concluded that the extent of a photochemical reaction is only dependent on the total energy absorbed and not the individual components, irradiation time and intensity (Bunsen-Roscoe Reciprocity Law).[423-427] Ideally, the specific combination of energy intensity and time used to produce the required number of photons necessary to form an image (or cause a photochemical reaction) should not affect the resulting image.[402] Halm later developed a graphical method for presenting reciprocity data which includes an example of reciprocity law failure (Figure 6-1).[424,427] The abscissa in Figure 6-1 is commonly referred to as image density, since the origin of the reciprocity law is based on the development of photographic and radiographic films. However, since its conception, the law has been applied to a number of systems ranging from erythema to polymer photodegradation.[424] Adherence to the reciprocity law (dependence on total energy absorbed only) is plotted as an ideal horizontal line, whereas failure is depicted as non-linearity. The degree of failure is determined as the deviation in the slope from the horizontal line.

When applied to photoinitiated polymerization, the polymerization kinetics greatly influence adherence to the reciprocity law. Zumbrum studied photopolymerization of multifunctional acrylates and methacrylates via FTIR and reported deviation from the reciprocity law for these systems.[402] The failure, in

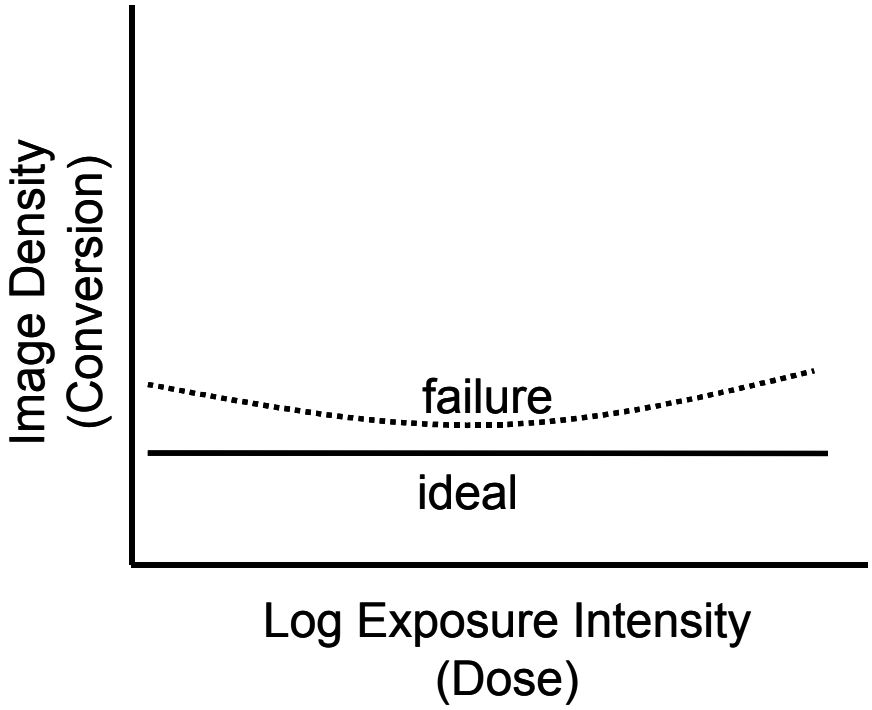

Figure 6-1. Halm's graphical method for determination of reciprocity law adherence.[424,427]

this case, was due in part to the photopolymerization reaction kinetics, as the theoretical photoinitated polymerization rate depends on intensity to the ½ power.[96,97,402] Experimentally, the reciprocity plot for Zumbrum's systems produced a sigmoidal curve, with combinations of low intensity and long irradiation times leading to low conversions. Conversely, combinations of high intensity short irradiation times lead to high conversions. Nevertheless, the reciprocity law is typically followed in the reported literature. In fact, in a recent review of the literature involving the reciprocity law, 62% of the 262 materials studied followed the reciprocity law.[424]

This report describes the effect of molecular mobility in terms of the polymer glass transition temperature (T_g) on the ability to crosslink coumarin-functionalized poly(alkyl acrylates) and poly(alkyl methacrylates). The effect of T_g and alkyl ester side chain composition on the dimerization of coumarin side chains is described. Coumarin groups were coupled with acrylic and methacrylic base copolymers via esterification of 2-hydroxyethyl acrylate side chains. The coumarin-modified poly(alkyl acrylates) and poly(alkyl methacrylates) were photocrosslinked via the coumarin photodimerization reaction upon irradiation in the UVA region. UV-Vis spectroscopy, differential scanning calorimetry (DSC), and gel fraction measurements were employed to monitor changes in the chemical structure of the coumarin-modified polymers.

6.3 EXPERIMENTAL SECTION

6.3.1 Materials.

7-Hydroxycoumarin, ethyl bromoacetate, 2,2'-azobisisobutyronitrile (AIBN) and thionyl chloride were purchased from Sigma Aldrich Chemical Company and used as received. Avery Dennison Chemical Company kindly provided the *n*-butyl acrylate (*n*-BA), 2-hydroxyethyl acrylate (HEA), methyl acrylate (MA), and 2-ethylhexyl acrylate (EHA), which were passed through a neutral alumina column to remove radical inhibitors. *n*-Butyl methacrylate (*n*-BMA), methyl methacrylate (MMA), 2-ethylhexyl methacrylate (EHMA), and *t*-butyl acrylate (*t*-BA) were purchased from Aldrich and passed through a neutral alumina column to remove radical inhibitors. All other solvents and reagents were purchased from commercial sources and were used without any further purification unless otherwise noted. THF was distilled from sodium/benzophenone under a nitrogen atmosphere prior to esterification.

6.3.2 Instrumentation.

^{1}H NMR spectra were recorded using either a Varian Unity 400 MHz or a Varian Inova 400 MHz spectrometer at 25 °C in $CDCl_3$. UV-Vis spectroscopy was performed using an Analytical Instrument Systems Inc. spectrometer equipped with fiber optic light guides, a DT1000CE light source, and an Ocean Optics USB2000 UV-Vis detector. Molecular weights were determined at 40 °C in chloroform or THF (HPLC grade) at 1 mL min^{-1} using polystyrene standards on a Waters 707 Autosampler equipped with 3 in-line PLgel 5 μm MIXED-C columns, a Waters 410 refractive index detector and an in-line Wyatt Technology

Corp. miniDAWN® multiple angle laser light scattering (MALLS) detector. DSC was performed with a Perkin Elmer Pyris 1 at a heating rate of 20 °C min^{-1} under nitrogen. The Tg was measured during the second heat using the midpoint of the transition. Irradiation temperature was measured with a Raytek Thermalert TX optical pyrometer. Homogenous films of 1 to 2 μm thickness were solvent cast from chloroform onto quartz microscope slides and drawn in a controlled manner using a doctor blade. Film thickness was measured using microcalipers.

6.3.3 UV Irradiation.

UVA irradiation was accomplished using a F300s series microwave powered electrodeless lamp source coupled with a LC-6B bench top conveyer manufactured by Fusion UV Systems, Inc. A “D” bulb (linear power output of 80 W cm^{-1}) was used with a glass filter, efficiently blocking wavelengths below 300 nm. The belt speed was set at 3 m min^{-1} unless otherwise noted. A fused silica, Tech Spec™ linear stepped neutral density filter (Edmund Optics) was used as an inline mask controlling light intensity during UVA irradiation of the polymers. The filter ranged from an optical density of 0 (100% transmission) to 2.0 (1% transmission) in 11 discrete steps and provided a combinatorial methodology to study reciprocity effects. UVA irradiance and effective energy density were measured before and after each sample set with an EIT UV Power Puck radiometer. Extent of photoreaction was monitored using UV-Vis spectroscopy. The temperature of the polymer samples in the Fusion system during the irradiation treatment ranged from 30 to 40 °C.

6.3.4 **Synthesis of Coumarin Precursors.**

The related synthesis of the 7-hydroxycoumarin derivatives is published elsewhere.[147,148] Briefly, 7-hydroxycoumarin (10.0 g, 61.6 mmol) was combined with ethyl bromoacetate (12.4 g, 73.9 mmol), potassium carbonate (12.5 g, 90 mmol), and acetone (450 mL) and refluxed for three hours. After salt filtration, the product was recrystallized from ethanol with an isolated yield of 90%. The product (7-ethoxycarbonylmethoxycoumarin) (7.05 g, 28.2 mmol) was subsequently hydrolyzed for 18 hours in a mixture of 1,4-dioxane (280 mL), water (400 mL) and sodium hydroxide (15.8 g, 395 mmol). The resulting product (7-carboxymethoxycoumarin) was extracted with a 3:1 chloroform/methanol mixture and recrystallized from ethanol with an isolated yield of 85%. The 7-carboxymethoxycoumarin (2.44 g, 11 mmol) was refluxed for three hours in thionyl chloride (20.0 mL 277 mmol) providing 7-chlorocarbonylmethoxycoumarin at a yield greater than 98%. Unreacted thionyl chloride was quantitatively removed under reduced pressure. ^{1}H NMR (400 MHz, $CDCl_3$, ppm): 7.65 (d, 1H, CH), 7.43 (d, 1H, Ar H), 6.86 (d, 1H, Ar H), 6.80 (s, 1H, Ar H), 6.31 (d, 1H, CH), 5.02 (s, 2H, CH_2).

6.3.5 **Synthesis of 10 mol% 2-Hydroxyethyl Acrylate Copolymers.**

The synthesis of a typical acrylate copolymer is described. The *n*-BA (10.0 g, 78.0 mmol) and 2-HEA (1.0 g, 8.61 mmol) monomers were added to a 100 mL round-bottomed flask with a magnetic stir bar. The reaction mixture was then diluted with ethyl acetate (49 mL, 80 vol%). Finally, the initiator, AIBN (22.3 mg,

0.2 wt%), was added to the reaction vessel. The reaction mixture equipped with a water condenser, sparged with nitrogen for 10 minutes, then placed in a 70 °C oil bath with a magnetic stirrer and allowed to polymerize for 24 h. The polymer was precipitated into approximately 600 mL 4:1 methanol:water solution. The isolated polymer product was dried in the vacuum oven at 65 °C for 24 h. A similar method was utilized to synthesize the series of copolymers (Table 6-1).

6.3.6 **Copolymer Modification with 7-Chlorocarbonylmethoxycoumarin.**

A typical coumarin modification of acrylic copolymers is described. Poly(*n*-BA-*co*-HEA) (3.60 g) was dissolved in 35 mL distilled THF then combined with triethylamine (0.625 g, 6.18 mmol) and stirred under nitrogen in a 100 mL round-bottomed flask. Triethylamine was added at a 25 mol% excess compared to the 7-chlorocarbonylmethoxycoumarin. 7-Chlorocarbonylmethoxycoumarin (1.19 g, 5.0 mmol) was dissolved in 12 mL distilled THF and added dropwise via an addition funnel to the poly(*n*-BA-*co*-HEA) and triethylamine mixture. The addition funnel was then rinsed with an additional 10 mL distilled THF. The reaction mixture was stirred at 0 °C overnight under a nitrogen blanket with the reaction vessel covered in aluminum foil to avoid ambient photoreactions. After filtration of the salt, the resulting polymer was precipitated into approximately 600 mL 4:1 methanol:water solution, stored in an aluminum foil covered 60 mL bottle, and dried in the vacuum over at 65 °C for 24 h. The purified yield was 74%.

Monomer	Charged mol% Monomer:HEA	^{1}H NMR mol% Monomer:HEA	M_w (g mol^{-1})	M_w/M_n
n-BA	90:10	89:11	273,000	3.65
n-BMA	90:10	89:11	163,000	1.82
t-BA	90:10	89:11	221,000	2.47
MA	90:10	90:10	390,000	2.50
MMA	90:10	90:10	138,000	1.63
EHA	90:10	88:12	248,000	3.73
EHMA	90:10	87:13	176,000	2.06

Table 6-1. Precursor alkyl acrylate and alkyl methacrylate copolymer compositions and molecular weights.

6.4 RESULTS AND DISCUSSION

6.4.1 Synthesis and Functionalization of Poly(alkyl acrylates) and Poly(alkyl methacrylates).

Polymerization of all seven acrylic or methacrylic monomers afforded the desired high molecular weights and molecular weight distributions typical of free radical polymerization (Table 6-1). Monomers were chosen to cover a wide range of glass transition temperatures (T_g), with copolymer T_g values after coumarin functionalization ranging from -54 °C to 105 °C. Each polymerization reaction was charged with 10 mol% HEA and ^{1}H NMR spectroscopy was utilized to confirm the copolymer composition (Table 6-1). Molar compositions were determined utilizing the ^{1}H NMR resonances due to the methyl group at the end of the aliphatic side chain of the monomer (1.0 ppm for *n*-BA) and the protons α to the hydroxyl group on the HEA (3.8 ppm).

As expected, functionalization of the acrylic copolymers using the coumarin acid chloride derivative depended on the selection of the monomer side group due to steric hindrance (Table 6-2). For example, a greater molar excess of coumarin acid chloride was required at identical reaction conditions to functionalize 5 mol% of the HEA when using monomers with the bulkier side groups. The poly(EHA) and poly(EHMA) copolymers required more than a 10-fold molar excess of coumarin acid chloride whereas the copolymers with smaller side groups such as poly(MA) and poly(MMA) required only 3-fold molar excess. The acid chloride was synthesized less than three days prior to the functionalization reaction to ensure that the reagents were fresh and dry.

Base Polymer	HEA:Coumarin molar ratio	Final Conc. HEA (mol%)	Final coumarin functionality (mol%)	T_g (°C)
EHA	1:10	8.0	4.0	-54
n-BA	1:3.5	7.0	4.0	-33
EHMA	1:12	6.0	7.0	3
MA	1:3	5.0	5.0	25
n-BMA	1:5	6.0	5.0	32
t-BA	1:5	6.0	4.0	51
MMA	1:3	5.0	5.0	105

Table 6-2. HEA:Coumarin ratios utilized to functionalize the poly(alkyl acrylates) and poly(alkyl methacrylates) and the final compositions and T_gs of the coumarin-functionalized copolymers.

The extent of copolymer coumarin modification was determined using ^{1}H NMR spectroscopy and resulted in 5.0 - 7.0 mol% coumarin functionality (Table 6-2). The T_g of each of the functionalized polymers is also shown in Table 6-2. The photodimerization of the coumarin-functionalized copolymers was expected to depend on the T_g; the higher T_g polymers (i.e., poly(MMA) and poly(*t*-BA)) were expected to be more difficult to crosslink than the lower T_g polymers due to the restricted chain mobility.

6.4.2 **UV Irradiation of Coumarin-Modified Copolymers.**

Polymer films were solvent cast onto quartz slides for the irradiation experiments. Three samples for each coumarin-functionalized polymer were irradiated and averaged to confirm UV-Vis reproducibility. The λ_{Max} absorbance near 325 nm in the UV-Vis absorbance spectrum of the coumarin-functionalized *n*-BA polymer is typical of 7-hydroxycoumarin containing polymers (Figure 6-2).[201,202,361,420] The reduced intensity of the coumarin double bond absorbance at 325 nm was used to measure the extent of dimerization. As the unsaturated coumarin moieties were converted to cyclobutane dimers (Figure 4-1), the extent of coumarin side group conjugation decreased, resulting in a decrease in absorbance at 325 nm and an increase at 248 nm. The intensity decrease was proportional to the consumption of the 3,4-olefin in the coumarin derivative. Figure 6-2 shows the typical decrease in absorbance (photocrosslinking of the coumarin functionalized poly(EHMA)) upon irradiation above 300 nm (UVA intensity ~ 2.2 J cm^{-2} min^{-1}).

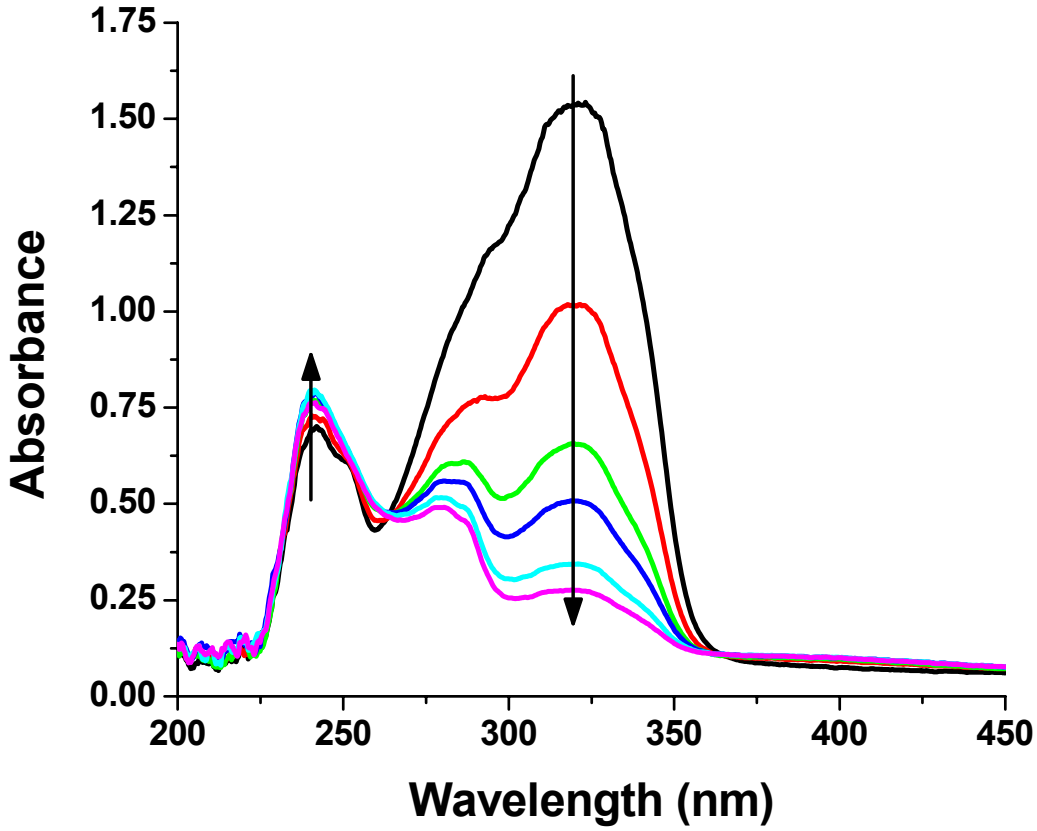

Figure 6-2. Typical UV absorbance of a coumarin-containing polymer (in this case, poly(EHMA)). Arrows indicate the change in absorbance due to coumarin dimerization with UVA irradiation.

The UV-Vis absorbance profiles for the coumarin-functionalized polymers studied are shown in Figure 6-3. As samples were irradiated, the absorbance at λ_{Max} initially decreased and then reached a plateau as the maximum coumarin consumption was approached. The sample temperature reached 30-40 °C in the Fusion system due to infrared heating during sample irradiation, and the absorbance profiles showed two distinct groups of data, polymers with a T_g below the irradiation temperature and polymers with a T_g above the irradiation temperature. The high T_g polymers (T_g = 51 and 105 °C) were irradiated at a temperature below their T_g and therefore consumed much less coumarin in the formation of the cyclobutane ring in the photoreaction due to the limited mobility of the coumarin side groups. The lower T_g functionalized polymers (T_g = -54 to 32 °C) were irradiated at a temperature above T_g, which allowed for increased chain mobility. The increased mobility allowed coumarin moieties to interact more frequently and consequently allowed for increased coumarin photoreaction.

Figure 6-4 shows the final percentage of coumarin groups consumed after exposure to approximately 22 J cm^{-2} of UVA light. The lower T_g polymers exhibited a 47 to 59% decrease in absorbance compared to approximately 17% for the higher T_g polymers. The greatest scatter measured in coumarin consumption occurred for the coumarin-functionalized poly(*n*-BMA), the T_g of which (32 °C) falls in the temperature range of the irradiation treatment (30 to 40 °C). This increased scatter in percent coumarin consumption was due to the presence of polymer chains with decreased mobility when the sample

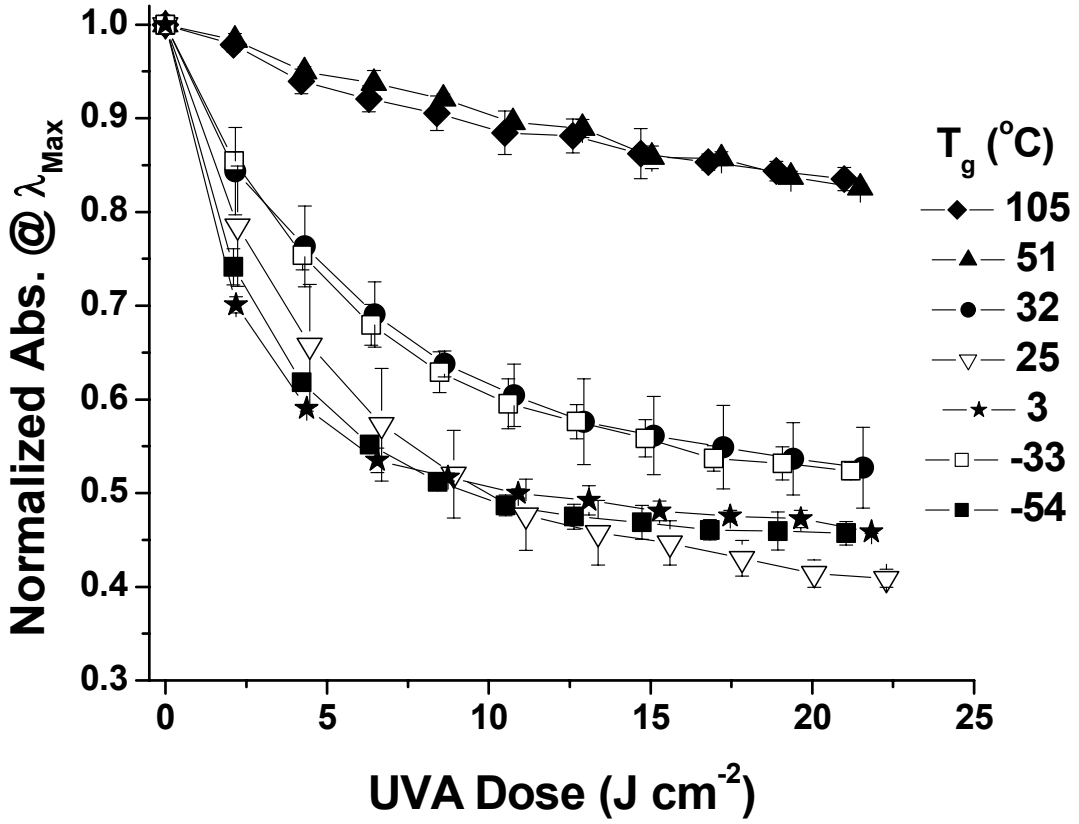

Figure 6-3. Consumption of coumarin groups as a function of irradiation dose and T_g for the coumarin-functionalized poly(alkyl acrylates) and poly(alkyl methacrylates).

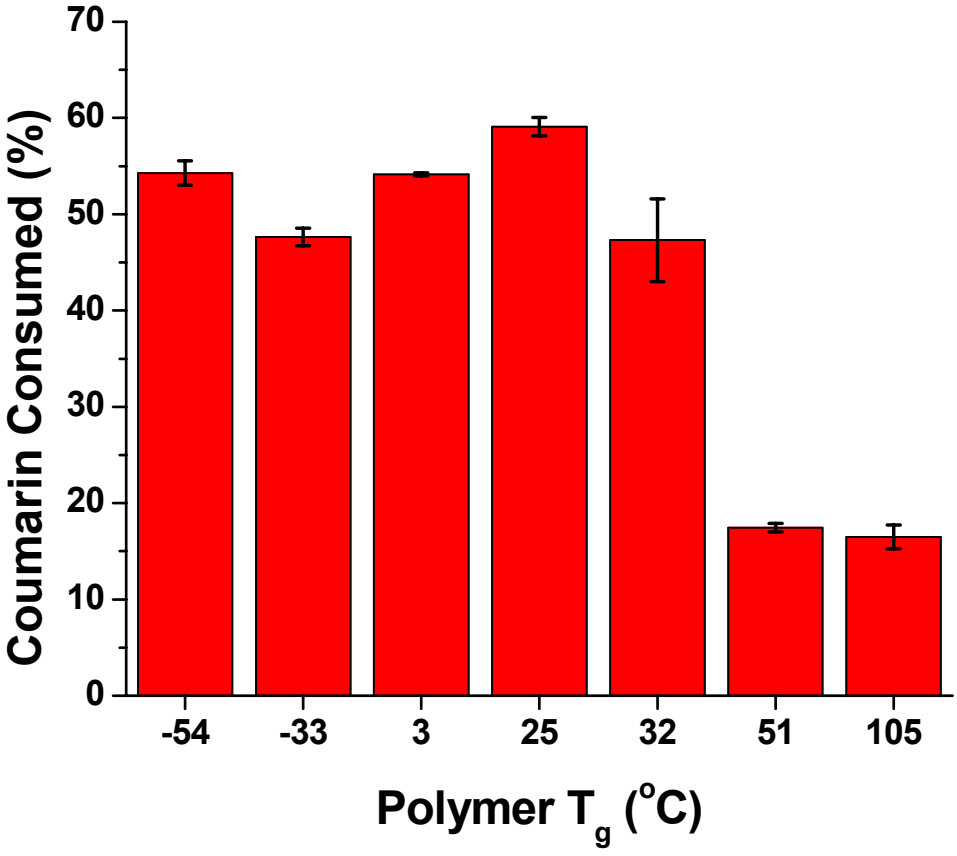

Figure 6-4. Percentage of coumarin consumed after coumarin-functionalized poly(alkyl acrylates) and poly(alkyl methacrylates) of various T_g were exposed to approximately 22 J cm^{-2} of UVA irradiation.

temperature did not uniformly exceed T_g during irradiation. As expected, photocrosslinking of the coumarin-functionalized polymers had an insignificant effect on polymer T_g. Table 6-3 shows the T_gs of the polymer series before and after irradiation with approximately 22 J cm^{-2} of UVA light.

In addition to chain mobility, alkyl ester side group composition was also considered as a possible factor restricting coumarin consumption during photoreaction. The composition of the alkyl ester side group played an important role in the photodimerization of the coumarin molecules (Figure 6-5). The MA based polymer had the highest coumarin consumption at 59%. The poly(2-EHA) and poly(2-EHMA) consumed approximately 54% followed by the poly(*n*-BA) and poly(*n*-BMA) with around 47%. The poly(MMA) and poly(*t*-BA) exhibited the lowest consumption at approximately 16%. The low percentage of coumarin consumption of the poly(MMA) and poly(*t*-BA) are attributed to the low mobility of the high T_g chains, several factors may contribute to the coumarin consumption for the other five polymers.

Pendant group bulkiness was expected to influence the coumarin consumption on irradiation. Indeed, poly(MA) has the pendant group chain and as anticipated, consumed the highest percentage of coumarin. The 2-ethylhexyl pendant group polymers (poly(EHA) and poly(EHMA)), however, showed greater consumption than the *n*-butyl side chain polymers (poly(*n*-BA) and poly(*n*-BMA)) although studies have shown that the 2-ethylhexyl side chain has a larger molar volume than the *n*-butyl side chains.[428,429] It was also evident that the α-methyl

Base polymer	T_g (°C) before irradiation	T_g (°C) after irradiation
EHA	-54	-53
n-BA	-33	-36
EHMA	3	9
MA	25	27
n-BMA	32	31
t-BA	51	49
MMA	105	101

Table 6-3. Glass transition temperatures of coumarin-functionalized poly(alkyl acrylates) and poly(alkyl methacrylates) before and after approximately 22 J cm^{-2} of UVA irradiation.

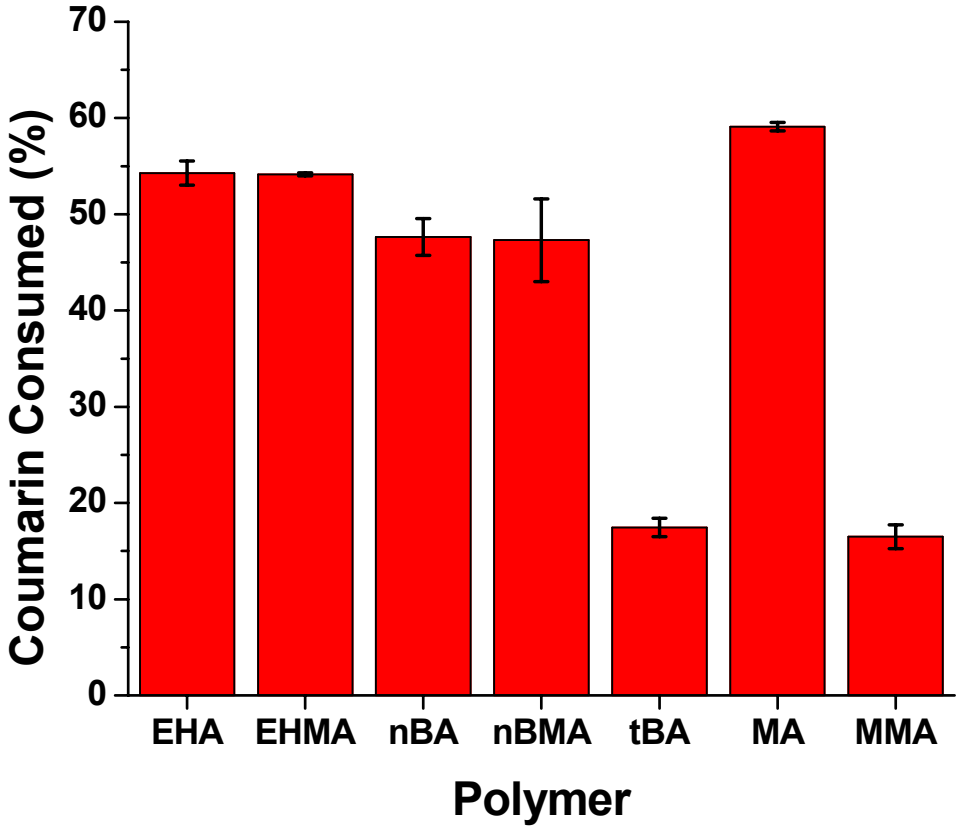

Figure 6-5. Percentage of coumarin consumed after approximately 22 J cm^{-2} of UVA irradiation based on copolymer side group composition.

on the backbone of the methacrylate polymer chains had no effect on the efficiency of the photoreaction as the poly(2-EHA) and poly(2-EHMA) as well as the poly(*n*-BA) and poly(*n*-BMA) consumed comparable percentages of coumarin even though the molar volumes of the poly(alkyl methacrylates) are significantly larger than those of the poly(alkyl acrylates).[428,429] The exception to this trend was the poly(MA) and poly(MMA). In this case, the α-methyl on poly(MMA) copolymer increased the T_g 70 °C, making the difference in coumarin consumption between poly(MA) and poly(MMA) attributable to T_g effects rather than the steric effect of the α-methyl group. Another interesting point in Figure 6 was the final coumarin consumption of poly(*t*-BA). The bulky *t*-butyl group was expected to have the greatest steric effect of all the side groups examined. While the data supported this hypothesis, the high T_g of the poly(*t*-BA) actually dictated the final coumarin consumption, as with the poly(MMA).

Solubility parameters were also investigated as a possible explanation to the observed trend in photoreaction efficiency, as the larger hydrophilic alkyl side chains may repel the more hydrophilic coumarin groups, limiting photodimerization. However, the polymer solubility parameters reported in the literature for polymers studied did not follow the observed trend.[428,430] While the specific gravity of the individual may also affect the rate and extent of conversion, it was not taken into consideration in this study.

The effect of side group composition was also studied using gel fraction measurements (Figure 6-6). A photocrosslinked polymer becomes insoluble

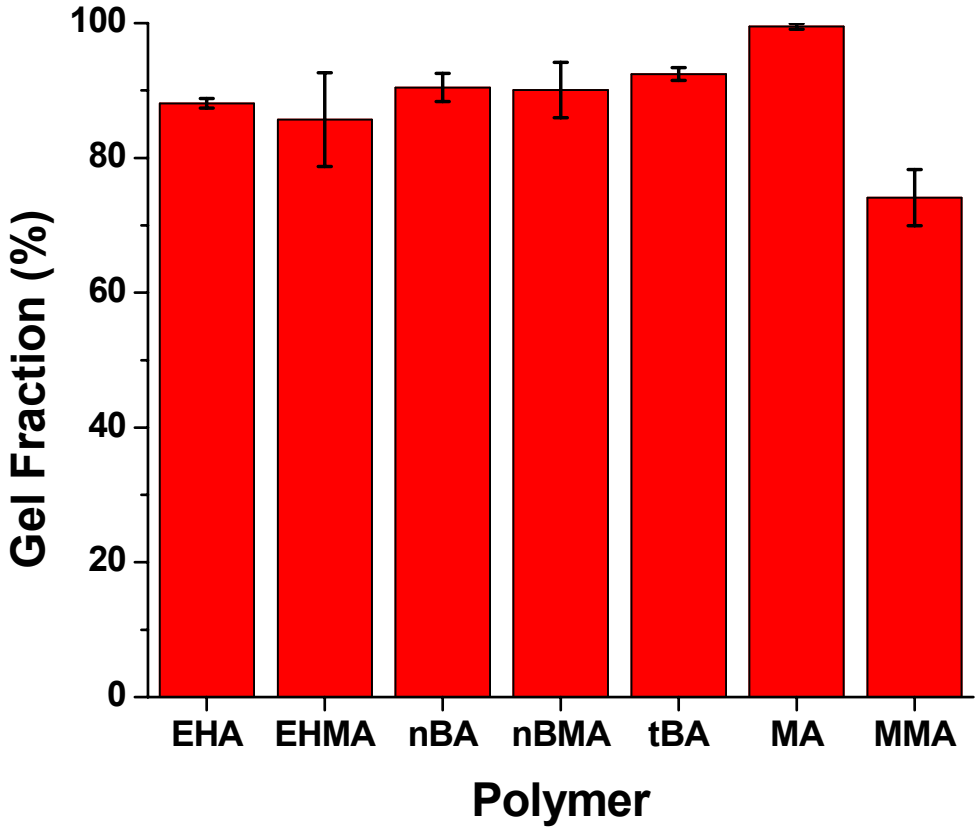

Figure 6-6. Gel fraction after approximately 22 J cm^{-2} of UVA irradiation based on copolymer side group composition.

after irradiation, forming a mixture of an insoluble gel and any remaining uncrosslinked product. Since only a few photoreactions per chain are necessary to form a crosslinked product, high gel fractions were expected.[95,159] Regardless of T_g, all seven of the coumarin-functionalized poly(alkyl acrylates) and poly(alkyl methacrylates) contained more than 75% gel after exposure to approximately 22 J cm^{-2} of UVA irradiation.

6.5 Reciprocity of Coumarin-functionalized EHMA polymers

The coumarin-functionalized 2-EHMA polymer was further evaluated to determine the effect of light intensity and irradiation time on the consumption of the coumarin groups. Figure 6-7 shows the effect of irradiation time on coumarin dimerization. The samples were placed on the conveyor and repeatedly passed under the UV lamp at approximately 3, 6, and 12 m s^{-1}, corresponding to doses of 2.2, 1.1, and 0.55 J cm^{-2} $pass^{-1}$, respectively. At a total dose of 2.2 J cm^{-2} (1 pass at 3 m s^{-1}, 2 passes at 6 m s^{-1}, and 4 passes at 12 m s^{-1}) the film that received 1.1 J cm^{-2} $pass^{-1}$ displayed a slightly higher percent of coumarin consumed than the other two samples. However, at a total dose of 11 and 22 J cm^{-2}, approximately 52 and 55% of the coumarin, respectively, was consumed in all of the films. This indicates that the extent of coumarin dimerization was independent of the individual doses studied (2.2, 1.1, and 0.55 J cm^{-2} $pass^{-1}$) and suggests reciprocity law adherence.

A neutral density linear step filter was utilized to determine the effect of light intensity on the coumarin dimerization reaction of the functionalized poly(EHMA). The first eight steps of the linear step filter were utilized, affording seven steps of

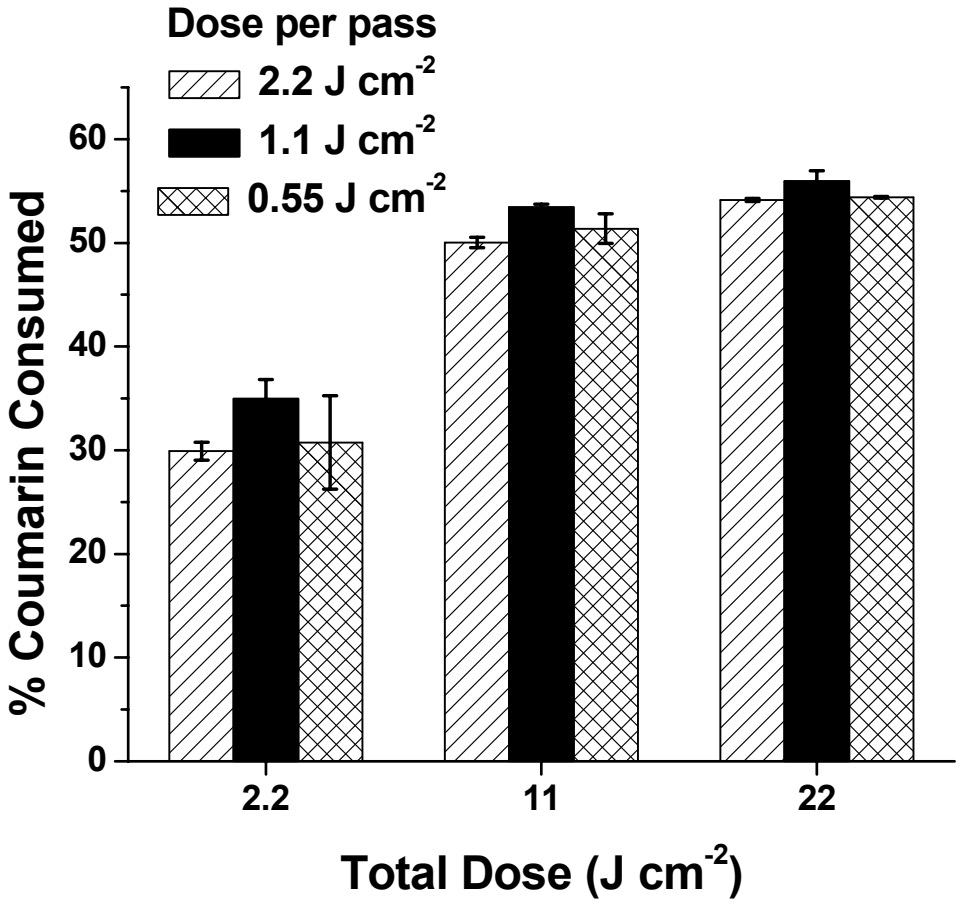

Figure 6-7. Percentage of coumarin consumed in films that received 2.2, 1.1, and 0.55 J cm^{-2} $pass^{-1}$ of UVA irradiation for a total dose of 2.2, 11 and 22 (J cm^{-2}).

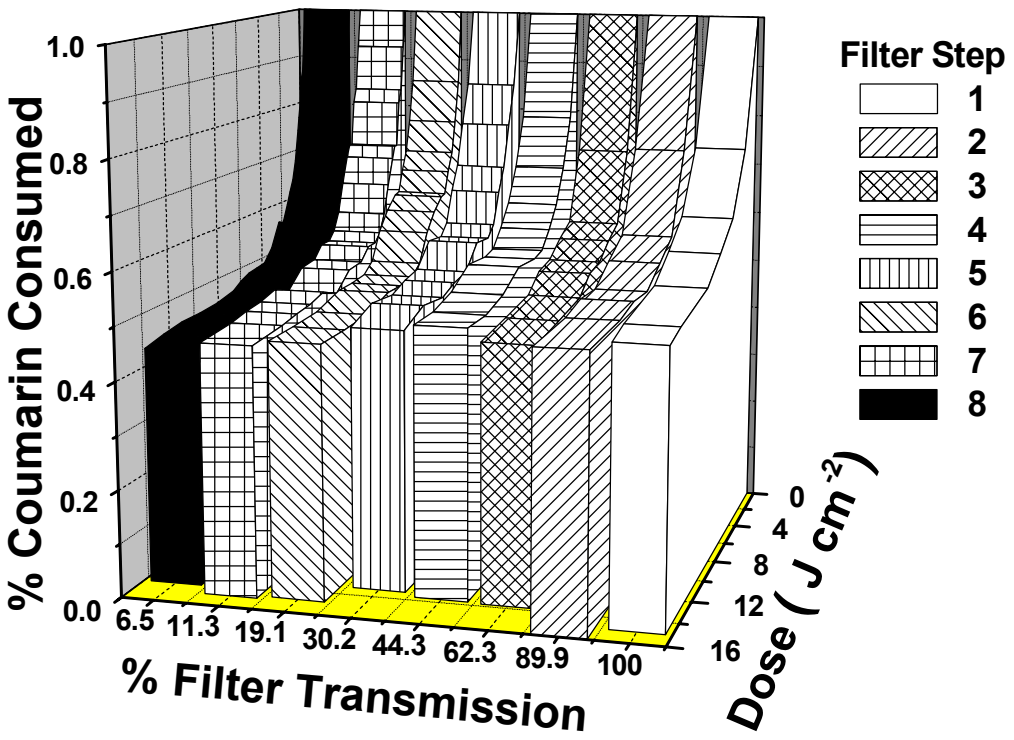

Figure 6-8. Waterfall-type plot of coumarin conversion versus dose utilizing the step filter.

filter transmission ranging from 6 to 100% (optical density between 1.4 and 0). The waterfall-type plot of coumarin conversion versus dose for each of the first seven steps of the filter is shown in Figure 6-8. Each sample displayed a similar reaction profile and thus similar conversions at the same dose (equal doses were achieved with additional passes under the UV lamp). Figure 6-9 shows the reciprocity plot for the coumarin-functionalized poly(EHMA) utilizing Halm's method at three doses (2, 8, and 15 J cm^{-2}).[424,426,427] The plot shows coumarin conversion (plotted on a log scale) versus the log of the exposure intensity. A flat line represents reciprocity law agreement, i.e. conversion is dependent only on the total energy absorbed (dose) and independent of the individual components of dose (intensity and irradiation time). Over the range studied, the polymer was in agreement with the reciprocity law with the exception of the high intensity (100% transmission) 2 J cm^{-2} sample. This deviation from the reciprocity law was attributed to Webb's intermittency effect at high irradiance.[426,431] Webb's intermittency effect is a result of the difference between constant irradiance and a pulsed light source (similar to the method of irradiation utilized in this study).

6.6 CONCLUSIONS

Coumarin-containing polymers with T_gs ranging from –54 to 105 °C were synthesized. UVA irradiation was utilized to crosslink the polymers via the dimerization of the coumarin groups. While the specific T_g was not an important factor in the dimerization of the coumarin groups, the polymer T_g relative to the irradiation temperature dictated the coumarin consumption. Polymers with a T_g

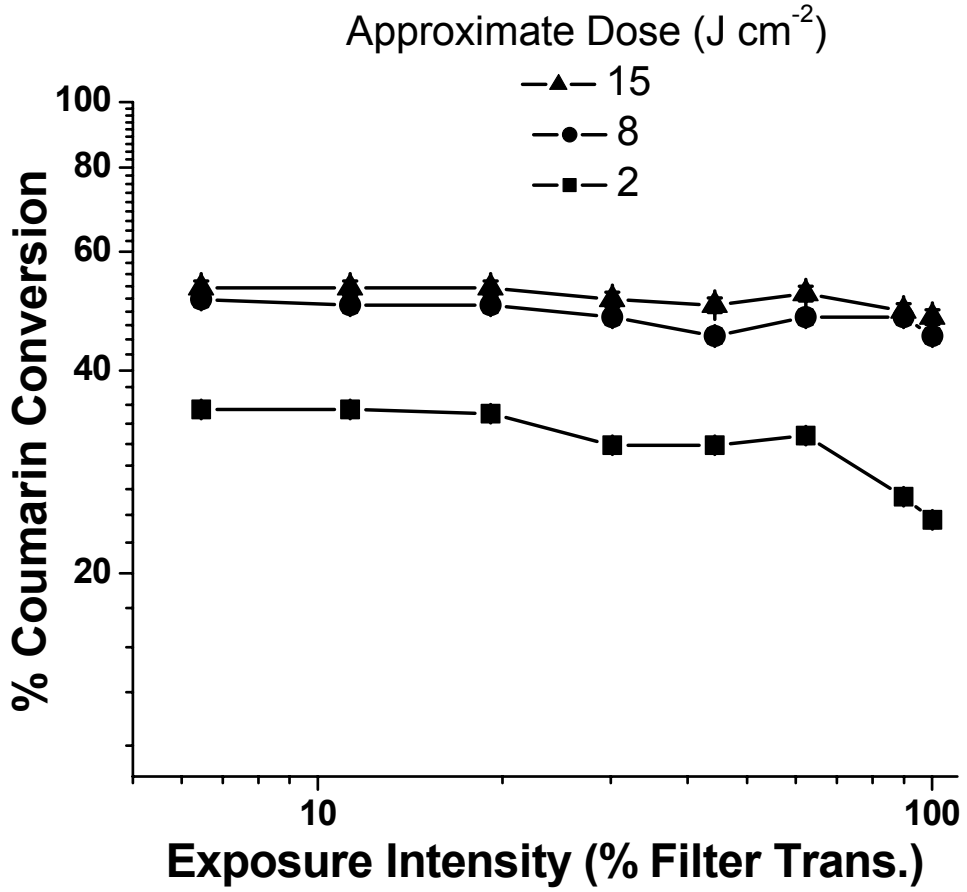

Figure 6-9. Halm-type plot of conversion versus exposure intensity showing reciprocity law agreement at doses of 15 and 8 J cm^{-2}.

above the irradiation temperature dimerized to a lesser extent than polymers with a T_g below the irradiation temperature. Alkyl ester side chain composition affected in coumarin dimerization, with the observed trend a result of a complex combination of factors possibly including molar volume, solubility parameters, etc. The α-methyl on the backbone of the poly(alkyl methacrylates) did not affect dimerization as there was no difference in the coumarin consumption efficiency between the poly(alkyl acrylates) and the poly(alkyl methacrylates) with identical alkyl ester side groups. The coumarin-functionalized acrylates obeyed the Bunsen-Roscoe reciprocity law indicating that the photodimerization of the coumarin groups depends only on the total energy absorbed (total irradiation dose) and is independent on the individual components of dose (irradiation time and intensity). This is an important advantage over photoinitiated crosslinking since low irradiation intensities are overcome with longer irradiation times, unlike photoinitiated reactions since the polymerization rate is dependent on irradiation intensity to the ½ power.

6.7 ACKNOWLEDGMENTS

The authors would like to thank the Center for Adhesive and Sealant Science and the National Science Foundation Summer Undergraduate Research Program at Virginia Tech for funding. This material is based upon work supported in part by the U.S. Army Research Laboratory and the U.S. Army Research Office under grant number DAAD19-02-1-0275 Macromolecular Architecture for Performance (MAP) MURI.

CHAPTER 7 THE DEVELOPMENT OF A LIGHT DEACTIVATABLE PSA VIA PHOTODIMERIZATION

Scott R. Trenor, Timothy E. Long[1], and Brian J. Love[2*]
[1] Department of Chemistry
[2] Department of Materials Science and Engineering
Virginia Polytechnic Institute and State University
Blacksburg, VA 24061
*To whom all correspondence should be addressed:

blove@vt.edu

7.1 ABSTRACT

Model photoreactive PSAs were developed to create a photodeactivatable PSA system. Coumarin-functionalized poly(2-ethylhexyl acrylate-*co*-hydroxyethyl acrylate) was prepared via traditional free radical polymerization followed with quantitative hydroxyl group esterification and studied as a model photoactive pressure sensitive adhesives (PSAs). The polymers were solution cast into films (1 - 2 μm thick for UV-Vis spectroscopy and 18 μm thick for gel fraction and peel strength studies) and photocrosslinked via dimerization of the coumarin derivatives with ultraviolet-A (UVA light irradiation (> 300 nm). UV-Vis spectroscopy indicated that approximately 60% of the coumarin groups photodimerized when exposed to 22 J cm^{-2} of UVA irradiation. The formation of reversible coumarin crosslinks gelled the model PSA and a 97% reduction in peel strength was measured. UVC irradiation was used to photocleave the coumarin dimers, reducing the crosslink density. This reduction in the crosslink density led to a 200% increase in the peel strength compared to the photocrosslinked

adhesive. This reversibility of the coumarin photodimerization and consequent peel strength modulation may provide a mechanism for the repeated use of these model adhesives.

Key words: UV crosslinking, PSA, photodimerization, coumarin

7.2 INTRODUCTION

Crosslinked materials are used as structural materials and hydrogels. Conventional methods for achieving crosslinking are often difficult to control and typically employ chain-like reactions using reactive species such as radicals or cations.[43,432-435] While these reactions often require the use of an initiator and the addition of thermal energy initiate crosslinking, alternative crosslinking methods, most notably photoactive crosslinking developed by Plambeck in the 1950's,[436] have sought to eliminate the need for special initiators and the use of the heat.

Webster and coworkers recently crosslinked acrylic based adhesive systems to create releasable PSA bandages.[24-26,104,437] The methacrylic functional sites were photocrosslinked using halogen lamps and sunlight as irradiation sources with Irgacure 784 as the photoinitiator. Peel strengths were reduced as much as 79% with 2 min of irradiation, and higher light intensities were found to achieve a greater reduction in peel strength as a function of time. [24-26,105-107] While this system was considered a breakthrough in medical grade PSAs, it does exhibit several drawbacks: diffusion of the photoinitiator may potentially lead to

nonhomogenous crosslinking and premature photocrosslinking may occur due to ambient lighting, causing the PSA to lose peel strength and fail prematurely.

Ebe and coworkers developed a releasable pressure-sensitive tape based on a precursor adhesive synthesized from *n*-butyl acrylate and acrylic acid.[438] Their adhesive mixtures leading to a 97% reduction in the peel strength upon UV exposure. The reduction in peel strength was attributed to a 2% volume contraction and an increase in the storage modulus at room temperature, which also led to a shift in the tan δ maximum from below 0 to over 60 °C. A change in fracture mechanism during peel testing from adhesive failure to mostly cohesive failure with UV irradiation was also reported.

Novel functional groups such as coumarin, cinnamate, and maleimides are also used as photocrosslinkers.[94,157-159,188,190,193,232,361,420] These small molecules undergo a $2\pi + 2\pi$ cycloaddition when exposed to UV irradiation and form crosslink points via non-radical radiative pathways negating the need for photoinitiators. 7-Hydroxycoumarin (Figure 1) and various derivatives undergo photodimerization reaction when irradiated in the ultraviolet-A (UVA) region of the electromagnetic spectrum (> 300 nm).[195,212,320,321,420] The dimer, which is composed of a cyclobutane ring, is subsequently cleaved when irradiated at wavelengths shorter than 290 nm (Figure 4-1). One distinct advantage of photocrosslinking via $2\pi + 2\pi$ cycloaddition is that these reactions do not suffer from oxygen inhibition, as do many photoinitated polymerizations.[59,85]

Here, we describe the synthesis of functional acrylic copolymers and the incorporation of photocrosslinking coumarin functionalities via a side group

esterification reaction. The performance of these photocrosslinkable polymers as an adhesive was evaluated before and after irradiation. The effects of light intensity and irradiation time were not included as part of this work as these materials were shown to follow the reciprocity law, i.e., the extent of photoreaction is dependent only on the total dose of irradiation and not the individual components of dose (irradiation intensity and time).[439] The photodimerization reaction was monitored the effects of irradiation on coumarin consumption, gel fraction and 90° peel strength were examined.

7.3 EXPERIMENTAL

7.3.1 Materials.

7-Hydroxycoumarin, ethyl bromoacetate, 2,2'-azobisisobutyronitrile (AIBN) and thionyl chloride were purchased from Sigma Aldrich Chemical Company and used as received. 2-Hydroxyethyl acrylate (HEA), 2-hydroxyethyl methacrylate (HEMA) and 2-ethylhexyl acrylate (EHA) were purchased from Aldrich and passed through a neutral alumina column to remove radical inhibitors. All other solvents and reagents were purchased from commercial sources and used without further purification unless otherwise noted. THF was distilled from sodium/benzophenone under a nitrogen atmosphere prior to polymer esterification reactions.

7.3.2 Instrumentation.

^{1}H NMR spectra were recorded using either a Varian Unity 400 MHz or a Varian Inova 400 MHz spectrometer at 25 °C in $CDCl_3$. UV-Vis spectroscopy was performed using an Analytical Instrument Systems Inc. spectrometer

equipped with fiber optic light guides, a DT1000CE light source, and an Ocean Optics USB2000 UV-Vis detector. Molecular weights were determined at 40 °C in chloroform or THF (HPLC grade) at 1 mL min^{-1} using polystyrene standards on a Waters 707 Autosampler equipped with 3 in-line PLgel 5 μm MIXED-C columns, a Waters 410 refractive index detector and an in-line Wyatt Technology Corp. miniDAWN® multiple angle laser light scattering (MALLS) detector. Differential scanning calorimetry (DSC) was performed with a Perkin Elmer Pyris 1 at a heating rate of 10 °C min^{-1} under nitrogen. The glass transition temperature (T_g) was measured during the second heat using the midpoint of the transition. Irradiation temperature was measured with a Raytek Thermalert TX optical pyrometer. Film thickness was measured using microcalipers or estimated from film coating weight. Two sets of peel samples were prepared for this study. The first set was measured with a TA.XT2i Texture Analyzer (Texture Technologies Corp., Scarsdale, NY/Stable Micro Systems, Godalming, Surrey, UK) utilizing a 90º peel wheel (aluminum) and PET backing materials. The second set of peel samples were tested on an Instron utilizing a 180º peel apparatus.

7.3.3 **UV Irradiation.**

UVA irradiation was accomplished using a F300s series microwave powered electrodeless lamp source coupled with a LC-6B bench top conveyer manufactured by Fusion UV Systems, Inc or an Hg arc lamp manufactured by ThermoOriel. In the Fusion system, “D” bulb (linear power output of 80 W cm^{-1}) was utilized in conjunction with a glass filter, which efficiently blocked

wavelengths below 300 nm. The belt speed was set at 6.1 m min^{-1}, providing a dose of approximately 1.1 J cm^{-2}. UVA irradiance and effective energy density were measured before and after each sample set with an EIT UV Power Puck radiometer. The UVA intensity of the Oriel system was 35 mW cm^{-2}. Exposure time controlled the sample dose. Extent of photoreaction was monitored using UV-Vis spectroscopy. The average of four samples was used to develop the conversion profiles. The temperature in the Fusion system during the irradiation treatment ranged from 30 to 40 °C.

7.3.4 **Synthesis of Coumarin Poly(EHA-*co*-HEA) Precursors.**

The related synthetic methodology of the 7-hydroxycoumarin derivatives is published elsewhere.[147,148] Briefly, 7-hydroxycoumarin (10.0 g, 61.6 mmol) was combined with ethyl bromoacetate (12.4 g, 73.9 mmol), potassium carbonate (12.5 g, 90 mmol), and acetone (450 mL) and refluxed for three hours. After salt filtration, the product was recrystallized from ethanol with an isolated yield of 90%. The product (7-ethoxycarbonylmethoxycoumarin) (7.05 g, 28.2 mmol) was subsequently hydrolyzed for 18 hours in a mixture of 1,4-dioxane (280 mL), water (400 mL) and sodium hydroxide (15.8 g, 395 mmol). The resulting product (7-carboxymethoxycoumarin) was extracted with a 3:1 chloroform/methanol mixture and recrystallized from ethanol with an isolated yield of 85%. The 7-carboxymethoxycoumarin (2.44 g, 11 mmol) was refluxed for three hours in thionyl chloride (20.0 mL 277 mmol) providing 7-chlorocarbonylmethoxycoumarin at a yield greater than 98%. Unreacted thionyl chloride was quantitatively removed under reduced pressure. ^{1}H NMR (400 MHz, $CDCl_3$, ppm): 7.65 (d, 1H,

CH), 7.43 (d, 1H, Ar H), 6.86 (d, 1H, Ar H), 6.80 (s, 1H, Ar H), 6.31 (d, 1H, CH), 5.02 (s, 2H, CH_2).

7.3.5 Synthesis of Precursor Copolymer.

The EHA (20.0 g, 104 mmol) and 2-HEA (3.54 g, 30.4 mmol) monomers were combined and diluted with ethyl acetate (95 mL, 75 vol%) and mixed under constant stirring in a 250 mL round-bottomed flask. Finally, the initiator, AIBN (47.2 mg, 0.2 wt%), was added to the reaction vessel. The reaction mixture was sparged with nitrogen for 10 minutes, then placed in a 65 °C oil bath and allowed to polymerize for 24 h. The polymer was precipitated into approximately 600 mL 4:1 methanol:water solution. The isolated polymer product was dried under vacuum at 65 °C for 24 h.

7.3.6 Copolymer Modification with 7-Chlorocarbonylmethoxycoumarin.

A typical coumarin modification of acrylic copolymers is described (Scheme 7-1). Poly(EHA-*co*-HEA) (5.00 g) was dissolved in 50 mL distilled THF then combined with triethylamine (0.913 g, 9.0 mmol) and stirred under nitrogen in a 100 mL round-bottomed flask. Triethylamine was added at a 20 mol% excess compared to the coumarin moiety. 7-Chlorocarbonylmethoxycoumarin (1.79 g, 7.52 mmol) was dissolved in 20 mL distilled THF and added dropwise via an addition funnel to the poly(EHA-*co*-HEA) and triethylamine mixture. The addition funnel was then rinsed with an additional 5 mL distilled THF. The reaction mixture was stirred at 0 °C overnight under a nitrogen blanket with a foil-covered reaction vessel. After filtration of the salt, the resulting polymer was precipitated

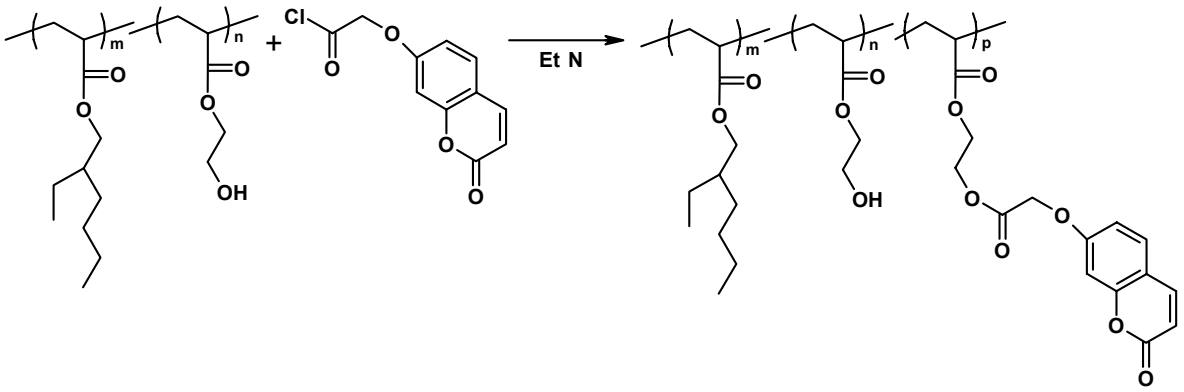

Scheme 7-1. Coumarin functionalization of EHA-*co*-HEA base polymer affording the photoactive model PSA.

into approximately 300 mL 3:1 methanol:water solution, stored in an aluminum foil covered 60 mL bottle, and dried in the vacuum over at 65 °C for 24 h. The purified yield was 74%.

7.3.7 **UV-Vis Spectroscopy, Gel Fraction and Peel Strength Sample Preparation.**

Homogenous films (1 to 2 μm thick) were solvent cast from chloroform onto quartz microscope slides and drawn using a doctor blade for the UV-Vis studies. Homogenous films of approximately 18 μm thickness were solvent cast from chloroform onto Mylar™ backing material and drawn using a doctor blade for the 90° peel tests. The solvent was removed under vacuum at 75 °C, and then a silicone release liner was applied to the adhesive layer forming a sandwich structure. The adhesive was exposed to the UV light through the Mylar™ film. Strips ~2.5 x 15 cm in size were cut from the sandwich structure and the adhesive tape was applied to the Texture Analyzer peel wheel attachment following removal of the release liner. After a 2 minute dwell, the 90° peel of the substrate was performed at 2 mm sec^{-1}. The second set of peel samples were applied to borosilicate glass microscope slides and irradiated through the glass, then peeled (180° peel test) at a rate of 5 mm sec^{-1} after a 10 min dwell time. The average force was recorded as the peel strength for both sample sets. The gel fraction samples were solvent cast directly onto a silicone release liner and drawn using a doctor blade.

7.4 RESULTS AND DISCUSSION

7.4.1 Synthesis and Modification of Poly(EHA-*co*-HEA) Random Copolymer.

The precursor poly(EHA-*co*-HEA) copolymer was synthesized via conventional free radical solution polymerization in ethyl acetate. AIBN initiated the polymerization and was added at 0.2 wt% compared to the total monomer weight. The resulting macromolecule exhibited a M_n of 75,300 g mol^{-1} with a molecular weight distribution of 3.74. The composition of the copolymer was examined using ^1H NMR spectroscopy and corresponded well with the feed ratios of 75 mol% EHA and 25 mol% HEA.

Modification of these EHA-*co*-HEA copolymers proceeded via an esterification reaction between the hydroxyl group of the HEA and the coumarin acid chloride derivative (Scheme 7-1). Manipulation of the molar ratio of hydroxyl functionality and coumarin derivative controlled the level of functionalization. Triethylamine was employed as an acid trap and was added in a 20% molar excess compared to the acid chloride to promote full conversion. Two coumarin-functionalized EHA-*co*-HEA copolymers were synthesized with coumarin concentrations of 6 and 10 mol% (Table 7-2). ^1H NMR of the modified EHA-*co*-HEA copolymers confirmed the synthesis of the two different levels of the coumarin functionality. The coumarin resonances were observed at 7.64, 7.44, 6.93, 6.30, and 4.84 ppm (Figure 7-1). A reduction in the peak area of the methylene adjacent to the hydroxyl at 3.75 ppm was observed along with the

EHA (mol%)	HEA (mol%)	Coumarin-functionalized HEA (mol%)	T_g (°C)
75	19	6.0	-36
75	15	10	-26

Table 7-1. Composition and glass transition temperature of the coumarin functionalized model PSAs.

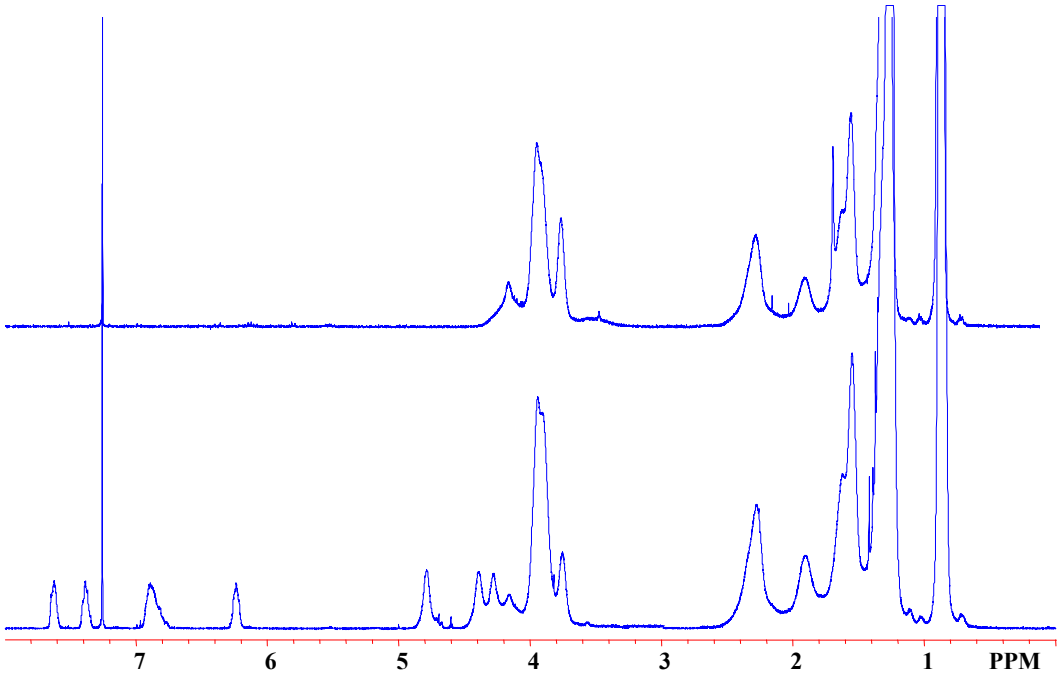

Figure 7-1. ^{1}H NMR spectra of the precursor poly(EHA-co-HEA) (upper) and a coumarin-functionalized poly(EHA-co-HEA) (lower).

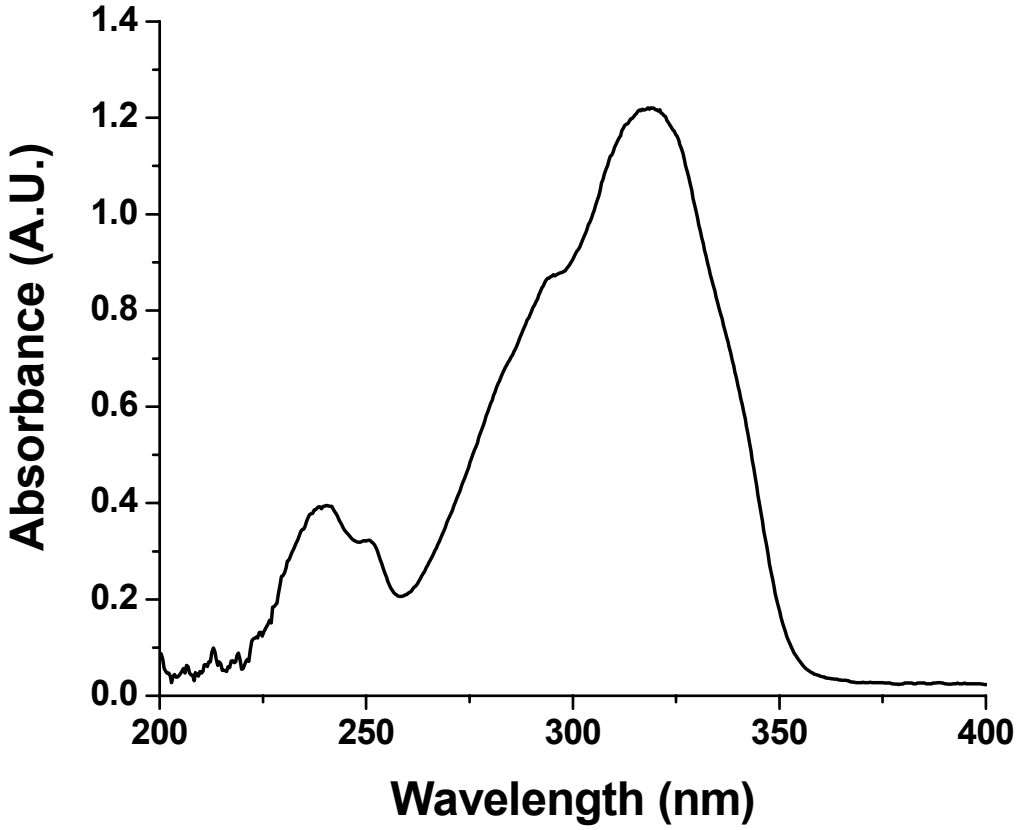

Figure 7-2. UV-Vis absorbance of 10 mol% coumarin functionalized poly(EHA-*co*-HEA) model PSA.

corresponding appearance of the methylene resonance adjacent to an ester linkage at approximately 4.42 ppm. Moreover, a new signal was observed in the UV-Vis spectrum of the polymer, characteristic of the double bond absorbance associated with the coumarin functionality at 319 nm (Figure 7-2).[148,201,420]

7.4.2 Irradiation and Evaluation of the Photocrosslinking Process.

UVA light photocrosslinked the coumarin-functionalized model PSAs in the bulk. The λ_{Max} absorbance at 319 nm in the UV-Vis absorbance spectrum is typical of 7-hydroxycoumarin containing polymers (Figure 7-2 and Figure 7-3). The intensity drop of the coumarin absorbance at 319 nm tracked the extent of dimerization. As the double bond was converted to the cyclobutane dimer (Figure 4-1), the extent of conjugation of the coumarin moiety was decreased, reducing the absorbance at 319 nm and an increase at 239 nm.[199,202,212,361,420] The intensity decrease was proportional to the consumption of the 3,4-olefin in the coumarin derivative, while an increase in the absorbance is indicative of cleavage of the cyclobutane rings and reversion to the original lactone structure.[361,420] Figure 7-3 shows the typical decrease in absorbance (photocrosslinking of 10 mol% coumarin-functionalized PSA) upon irradiation above 300 nm (UVA intensity ~ 1.1 J cm^{-2} $pass^{-1}$).

Figure 7-4 shows the normalized UV-Vis absorbance profiles at 319 nm for both coumarin-functionalized PSAs as a function of dose. As samples were irradiated, the absorbance at λ_{Max} initially decreased and then plateaued as the maximum coumarin consumption was approached. This maximum was

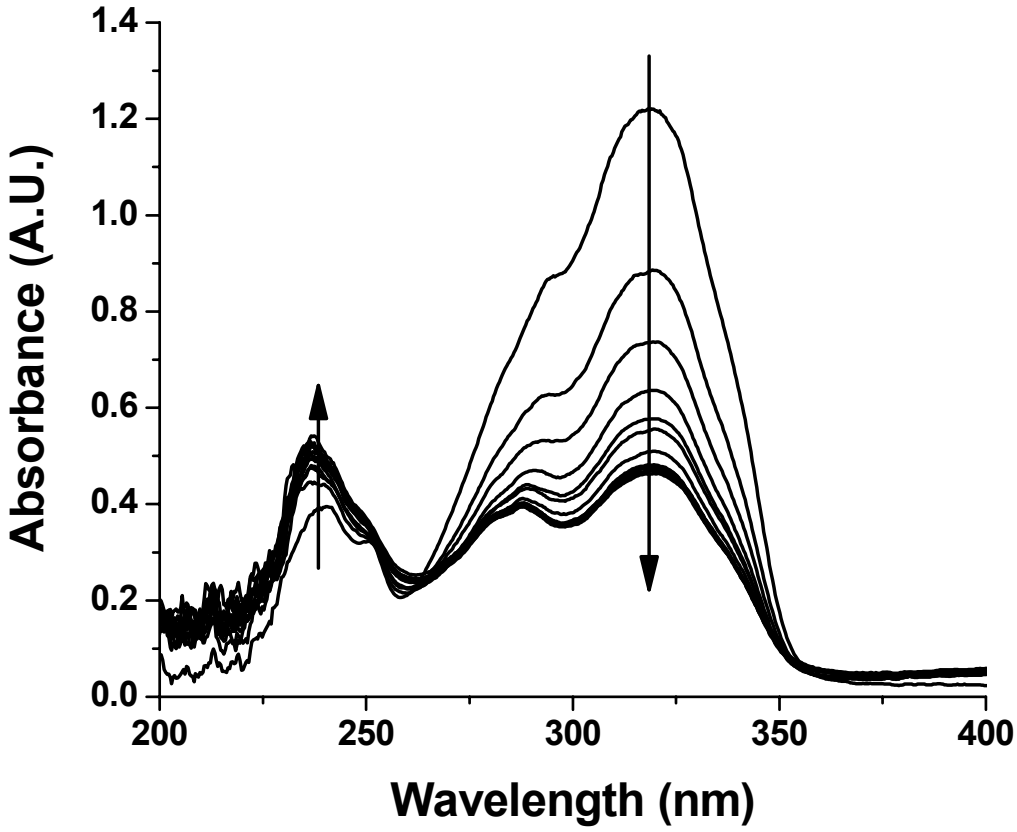

Figure 7-3. Decrease in the absorbance at 319 nm and increase in the absorbance at 239 nm as function of increasing UVA radiation dose.

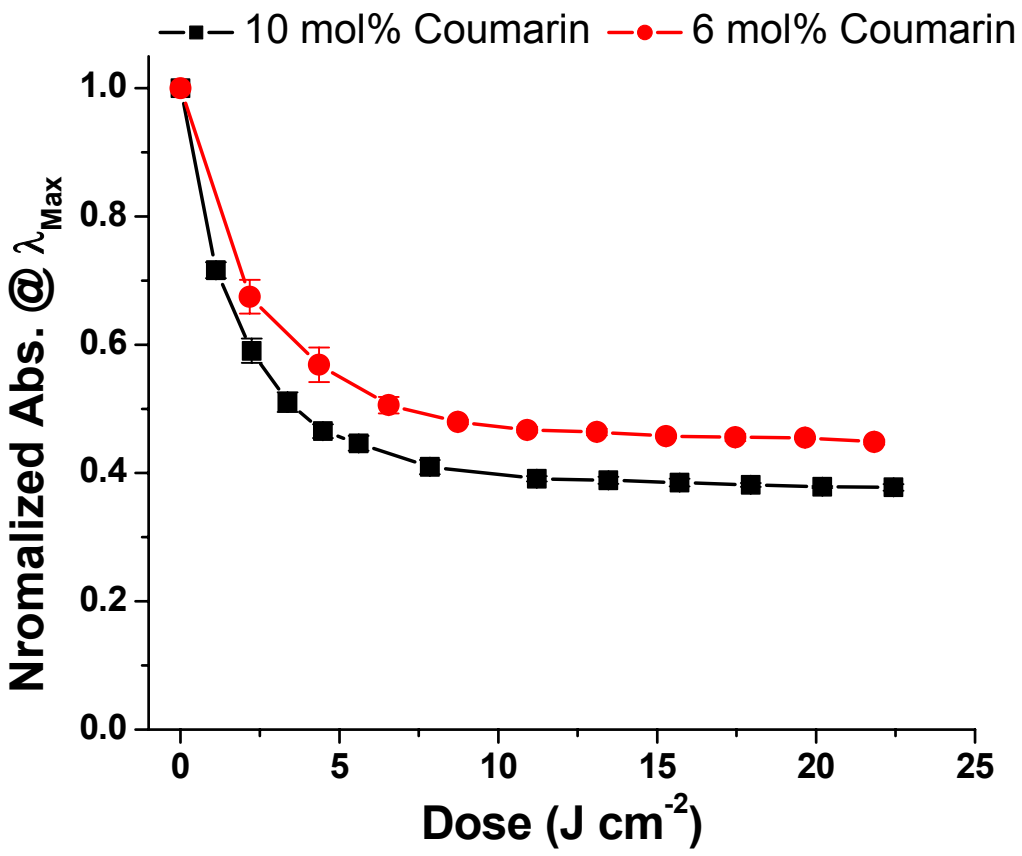

Figure 7-4. Comparison of coumarin consumption as a function of dose for the 6 and 10 mol% coumarin-functionalized model PSAs.

controlled by a combination of factors including chain mobility and coumarin concentration. The 10 mol% coumarin containing PSA had faster coumarin conversion than the 6 mol% coumarin PSA. This was expected, as the probability of photodimerization reaction depends on coumarin group proximity, and the 10 mol% sample had 65% more coumarin than the 6 mol% sample. The increased contact of coumarin groups in the 10 mol% sample led to a higher coumarin consumption rate. Likewise, the 10 mol% sample displayed a higher extent of reaction, as there were more coumarin groups to react before the crosslinking reaction hindered the chain mobility to the extent that unreacted coumarin groups could not "find" other coumarin moieties with which to react. Previous studies indicated that the T_g of these polymers was insensitive to photocrosslinking.[439]

A distinct advantage to this coumarin-functionalized acrylate system is its stability in ambient light. The methacrylate-functionalized PSAs developed by Webster and coworkers crosslinked on exposure to low doses of ambient light.[24-26] Figure 7-5 shows the effect of ambient light exposure on the 6 mol% coumarin-functionalized model PSA. The laboratory is illuminated with fluorescent lighting at a UVA intensity of 0.15 $\mu W\ cm^{-2}$, which corresponds to a dose of 540 $mJ\ cm^{-2}\ h^{-1}$. Over seven days, less than 2 mol% of the coumarin was consumed, which is within the day to day precision of the spectrometer. This ambient light stability allows for everyday use of the adhesive without a light shield or special lighting. In Webster's work, however, the photoactive adhesive

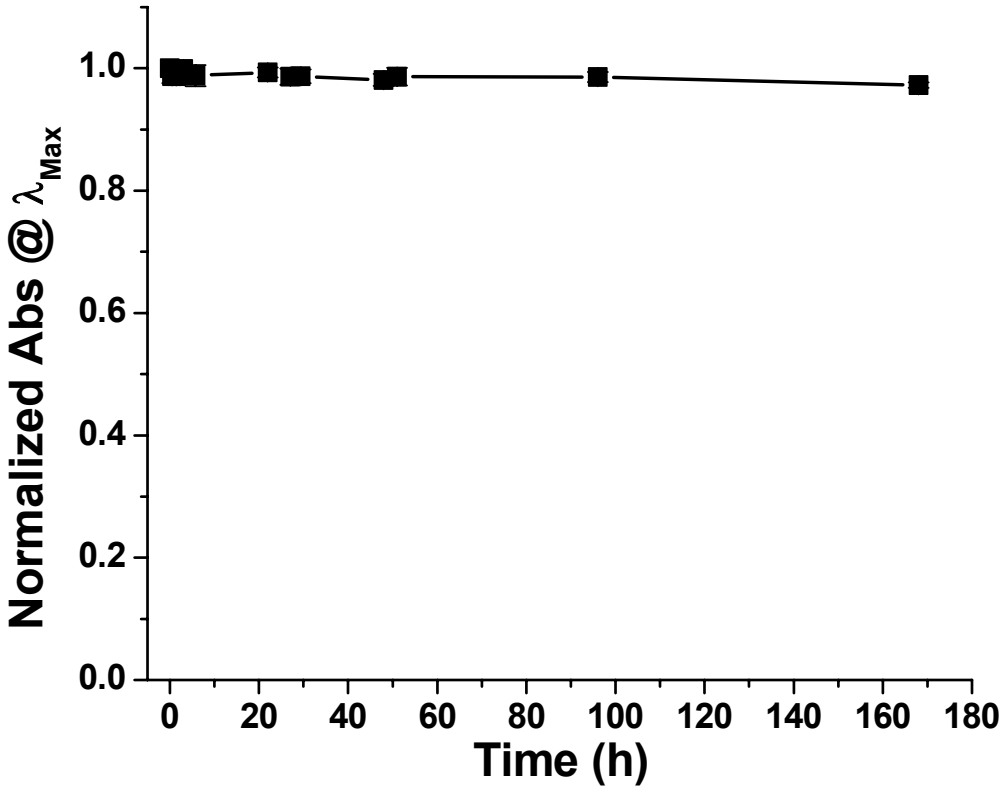

Figure 7-5. Coumarin consumption as a function of irradiation time on exposure to ambient light (6 mol% coumarin-functionalized model PSA).

lost 82% of its peel strength (thus extensively crosslinked) with 10 minutes of irradiation with a 60 W incandescent bulb.[26]

The evolution of gelled polymer was measured via soxhlet extraction in THF. A photocrosslinked polymer becomes significantly insoluble in THF after irradiation, forming a mixture of an insoluble gel and any remaining uncrosslinked product. Since only a few photoreactions per chain are necessary to form a crosslinked product, high gel fractions were expected.[95,159] Figure 7-6 shows the generation of gel as a function of UVA dose. Gel development was inversely proportional to the consumption of coumarin groups. The gel fraction quickly increased then plateaued after exposure to approximately 11 J cm^{-2} of UVA light (10 passes under the UV lamp). Polymer gel fraction increased to a maximum of 86 and 89% for the 5 and 10 mol% polymers, respectively.

7.4.3 **Effect of Irradiation on Peel Strength.**

7.4.3.1 *Irradiated-then-bonded.* In this first set of peel strength data, the adhesive was irradiated before forming the bond with the substrate. As the PSAs were crosslinked with UVA irradiation, the peel strengths decreased from their initial values of 2.58 and 1.61 N per cm-width for the 10 and 6 mol% PSAs, respectively. The dose-dependent peel strength data was normalized in Figure 7-7 to the nonirradiated peel strength to ease comparison of the two sets of data since initial peel strengths differed between the two PSAs. All samples failed via an apparent adhesive mechanism with the exception of the nonirradiated 6 mol% sample, which failed cohesively. With less than 2 J cm^{-2} of UVA irradiation, the

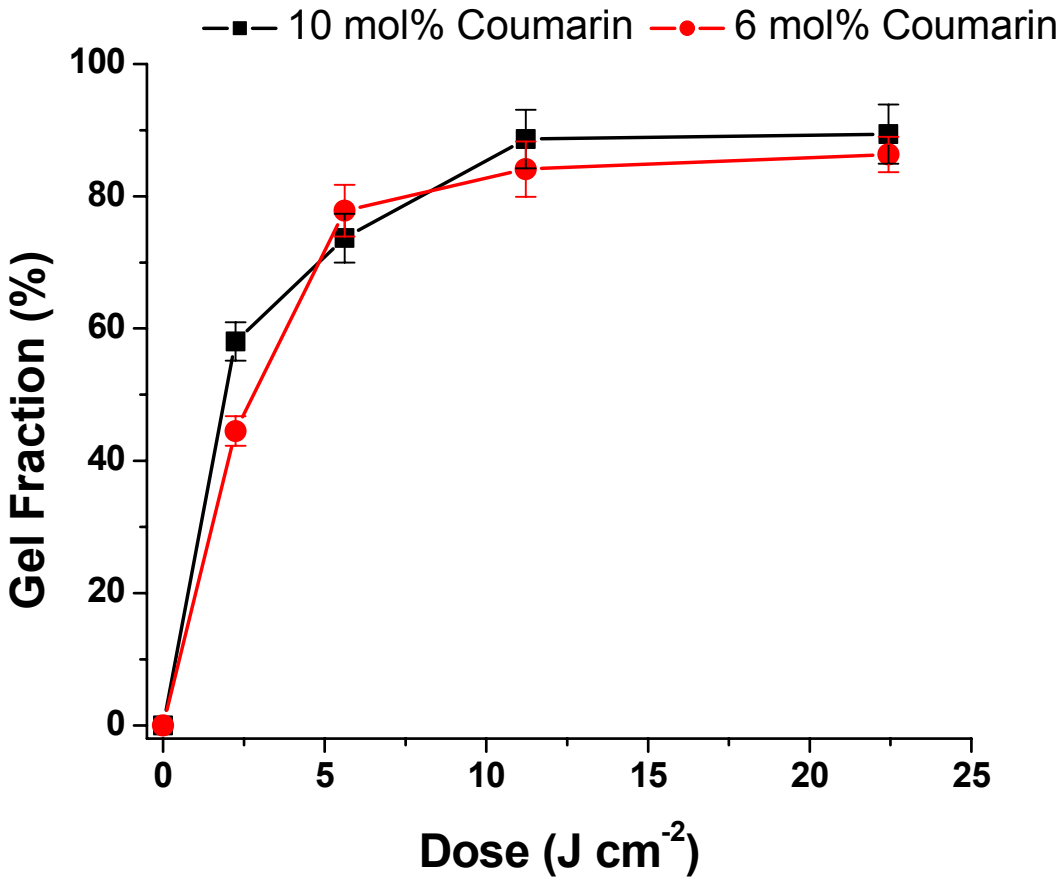

Figure 7-6. Evolution of gel fraction of the 6 and 10 mol% coumarin-functionalized model PSAs as a function of UVA irradiation.

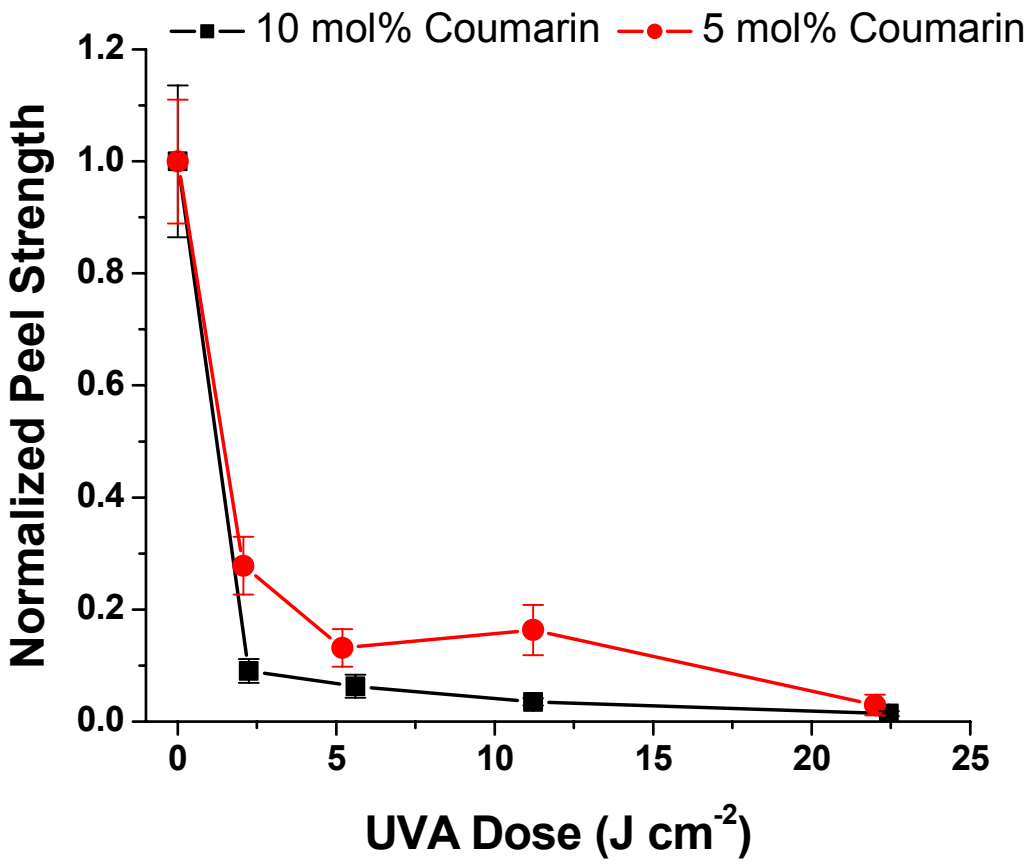

Figure 7-7. Decrease in the normalized average peel strength of the 6 and 10 mol% coumarin-functionalized model PSAs as a function of UVA dose.

peel strengths of the 10 and 6 mol% samples decreased 90 and 70%, respectively. As in the case of the UV-Vis data and the gel fraction measurements, subsequent irradiation offered little change in the peel strengths. After approximately 22 J cm^{-2} of UVA light, the peel strengths decreased greater than 97% of the initial values. Figure 7-8 summarizes the effect of UVA irradiation on the 10 mol% coumarin-functionalized model PSA. As the PSA was irradiated, the coumarin groups photodimerized. Since the irradiation was performed before the model adhesives were applied to the test substrate, the reduced peel strength was attributed to reduced viscous flow of the already crosslinked adhesives and thus an inability to properly wet the substrate and form an adhesive bond.[10]

7.4.3.2 *Bonded-then-irradiated.* A second set of peel samples was irradiated following the formation of the adhesive bond with glass microscope slides. The composition of this set of model PSAs varied slightly from the adhesives used throughout this rest of this report (Table 7-2). Irradiation of the adhesive through the bond substrate was performed with the ThermoOriel irradiation system. The UVA intensity was 35 mJ cm^{-2}). The effect of irradiation time on the gel fraction and peel strength is shown in Figure 7-9. As the adhesive was irradiated through the glass slide, the gel fraction of the adhesive increased to a maximum of 64%, while the adhesive peel strength decreased from 2.5 to 0.70 N per cm-width. The failure mechanism also changed with dose. The non-irradiated peel samples failed cohesively, while the irradiated samples failed adhesively. In

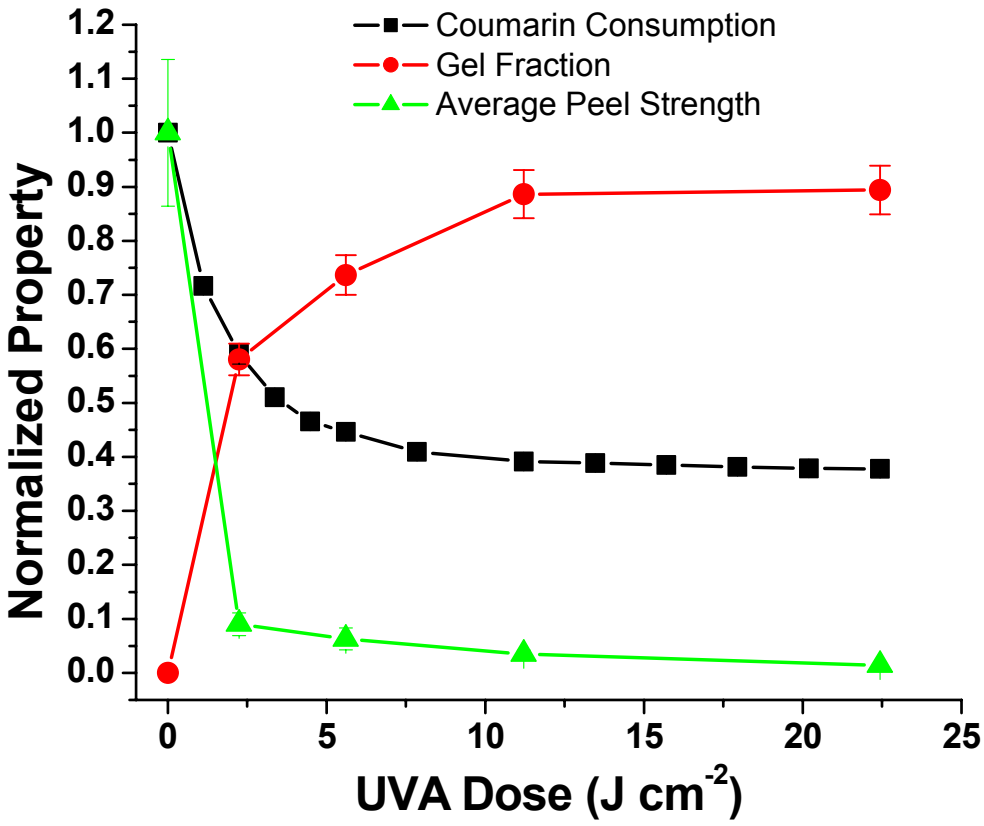

Figure 7-8. Effects of UVA irradiation on coumarin consumption, gel fraction, and 90° peel strength for the 10 mol% coumarin-functionalized model PSA.

M_n	M_w/M_n	EHA (mol%)	HEMA (mol%)	Coumarin-functionalized HEMA (mol%)
53,000	3.30	80	10	10

Table 7-2. Composition of the model PSA used for the glass substrate 180° peel tests.

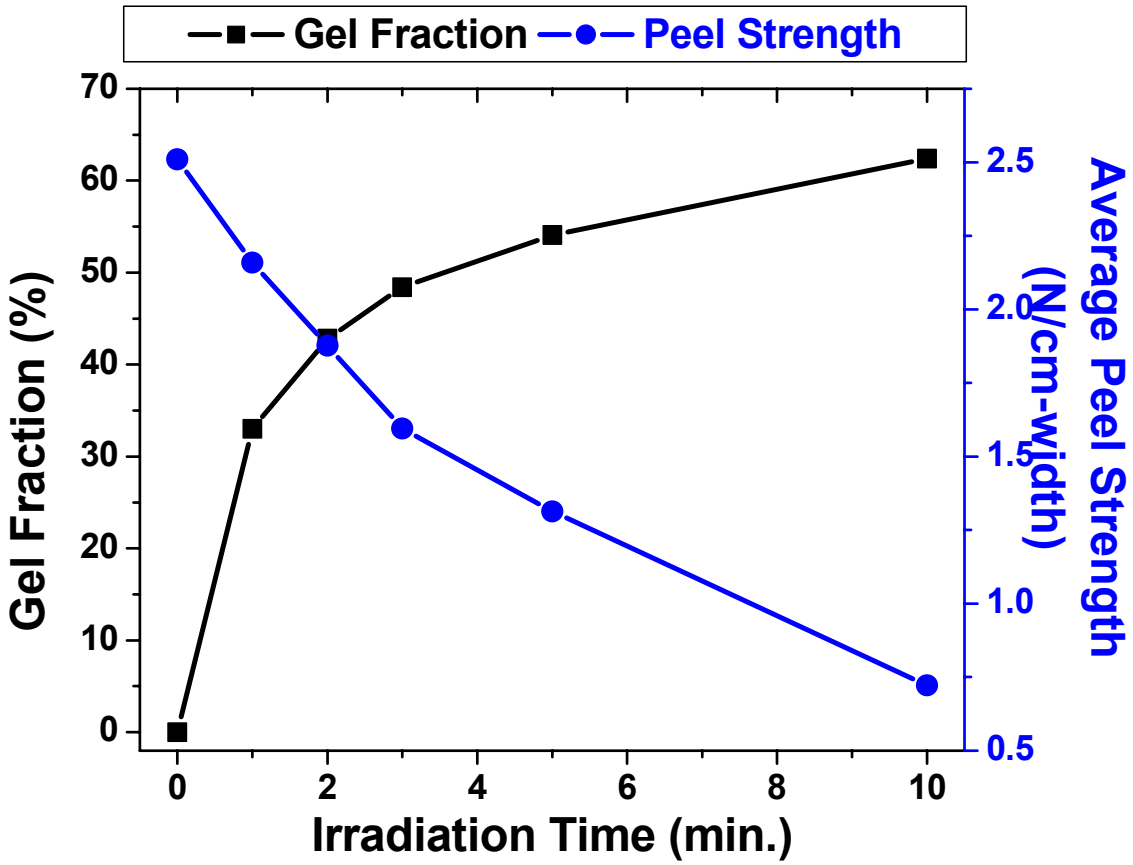

Figure 7-9. The increase in gel fraction and the decrease in peel strength for the bonded-then-irradiated samples.

addition, fibrillation was observed in the non-irradiated sample whereas no fibrillation was observed following irradiation. While the reduced peel strength of the irradiated-then-bonded samples was attributed to a lack of wetting, this adhesive had wetted the substrate before UV exposure. Thus, the lower peel strength in the bonded-then-irradiated sample was attributed to a decrease in the chain mobility resulting in a decrease in the ability of the adhesive to dissipate energy during peel testing.[10]

One additional advantage for coumarin photodimerization crosslinking of PSAs is the ability to reverse the cyclobutane ring that forms the polymer crosslink point with UVC irradiation (< 290 nm). This feature may lead to the ability to reuse the PSA. Initial data (Figure 7-10) from the 5 mol% functionalized PSA shows a 200% increase in the peel strength of the UVA irradiated adhesive following subsequent UVC irradiation. Further tuning of the PSA system could afford higher initial peel strengths and optimize reversibility.

7.5 CONCLUSIONS

This studied demonstrated the ability to utilize coumarin photodimerization to reduce the peel strengths of model PSAs. Photocrosslinkable model PSAs were prepared from a quantitative esterification reaction of poly(2-ethylhexyl acrylate-*co*-hydroxyethyl acrylate) and an acid chloride derivatized 7-hydroxycoumarin. The coumarin groups in the polymer dimerized and the gel fraction of the coumarin-modified PSAs increased with increasing UV irradiation. The increase in the gel fraction contributed to as much as a 97% decrease in the peel strength

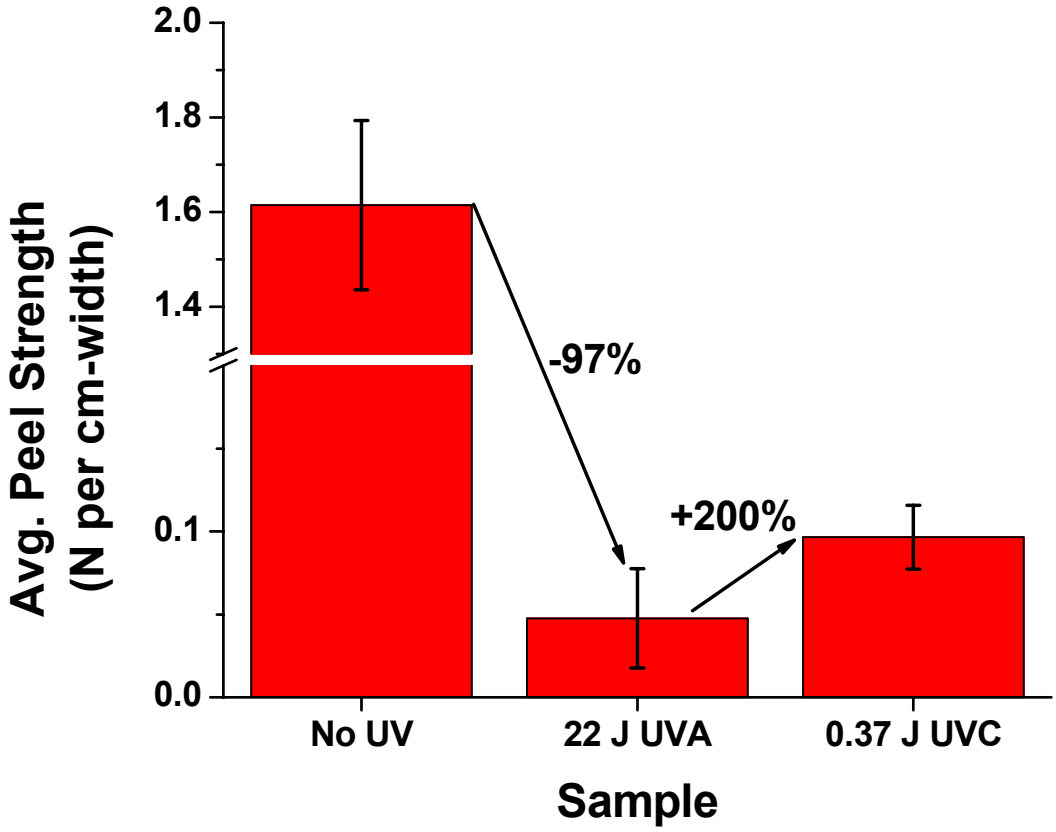

Figure 7-10. The effect of irradiation of the 6 mol% coumarin-functionalized model PSA affording a possible route for repeated use.

when exposed to 22 J cm^{-2} of UVA irradiation. The decrease in peel strength upon irradiation of the two sets of model PSAs (irradiated-then-bonded and bonded-then-irradiated) was attributed to two different mechanisms. The decrease peel strength of the irradiated-then-bonded samples was attributed to a lack of wetting, while the decrease in the bonded-then-irradiated samples was attributed to a decrease in the energy dissipation of the model PSA. Photocrosslinkable polymers synthesized with coumarin functionalities are stable on exposure to ambient light, a trait not achieved in previously published studies involving photocrosslinkable PSAs. If optimized for adhesive applications (with the addition of higher T_g monomers), this system may have increased initial peel strengths and similar decreases in peel strength with irradiation. In addition, systems utilizing coumarin photodimerization possess a significant advantage over other photoreversible systems due to the ability to reverse the loss of adhesive strength on demand via the photocleavage of the coumarin dimers with UVC irradiation.

7.6 ACKNOWLEDGMENTS

The authors gratefully acknowledge financial support from the Center for Adhesive and Sealant Science (CASS) at Virginia Tech, and the Adhesive and Sealant Council Education Foundation. This material is based upon work supported in part by the U.S. Army Research Laboratory and the U.S. Army Research Office under grant number DAAD19-02-1-0275 Macromolecular Architecture for Performance (MAP) MURI.

CHAPTER 8 DESIGN AND SYNTHESIS OF UV-CURABLE ACRYLIC HOT MELT ADHESIVES VIA A PHOTOCROSSLINKABLE CINNAMATE FUNCTIONALITY

Scott R. Trenor, Jeremy R. Lizotte, Brian J. Love, and Timothy E. Long
Virginia Tech
Department of Materials Science and Engineering
Department of Chemistry
Blacksburg, VA 24061-0212

8.1 ABSTRACT

Multicomponent acrylic random copolymers were synthesized via conventional free radical polymerization to incorporate maleic anhydride or 2-hydroxyethyl acrylate units into the polymer backbone. The anhydride and hydroxyl functionality were subsequently reacted with photoactive cinnamate derivatives possessing an appropriate functional group. The ring opening reaction associated with maleic anhydride modification attached the photoactive cinnamate functionality to the polymer backbone and provided an adjacent carboxylic acid functionality. The pendant hydroxyl group characteristic of 2-hydroxyethyl acrylate was reacted with cinnamoyl chloride to attach the photoactive cinnamate group. Both ^{1}H NMR analysis and UV Vis spectroscopy indicated cinnamate functionalization.

Key words: UV crosslinkable, free radical polymerization, photodimerization, polymer modification

8.2 INTRODUCTION

Acrylate based copolymers are utilized in a number of pressure sensitive adhesive (PSA) applications.[2,10,21,45] Because high molecular weights are required in order to achieve good adhesive properties with acrylic-based PSAs, these materials typically have high viscosities in the processing temperature regime. As a result, acrylic PSAs are usually applied from an organic solvent rather than from the melt. In reducing solvent use, a recent goal in the field is to synthesize acrylic-based PSAs applied as hot melts. Schumacher and coworkers have recently developed a photoreactive acrylic hot-melt adhesive.[32,34,41,48-53] They incorporated vinyl derivatives of a common photoinitiator (benzophenone) into the polymer composition. When irradiated between 220 and 280 nm, the benzophenone decomposes, forming radicals which react with tertiary carbons in the polymer to form crosslinks.[34,53] This reaction increases the adhesive molecular weight and forms a lightly crosslinked gel. These researchers reported that as UV dose was increased, the gel fraction and cohesive strength increased, while the adhesion and tack decreased.[41]

In addition to the aforementioned photoinitiated radical crosslinking reactions, reactions involving novel functional groups that efficiently crosslink polymers via non-radical radiation pathways were also examined.[94,188,190,193,232,361,420] Crosslinking via non-radical pathways afforded the first synthetic photoreactive polymers via photodimerization of poly(vinyl cinnamate).[154,157,403] The photocrosslinking route for the coumarin and cinnamate molecules involves the formation of a cyclobutane ring via a [2π+2π] cycloaddition (Figure 8-1).[58,358]

Cinnamate derivatives were recently utilized to crosslink a number of acrylic liquid crystalline polymers with good success.[169,172,176,242-244,247,250,251] The advantage to the cycloaddition crosslinking process is reduction of postcure events induced via addition of reactive elements. In addition, the cycloaddition pathway is not thermally allowed.

This report describes the synthesis of functional acrylate multicomponent copolymers and subsequent modification to incorporate a photoactive crosslinking cinnamate functionality. The goal was to synthesize acrylic systems that are applicable as hot melt adhesives. The incorporation of the photoactive cinnamate group at low concentrations allows for chain extension and possibly low levels of crosslinking affording the high molecular weights necessary for use as pressure sensitive adhesives. The photoactive groups were introduced via two reaction pathways: an esterification reaction involving an acid chloride reaction and the ring opening of a cyclic anhydride. The ring opening pathway was utilized to monitor and optimize model reactions for the addition of the photoactive group via the maleic anhydride pathway. A second chapter to follow will describe the UV curing and the adhesive characterization of acrylic hot melt adhesives.

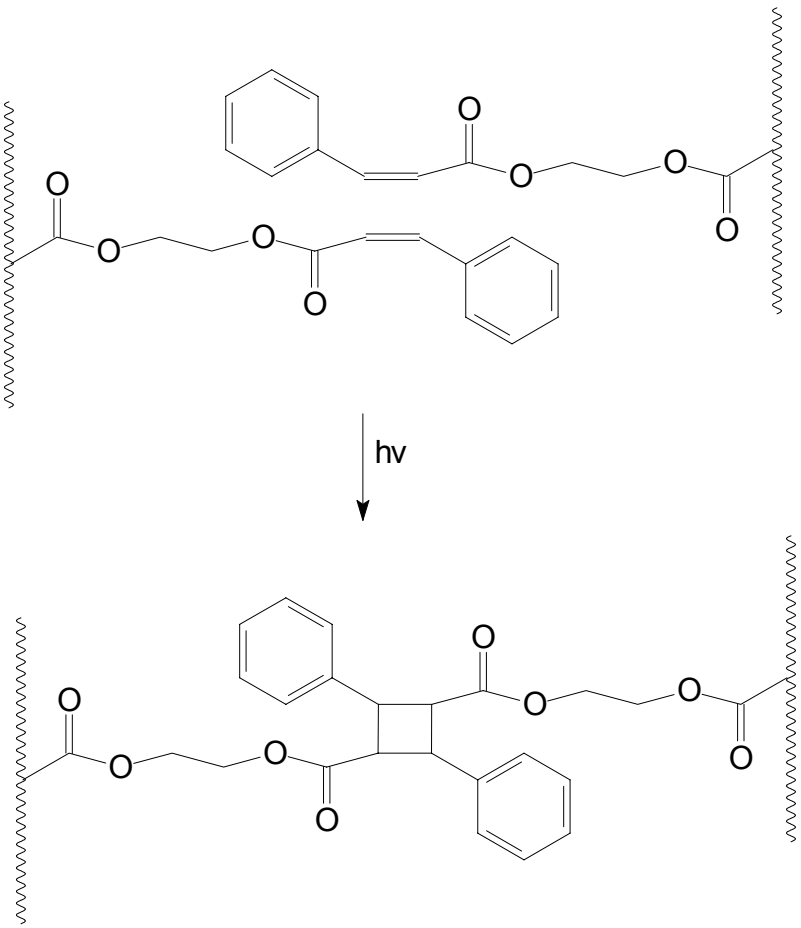

Figure 8-1. Photoinduced dimerization of cinnamate functionality attached to a polymer chain.

8.3 EXPERIMENTAL

8.3.1 **Materials.**

Avery Dennison Chemical Company provided the *n*-Butyl acrylate (*n*BA), 2-hydroxyethyl acrylate (HEA), methyl acrylate (MA), and 2-ethylhexyl acrylate (EHA) which were passed through a neutral alumina column to remove radical inhibitors. Maleic anhydride (MAH), succinic anhydride (SAH), and 2,2'-azobisisobutyronitrile (AIBN) were purchased from Aldrich and used as received. Ethylene glycol, triethyl amine, cinnamoyl chloride, and all other solvents were purchased from Acros. All of the solvents were used as received with the exception of the ethylene glycol. The ethylene glycol was dried in a vacuum oven for 24 h at 80 °C prior to use.

8.3.2 **Instrumentation.**

^{1}H NMR spectra were recorded using either a Varian Unity 400 MHz or a Varian Inova 400 MHz spectrometer at 25 °C in CDCl3. UV-Vis spectroscopy was performed using an Analytical Instrument Systems Inc. spectrometer equipped with fiber optic light guides, a DT1000CE light source, and an Ocean Optics USB2000 UV-Vis detector. Molecular weights were determined at 40 °C in chloroform or THF (HPLC grade) at 1 mL min^{-1} using polystyrene standards on a Waters 707 Autosampler equipped with 3 in-line PLgel 5 μm MIXED-C columns, a Waters 410 refractive index detector and an in-line Wyatt Technology Corp. miniDAWN® multiple angle laser light scattering (MALLS) detector. *In situ* FTIR monitoring was performed with an ASI Mettler-Toledo ReactIR 4000 apparatus with a stainless steel dicomp insertion probe. DSC was performed

with a Perkin Elmer Pyris 1 at a heating rate of 20 °C min^{-1} under nitrogen. The T_g was measured during the second heat using the midpoint of the transition. Parallel plate (25 mm, 2% strain, 10 Hz) rheology was performed using a TA Instruments AR 1000. The viscosity was measured during a temperature ramp from 20 to 180 °C at 2 °C min^{-1}. Homogenous films (1 to 2 μm thick) were solvent cast from chloroform onto quartz microscope slides and drawn using a doctor blade. Film thickness was measured using microcalipers.

8.3.3 Succinic Anhydride Model System Study.

The ring opening reaction of succinic anhydride with *n*-butanol was utilized as a model system to optimize reaction the conditions for the maleic anhydride ring opening reaction. A 100 mL 3-neck round bottom flask equipped with a water condenser and a nitrogen inlet/outlet was attached to the ASI Mettler-Toledo ReactIR 4000 apparatus with a stainless steel dicomp insertion probe and purged with nitrogen. The third neck of the round bottom flask was equipped with a thermocouple to monitor reaction temperature. A background of the empty round bottom flask was taken, then succinic anhydride (8.00 g, 79.9 mmol), *n*-butanol (5.92 g, 79.9 mmol), 72.0 g of toluene and the appropriate catalyst (either *p*-toluene sulfonic acid or titanium isopropoxide at 0.5 mol% of succinic anhydride) were added to the flask. The solution was heated to 100 °C in an oil bath and stirred with a magnetic stir bar. The FTIR was started when the reaction mixture reached 90 °C, and a spectrum was taken at intervals of either five or ten minutes for 24 h. The IR absorbances at 1790 and 1742 cm^{-1}

corresponding to the succinic anhydride ring and monobutyl ester of butanedioic acid (product), respectively, were utilized to determine conversion.

8.3.4 **Synthesis of Maleic Anhydride Containing Acrylic Copolymer.**

The synthesis of a typical MAH mulit-component copolymer is described. The MA (4.82 g, 56.0 mmol), *n*BA (22.6 g, 176 mmol), and EHA (13.6 g, 73.8 mmol) monomers were added to a 250 mL round-bottomed flask with a magnetic stir bar. Maleic anhydride (3.28 g, 33.4 mmol) was then added to the reaction flask. The reaction mixture was then diluted with ethyl acetate (34 mL) to 45 wt% solids. Finally, the initiator, AIBN (442 mg, 1 wt% compared to monomer), was added to the reaction vessel. The reaction mixture was sparged with nitrogen for 15 minutes. The polymerization vessel was subsequently equipped with a water condenser and a nitrogen inlet/outlet. The flask was placed in an 85 °C oil bath with a magnetic stirrer and allowed to polymerize for 24 h under a nitrogen blanket. The polymer was diluted with ethyl acetate (25 mL) and precipitated into methanol. The isolated polymer product was dried in the vacuum oven at 65 °C for 24 h. The purified yield was 93%.

8.3.5 **Synthesis of HEA Containing Acrylic Copolymer.**

The synthesis of a typical HEA mulit-component copolymer is described. The MA (4.59 g, 53.3 mmol), *n*BA (22.2 g, 173 mmol), EHA (13.52 g, 73.4 mmol), and HEA (4.00 g, 34.4 mmol) monomers were added to a 250 mL round-bottomed flask with a magnetic stir bar. The reaction mixture was then diluted with ethyl acetate (34 mL) to afford 45 wt% solids. Finally, the initiator, AIBN (444 mg, 1 wt% compared to monomer), was added to the reaction vessel. The reaction

mixture was sparged with nitrogen for 15 minutes. The polymerization vessel was subsequently equipped with a water condenser and a nitrogen inlet/outlet. The flask was placed in an 85 °C oil bath with a magnetic stirrer and allowed to polymerize for 24 h under a nitrogen blanket. The polymer was diluted with ethyl acetate (25 mL) and precipitated into methanol. The isolated polymer product was dried in the vacuum oven at 65 °C for 24 h. The purified yield was 94%.

8.3.6 **Synthesis of Aliphatic Hydroxyl Cinnamate Derivative.**

The detailed synthesis of the ethylene glycol based cinnamate derivative is described in the literature.[247] Triethyl amine (22.9 g, 226 mmol) was added to freshly distilled acetone (50 mL) in a 250 mL 2-neck round-bottomed flask with a magnetic stir bar. Ethylene glycol (44.5 g, 717 mmol) was added to the triethylamine solution. One neck was fitted with a nitrogen outlet and the other neck was fitted with a 250 mL addition funnel sealed with a rubber septum. The flask was placed in an ice cooled 0 °C water bath. An acetone (75 mL) solution of cinnamoyl chloride (27.1 g, 113 mmol) was also prepared in a separate flask. The cinnamoyl chloride was added dropwise via an addition funnel to the ethylene glycol over 30 min under nitrogen. The reaction began to turn a light yellow color and precipitation of the triethylamine salt was observed. After 16 h, the reaction mixture was filtered through filter paper and the residual acetone solvent was removed *in vacuo*. The reaction mixture was redissolved in dichloromethane and washed with water five times to extract the residual salt. The dichloromethane solution was dried with magnesium sulfate and the

dichloromethane was removed *in vacuo*. The product was collected as an orange-yellow oil in 92% yield.

8.3.7 **Modification of the Maleic Anhydride Containing Copolymers.**

The maleic anhydride-containing polymer in (9.21 g) was transferred to a 100 mL round-bottomed flask with a magnetic stir bar. The purified ethylene glycol cinnamate derivative (2.07 g, 10.8 mmol) was added to the reaction flask and diluted with toluene to produce a 30 wt% solids solution. The flask was equipped with a water condenser and nitrogen atmosphere. The toluene reaction mixture was heated in a 105 °C oil bath and stirred for 18 h. The modified polymer product was precipitated into hexanes and dried in a vacuum oven at 65 °C for 24 h. The catalyzed functionalization reactions were prepared similarly with the catalysts (*p*-toluene sulfonic acid or titanium isopropoxide) added at 1:3 molar ratio compared to the maleic anhydride concentration of the polymer.

8.3.8 **Modification of the HEA Containing Copolymers.**

A typical coumarin modification of HEA containing copolymers is described. The polymer (5.40 g) was dissolved in 43 mL distilled THF then combined with triethylamine (0.389 g, 3.84 mmol) and stirred under nitrogen in a 100 mL round-bottomed flask. Triethylamine was added at a 20 mol% excess compared to the cinnamoyl chloride. Cinnamoyl chloride (387 mg, 2.33 mmol) was dissolved in 3 mL distilled THF and added dropwise via an addition funnel to the polymer and triethylamine mixture. The addition funnel was then rinsed with an additional 1 mL distilled THF. The reaction mixture was stirred at 0 °C overnight under a nitrogen blanket with the reaction vessel covered in aluminum foil to avoid

ambient photoreactions. The modified polymer product was filtered to remove the triethylamine salt, precipitated into methanol, and dried in the vacuum oven at 65 °C for 24 h.

8.3.9 **UV-Vis Spectroscopy Sample Preparation.**

Homogenous films (1 - 2 μm thick) were solvent cast from chloroform onto quartz microscope slides and drawn using a doctor blade for the UV-Vis studies. Film thickness was measured using microcalipers.

8.4 RESULTS AND DISCUSSION

8.4.1 **Synthesis and Modification of HEA Containing Random Copolymers.**

The HEA copolymers were synthesized via a conventional free radical solution polymerization in ethyl acetate. AIBN initiated the polymerization and was added at 1.0 wt% compared to the total monomer weight. The resulting macromolecule had a weight average molecular weight of 342,00 g mol^{-1} with a molecular weight distribution of 4.06. The composition of the copolymers was examined using ^{1}H NMR spectroscopy and corresponded well with the feed ratios. The copolymers possessed 20 mol% EHA, 53 mol% *n*BA, 16 mol% MA and 11 mol% HEA.

Modification of these copolymers proceeded via quantitative esterification between the hydroxyl group of the HEA and the cinnamoyl chloride (Scheme 8-1(a)). Manipulation of the molar ratio of hydroxyl functionality and cinnamoyl chloride was utilized to control the level of functionalization. Triethylamine was

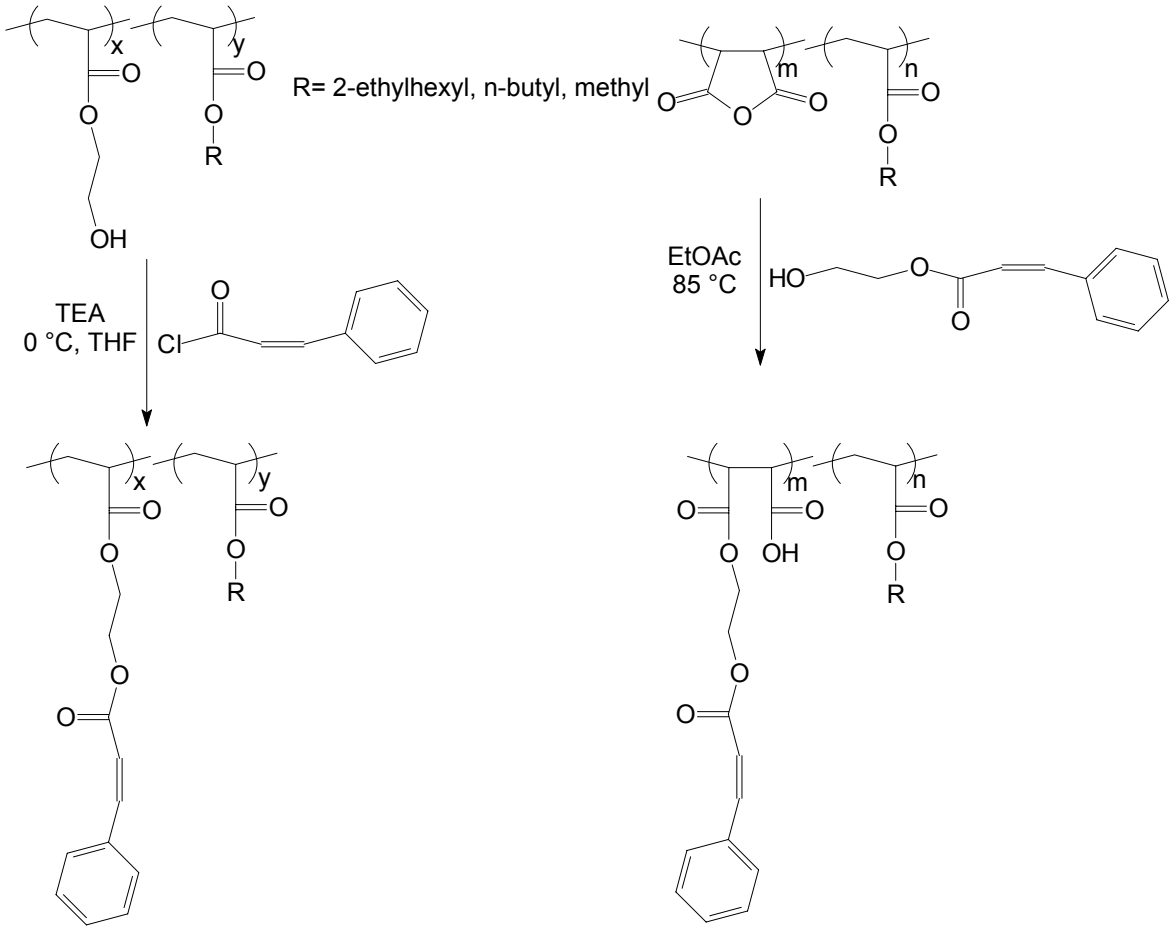

Scheme 8-1. Post-polymerization introduction of photoactive cinnamate functional groups.

employed as an acid trap and was added in a 20% excess compared to the acid chloride to promote full conversion. ^{1}H NMR of the modified polymers confirmed the presence of different levels of the cinnamate functionality. The resonances associated with the cinnamate group are apparent at 6.5 ppm and from 7.3-7.6 ppm. The disappearance of the methylene adjacent to the hydroxyl at 3.75 ppm was observed along with the corresponding appearance of the methylene resonance adjacent to an ester linkage at approximately 4.3 ppm. Moreover, a new signal was observed in the UV-Vis spectrum of the polymer characteristic of the double bond absorbance at 278 nm associated with the cinnnamate functionality (Figure 8-2).

8.4.2 **Synthesis and Modification of MAH Containing Random Copolymers.**

The MAH multicomponent copolymers were synthesized similar to the HEA copolymers via free radical solution polymerization in ethyl acetate using AIBN initiator at 1.0 wt% compared to the monomer weight. The resulting macromolecules had a M_w = 167,800 g mol^{-1} with a molecular weight distribution of 3.27, typical of free radical polymerizations. The composition of the copolymer was investigated using ^{1}H NMR and corresponded well with the initial monomer feed ratios. The copolymers possessed 53 mol% *n*BA, 17 mol% EHA, 20 mol% MA and 10 mol% MAH. The reactivity ratios of MAH and the acrylates utilized as comonomers indicate that the incorporation of the MAH groups may at the beginning of the reaction.[440,441] Figure 8-3 shows the viscosity of the

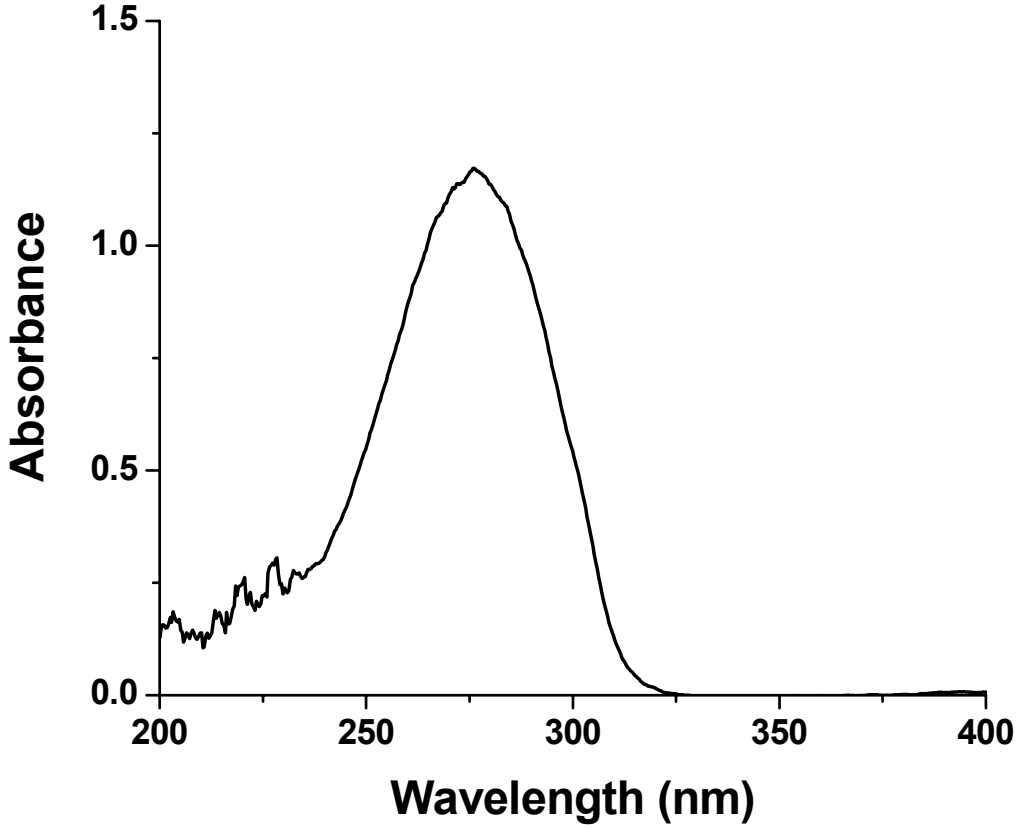

Figure 8-2. UV absorbance of the cinnamate-functionalized HEA containing random copolymer.

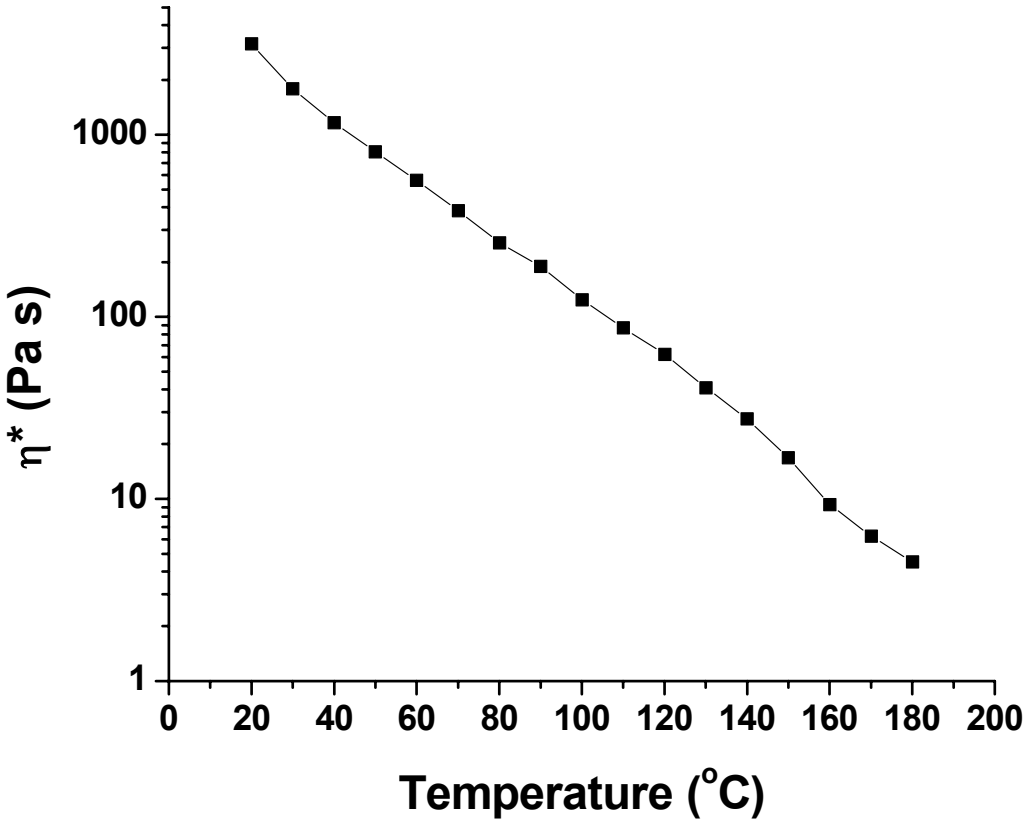

Figure 8-3. Viscosity of the MAH-containing polymer as a function of temperature.

MAH-containing copolymer as a function of temperature. The viscosity at 150 °C is similar to the viscosity of BASF's commercially available UV-curable PSA (10 Pa s at 140 °C).[54]

In addition to the copolymer, a cinnamate derivative possessing an aliphatic hydroxyl functionality was synthesized. Cinnamate functionalized molecules were synthesized via an esterification reaction of cinnamoyl chloride and the ethylene glycol (Scheme 8-2). The molar excess of the diol was maintained at a high level to ensure that both hydroxyl groups were not significantly functionalized, the reaction products were isolated in greater than 90% yield. The ethylene glycol cinnamate derivative (EG-Cinn) tended to difunctionalize. Molar ratios from 1.5:1 up to 6:1 were investigated and the percentage of difunctionalized diol steadily decreased with the increase in molar ratio (Table 8-1). Consequently, a molar ratio of 6:1 was employed to obtain a product that was only 9.5% difunctionalized (peak at 4.4 ppm). The ^{1}H NMR of the purified product is shown in Figure 8-4b. The percentage of doubly substituted cinnamate molecules was accounted for in the functionalization reactions.

The synthesized cinnamate derivatives were subsequently employed in the ring opening reaction of the maleic anhydride unit in the polymer backbone Scheme 8-1(b). The modification reaction resulted in the attachment of a cinnamate functionality to the polymer backbone via an aliphatic spacer consisting of two methylene units. Moreover, a carboxylic acid group was formed directly adjacent to the cinnamate group. The carboxylic acid group is known to increase the cohesive strength of adhesives and may aid in the photoreaction by

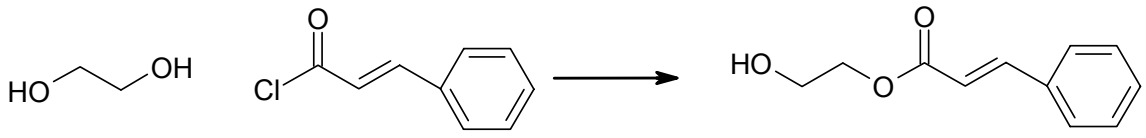

Scheme 8-2. Synthesis of cinnamate based alcohols.

Molar Ratio		mol% difunctionalized
Cinnamoyl Chloride	**Ethylene Glycol**	
1	1.5	35
1	4	14
1	6	9.5

Table 8-1. The effect of the molar ratio of acid chloride to ethylene glycol on the level of difuctionalization.

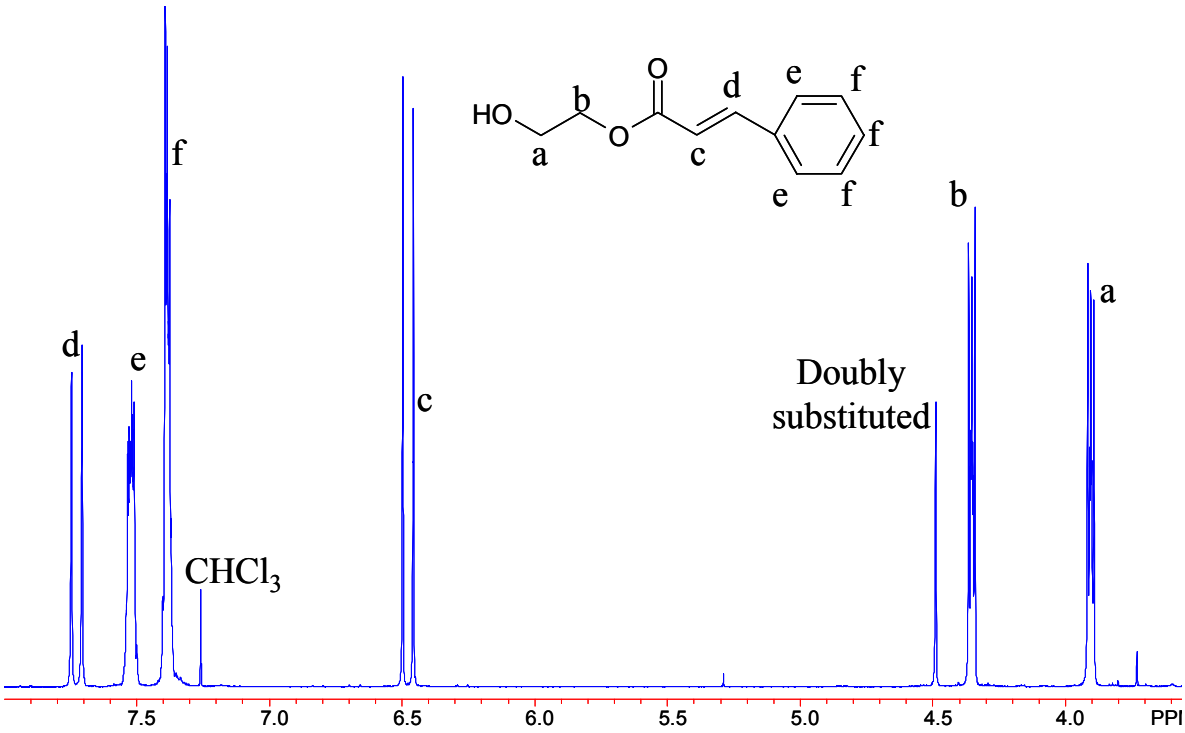

Figure 8-4. ^{1}H NMR spectra of the synthesized cinnamate derivatives possessing an aliphatic hydroxyl functionality.

directing adjacent cinnamate groups into close proximity.[2,15] After functionalization, a new absorbance at λ_{Max} = 278 nm was observed (Figure 8-5) similar to that of the cinnamate-functionalized HEA polymers.

The effect of polymer composition on the modification reaction was investigated using copolymers of maleic anhydride and a single additional acrylate monomer. It is well known that steric hindrance affects the ability to functionalize polymers.[96] Copolymers of maleic anhydride (10 mol%) with MA, *n*BA, and EHA were prepared in a manner identical to the multicomponent copolymer systems. The number average molecular weights of the resulting copolymers ranged from 70,000 g mol^{-1} to 300,000 g mol^{-1} with molecular weight distributions typical of free radical polymerizations (1.93 - 3.03). The bicomponent copolymers were functionalized in a 10 wt% ethyl acetate solution at 85 °C using a 1.5:1.0 molar ratio of cinnamate derivative to anhydride functionality. ^{1}H NMR was employed to determine the level of functionalization for the copolymers, and resonances characteristic of the cinnamate functionality were observed at 6.5 ppm and at 7.3-7.6 ppm. The appearance of a new methylene resonance was observed at 4.3 ppm corresponding to the methylene adjacent to the newly formed ester linkage. Table 8-2 highlights the percent MAH conversion corresponding to polymer modification. The *n*BA and EHA copolymers exhibited only slight degrees of modification, while the methyl acrylate copolymer possessed a high level of cinnamate functionalization. As expected, this result suggested that steric crowding from the larger alkyl ester chains of *n*BA and EHA inhibit the modification reaction.

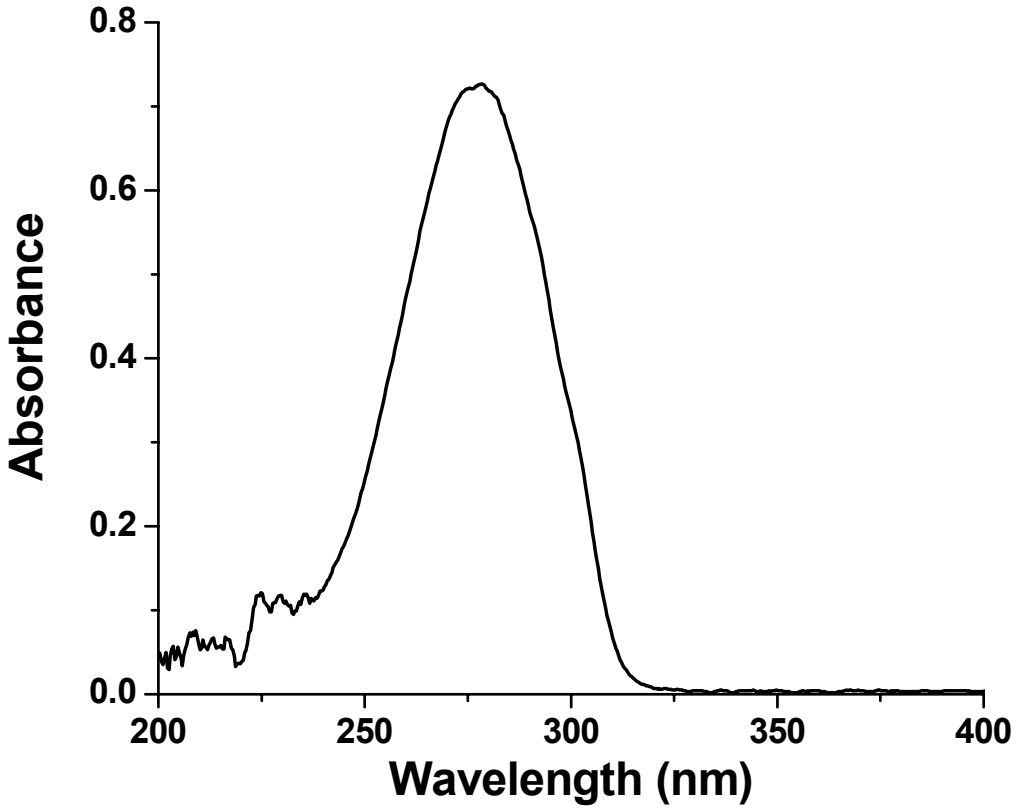

Figure 8-5. UV absorbance of the EG-Cinn functionalized MAH containing random copolymer.

alkyl acrylate	mol% cinnamate	MAH conversion
methyl acrylate	4.0[a]	40 %
n-butyl acrylate	<1.0	<10 %
2-ethylhexyl acrylate	<1.0	<10 %

Table 8-2. Levels of cinnamate functionalization in bicomponent copolymers of alkyl acrylate and maleic anhydride.

[a] methyl acrylate copolymer modification resulted in a slightly gelled system and the calculated mol% cinnamate is based on the soluble fraction.

The effect of a molar excess of EG-Cinn relative to the maleic anhydride concentration was also studied. The maleic anhydride containing polymers were functionalized in a 50 wt% ethyl acetate solution at 85 °C using various molarratios of cinnamate derivative to maleic anhydride functionality. ^{1}H NMR was employed to study the different levels of functionalization for the copolymers. Table 8-3 highlights the percent MAH conversion corresponding to polymer modification. As expected, increasing the EG-Cinn:MAH molar ratio, increased the conversion of maleic anhydride.

8.4.3 Succinic Anhydride Model System.

Further investigation of the polymer modification reaction involved use of *in situ* FTIR spectroscopy. A model system of succinic anhydride and *n*-butanol was utilized to the optimize polymer reaction conditions. A typical waterfall plot of the reaction in Figure 8-6 shows the disappearance of the succinic anhydride peak and the appearance of two carbonyl two peaks corresponding to the formation of the monobutyl ester of butanedioc acid. *p*-Toluene sulfonic acid and titanium isopropoxide were investigated as possible reaction catalysts (both added at 0.5 mol% compared to the succinic anhydride). Figure 8-7(a) shows the disappearance of the succinic anhydride and Figure 8-7(b) shows the formation of the monobutyl ester of butanedioc acid. Both catalysts studied increased the model reaction rate, with the *p*-TSA having a higher catalytic effect. This is evident from Figure 8-7(b), which shows the growth of the peak at 1738 cm^{-1}. The first data point (t = 0) from the formation of the monobutyl ester of

EG-Cinn:MAH	mol% cinnamate	MAH conversion
1.5:1.0	2.5	25 %
3.0:1.0	3.8	38 %
4.5:1.0	5.6	56 %

Table 8-3. Effect of EG-Cinn concentration on final maleic anhydride conversion.

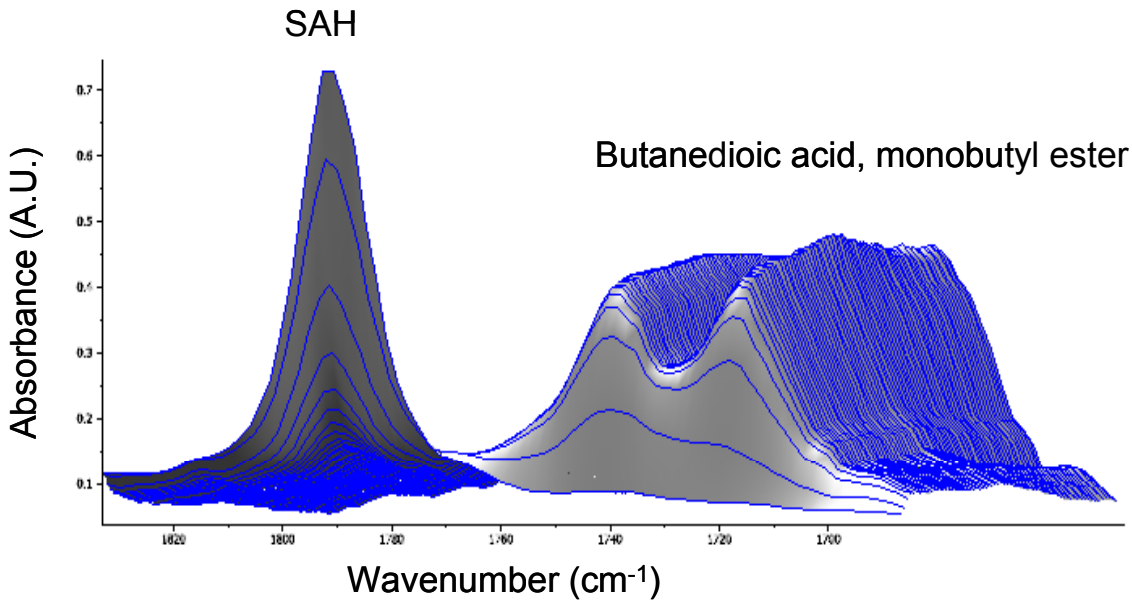

Figure 8-6. Real-time FTIR waterfall plot of succinic anhydride ring opening model reaction.

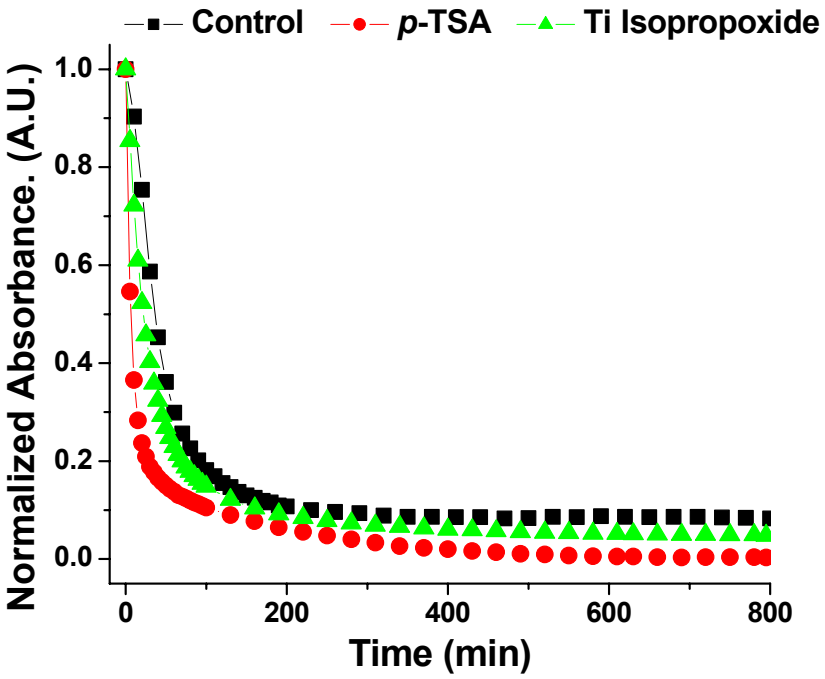

(a)

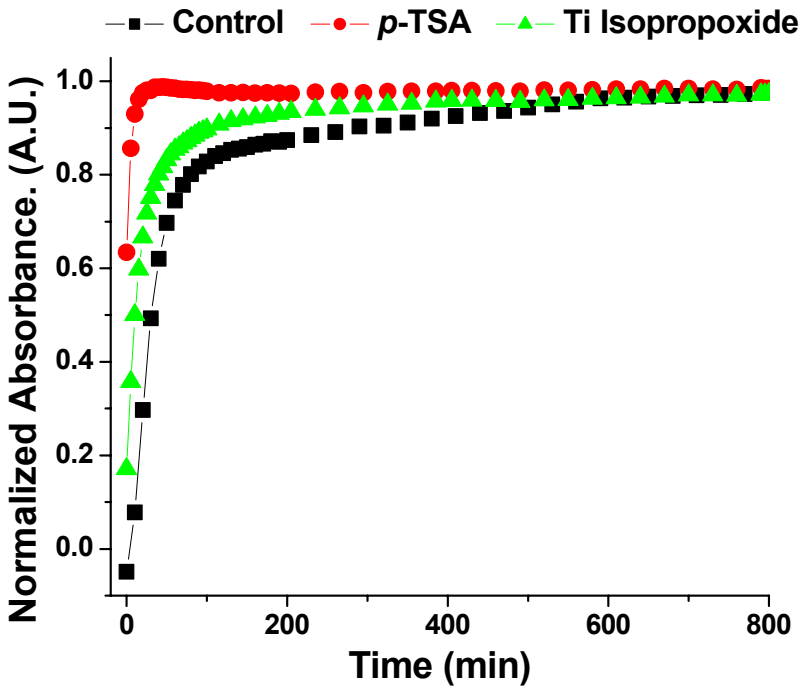

(b)

Figure 8-7. Real-time FTIR profiles of (a) disappearance of SAH (1790 cm^{-1}) and (b) formation of the monobutyl ester of butanedioc acid (1738 cm^{-1}).

butanedioc acid was at 0.63, indicating that 63% of the reaction had completed before the first spectrum was taken. The results from the model system indicated that the *p*-TSA catalyst would provide the best reaction conditions with which to ring open the maleic anhydride linkage.

8.4.4 Transfer of the Model System Results to the Polymer Modification Reactions.

Since the addition of the Ti isopropoxide and *p*-TSA increased the reaction rate of the model system, the polymer functionalization reactions were also performed with the individual catalysts. Each catalyst was added at a 1:3 molar ratio relative to the MAH in the polymer (i.e., 5 wt% of the *p*-TSA relative to the polymer mass) and the reactions were performed in toluene at 100 °C for 18 h. ^{1}H NMR was utilized to confirm the attachment of the photoactive group and determine the level of functionalization (Table 8-4).

As in the model system, both catalysts greatly increased the extent of maleic anhydride ring-opening reaction. Unfortunately, the polymers functionalized in the presence of catalyst were highly gelled following the modification reaction due to transesterification reactions. A second functionalization reaction in the presence of the Ti isopropoxide catalyst was performed at ½ the catalyst concentration (i.e., at a 1:6 molar ratio relative to the MAH in the polymer). The reaction also resulted in a gelled polymer with 100% maleic anhydride conversion.

Catalyst	mol% cinnamate	MAH conversion
None	2.2	22%
p-TSA	~10[a]	~ 100%[a]
Ti isopropoxide	~10[a]	~ 100%[a]

Table 8-4. The effect of catalyst on the level of polymer functionalization.
[a] soluble fraction.

8.5 CONCLUSIONS

The copolymer compositions containing 2-hydroxyethyl acrylate and maleic anhydride represent viable precursor polymers for introducing photoactive cinnamate groups via an acid chloride reaction and an anhydride ring opening reaction, respectively. The maleic anhydride based polymers were more difficult to functionalize than the HEA containing polymers. While the degree of functionalization for both systems depended on the steric bulk of the alkyl ester side chains of the comonomers, the maleic anhydride polymers proved more difficult to functionalize due to the proximity of the reaction site to the polymer backbone. The level of functionalization for both reactions was controlled by varying the molar ratio of the cinnamate derivative relative to either the HEA or the maleic anhydride in the polymer. The low level of functionalization in both systems was desired to promote chain-extension rather than crosslinking during irradiation. The model system provided valuable insights into possible methodologies to increase the degree of functionalization in the maleic anhydride copolymers. Unfortunately, initial experiments utilizing the chosen catalysts resulted in already crosslinked polymers. Since the desired polymer should contain approximately 2 mol% of cinnamate groups, future research will focus on achieving the desired level of cinnamate functionality, while reducing the amount of cinnamate charged into the reaction.

8.6 ACKNOWLEDGMENTS

The authors gratefully acknowledge financial support from the Avery Dennison Chemical Company, the Center for Adhesive and Sealant Science

(CASS) at Virginia Tech, and the Adhesive and Sealant Council Education Foundation. This material is based upon work supported in part by the U.S. Army Research Laboratory and the U.S. Army Research Office under grant number DAAD19-02-1-0275 Macromolecular Architecture for Performance (MAP) MURI.

CHAPTER 9 IRRADIATION AND ADHESIVE CHARACTERIZATION OF UV-CURABLE ACRYLIC HOT MELT ADHESIVES VIA A PHOTOCROSSLINKABLE CINNAMATE FUNCTIONALITY

Scott R. Trenor, Jeremy R. Lizotte, Brian J. Love, and Timothy E. Long
Virginia Tech
Department of Materials Science and the Department of Chemistry
Blacksburg, VA 24061-0212

9.1 SUMMARY

Multicomponent acrylate random copolymers were synthesized via conventional free radical polymerization methodologies to incorporate maleic anhydride or 2-hydroxyethyl acrylate units into the polymer backbone.[257] The anhydride and hydroxyl functionality were subsequently reacted with a photoactive cinnamate derivative possessing an appropriate functional group. The ring opening reaction associated with maleic anhydride modification resulted in attachment of the photoactive cinnamate functionality to the polymer backbone and the production of an adjacent carboxylic acid functionality. The photoactive macromolecules were subjected to irradiation (>300 nm) resulting in crosslinked polymeric materials. UV-Vis data indicated that the majority of the curing occurred during the first irradiation step with little additional curing during the postcure irradiations. Similarly, the peel strength and gel fraction increased with

the initial irradiation step. The gel fraction continued to either increase with the postcure irradiation, while the peel strength increased for the cinnamate-functionalized MAH PSA and decreased (cinnamate-functionalized EHA PSA).

Key words: UV crosslinkable, hot melt adhesives, photodimerization,

9.2 INTRODUCTION

There are currently three major types of pressure sensitive adhesives (PSA) available: solvent based acrylics, emulsions (aqueous based) and hot melt adhesives (SIS and SBS materials).[1,2,32-38] Hot melts and emulsion adhesives are growing in popularity due to the significant environmental issues associated with solvent-based adhesives, and the zero-emission hot melts are showing the highest growth rates. Hot melt adhesives are quite attractive because they possess high tack and a wide range of possible formulations with the addition of tackifiers and plasticizers. However, they have only moderate heat resistance and may be susceptible to oxidation of the residual double bonds.

Acrylic-based polymers are utilized in a number of PSA applications, but have the draw-back of solvent emission.[2,10,21,45] Since high molecular weights are required to achieve good adhesive properties with acrylic PSAs, these materials typically have high melt viscosities in the processing temperature regime and are applied from an organic solvent rather than from the melt. In order to develop acrylic-based PSAs that are applicable as hot melt adhesives, an increase in the polymer molecular weight must occur between the processing step (low molecular weight for facile processing) and the application or bonding step (higher molecular weight for adequate adhesion). UV curable hot melt and warm

melt PSAs are under development as potential melt processable, zero-emission acrylic adhesives.

Warm melt PSAs typically consist of a low molecular weight polyurethane or polyester acrylate, a mixture of acrylic monomers, tackifiers, antioxidants, and a photoinitiator.[35,37,46,47] The mixtures are typically coated at or above room temperature, then photopolymerized/crosslinked with UV irradiation. While these systems show some promise, they have a number of shortcomings including high material costs, residual monomer after curing and low heat resistance, among others.

Schumacher and coworkers recently developed a photoreactive acrylic hot-melt adhesive, incorporating vinyl derivatives of a common photoinitiator (benzophenone).[32-34,41,48-53] When irradiated between 220 and 280 nm, the benzophenone decomposes, forming a radical which then reacts with a tertiary carbon in the polymer to form a crosslink.[34,53,55,56] This reaction increases the molecular weight of the adhesive and begins to form a lightly crosslinked gel. As the UV dose was increased, the gel fraction and cohesive strength increased, and the adhesion and tack decreased.[41] Mehnert and coworkers studied the photocrosslinking of Schumacher's UV-curable PSA with real-time FTIR.[55,56] While the reaction stopped as soon as the light was removed, the system was easily over-cured, and the reaction rate and extent of reaction was significantly dependent on temperature. An additional shortfall of Schumacher's adhesive is the ease with which it crosslinks upon subsequent irradiation. Subsequent irradiation (for example during the ink curing process in label making) can further

crosslink the system, leading to reduced peel strengths similar to the releasable adhesives synthesized by Webster et al.[24-26,55,56]

An additional route to photocrosslinking polymers involves photoactive groups that react via non-radical radiation pathways.[94,188,190,193,232,361,420] Crosslinking via non-radical pathways afforded the first synthetic photoreactive polymers via photodimerization of poly(vinyl cinnamate).[154,157,403] UV irradiation of coumarin and cinnamate molecules provides a photocrosslinking route involving the formation of a cyclobutane ring via a [2π+2π] cycloaddition (Figure 8-1).[58,358] Cinnamate derivatives were recently used to crosslink a number of acrylic liquid crystalline polymers with good success.[169,172,176,242-244,247,250,251] There are a number of advantages to the cycloaddition crosslinking reaction over free radical methodologies. For example, cinnamate photodimerization reactions need two unreacted molecules to form a crosslink, so irradiation will only cause a reaction if two cinnamate groups "find" each other. This is in contrast to the benzophenone pathway, in which irradiation forms a radical that can react with any tertiary carbon to form a crosslink. In addition, the cycloaddition pathway is not thermally allowed and is not affected by fluctuations in the cure temperature as were the Schumacher adhesives.[91,184,243,420,439]

This report describes the characterization and curing behavior of UV-curable acrylic PSAs. UV irradiation was utilized to photo-chain-extend and photocrosslink the PSAs. Two polymers containing cinnamate functionalities were synthesized using different methods for cinnamate functionalization. The first polymer was functionalized via an esterification reaction between

hydroxyethyl acrylate and cinnamoyl chloride, while the second was functionalized via a ring opening reaction of maleic anhydride and an ethylene glycol derivatized cinnamate. The maleic anhydride pathway positions an acid functionality alpha to the cinnamate group on the polymer backbone. In addition to increasing peel strength, the acid groups may help position cinnamate groups closer to each other and increase the photodimerization reaction rate and extent.[15,185] The subsequent photocuring and adhesive properties (peel strength) are the two UV-curable acrylic PSAs are described.

9.3 EXPERIMENTAL

9.3.1 **Materials.**

Avery Dennison Chemical Company provided the *n*-Butyl (*n*BA), 2-hydroxyethyl (HEA), methyl (MA), and 2-ethylhexyl acrylate (EHA), which were passed through a neutral alumina column to remove radical inhibitors prior to use. Maleic anhydride (MAH), succinic anhydride (SAH), and 2,2'-azobisisobutyronitrile (AIBN) were purchased from Aldrich and used as received. Ethylene glycol, triethylamine and cinnamoyl chloride were purchased from Acros. The ethylene glycol was dried in a vacuum oven for 24 h at 80 °C prior to use. All other solvents were purchased from Acros and used as received.

9.3.2 **Instrumentation.**

^{1}H NMR spectra were recorded using either a Varian Unity 400 MHz or a Varian Inova 400 MHz spectrometer at 25 °C in $CDCl_3$ at ambient temperature. UV-Vis spectroscopy was performed using an Analytical Instrument Systems Inc. spectrometer equipped with fiber optic light guides, a DT1000CE light source,

and an Ocean Optics USB2000 UV-Vis detector. Molecular weights were determined at 40 °C in chloroform or THF (HPLC grade) at 1 mL min^{-1} using polystyrene standards on a Waters 707 equipped with 3 in-line PLgel 5 μm MIXED-C columns, a Waters 410 refractive index detector and an in-line Wyatt Technology Corp. miniDAWN multiple angle laser light scattering (MALLS) detector.

9.3.3 **Synthesis of Maleic Anhydride Containing Acrylic Copolymer.**

The synthesis of a typical MAH mulit-component copolymer is described. The MA (4.82 g, 56.0 mmol), *n*BA (22.6 g, 176 mmol), and EHA (13.6 g, 73.8 mmol) monomers were added to a 250 mL round-bottomed flask with a magnetic stir bar. Maleic anhydride (3.28 g, 33.4 mmol) was then added to the reaction flask, and the reaction mixture was diluted with ethyl acetate (34 mL) to 45 wt% solids. Finally, the initiator, AIBN (442 mg, 1 wt% compared to monomer), was added to the reaction vessel. The reaction mixture was sparged with nitrogen for 15 minutes. The polymerization vessel was subsequently equipped with a water condenser and a nitrogen inlet/outlet. The flask was placed in an 85 °C oil bath with a magnetic stirrer and allowed to polymerize for 24 h under a nitrogen blanket. The polymer was diluted with ethyl acetate (25 mL) and precipitated into methanol. The isolated polymer product was dried in the vacuum oven at 65 °C for 24 h. The purified yield was 93%. The HEA containing copolymer was synthesized similar to the MAH-containing copolymer with HEA substituted for MAH. The purified yield was 94%.

9.3.4 **Modification of the Maleic Anhydride Containing Copolymers.**

The maleic anhydride-containing polymer (9.21 g) was transferred to a 100 mL round-bottomed flask with a magnetic stir bar. The purified ethylene glycol cinnamate derivative (2.07 g, 10.8 mmol) was added to the reaction flask. The reaction mixture was diluted with toluene to produce a 30 wt% solids solution. The flask was equipped with a water condenser and nitrogen atmosphere, and the toluene reaction mixture was heated in a 105 °C oil bath and stirred for 18 h. The modified polymer product was precipitated into hexanes and dried in the vacuum oven at 65 °C for 24 h. The catalyzed functionalization reactions were prepared in a similar manner with the catalysts (*p*-toluene sulfonic acid or titanium isopropoxide) added at 1:3 molar ratio compared to the maleic anhydride concentration of the polymer.

9.3.5 Modification of the HEA Containing Copolymers.

A typical coumarin modification of HEA containing copolymers is described. The polymer (5.40 g) was dissolved in 43 mL distilled THF then combined with triethylamine (0.389 g, 3.84 mmol) and stirred under nitrogen in a 100 mL round-bottomed flask. Triethylamine was added at a 20 mol% excess compared to the cinnamoyl chloride. Cinnamoyl chloride (387 mg, 2.33 mmol) was dissolved in 3 mL distilled THF and added dropwise via an addition funnel to the polymer and triethylamine mixture. The addition funnel was then rinsed with an additional 1 mL distilled THF. The reaction mixture was stirred at 0 °C overnight under a nitrogen blanket with the reaction vessel covered in aluminum foil to avoid ambient photoreactions. The modified polymer product was filtered to remove

the triethylamine salt, precipitated into methanol, and dried in the vacuum oven at 65 °C for 24 h.

9.3.6 **Irradiation System.**

A Fusion UV Systems, Inc. F300s series microwave powered electrodeless lamp source coupled with a LC-6B bench top conveyer was utilized for the irradiation studies. An “H” or “D” bulb (linear power output of 80 W cm^{-1}) was utilized in the lamp depending on the cure step. Table 9-1 lists the typical output of the lamp in the UVA (320 – 390 nm), UVB (280 - 320 nm) and UVC (250 - 260 nm) regions of the electromagnetic spectrum as measured with the Power Puck. The belt speed was set at 18.3 m min^{-1} for all irradiations unless otherwise noted. UVA irradiance and effective dose were measured before and after each sample set with an EIT UV Power Puck radiometer. Test samples were irradiated with the H bulb for the first pass (cure step), then irradiated six times with the D bulb (postcure).

9.3.7 **UV-Vis Spectroscopy and Gel Fraction Sample Preparation.**

Homogenous films of 1 - 2 μm thickness were solvent cast from chloroform onto quartz microscope slides and drawn using a doctor blade for the UV-Vis studies. Film thickness was measured using microcalipers. Homogenous films (25 to 30 μm thick) were solvent cast from chloroform onto a silicone release liner and drawn using a doctor blade for the gel fraction studies. Both sets of samples were placed onto the conveyor and exposed to UV at 18.3 m min^{-1}. Gel fractions were determined using soxhlet extraction in refluxing THF for a minimum of 4 hours.

Bulb	UVA ($W\ cm^{-2}$)	UVB ($W\ cm^{-2}$)	UVC ($mW\ cm^{-2}$)
H	1.58	1.43	54
D	3.50	1.14	30

Table 9-1. Typical lamp output.

9.3.8 Peel Strength Sample Preparation.

Homogenous films of 28 to 30 g m^{-2} film weight were solvent cast from chloroform onto Mylar™ backing material and drawn using a doctor blade. After casting, the peel samples were dried in a preheated 65 °C oven for 4 hours. The peel samples were then irradiated with the H bulb with the adhesive facing the irradiation source. Following H bulb irradiation, a silicone release liner was placed on top of the adhesive forming a sandwich structure (Figure 9-1). The sandwich was then irradiated with the D bulb six times, with the radiation passing through the Mylar™ backing material. For the peel testing, the release liner was removed and the adhesive was applied to a stainless steel coupon (from ChemInstruments) and passed over (back and forth one time) with a 2.0 kg (4.5 lb) roller. The 90° peel test were performed at 305 mm min^{-1} (12 inches min^{-1}) following a 10 min. dwell time.

9.4 Results and Discussion

9.4.1 Polymer Synthesis and Characterization.

The synthesis, functionalization and characterization of the polymers in this study were described in the previous chapter (Chapter 8). Two precursor polymer compositions were synthesized. The first consisted of *n*BA, EHA, MA and MAH (referred to as the MAH polymer) while the second consisted of *n*BA, EHA, MA and HEA (referred to as the HEA polymer). Each polymer was subsequently functionalized via one of two pathways (Scheme 8-1). The MAH polymer was reacted with an ethylene glycol cinnamate derivative via a ring

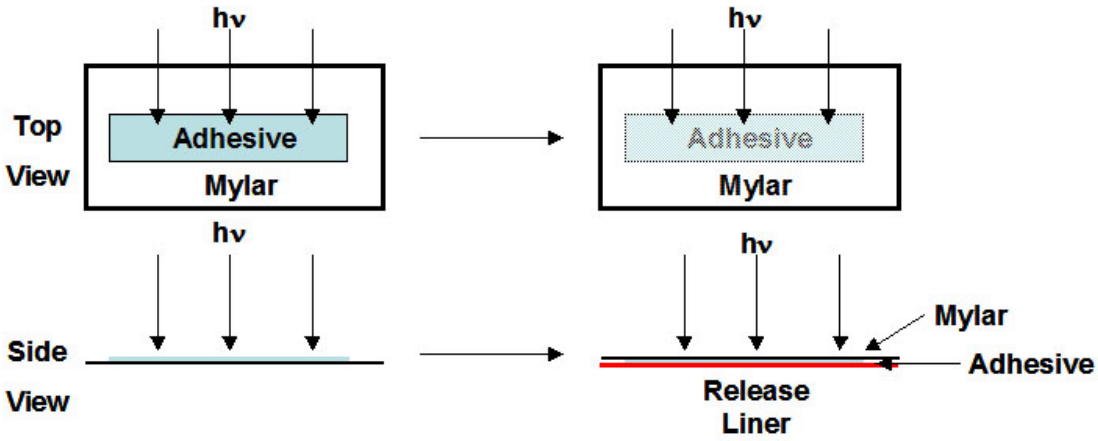

Figure 9-1. Peel testing sample preparation showing irradiation of the adhesive in the cure and the postcure steps.

opening reaction of the maleic anhydride repeat unit. The HEA polymer was functionalized via an esterification reaction between cinnamoyl chloride and the hydroxyl functionality of the HEA. While both reactions result in cinnamate functionalized polymers with the photoreactive cinnamate double bond at an equivalent distance from the polymer backbone, the cinnamate in the MAH polymer is adjacent to an acrylic acid functionality. This acrylic acid group was thought to aid in the photodimerization reactions by possibly bringing multiple cinnamate groups into close proximity via hydrogen bonding interactions. Since the dimerization reaction necessitates the presence of two cinnamate groups, the hydrogen bonding of the acid groups may aid the extent of reaction. Table 9-2 summarizes the characterization data of the two cinnamate-functionalized PSAs.

9.4.2 Irradiation and Evaluation of the Photocrosslinking Process.

The polymeric materials were cast as films (1 - 2 μm thick) from chloroform onto quartz substrates. The cast films were exposed to UV irradiation via a conveyor system that carried the sample under the microwave UV source. The irradiation process involved exposure to two different UV microwave bulbs. The first pass was exposure to an H bulb that emits radiation more heavily focused in the UVC and UVB region of the spectrum. The next six passes under the D bulb exposed the sample to longer wavelengths and is referred to as the “postcure step”. These conditions mimicked the initial curing step of an adhesive (H bulb exposure) and the irradiation in subsequent ink curing steps in a typical commercial adhesive label-making process (D bulb exposure).

UV-Vis spectroscopy was used to monitor the disappearance of the double bond involved in the photodimerization reaction. A λ_{max} for the double bond absorbance was observed at 278 nm (Figure 8-2).

Figure 9-2 shows the typical change in absorbance as a function of cure step (first H bulb cure then the 6 subsequent postcure passes with the D bulb). The cinnamate dimerization conversion profiles are shown in Figure 9-3 for the cinnamate-containing polymers functionalized via the maleic anhydride and the HEA methodologies. The shapes of the curves in Figure 9-3 provide interesting insight into the polymer photoreactions.

As the polymers were irradiated with the H bulb, approximately 31% of the cinnamate was consumed via the $2\pi + 2\pi$ photodimerization reaction. On postcure with the D bulb, less than 6% of the cinnamate groups continue to react. This phenomenon was attributed to two factors. First, the H bulb provides a higher intensity in the shorter wavelengths (<300 nm) than the D bulb (Table 9-1). This shift in intensity is significant since the peak absorbance of the cinnamate groups is at 278 nm. Thus, less light is absorbed from the D bulb, resulting in fewer photoreactions. Second, crosslinking via the photodimerization reaction is self-limiting. As the polymer crosslinks or chain-extends, the viscosity of the system increases and it becomes increasingly difficult for two cinnamate groups to come in close enough proximity to dimerize. This is a distinct advantage over the other UV curable acrylic methodologies such as the benzophenone photoinitiated reactions, in that once the benzophenone excited

PSA	Composition (mol %)						M_n	M_w/M_n
	***n*BA**	**EHA**	**MA**	**MAH**	**HEA**	**Cinn**		
MAH	53	17	20	8.8	N/A	2.2	51,300	3.27
HEA	53	20	16	N/A	8.9	2.1	84,300	4.06

Table 9-2. Composition and molecular weight of cinnamate-functionalized acrylic PSAs.

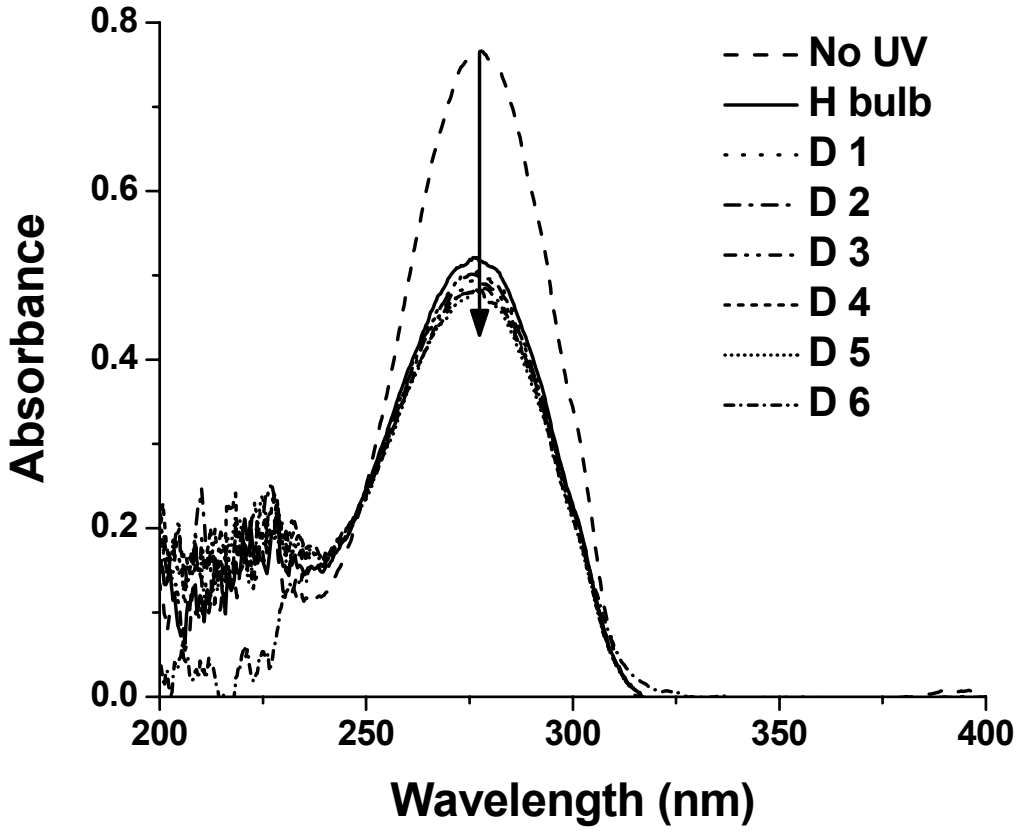

Figure 9-2. Typical UV absorbance of the cinnamate containing polymers (No UV) and subsequent decrease in absorbance as a function of cure step.

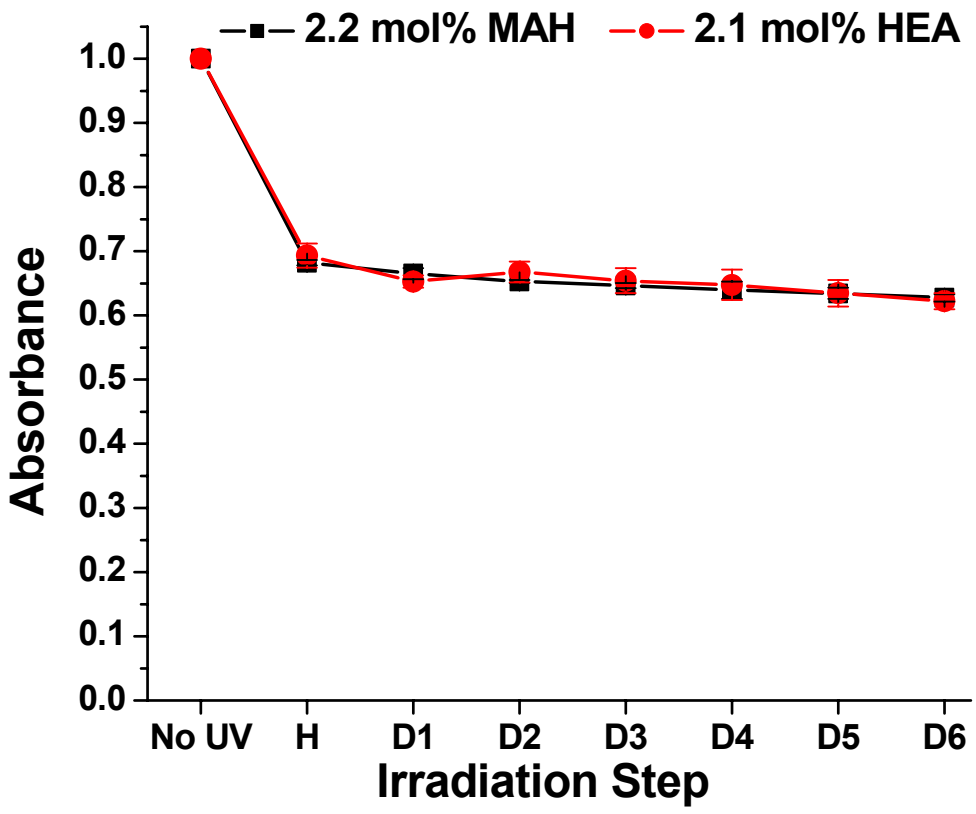

Figure 9-3: Typical double bond consumption profile for cinnamate modified random copolymers (H = H bulb cure and D# = D bulb postcure step number).

triplet is formed, the radical needs only to find a tertiary carbon with which to react and further increase the crosslinking density. Therefore, the possibility of over curing the adhesive and subsequent decrease in the peel strength is greatly reduced.

The comparison of the reaction profiles of the cinnamate groups in both PSAs indicates the role that the acrylic acid groups play in the photodimerization reaction. The ring opening of the maleic anhydride with the EG-Cinn derivative forms an acrylic acid group adjacent to the cinnamate side group. The acrylic acid functionality was thought to aid in the photoreaction via hydrogen bonding and thus bring the cinnamate groups closer together.[184,185] Within the scatter of the measurements, there was no difference in the photodimerization reaction of the two polymers. Therefore, the adjacent acrylic acid groups did not influence the extent or rate of photodimerization.

9.4.3 **The Effect of Irradiation on the Gel Fraction.**

The effect of irradiation from the cure step (H bulb) and the postcure steps (D bulb) on the gel fraction is shown in Figure 9-4 for the cinnamate-functionalized EHA and MAH PSAs. As the MAH and HEA PSAs were irradiated with the H bulb, 20 and 5 wt% gel was formed, respectively, via the crosslinking of the cinnamate groups. The postcure irradiation (6 passes under the D bulb) increased the gel fraction of both polymers. Post curing of the cinnamate-functionalized HEA polymer increased the percent gel to 60%, while the cinnamate-functionalized MAH polymer increased to 17%. Since the HEA PSAs had higher initial molecular weights, each chain had more repeat units and thus

more cinnamate groups than the MAH based PSAs. Thus, higher gel fractions formed more readily with the HEA polymers. Once again, it was not desirable to further increase the gel fraction due to potential decreases in the adhesive peel strengths.[1,2,15,22]

9.4.4 The Effect of Irradiation on Adhesive Peel Strengths.

The effect of irradiation on the average peel strength of the cinnamate-functionalized HEA copolymer is shown in Figure 9-5. As the adhesive was cured via irradiation with the H bulb, chain-extension and crosslinking increased the peel strength of the adhesive from 4.9 to 5.6 N per cm-width. Further irradiation (postcuring with the D bulb) slightly decreased the peel strength to 5.1 N per cm-width. This was expected as higher gel content typically leads to lower peel strengths.[1,2,15,22] The failure mechanism in all cases was cohesive, indicating that the cohesive strength of the adhesive was low. This result was not expected as increasing the gel fraction of an adhesives typically increases the cohesive strength of the adhesive.[1-3,22]

Figure 9-6 illustrates the effect of irradiation on the average peel strength of the cinnamate-functionalized MAH copolymers. The peel strength of the non-irradiated adhesive (4.8 N per cm-width) was similar to that of the non-irradiated HEA based sample (4.9 N per cm-width) even though the M_w of the MAH based polymer was significantly lower (Table 9-2). The higher molecular weight polymer should have higher peel strengths due to the increased number of entanglements per chain.[10] The similar peel strengths were attributed to the

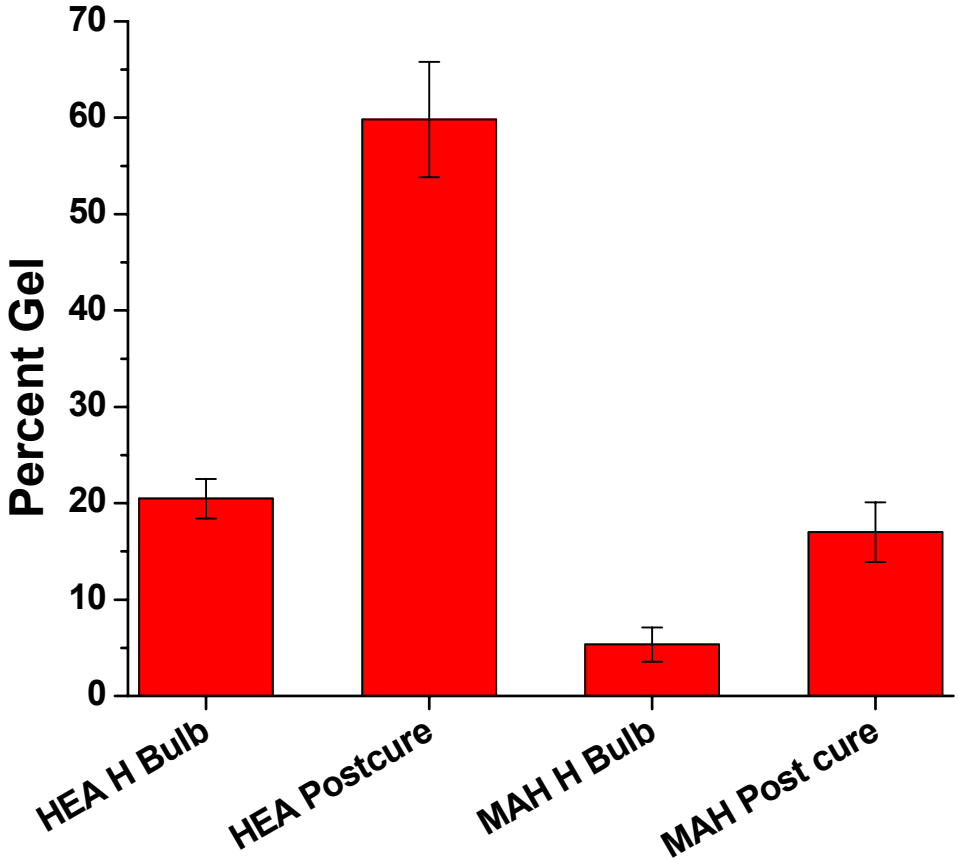

Figure 9-4. Gel fraction for the cinnamate-functionalized HEA and MAH copolymers after cure and postcure steps.

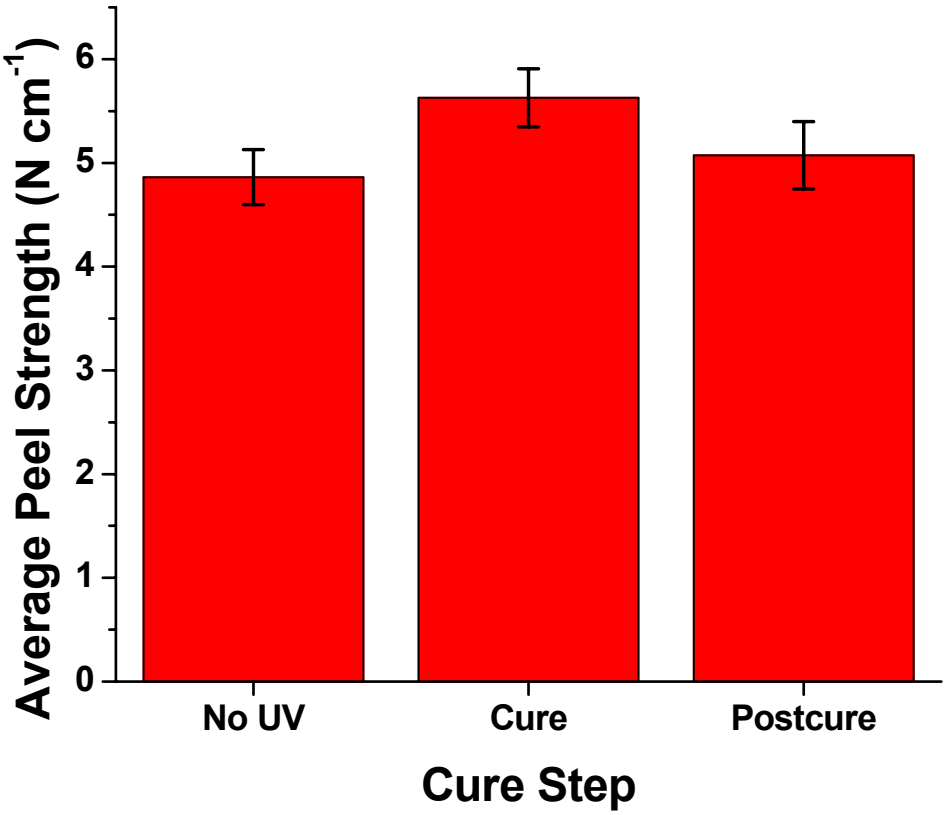

Figure 9-5. The effect of irradiation on the peel strength on the cinnamate-functionalized HEA copolymer.

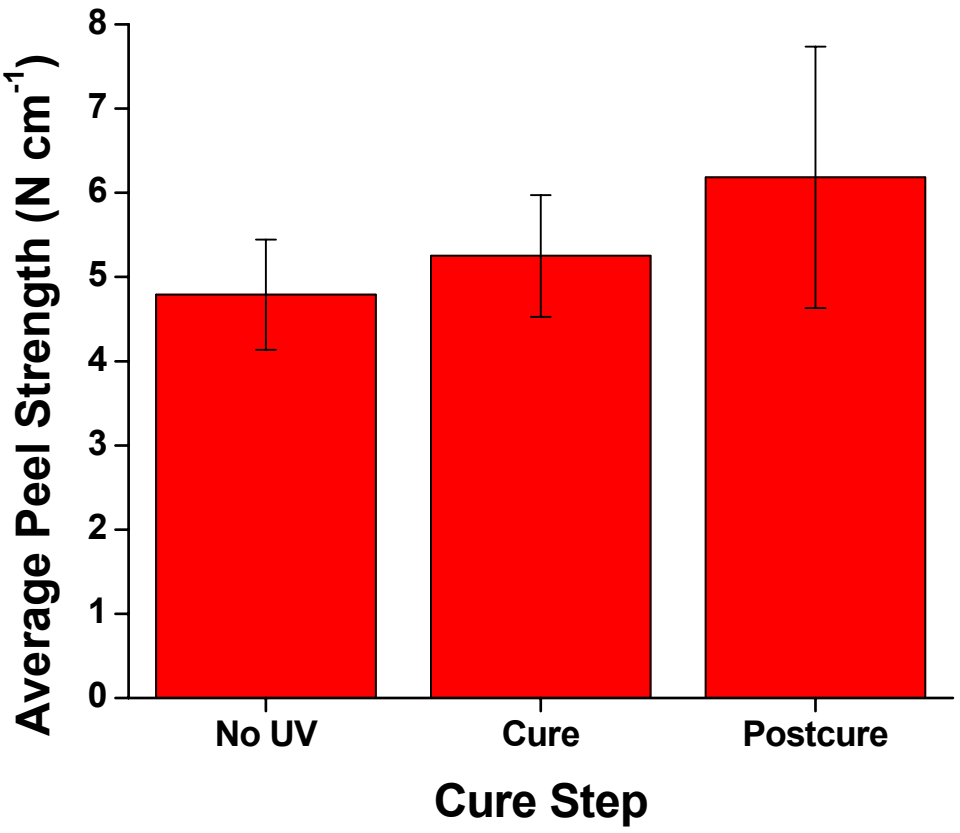

Figure 9-6. The effect of irradiation on the peel strength on the cinnamate-functionalized MAH copolymer.

presence of acrylic acid in the cinnamate-functionalized MAH PSA. Cure of the MAH PSAs (H bulb) led to a slight increase in the peel strength from 4.8 to 5.3 N per cm-width. The postcure step further increased the peel strength to 6.2 N per cm-width. The peel strengths of the cinnamate-functionalized MAH PSAs did not decrease with postcure irradiation as was the case for the cinnamate-functionalized HEA PSAs. This was attributed to the relatively low amounts of gel in the cinnamate-functionalized MAH PSAs after postcure (17%) versus that of the cinnamate-functionalized HEA PSAs (60%).

Another difference between the cinnamate-functionalized HEA adhesive and the cinnamate functionalized MAH adhesive was the mode of failure. As previously mentioned, all of the cinnamate-functionalized HEA adhesives (nonirradiated, H bulb cure and D bulb postcured) failed cohesively in all tests. However, the nonirradiated cinnamate-functionalized MAH adhesive failed predominantly via an adhesive mechanism (> 90% adhesive failure from visual inspection). This was expected as the presence of acrylic acid has been shown to increase the cohesive strength of adhesives and thus promote adhesive failure.[1,10,15] As the adhesive was irradiated, the failure mechanism became more adhesive and a stick-slip failure became prominent leading to the large scatter in the measurements.[2,15]

Static shear testing was performed on the cinnamate-functionalized HEA and MAH PSAs before and after curing using stainless steal substrates an a 12.7 x 12.7 mm (0.5 x 0.5 inch) Mylar-backed adhesive tape. The time to failure at a loading of 500 g is shown in Figure 9-7. The HEA based PSA displayed little

change in the shear holding time with irradiation failing at 2.3 and 2.2 min for the uncured and cured adhesives, respectively. However, the MAH based PSA showed a substantial change upon curing. The shear holding time increased from 30 s for the uncured sample to nearly 2 min for the cured sample. UV irradiation induced chain-extension and light crosslinking of the lower molecular weight MAH-based PSA (compared to the HEA-based PSA) had a pronounced effect on the MAH based PSA shear holding time.

9.5 CONCLUSIONS

The copolymer compositions containing HEA and MAH represent viable precursor polymers for the introduction of a photoactive cinnamate group. Irradiation of the adhesives with the H bulb (cure step) consumed ~31% of the cinnamate groups regardless of the polymer structure. The consumption of the cinnamate groups increased the molecular weight and gel fraction of the adhesive. Postcuring of the adhesives with the D bulb in a manner that simulated the ink-curing step in an industrial label making procedure minimally affected the extent of dimerization. The gel fractions of the cinnamate-functionalized HEA adhesives increased from 0 to 20 and 60% for the cure and postcure steps, respectively. Similarly, the gel fractions of the cinnamate-functionalized MAH adhesives increased from 0 to 5 and 17% for the cure and postcure steps, respectively. The increase in the adhesive molecular weight and gel fraction led to slight increases in the average peel strengths of the adhesives and a decrease in the peel strength of the postcured cinnamate-functionalized

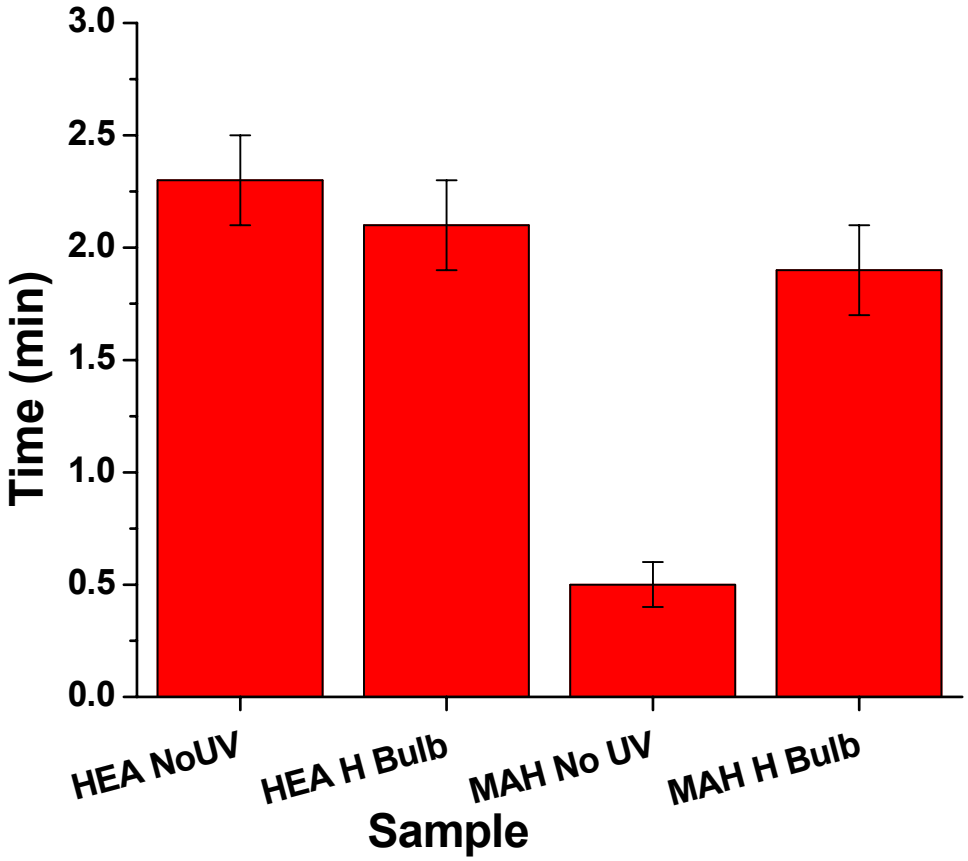

Figure 9-7. The effect of irradiation on the shear holding time of the cinnamate-functionalized HEA and MAH based PSAs.

HEA PSA. While the presence of acrylic acid groups adjacent to the cinnamate groups did not aid in the rate or extent of the photoreactions, they did increase the cohesive strength of the adhesive and promote a predominately adhesive failure mechanism. The results of this work indicate that both systems are candidates as UV-curable hot melt adhesives.

9.6 ACKNOWLEDGMENTS

The authors gratefully acknowledge financial support from the Avery Dennison Chemical Company, the Center for Adhesive and Sealant Science (CASS) at Virginia Tech, and the Adhesive and Sealant Council Education Foundation. The authors would specifically like to thank Dr. Yi Wei at Avery Dennison for the shear testing. This material is based upon work supported in part by the U.S. Army Research Laboratory and the U.S. Army Research Office under grant number DAAD19-02-1-0275 Macromolecular Architecture for Performance (MAP) MURI.

CHAPTER 10 ELECTROSPINNING AND PHOTOCROSSLINKING OF CINNAMATE-FUNCTIONALIZED POLY(METHYL METHACRYLATE-CO-2-HYDROXYETHYL ACRYLATE)

Scott R. Trenor, Pankaj Gupta, Timothy E. Long, and Garth L. Wilkes
Department of Chemical Engineering
and
Department of Chemistry
Virginia Polytechnic Institute and State University
Blacksburg, VA 24061

10.1 SUMMARY

Photocrosslinked electrospun fibers were made in a single step process. Random copolymers of methyl methacrylate and hydroxyethyl acrylate were synthesized via free radical polymerization and subsequently functionalized with cinnamoyl chloride via a side group esterification reaction with varying degrees of cinnamate functionality. The cinnamate-functionalized polymers were photocrosslinked *in situ* during the electrospinning of the fibers. Photocrosslinking via $2\pi + 2\pi$ photodimerization of cinnamate derivatives led to insoluble non-woven fiber mats without the need for photoinitiators. The cinnamate-functionalized terpolymers were also irradiated in the film state. While similar percentages of cinnamates were consumed during both photocrosslinking processes, the films were still soluble after the irradiation.

Keywords: electrospinning, photocrosslinking, cinnamate

10.2 INTRODUCTION

Traditionally, polymer fibers are spun using pressure-driven flow through an extruder, which yield fibers on the order of 10-100 μm in diameter.[442] However, fibers on the order of 100 nm in diameter are achievable with electrospinning. Electrospinning uses an electrostatic potential to charge a polymer solution or melt. The charged solution is emitted from a syringe forming a charged fluid jet in the presence of an electric field, providing the polymer possesses sufficient molecular entanglements.[442-446] The charged jet follows a chaotic trajectory of stretching and splaying until it reaches its grounded target, thus completing the circuit.

If sufficient entanglements are not present, the jet breaks up into small droplets leading to the well-known phenomenon, electrospraying. However, if the polymer solution possess sufficient chain overlap and entanglements, it does not break up and undergoes a bending instability that causes a whip-like motion between the capillary tip and the grounded target.[447] This bending instability accounts for the high degree of single fiber drawing, which results in submicron size fibers.[442] The small fiber size and disordered deposition onto the grounded target yield nonwoven, three-dimensional, fiber mats with a high specific surface area. The unique fibers are suitable as filtration devices, membranes, vascular grafts, protective clothing, and tissue scaffolding applications.[442,444-446,448-452]

Recent efforts have targeted the synthesis of functional fibers via simultaneous electrospinning of two polymer solutions yielding bicomponent submicron fibers with properties of each polymer component and the

incorporation of acrylic functionalities for subsequent photocrosslinking.[450,453,454] Greiner and coworkers recently synthesized and subsequently electrospun poly(vinyl alcohol) containing either thienyl acrylate groups or incorporated tetraethyleneglycol diacrylate and ammonium persulfate. Subsequent UV irradiation of the electrospun fibers produced crosslinked fiber mats, insoluble in both water and steam.[453,454]

Derivatives of cinnaminic acid (Figure 10-1) photodimerize ($2\pi+2\pi$ cycloaddition) when irradiated in the ultraviolet-B (UVB) region of the electromagnetic spectrum.[91,156,157,167,181,247,403,420] Crosslinking via non-radical pathways afforded the first synthetic photoreactive polymers via photodimerization of poly(vinyl cinnamate) and the crosslinked fiber mat (thienyl acrylate route) in Greiner's study.[154,157,403,453,454] The photocrosslinking route for cinnamate molecules involves the formation of a cyclobutane ring via a [$2\pi+2\pi$] cycloaddition (Figure 10-1).[58,358] Cinnamate derivatives were recently utilized to crosslink a number of acrylic liquid crystalline.[169,172,176,242-244,247,250,251]

This work describes the use of cinnamate groups to photocrosslink fibers during electrospinning. Poly(methyl methacrylate-*co*-hydroxyethyl acrylate) was synthesized and subsequently functionalized with cinnamoyl chloride via a side group esterification reaction. The cinnamate-functionalized polymers were irradiated with UV light during electrospinning, thus forming and crosslinking the electrospun fibers in a single processing step. The extent of the

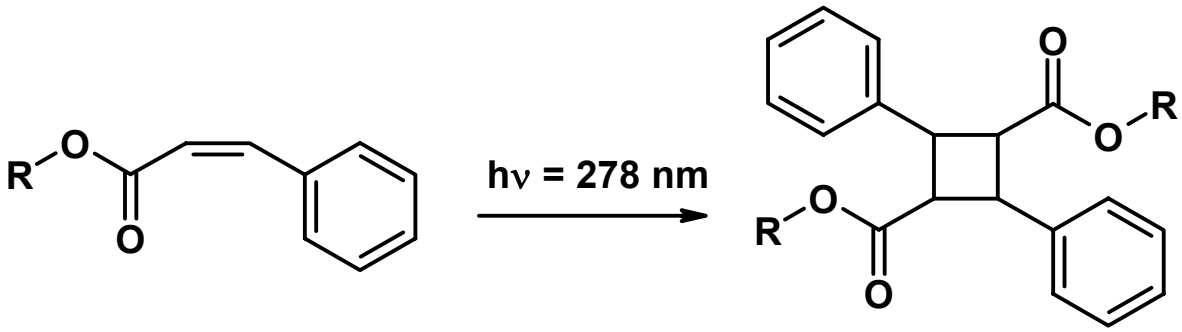

Figure 10-1. Photodimerization of cinnamate derivatives.

photoreactions was monitored with FTIR and gel fraction measurements. The results from electrospinning were compared to irradiated films with the same polymer composition.

10.3 Experimental Section

10.3.1 Materials.

Cinnamonyl chloride, ethyl acetate, and 2,2'-azobisisobutyronitrile (AIBN) and dimethyl formamide (DMF) were purchased from Sigma Aldrich. 2-hydroxyethyl acrylate (HEA) and methyl methacrylate (MMA) were purchased from Aldrich and passed through a neutral alumina column to remove radical inhibitors. All other solvents and reagents were purchased from commercial sources and were used without any further purification unless otherwise noted. THF was distilled from sodium/benzophenone under a nitrogen atmosphere prior to polymer/acid chloride reactions.

10.3.2 Instrumentation.

^{1}H NMR spectra were recorded using either a Varian Unity 400 MHz or a Varian Inova 400 MHz spectrometer at 25 °C in $CDCl_3$. UV-Vis spectroscopy was performed using an Analytical Instrument Systems Inc. spectrometer equipped with fiber optic light guides, a DT1000CE light source, and an Ocean Optics USB2000 UV-Vis detector. Molecular weights were determined at 40 °C in THF (HPLC grade) at 1 mL min^{-1} using polystyrene standards on a Waters 707 Autosampler equipped with 3 in-line PLgel 5 μm MIXED-C columns, a Waters 410 refractive index detector and an in-line Wyatt Technology Corp. miniDAWN® multiple angle laser light scattering (MALLS) detector. Solution rheology was

performed with a VOR Bohlin strain-controlled solution rheometer at 25 ± 0.2 °C using a concentric cylinder geometry. Differential scanning calorimetry (DSC) was performed with a Perkin Elmer Pyris 1 at a heating rate of 10 °C min^{-1} under nitrogen. The glass transition temperature (T_g) was measured during the second heat using the midpoint of the transition. Electrospun fiber diameter and morphology were analyzed using a Leo 1550 field emission scanning electron microscope (FESEM). Fibers were mounted onto an SEM disk, and sputter-coated with a Pt/Au layer. IR spectroscopy of the thin films was performed with an Olympus Bx51 microscope modified with a SensIR IlluminatIR all reflecting objective and stage. IR spectroscopy of the electrospun fibers was performed with a Nicolet 510 FTIR Spectrometer.

10.3.3 **Synthesis of 85:15 mol% MMA:HEA Precursor Copolymers.**

The synthesis of the precursor copolymer is described. The MMA (40.0 g, 465 mmol) and HEA (9.52 g, 81.9 mmol) monomers were added to a 250 mL round-bottomed flask with a magnetic stir bar. The reaction mixture was then diluted with ethyl acetate (205 mL, 80 vol%). Finally, the initiator, AIBN (40.3 mg, 0.1 wt%), was added to the reaction vessel, then equipped with a water condenser. The reaction mixture was sparged with nitrogen for 10 minutes, then placed in a 75 °C oil bath with a magnetic stirrer and polymerized for 24 h. The polymer was precipitated into methanol, then dried in the vacuum oven at 65 °C for 24 h. ^{1}H NMR analysis indicated 13 mol% HEA was incorporated into the copolymer. The poly(methyl methacrylate-*co*-hydroxyethyl acrylate) (poly(MMA-

co-HEA) copolymer weight average molecular weight (measured with MALLS) was 334,000 g mol^{-1} with a molecular weight distribution of 1.96.

10.3.4 **Copolymer Modification with Cinnamonyl Chloride.**

A typical cinnamate modification of MMA/HEA copolymers is described. Poly(MMA-*co*-HEA) (5.00 g) was dissolved in 40 mL freshly distilled THF then combined with triethylamine (0.644 g, 6.37 mmol) and stirred under nitrogen in a 50 mL round-bottomed flask. Cinnamonyl chloride (1.06 g, 6.37 mmol) was dissolved in 5 mL distilled THF and added dropwise via an addition funnel to the poly(MMA-*co*-HEA) and triethylamine solution. The addition funnel was then rinsed with an additional 5 mL distilled THF. The reaction mixture was stirred at 0 °C overnight under nitrogen with the reaction vessel covered in aluminum foil to avoid ambient photoreactions. After filtration of the salt, the resulting polymer was precipitated into approximately 300 mL 4:1 methanol:water solution, stored in an aluminum foil covered 60 mL bottle, and dried in the vacuum over at 65 °C for 24 h. The purified yield was 90%. Table 10-1 lists the compositions of the three cinnamate-functionalized terpolymers synthesized for this study.

10.3.5 *In situ* UV Irradiation of Electrospun Fibers

The three terpolymers were dissolved separately in DMF at a concentration of 20 wt%. These solutions were later electrospinning. The schematic of the electrospinning apparatus along with the UV source is shown in Figure 10-2. Electrospinning was performed in a vertical configuration

Cinn:HEA molar ratio	mol% MMA	mol% HEA	mol% Cinn	T_g (°C)
3:1	87	0	13	91
1:1	86	5	9.0	94
0.5:1	86	10	4.0	99

Table 10-1. Cinnamate reaction conditions and functionalized polymer composition.

where the fibers were electrostatically conveyed in the upward direction to the grounded target. This approached minimized the effect of IR heating from the lamp. A quartz tube protected the fibers from the cooling air outlet from the lamp. The terpolymer solution was filled in the syringe that was connected to a Teflon needle (0.7 mm internal diameter). The free-end of the Teflon needle was placed at the entrance of a 15 cm long quartz tube (15 cm internal diameter). A grounded steel wire mesh (collector/target) was positioned 5 cm away from the opposite end of the quartz tube, thereby making the total distance between the Teflon needle tip and target ~20 cm. A platinum electrode dipped in the polymer solution was connected to a high voltage DC power supply of positive polarity. The polymer flow rate was controlled with a syringe pump connected to the syringe.

For each of the three terpolymer solutions, electrospinning was performed at a voltage of 15kV, a flow rate of 3ml/h, a tip to target distance of 20 cm and a concentration of 20wt% in DMF. At the tip of the needle, the solution was observed to elongate into a conical shape, also referred to as the Taylor cone in the literature.[442-444,450] A jet was observed to emanate from the surface of the Taylor cone that traveled through the quartz tube to the grounded target. During its travel through the quartz tube, the jet was exposed to UVB irradiation (13.5 mJ cm^{-2} at an intensity of 0.135 W cm^{-2} as measured with the Power Puck) to cure the cinnamate groups. Samples collected for 10 min with and without UV curing were dried under reduced pressure at 40^{o}C for 8h before

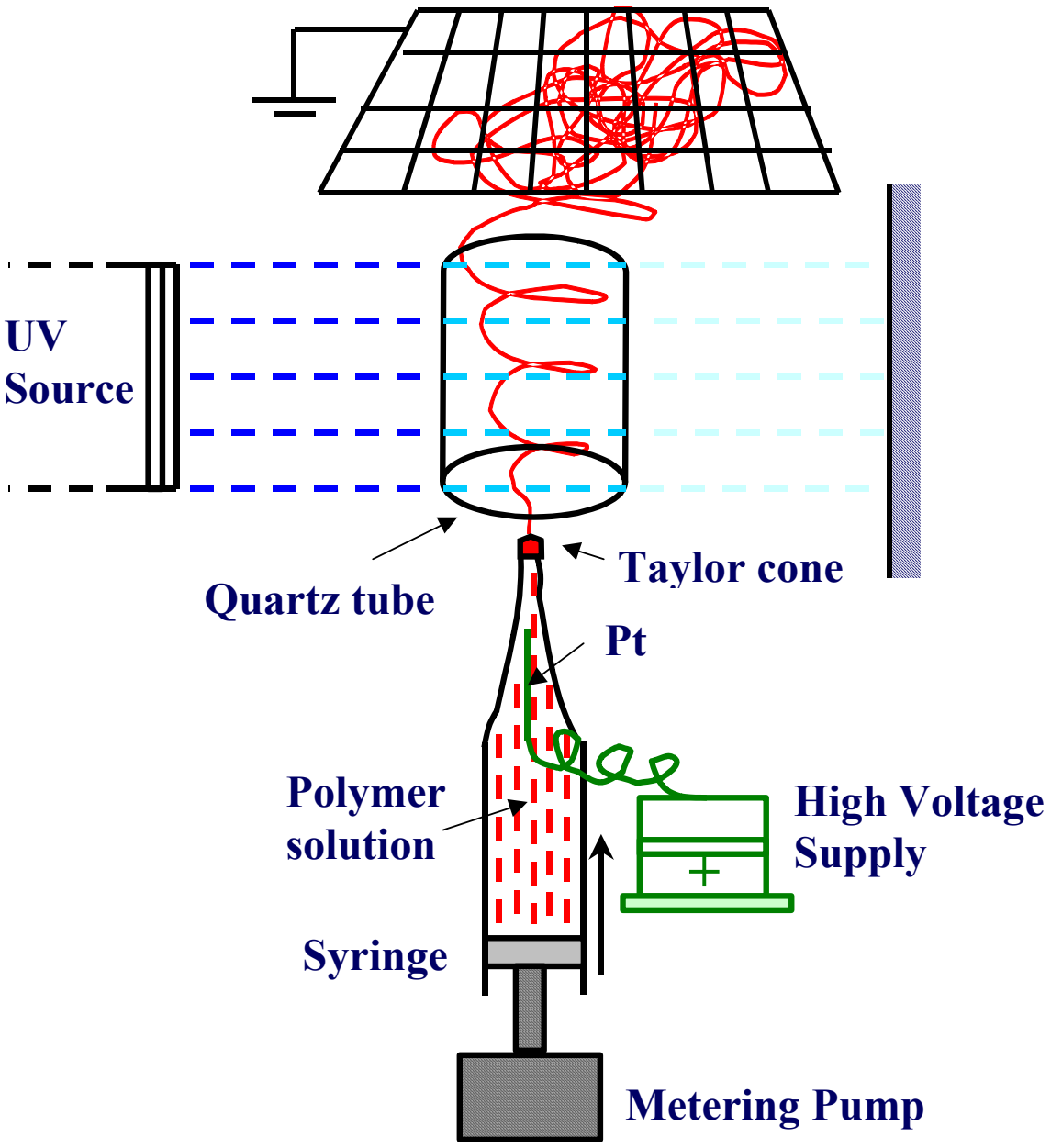

Figure 10-2. Schematic of electrospinning apparatus.

being investigated for morphological changes, if any, in addition to the infrared characterization and solvent extraction.

10.3.6 UV Irradiation of Polymer Films.

UVA irradiation was accomplished using a F300s series microwave powered electrodeless lamp source coupled with a LC-6B bench top conveyer manufactured by Fusion UV Systems, Inc. A "V" bulb (linear power output of 80 W cm^{-1}) was utilized to minimize the intensity in the UVB region. The belt speed was set at 87 m min^{-1} for all irradiations. This speed was selected to mimic the irradiation conditions of the electrospun fibers (13.5 mJ cm^{-2}). The UVB exposure for the films at 87 m min^{-1} was 14.6 mJ cm^{-2}. UVB irradiance and effective energy density were measured before and after each sample set with an EIT UV Power Puck radiometer. Extent of photoreaction was monitored using FTIR spectroscopy. Homogenous films (less than 1 μm thick) were solvent cast from chloroform onto low e-glass microscope slides and drawn using a doctor blade for FTIR spectroscopy. The extent of crosslinking was measured using soxhlet extractions of irradiated 20-25 μm thick.

10.4 Results and Discussion

10.4.1 Synthesis and Modification of Poly(MMA-co-HEA).

The precursor poly(MMA-*co*-HEA) copolymer was synthesized via an AIBN initiated conventional free radical solution polymerization in ethyl acetate. The resulting copolymer exhibited a weight average molecular weight of 333,000 g mol^{-1} with a molecular weight distribution of 1.96. The composition of the

copolymer was examined using ^{1}H NMR spectroscopy and corresponded well with the feed ratios of 87 mol% MMA and 13 mol% HEA.

Modification of these MMA-*co*-HEA copolymers proceeded via an esterification reaction between the hydroxyl group of the HEA and the cinnamate acid chloride derivative (Scheme 10-1). Manipulation of the molar ratio of cinnamoyl chloride to the hydroxyl functionality was utilized to control the level of functionalization. Three cinnamate-functionalized MMA-*co*-HEA copolymers were synthesized with cinnamate concentrations of 4.0, 9.0 and 13 mol% (Table 10-1). ^{1}H NMR of the modified MMA-*co*-HEA copolymers confirmed functionalization of the copolymers with three different levels of the cinnamate functionality. The resonances associated with the cinnamate group were apparent at 7.73, 7.52, 7.38, and 6.49 ppm. A reduction in the peak area of the methylene adjacent to the hydroxyl at 3.75 ppm was observed along with the corresponding appearance of the methylene resonance adjacent to an ester linkage at approximately 4.42 ppm. The IR spectra of the 10 mol% cinnamate-functionalized copolymer is shown in Figure 10-3(a) and (b). The arrow in Figure 10-3(b) highlights the absorbance of the C=C bond stretch associated with the cinnamate group. Decreases in the absorbance of this C=C stretch were used to determine the extent of photodimerization. Moreover, a new signal was observed in the UV-Vis spectrum of the polymer characteristic of the double bond absorbance associated with the cinnamate functionality at 278 nm (Figure 10-4).[152,169,181]

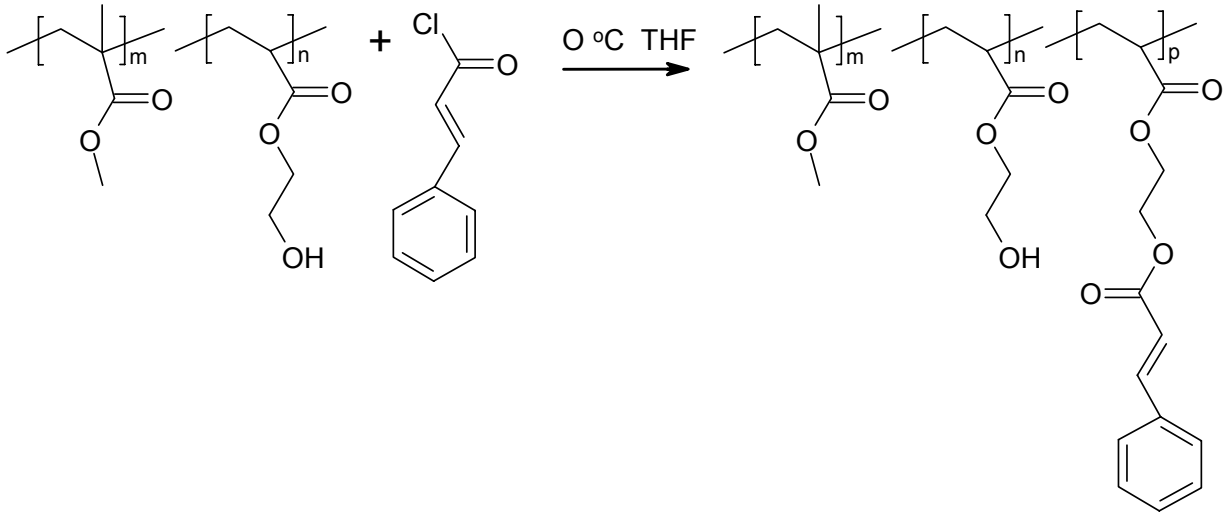

Scheme 10-1. Cinnamate functionalization of poly(MMA-*co*-HEA).

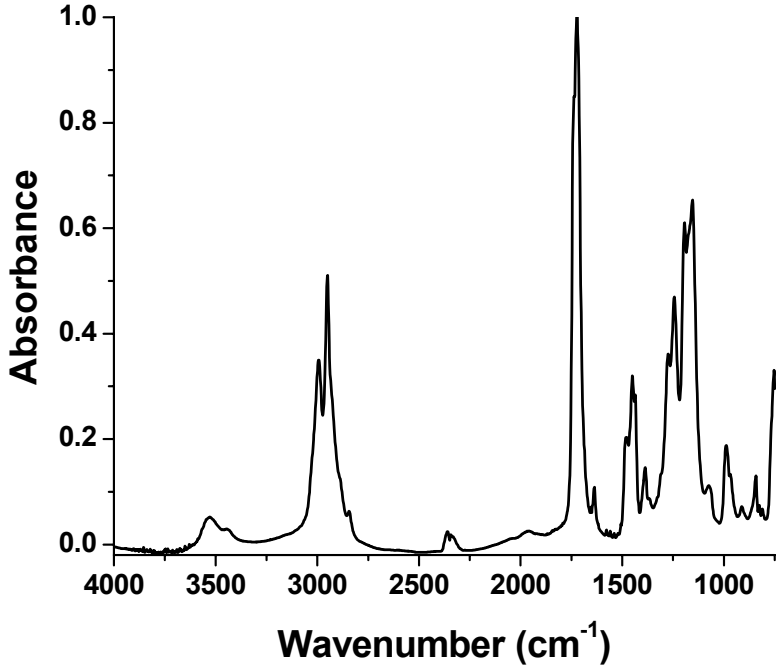

(a)

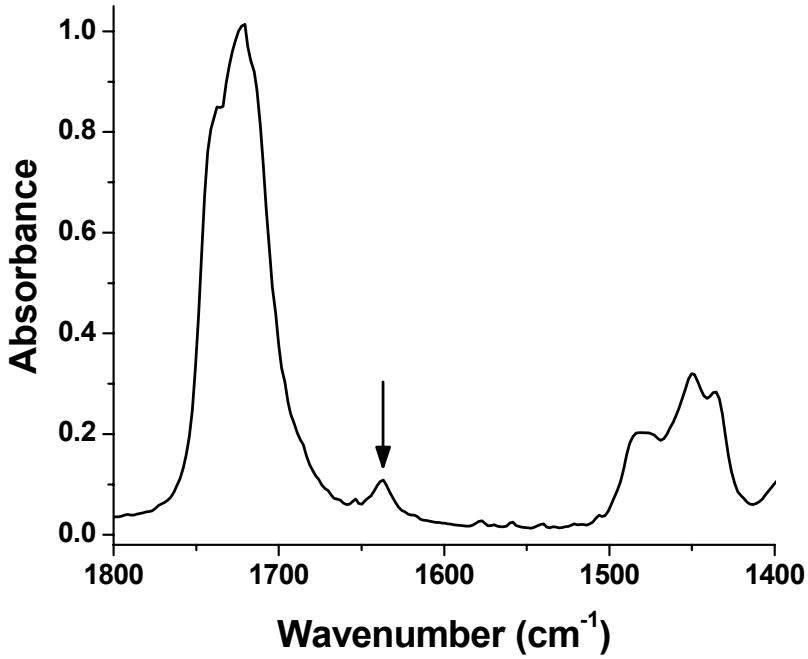

(b)

Figure 10-3. (a) and (b) FTIR spectra of cinnamate-functionalized poly(MMA-*co*-HEA). Arrow in (b) indicates C=C in cinnamate group.

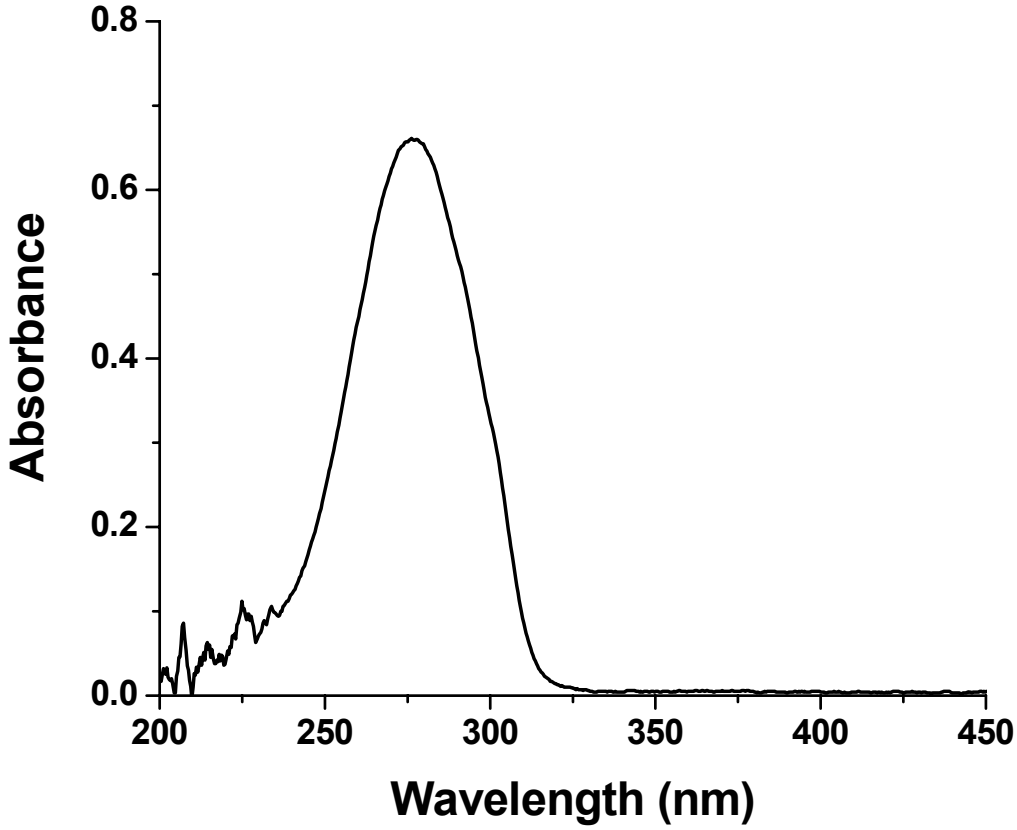

Figure 10-4. Typical UV absorbance on the cinnamate-functionalized poly(MMA-*co*-HEA).

10.4.2 *In situ* UV Irradiation of the Electrospun Fibers.

The cinnamate-functionalized terpolymers were irradiated during electrospinning. The SEM micrographs corresponding to the uncured and cured fibrous mats for the 4, 9 and 13 mol% cinnamate functionalized terpolymers are shown in Figure 10-5, Figure 10-6, and Figure 10-7, respectively. No distinct morphological change was observed between the non-irradiated and irradiated fibers. Fibers of the terpolymer containing the least amount of cinnamate (4 mol%) had a relatively larger diameter (2 - 4 μm) compared to the fibers of the other two terpolymers (200 - 600 nm). The fibers from the 4 mol% cinnamate functionalized terpolymers were also free of bead defects, unlike the other two compositions that displayed a beaded fiber morphology. This was expected as the viscosity of the 4 mol% cinnamate-containing polymer solution was 2,800 cP, while that of 9 mol% cinnamate-containing polymer was 670 cP (the viscosity of the 13 mol% polymer was not measured, but visually had a similar viscosity to the 9 mol% sample). It is speculated that this might account for the differences in the fiber diameter.

Absorbance of the uncured and cured electrospun mats in the infrared region of the electromagnetic spectrum was measured on a Nicolet 510 FTIR Spectrometer. The C=C peak was observed at 1637 cm^{-1}. To account for the thickness variations in the fibrous mats, all the peak intensities were normalized with that corresponding to the $C\text{-}CH_3$ bending observed at 1388 cm^{-1}.

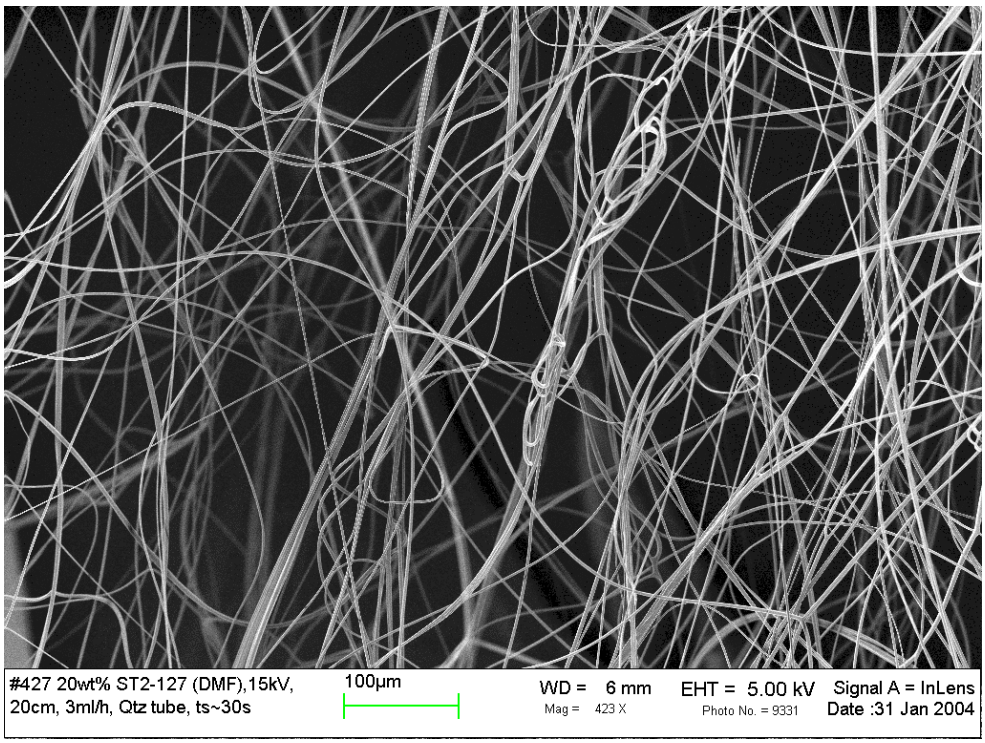

(a)

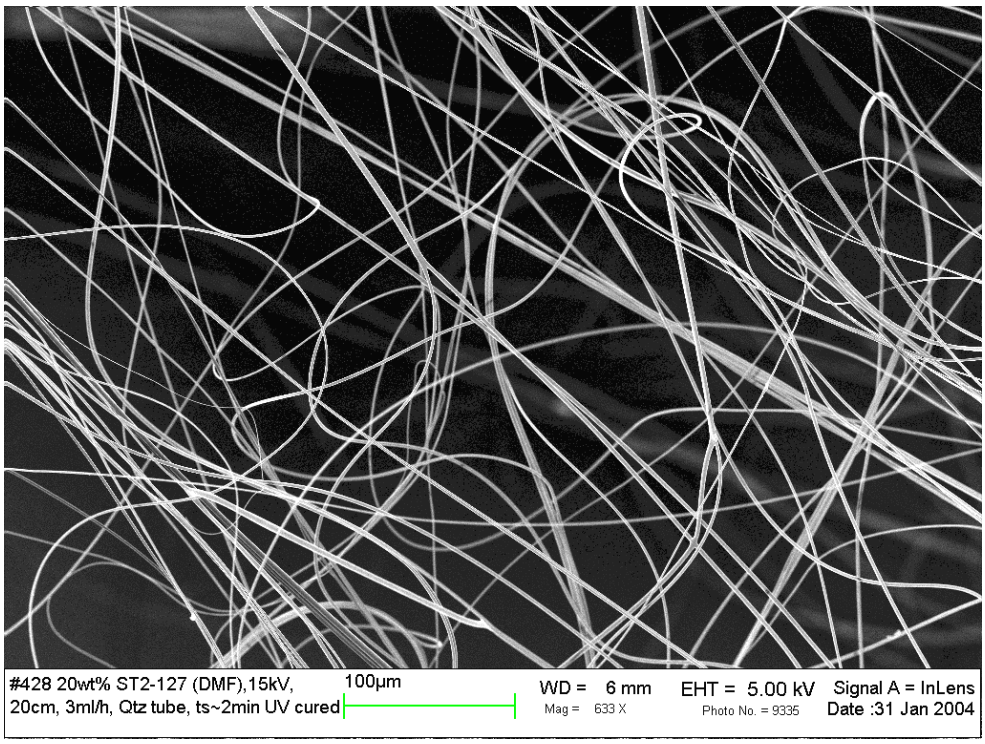

(b)

Figure 10-5. 4 mol% cinnamate-functionalized terpolymer fibers (a) without and (b) with exposure to UV irradiation.

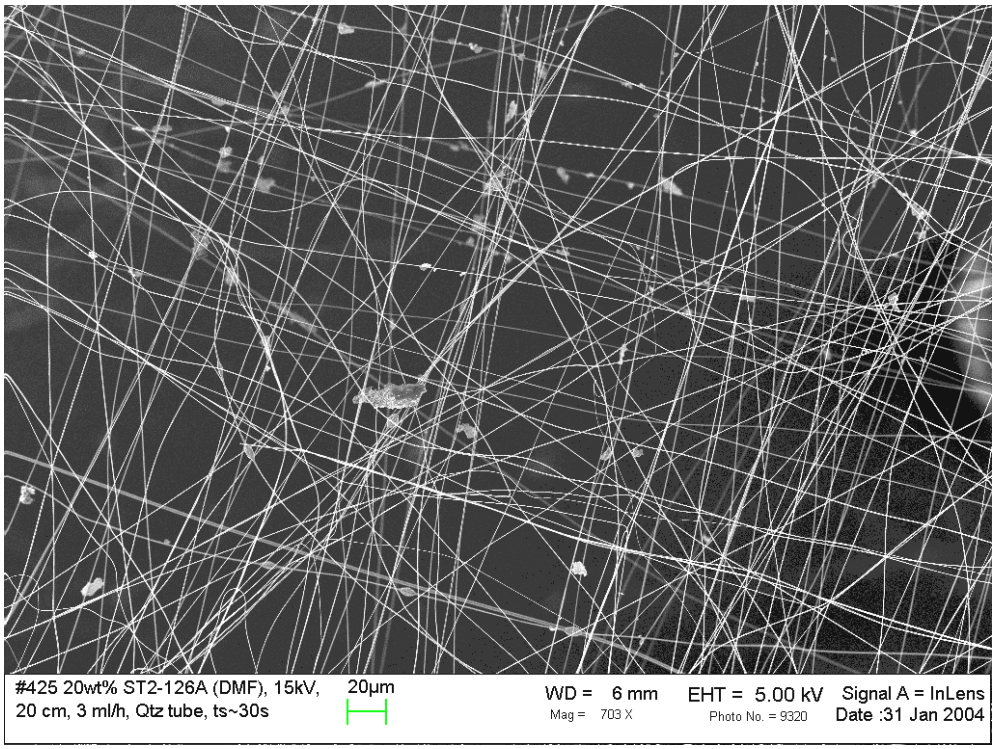

(a)

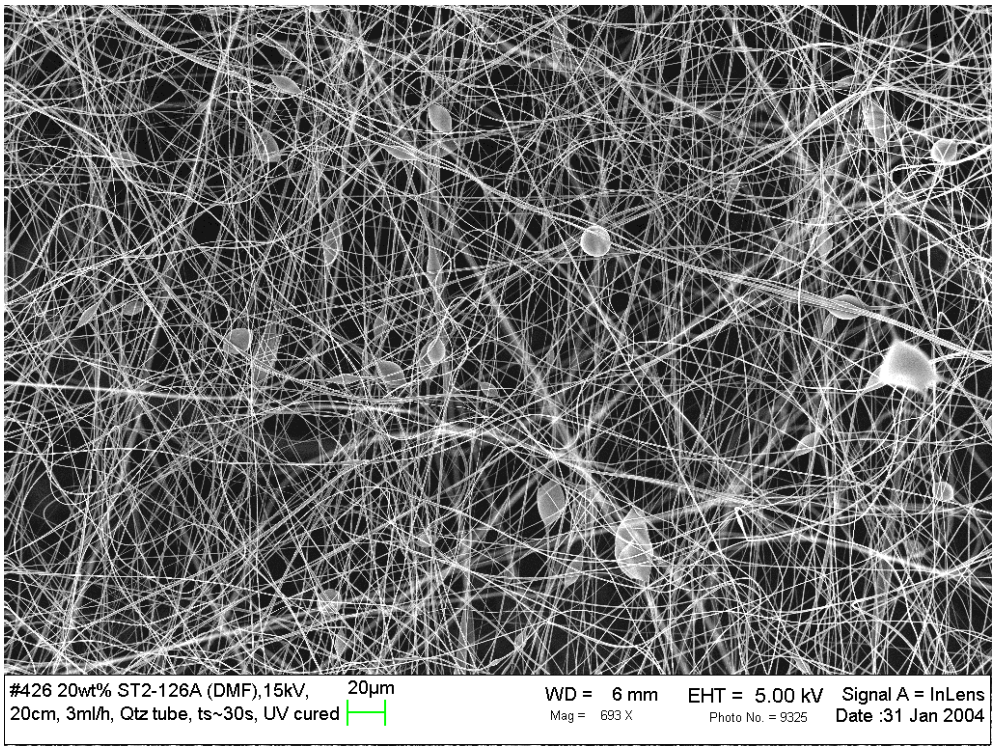

(b)

Figure 10-6. 9 mol% cinnamate-functionalized terpolymer fibers (a) without and (b) with exposure to UV irradiation.

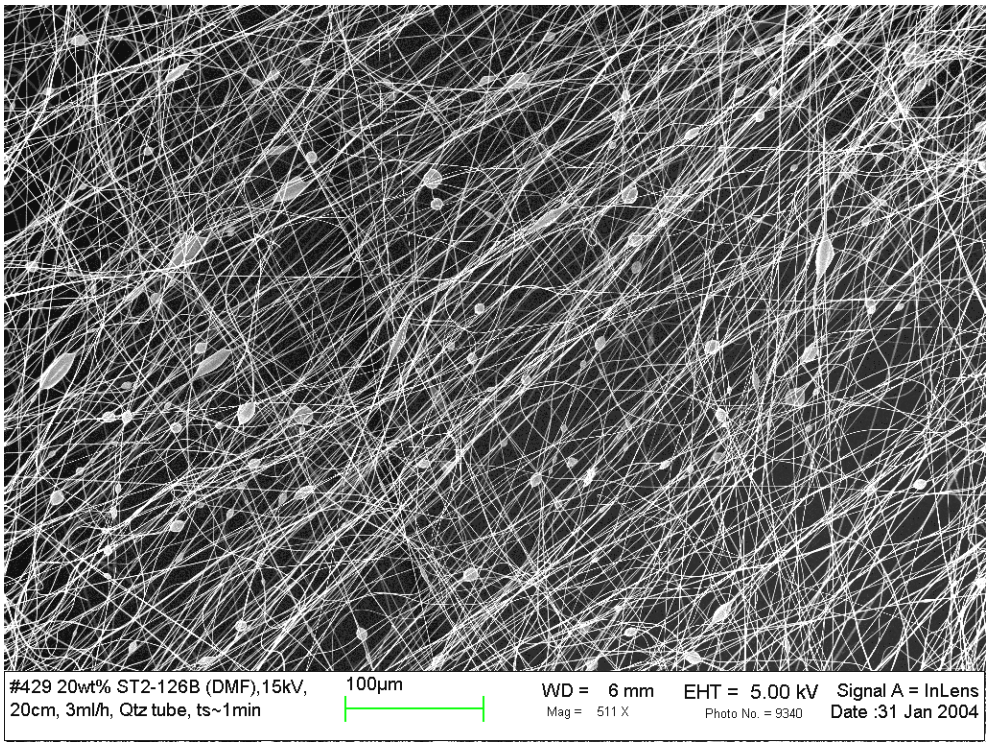

(a)

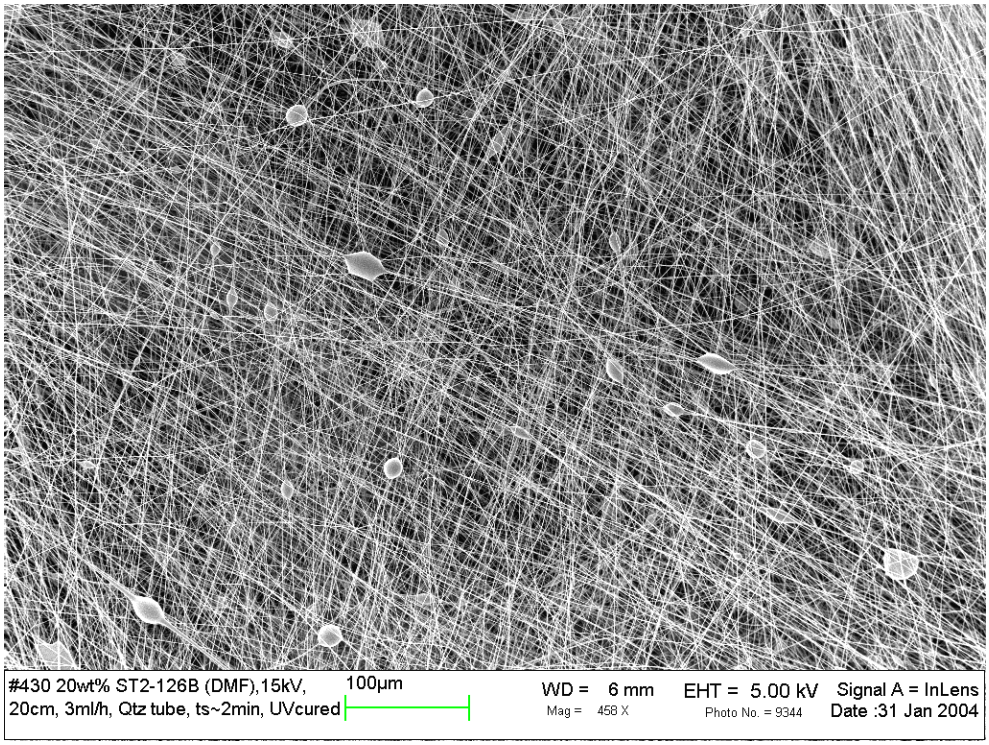

(b)

Figure 10-7. 13 mol% cinnamate-functionalized terpolymer fibers (a) without and (b) with exposure to UV irradiation.

A typical FTIR spectrum of the crosslinked and noncrosslinked fibers is shown in Figure 10-8. It can be seen that the peak intensity at 1637 cm^{-1} decreases after UV curing in this sample as well as in the other two terpolymers investigated. It is noted that the crosslinking of the cinnamate functionality occurs between the chains present in a given fiber and not between the fibers themselves. As the peak intensity at 1637 cm^{-1} is directly proportional to the concentration of the double bonds in the cinnamate group (Beer's Law), an estimate of the relative degree of crosslinking of the polymeric chains can be obtained by calculating the mathematical quantity $1-I/I_o$, where, I is the normalized peak intensity of the cured fibrous mat and I_o corresponds to the normalized peak intensity of the uncured fibrous mat. These results are plotted in Figure 10-9 along with the average gel fraction (obtained from the solvent extraction experiments) for each photocured fibrous mat. The extent of crosslinking, as measured by these two techniques, distinctly increases with increasing cinnamate concentration.

10.4.3 UV Irradiation of the Polymer in the Film State.

The 4, 9 and 13 mol% cinnamate-functionalized polymers were solution cast onto quartz low e-glass slides (IR study) or silicone release paper (gel fraction measurements) and irradiated in the Fusion UV conveyor system. The belt speed was set at the systems maximum of 87 m min^{-1} affording a UVB dose of 14.6 mJ cm^{-2}. The extent of photodimerization was measured with FTIR-ATR using the C=C stretch at 1638 cm^{-1} (Figure 10-3(b)). Figure 10-10 shows the percent of cinnamate consumed after exposure to 14.6 mJ cm^{-2} of UVB

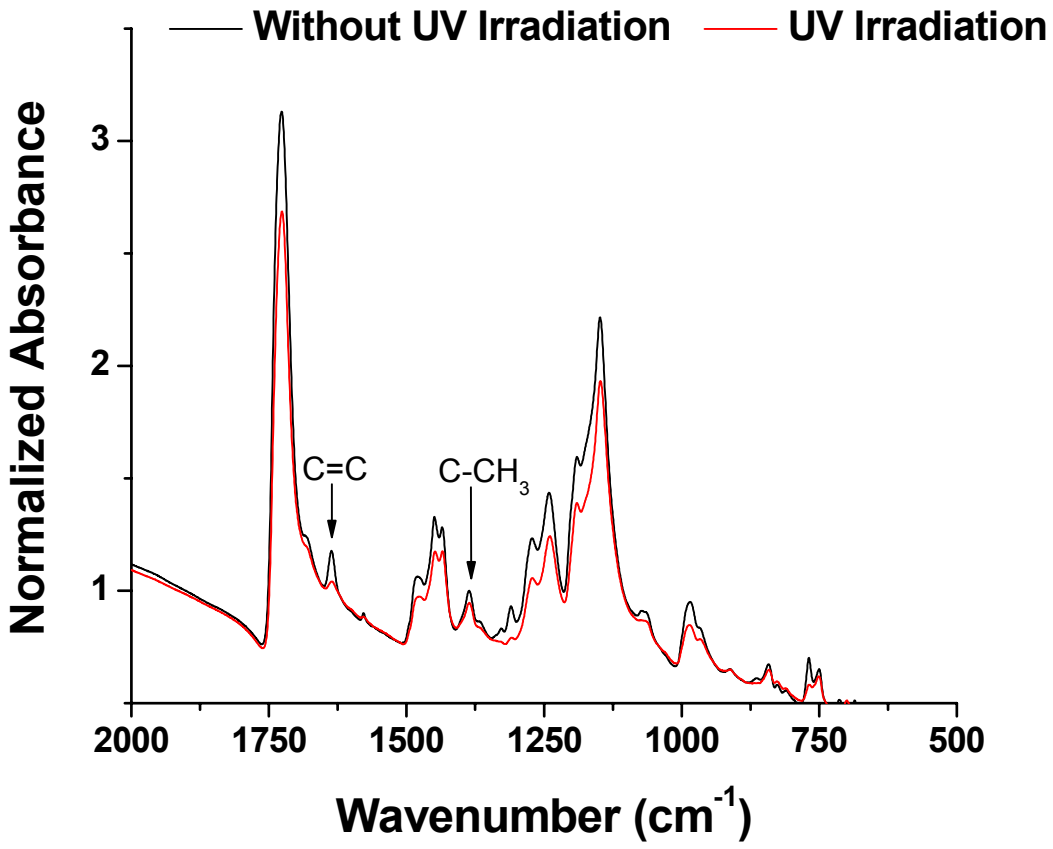

Figure 10-8. Typical normalized IR absorbance of the cinnamate-functionalized terpolymer fibers (in this case, 13 mol% cinnamate).

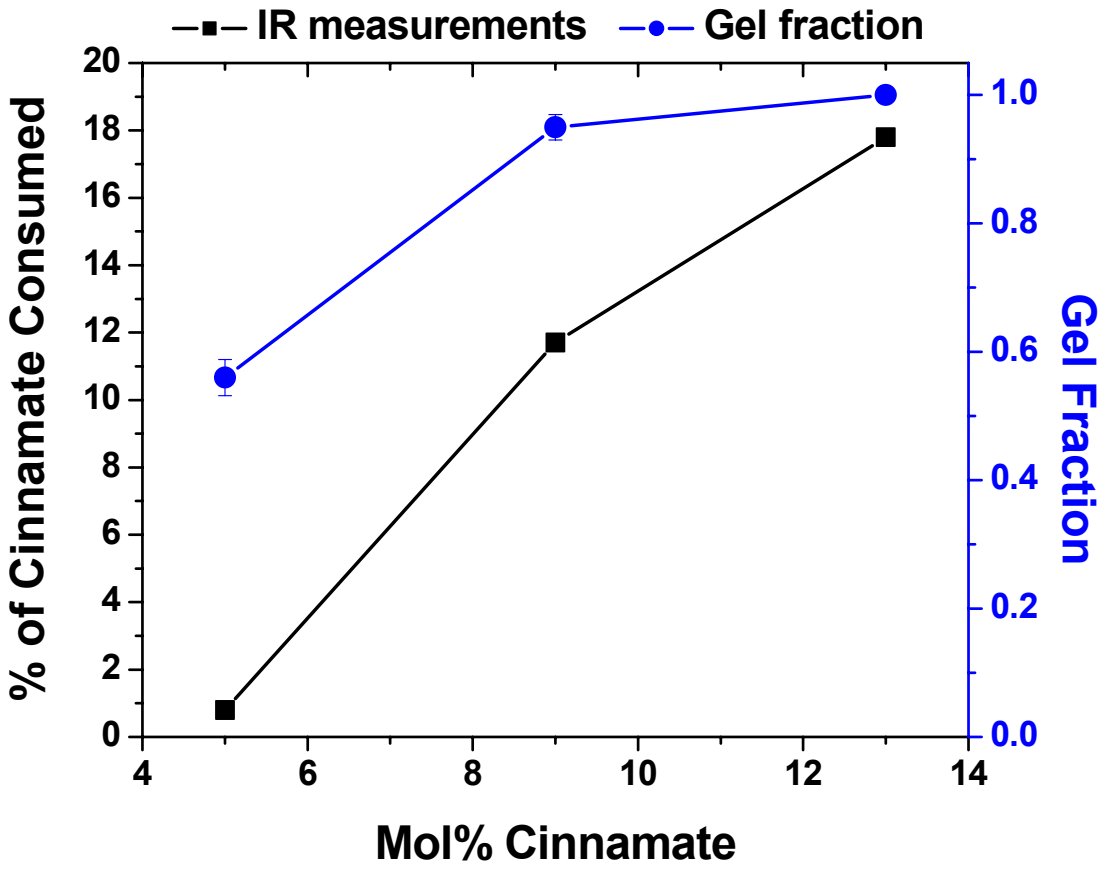

Figure 10-9. Percent of cinnamate consumed via photodimerization and gel fraction as a function of cinnamate concentration after exposure to approximately 13.5 mL cm^{-2} UVB irradiation.

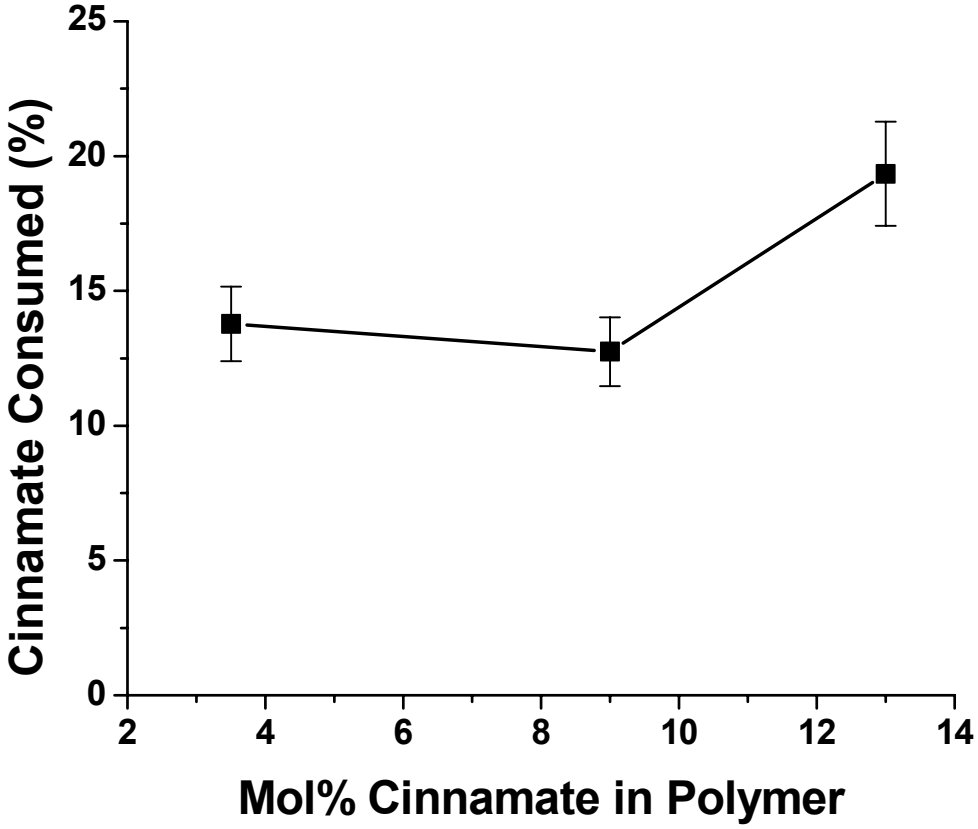

Figure 10-10. Percent of cinnamate groups dimerized as a function of mol% of cinnamate in the cinnamate-functionalized poly(MMA-co-HEA) after exposure to14.6 mJ cm^{-2} of UVB irradiation.

irradiation. The 14.6 mJ cm^{-2} of UVB irradiation consumed ~13% of the cinnamate groups in the 4 and 9 mol% samples, whereas 19% of the cinnamate groups were consumed in the 13% sample. The increased consumption in the 13% sample was attributed to the higher cinnamate concentration in the polymer. Soxhlet extraction of the 20 – 25 μm thick films indicated that the films were not crosslinked as 0% gel was measured for all samples. However, GPC measurements indicated increased molecular weight with the UV irradiation (Table 10-2). Thus, while there was insufficient cinnamate dimerization for crosslinking, cinnamate dimerization occured leading to molecular weight increases. Irradiation of thinner films and higher dose will provide further insight into these results.

10.5 CONCLUSIONS

Three terpolymers containing MMA and various concentrations of HEA and cinnamate-functionalized HEA were synthesized. The terpolymers were subsequently irradiated during electrospinning forming crosslinked fibrous mats in a single step. The *in situ* photocrosslinking of the 0.2 - 4 nm diameter fibers was highly efficient forming up to 100% gel. The terpolymers were also cast into films and subsequently irradiated. Similar cinnamate consumption was observed for the irradiated cast films and irradiated fibers with the exception of the 4 mol% cinnamate-functionalized terpolymer (Table 10-3). However, the molecular weights of the irradiated fibers and films varied greatly. Irradiation of the electrospun fibers led to gel formations between 56 and 100%

Sample	M_n (g mol^{-1})	M_w (g mol^{-1})
MMA-*co*-HEA Precursor	170,000	334,000
4.0 mol% Cinnamate + UV	350,000	781,000
9.0 mol% Cinnamate + UV	412,000	879,000
13 mol% Cinnamate + UV	450,000	924,000

Table 10-2. Molecular weights of the irradiated cinnamate-functionalized poly(MMA-co-HEA).

Cinnamate concentration (mol%)	% of cinnamate consumed during irradiation	
	Fiber	Film
4	0.8	13 $\pm$ 1.4
9	12	13 $\pm$ 1.3
13	18	20 $\pm$ 2.0

Table 10-3. Comparison of cinnamate consumption via the photodimerization for the electrospun fibers and solution cast films.

depending on cinnamate concentration, whereas the irradiated films were completely soluble in organic solvents. GPC analysis of the irradiated films indicated that the irradiation and subsequent photodimerization of the cinnamate groups led primarily to chain-extension as the molecular weight of the irradiated fibers increased from the non-cured molecular weights with higher cinnamate concentrations leading to higher final molecular weights. This difference was attributed, in part, to the difference in the thickness of the fibers (up to 4 μm thick) and the films (20 – 25 μm thick) and the mobility of the cinnamate groups during irradiation. During electrospinning, the polymer has increased mobility versus the film state. Future work will study the total dose necessary for gelation of the films and the effect of polymer branching on the photocrosslinking efficiency.

10.6 Acknowledgments

This material is based upon work supported in part by the U.S. Army Research Laboratory and the U.S. Army Research Office under grant number DAAD19-02-1-0275 Macromolecular Architecture for Performance (MAP) MURI.

CHAPTER 11 FUTURE WORK

11.1 INVESTIGATION OF CRYSTALLIZATION RATE OF COUMARIN DIMER-LINKED PEG.

Many researchers have studied the effects of various molecular parameters on the crystallization rate and crystal structure of PEG and PEO including molecular weight, chain endgroup size and endgroup polarity, among others.[406-412] Chain-extension via coumarin dimerization forms a polymer with a coumarin dimer in the middle of the chain. The effect of the mid-chain "defect" on the crystallization kinetics could be studied. Since the defects are in the middle of the chain (for dimer) or spaced at a pre-determined spacing (dependent on the degree of chain-extension and PEG starting molecular weight), the mobility and formation of the crystals may be affected more so than in the chain end situation. Various spacings (MW between coumarin dimers) as well as multiple molecular weights (function of irradiation dose) could be synthesized and studied.

11.2 THE EFFECT OF CROSSLINK/CHAIN EXTENSION POINT PLACEMENT IN POLYMER BACKBONE.

Utilizing stable free radical polymerization one could synthesize block copolymers such as, poly((HEA-*co*-*n*BA)-*b*-*n*BA) where the HEA containing block is short (<5K) and the pure *n*BA block is large (>50K). The block copolymers could be subsequently modified via the hydroxyl group with a cinnamate or coumarin group. Irradiation of the photoactive polymer could result in a star shaped copolymer that is reversible depending on the wavelength of light

irradiation. Changing the monomer incorporation to synthesize poly(*n*BA-*b*-(HEA-*co*-nBA)-*b*-*n*BA) where the HEA containing block is short and with larger *n*BA blocks will provide a polymer with functionalizable groups in the middle of the chain. Thus, subsequent functionalization will afford a macromolecule with the photoactive groups in the middle of the chain. Irradiation of this polymer would lead to a crosslinked center block with dangling arms (*n*BA blocks).

11.3 REVERSIBLE/RELEASABLE SURFACES.

A surface that can release molecules or macromolecules could be prepared by grafting coumarin dimers on the surface of a substrate. This is achievable by attaching a polymer to one side of a coumarin dimer and the substrate to the second side (Figure 11-1). UVC irradiation of the functionalized surface would cleave the coumarin dimer and release the polymer (or whatever is attached to the coumarin dimer).

11.4 ADHESION STUDIES.

There are a number of research possibilities in the field of adhesives. The irradiation of incorporated cinnamate or coumarin groups in PSAs allows for the study of controlled amounts of chain-extension/crosslinking on adhesive properties. Varying the dose would provide an easier methodology to control the crosslink density than thermally or photoinitiated crosslinking. DMA and rheological studies coupled with peel and shear testing could help determine the cross-over point where increased gel content adversely affects the peel strength. This study would be greatly aided by the use of the neutral density step filter.

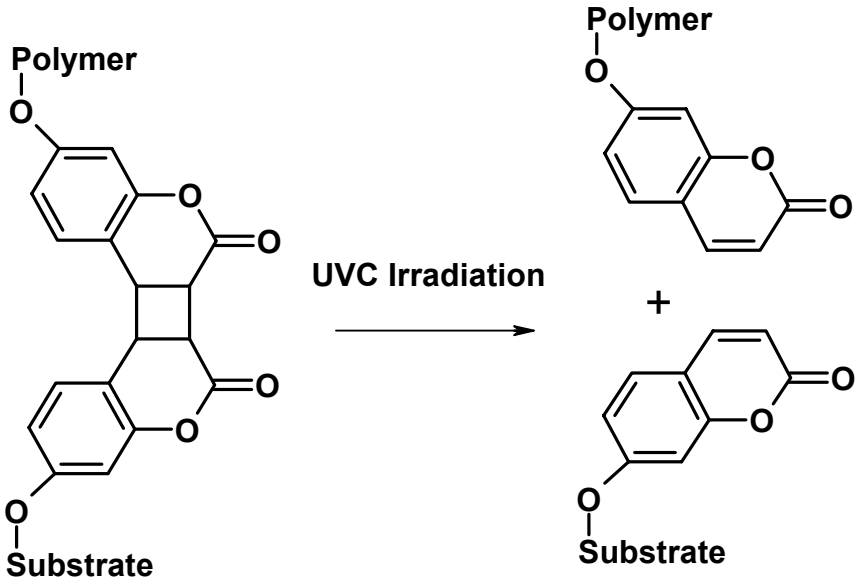

Figure 11-1. Schematic of releasable surfaces.

Utilizing the filter as a mask would provide up to 11 samples with different degrees of dimerization. The 11 samples could individually be tested using dynamic mechanical analysis while the peel testing could be done in a combinatorial manner using the gradient peel methodologies developed by Stafford and coworkers NIST.[455]

11.5 REVERSIBLE COUPLING.

There are also a number of possibilities to be explored regarding reversible coupling. One example would be to attach a photoreactive group via a spacer to the center of a star or hyperbranched polymer. Irradiation could lead to star and hyperbranch polymer dimers, which could later be cleaved. Similar methodologies could be utilized to synthesize stars polymers with releasable arms. An additional possibility is the synthesis of reversible block copolymers. They could be synthesized by functionalizing polymer chain ends with the photoactive groups, then mixing two or more of the functionalized polymers and irradiating the mixture. If a hydrophobic polymer is chosen (for example ethylene/propylene) and mixed with another incompatible hydrophobic polymer the coumarin functionalities of the two polymers should be present at the interface of the two polymers. Thus, irradiation of the mixture could lead to formation of a mixture of block copolymers with incompatible blocks. The copolymers could later be cleaved via 254 nm irradiation.

11.6 PHOTO-RHEOLOGICAL CONTROL.

Utilizing light to control polymer molecular weight in mixtures with solvents could allow for the use of light to control the viscosity of solutions via the coumarin dimerization reaction.

11.7 COMBINING HYDROGEN-BONDING AND PHOTOACTIVITY.

A few research groups have begun to study utilizing light to lock-in hydrogen-bonded structures processes utilizing complex chemistries (Section 2.2.4). However, combining self complementary multiple hydrogen bonding and a photoactive group could provide interesting systems. One could use the hydrogen bonding groups to self assemble or form a desired molecular topology. Subsequent irradiation of the polymer would lock in the structure permanently or until irradiation cleave the coumarin photodimers. The combination of self complementary multiple hydrogen bonding groups and photodimerizable groups into a single polymer would provide for two methodologies to manipulate the crosslink density. Thermal control is accomplished by heating and dissociating the hydrogen bonding groups and light would dimerize the photoactive groups.

CHAPTER 12 OVERALL CONCLUSIONS

Coumarin and cinnamate derivatives were positioned as polymer chain ends and side groups to synthesize photoactive macromolecules. The cinnamates and coumarins were reacted onto the polymers via one of two pathways. Polymers were functionalized with coumarin groups via an esterification reaction between hydroxyl functionalities and an acid chloride derivatized coumarin group. In addition to the esterification reaction, cinnamates were also coupled to polymers via a ring opening reaction between a hydroxyl functionalized cinnamate derivative and a maleic anhydride repeat unit copolymerized into the polymer. While both functional groups undergo a [$2\pi + 2\pi$] photodimerization reaction (coumarin groups in the UVA and cinnamate groups in the UVB), the coumarin dimers are subsequently photocleaved when irradiated below 254 nm. The photodimerization reaction was used to chain extend or crosslink the polymers in this study, while the coumarin photocleavage was utilized to depolymerize chain-extended macromolecules.

Coumarin groups were initially used to chain extend PEG oligomers. PEG monols and diols (approximately 2,000 g mol^{-1}) were endcapped with coumarin functionalities via the aforementioned esterification reaction. UVA irradiation (110 J cm^{-2}) of the coumarin-functionalized PEGs diols doubled the number average molecular weight of the oligomers and broadened the molecular weight distribution from 1.04 to 2.75. Both increases indicated that the UVA irradiation caused the photodimerization of the coumarin endgroups, which in turn, increased the size of the molecules. Subsequent UVC irradiation (2 J cm^{-2})

photocleaved the coumarin groups, reverting the chain-extended PEGs to their original M_n and decreasing the polydispersity to 1.08.

The coumarin groups were then incorporated into poly(alkyl acrylates) and poly(alkyl methacrylates) via the esterification reaction to determine the effects of polymer T_g and composition on the photodimerization reaction and subsequent crosslinking. Varying the composition of the individual polymers, the coumarin-functionalized polymers possessed T_gs between –54 and 105 °C. The UV-Vis data monitoring the conversion of the coumarin groups revealed an interesting trend. While the absolute difference between T_g and irradiance temperature did not affect the rate or extent of photodimerization reaction, polymers with a T_g greater than the irradiance temperature displayed less reaction than those with a T_g lower than the irradiance temperature. Furthermore, the alkyl ester side groups dictated the final extent of conversion for polymers with a T_g lower than the irradiation temperature. Steric crowding of the coumarin groups from the larger alkyl ester side groups was not the only factor which controlled the extent of reaction, however. Irradiation of the coumarin-functionalized poly(HEMA-co-HEA) using a neutral density linear step filter provided some insight into the system reciprocity. For the intensities studied, the coumarin-functionalized polymers obeyed the reciprocity law in that the extent of photodimerization was only dependent on the total UVA dose and not the individual components of dose (power and irradiation time).

Coumarin-functionalized poly(EHA-*co*-HEA) was subsequently utilized as a a model PSA. Photodimerization of the coumarin groups crosslinked the model

PSAs and decreased the PSA peel strength as much as 97%. Two different types of strength decreases were observed. For the first, the PSAs were irradiated before they were bonded to the substrate. The decrease in peel strength was attributed to a decrease in the ability of the adhesive to wet the substrate. The second type of peel strength decrease was observed for samples that were bonded before irradiation. The decrease in peel strength in the second case was attributed to a decrease in the chain mobility, which resulted in a subsequent decrease in the ability of the adhesive to dissipate energy during peel testing. The reversibility on the coumarin photodimerization reaction was utilized to uncrosslink the model PSA and resulted in increased peel strengths compared to the fully crosslinked PSA.

Cinnamate groups were utilized in the design of an UV-curable acrylic PSA. The cinnamate groups were placed onto the polymer via two methodologies. The first was the side group esterification reaction between a hydroxyl group on the polymer and cinnamoyl chloride. The second method involved the ring opening of a maleic anhydride on the polymer backbone and a hydroxyl derivatized cinnamate. This reaction positioned an acrylic acid group adjacent to the cinnamate group. Photodimerization of the cinnamate groups increased the polymer molecular weight and slightly crosslinked the PSA, both leading to increases in the peel strength, although extensive crosslinking led to a decrease in the peel strength.

Cinnamate groups were also utilized to photocrosslink fibers during electrospinning. Cinnamate-functionalized poly(MMA-*co*-HEA) were irradiated

during the electrospinning process forming highly crosslinked fibers between 200 and 4000 nm in diameter. Higher cinnamate concentrations produced higher gel fractions when photocrosslinked during electrospinning.

CHAPTER 13 LITERATURE CITED

(1) Everaerts, A. I.; Clemens, L. M. In *Surfaces, Chemistry and Applications*; Chaudhury, M., Pocius, A. V., Eds.; Elsevier: New York, 2002; Vol. 2.
(2) Satas, D. In *Handbook of Pressure Sensitive Adhesive Technology*; Satas, D., Ed.; Van Nostrand Reinhold: New York, 1989.
(3) Dahlquist, C. A. In *Handbook of Pressure Sensitive Adhesive Technology*; 2 ed.; Satas, D., Ed.; Van Nostrand Reinhold: New York, 1989.
(4) Chang, E. P. *Journal of Adhesion* **1991**, *34*, 189.
(5) Chang, E. P. *Journal of Adhesion* **1997**, *60*, 233.
(6) Yang, H. W. H.; Chang, E. P. *Trends in Polymer Science* **1997**, *5*, 380.
(7) Berg, J. C. In *Surfaces, Chemistry and Applications*; Chaudhury, M., Pocius, A. V., Eds.; Elsevier: New York, 2002; Vol. 2.
(8) Yarusso, D. J. In *The Mechanics of Adhesion*; Dillard, D. A., Pocius, A. V., Eds.; Elsevier: New York, 2002; Vol. 1.
(9) Dahlquist, C. A. *Adhesion: Fundamentals and Practice*; McLaren, 1966.
(10) Tobing, S. D.; Klein, A. *Journal of Applied Polymer Science* **2001**, *79*, 2230.
(11) Tse, M. F. *Journal of Adhesion Science and Technology* **1989**, *3*, 551.
(12) Ajji, A.; Carreau, P. J.; Schreiber, H. P. *Journal of Polymer Science Part B-Polymer Physics* **1986**, *24*, 1983.
(13) Zosel, A. *International Journal of Adhesion and Adhesives* **1998**, *18*, 265.
(14) Aymonier, A.; Papon, E.; Villenave, J. J.; Tordjeman, P.; Pirri, R.; Gerard, P. *Chemistry of Materials* **2001**, *13*, 2562.
(15) Satas, D. In *Handbook of Pressure Sensitive Adhesive Technology*; 2 ed.; Satas, D., Ed.; Van Nostrand Reinhold: New York, 1989.
(16) Lakrout, H.; Creton, C.; Ahn, D. C.; Shull, K. R. *Macromolecules* **2001**, *34*, 7448.
(17) Crosby, A. J.; Shull, K. R. *Journal of Polymer Science Part B-Polymer Physics* **1999**, *37*, 3455.
(18) Chen, W. L.; Shull, K. R. *Macromolecules* **1999**, *32*, 6298.
(19) Creton, C.; Hooker, J.; Shull, K. R. *Langmuir* **2001**, *17*, 4948.
(20) Creton, C.; Fabre, P. In *The Mechanics of Adhesion*; Dillard, D. A., Pocius, A. V., Eds.; Elsevier: New York, 2002; Vol. 1.
(21) Tobing, S. D.; Klein, A. *Journal of Applied Polymer Science* **2001**, *79*, 2558.
(22) Hammond, F. H. In *Handbook of Pressure Sensitive Adhesive Technology*; 2 ed.; Satas, D., Ed.; Van Nostrand Reinhold: New York, 1989.
(23) Asahara, J.; Hori, N.; Takemura, A.; Ono, H. *Journal of Applied Polymer Science* **2003**, *87*, 1493.
(24) Webster, I. *International Journal of Adhesion and Adhesives* **1999**, *19*, 29.
(25) Chivers, R. A.; Webster, I. Adhesion '99, Cambridge, UK, 1999; p 37.
(26) Boyne, J. M.; Millan, E. J.; Webster, I. *International Journal of Adhesion and Adhesives* **2001**, *21*, 49.

(27) Gent, A. N.; Hamed, G. R. *Journal of Applied Polymer Science* **1977**, *21*, 2817.
(28) Kinloch, A. J.; Williams, J. G. In *The Mechanics of Adhesion*; Dillard, D. A., Pocius, A. V., Eds.; Elsevier: New York, 2002; Vol. 1.
(29) Charmeau, J. Y.; Gerin, P. A.; Vovelle, L.; Schirrer, R.; Holl, Y. *Journal of Adhesion Science and Technology* **1999**, *13*, 203.
(30) Kinloch, A. J.; Lau, C. C.; Williams, J. G. *International Journal of Fracture* **1994**, *66*, 45.
(31) Drzal, P. L.; Shull, K. R. *Macromolecules* **2003**, *36*, 2000.
(32) Schumacher, K.-H.; Sanborn, T. *Adhesives & Sealants Industry* **2001**, *8*, 42.
(33) Paul, C. W. In *Surfaces, Chemistry and Applications*; Chaudhury, M., Pocius, A. V., Eds.; Elsevier: New York, 2002; Vol. 2.
(34) Schumacher, K.-H.; Sanborn, T. Annual meeting of the Adhesion Society, Williamsburg, VA, 2001; p 165.
(35) Malik, R. *RadTech Report* **2001**, *15*, 25.
(36) Malik, J.; Clarson, S. J. *International Journal of Adhesion and Adhesives* **2002**, *22*, 283.
(37) Malik, R. *Adhesives Age* **2002**, *45*, 35.
(38) Malik, J.; Goldslager, B. A.; Clarson, S. J. *Surface Engineering* **2003**, *19*, 121.
(39) Dobmann, A. *Adhesive Technology* **2000**, *17*, 14.
(40) Dobmann, A. *Adhesives Age* **2002**, *45*, 26.
(41) Schumacher, K.-H.; Dussterwald, U.; Fink, R. *Adhesive Technology* **2000**, *17*, 18.
(42) Kim, J. K.; Kim, W. H.; Lee, D. H. *Polymer* **2002**, *43*, 5005.
(43) Staeger, M.; Finot, E.; Brachais, C. H.; Auguste, S.; Durand, H. *Applied Surface Science* **2002**, *185*, 231.
(44) Han, C. D.; Kim, J.; Baek, D. M. *Journal of Adhesion* **1989**, *28*, 201.
(45) Tobing, S. D.; Klein, A. *Journal of Applied Polymer Science* **2000**, *76*, 1965.
(46) Sciangola, D. A. *Adhesives Age* **2000**, *43*, 25.
(47) Quirk, B. *Adhesives Age* **2000**, *43*, S5.
(48) Balzer, V.-D.; Erhardt, U.; Ladenberger, V.; Meyer, H.; Bruchmann, B.; Schumacher, K.-H. In *Scifinder*; BASF AG: WO 2002-EP11109 20021004, 2003.
(49) Fink, R.; Schumacher, K.-H.; Duesterwald, U.; Erhardt, U.; Meyer, H. In *Scifinder*; BASF AG: Germany DE 2001-10134261 20010718, 2003.
(50) Fink, R.; Stoeckelmann, E.; Ladenberger, V.; Schumacher, K.-H. In *Scifinder*; BASF AG: Eur. Pat. Appl. EP 1213306 A2 20020612, 2003.
(51) Jung, M.; Schumacher, K.-H.; Fink, R. In *Scifinder*; BASF AG: Germany DE 2002-10208843 20020301, 2003.
(52) Meyer, H.; Becker, H.; Erhardt, U.; Schumacher, K.-h.; Jung, M.; Henkelmann, J. In *Scifinder*; BASF AG: Germany DE 10206987 A1 20030821, 2003.
(53) Schumacher, K.-H.; Sanborn, T. *Adhesives Age* **2003**, *46*, 38.

(54) BASF; http://www.basf.com/businesses/consumer/dispersions/usa/pressure/acresin3532.html, 2004.
(55) Scherzer, T.; Tauber, A.; Mehnert, R. *Vibrational Spectroscopy* **2002**, *29*, 125.
(56) Tauber, A.; Scherzer, T.; Mehnert, R. *Journal of Coatings Technology* **2002**, *74*, 41.
(57) Peiffer, R. In *Photopolymerization Fundamentals and Applications*; American Chemical Society: Washington D.C., 1997; Vol. 673.
(58) Reiser, A. *Photoreactive Polymers: The Science and Technology of Resists*; Wiley-Interscience, 1989.
(59) Fouassier, J.-P. *Photoinitiation, Photopolymerization, and Photocuring : Fundamentals and Applications*; Hanser Gardner: New York, 1995.
(60) Allen, N. *TRIP* **1993**, *1*, 213.
(61) Kindernay, J.; Blazkova, A.; Ruda, J.; Jancovicova, V.; Jakubikova, Z. *Journal of Photochemistry and Photobiology a-Chemistry* **2002**, *151*, 229.
(62) Allonas, X.; Lalevee, J.; Fouassier, J. P. *Journal of Photochemistry and Photobiology a-Chemistry* **2003**, *159*, 127.
(63) Braslavsky, S. E.; Heibel, G. E. *Chemical Reviews* **1992**, *92*, 1381.
(64) Khudyakov, I. V.; Fox, W. S.; Purvis, M. B. *Industrial & Engineering Chemistry Research* **2001**, *40*, 3092.
(65) Decker, C.; Decker, D.; Morel, F. *Photopolymerization* **1997**, *673*, 63.
(66) Dietz, J. E.; Cowans, B. A.; Scott, R. A.; Peppas, N. A. *Photopolymerization* **1997**, *673*, 28.
(67) Lovell, L. G.; Newman, S. M.; Donaldson, M. M.; Bowman, C. N. *Dental Materials* **2003**, *19*, 458.
(68) Hacioglua, B.; Berchtolda, K. A.; Lovella, L. G.; Jun Niea; Bowman, C. N. *Biomaterials* **2002**, *23*, 4057.
(69) Jansen, J.; Dias, A. A.; Dorschu, M.; Coussens, B. *Macromolecules* **2003**, *36*, 3861.
(70) Decker, C.; Zahouily, K. *Radiation Physics and Chemistry* **2002**, *63*, 3.
(71) Decker, C.; Bendaikha, T. *Journal of Applied Polymer Science* **1998**, *70*, 2269.
(72) Decker, C.; Zahouily, K.; Decker, D.; Nguyen, T.; Viet, T. *Polymer* **2001**, *42*, 7551.
(73) Dolez, P.; Marek, M.; Love, B. J. *Journal of Applied Polymer Science* **2001**, *82*, 546.
(74) P. Dolez, C. W., A. Goff, B. Love *Journal of the Society of Underwater Technology* **2002**, *In Print*.
(75) Suggs, A. E.; Dolez, P. I.; Love, B. J. *Journal of Adhesion Science and Technology* **2002**, *In Press*.
(76) Yu, C.; Davey, M. H.; Svec, F.; Fréchet, J. M. J. *Analytical Chemistry* **2001**, *73*, 5088.
(77) Yu, C.; Xu, M. C.; Svec, F.; Fréchet, J. M. J. *Journal of Polymer Science Part a-Polymer Chemistry* **2002**, *40*, 755.

(78) Benson, R. S. *Nuclear Instruments and Methods in Physics Research B* **2002**, *191*, 752.
(79) Anseth, K. S.; Burdick, J. A. *Mrs Bulletin* **2002**, *27*, 130.
(80) Anseth, K. S.; Shastri, V. R.; Laurencin, C. T.; Langer, R. *Abstracts of Papers of the American Chemical Society* **1996**, *211*, 228.
(81) Anseth, K. S.; Svaldi, D. C.; Laurencin, C. T.; Langer, R. *Photopolymerization* **1997**, *673*, 189.
(82) Muggli, D. S.; Burkoth, A. K.; Anseth, K. S. *Journal of Biomedical Materials Research* **1999**, *46*, 271.
(83) Toru Kawadaa, Y. N., Can Zhenga, Shoji Ohyab,; Kannna Okudab, K. S. *Biomaterials* **2002**, *23*, 3169.
(84) Crivello, J. V.; Narayan, R.; Sternstein, S. S. *Journal of Applied Polymer Science* **1997**, *64*, 2073.
(85) Crivello, J. V.; Sangermano, M. *Journal of Polymer Science Part a-Polymer Chemistry* **2001**, *39*, 343.
(86) Kannurpatti, A. R.; Goodner, M. D.; Lee, H. R.; Bowman, C. N. *Photopolymerization* **1997**, *673*, 51.
(87) Lovell, L. G.; Elliott, B. J.; Brown, J. R.; Bowman, C. N. *Polymer* **2001**, *42*, 421.
(88) Hutchison, J. B.; Haraldsson, K. T.; Hawker, C. J.; Bowman, C. N.; Anseth, K. S. *PMSE Preprints* **2002**, *87*, 162.
(89) Ma, H.; Davis, R.; Bowman, C. *Macromolecules* **2000**, *33*, 331.
(90) Decker, C.; Viet, T. N. T. *Journal of Applied Polymer Science* **2000**, *77*, 1902.
(91) Visconte, L. L. Y.; Andrade, C. T.; Azuma, C. *Journal of Applied Polymer Science* **1998**, *69*, 907.
(92) Andreopoulos, F. M.; Roberts, M. J.; Bentley, M. D.; Harris, J. M.; Beckman, E. J.; Russell, A. J. *Biotechnology and Bioengineering* **1999**, *65*, 579.
(93) Kuckling, D.; Adler, H. J.; Arndt, K. F.; Wolff, T.; Hoffmann, J.; Fischer, W. J. *Macromolecular Symposia* **1999**, *142*, 111.
(94) Kuckling, D.; Adler, H. J. P.; Arndt, K. F.; Hoffmann, J.; Plotner, M.; Wolff, T. *Polymers for Advanced Technologies* **1999**, *10*, 345.
(95) Decker, C. *Pigment & Resin Technology* **2001**, *30*, 278.
(96) Odian, G. *Principles of Polymerization*; 3rd ed.; John Wiley and Sons, Inc.: New York, 1991.
(97) Chanda, M. *Advanced Polymer Chemistry: A Problem Solving Guide*; Marcel Dekker, Inc: New York, 2000.
(98) Urankar, E. J.; Fréchet, J. M. J. *Chemistry of Materials* **1997**, *9*, 2861.
(99) Havard, J. M.; Vladimirov, N.; Fréchet, J. M. J.; Yamada, S.; Willson, C. G.; Byers, J. D. *Macromolecules* **1999**, *32*, 86.
(100) Havard, J. M.; Shim, S. Y.; Fréchet, J. M. J.; Lin, Q. H.; Medeiros, D. R.; Willson, C. G.; Byers, J. D. *Chemistry of Materials* **1999**, *11*, 719.
(101) Adronov, A.; Gilat, S. L.; Fréchet, J. M. J.; Ohta, K.; Neuwahl, F. V. R.; Fleming, G. R. *Journal of the American Chemical Society* **2000**, *122*, 1175.

(102) Adronov, A.; Robello, D. R.; Fréchet, J. M. J. *Journal of Polymer Science Part a-Polymer Chemistry* **2001**, *39*, 1366.
(103) Havard, J. M.; Yoshida, M.; Pasini, D.; Vladimirov, N.; Fréchet, J. M. J.; Medeiros, D. R.; Patterson, K.; Yamada, S.; Willson, C. G.; Byers, J. D. *Journal of Polymer Science Part a-Polymer Chemistry* **1999**, *37*, 1225.
(104) Mayrovitz, H.; Carta, S. *Advances in Wound Care* **1996**, *9*, 38.
(105) Webster, I. World Patent #WO 96/29374, 1996.
(106) Webster, I. World Patent #WO 99/18136, 1999.
(107) Webster, I.; Smith & Nephew: US Patent # 6,184,264 B1, 2001.
(108) Elisseeff, J.; Anseth, K.; Sims, D.; McIntosh, W.; Randolph, M.; Yaremchuk, M.; Langer, R. *Plastic and Reconstructive Surgery* **1999**, *104*, 1014.
(109) Anseth, K. S.; Metters, A. T.; Bryant, S. J.; Martens, P. J.; Elisseeff, J. H.; Bowman, C. N. *Journal of Controlled Release* **2002**, *78*, 199.
(110) Trudel, J.; Massiaa, S. P. *Biomaterials* **2002**, *23*, 3299.
(111) Okino, H.; Nakayama, Y.; Tanaka, M.; Matsuda, T. *Journal of Biomedical Materials Research* **2002**, *59*, 233.
(112) Nakayama, Y.; Matsuda, T. *Journal of Biomedical Materials Research* **1999**, *48*, 511.
(113) Matsuda, T.; Magoshi, T. *Biomacromolecules* **2002**, *3*, 942.
(114) Mizutani, M.; Matsuda, T. *Journal of Biomedical Materials Research* **2002**, *62*, 387.
(115) Matsuda, T.; Mizutani, M. *Journal of Biomedical Materials Research* **2002**, *62*, 395.
(116) Magoshi, T.; Matsuda, T. *Biomacromolecules* **2002**, *3*, 976.
(117) Nuttelman, C. R.; Henry, S. M.; Anseth, K. S. *Biomaterials* **2002**, *23*, 3617.
(118) John, G.; Morita, M. *Macromolecules* **1999**, *32*, 1853.
(119) Shirai, M.; Morishita, S.; Okamura, H.; Tsunooka, M. *Chemistry of Materials* **2002**, *14*, 334.
(120) Shirai, M.; Kawaue, A.; Okamura, H.; Tsunooka, M. *Chemistry of Materials* **2003**, *15*, 4075.
(121) Yamauchi, K.; Lizotte, J. R.; Long, T. E. *Macromolecules* **2002**, *35*, 8745.
(122) Sijbesma, R. P.; Beijer, F. H.; Brunsveld, L.; Folmer, B. J. B.; Hirschberg, J.; Lange, R. F. M.; Lowe, J. K. L.; Meijer, E. W. *Science* **1997**, *278*, 1601.
(123) Janssen, H. M.; Peeters, E.; Zundert, M. F. v.; Genderen, H. M. v.; Meijer, E. W. *Macromolecules* **1997**, *30*, 8113.
(124) Folmer, B. J. B.; Cavini, E.; Sijbesma, R. P.; Meijer, E. W. *Chemical Communications* **1998**, 1847.
(125) Beijer, F. H.; Sijbesma, R. P.; Kooijman, H.; Spek, A. L.; Meijer, E. W. *Journal of the American Chemical Society* **1998**, *120*, 6761.
(126) Beijer, F. H.; Kooijman, H.; Spek, A. L.; Sijbesma, R. P.; Meijer, E. W. *Angewandte Chemie-International Edition* **1998**, *37*, 75.
(127) Yamauchi, K.; Lizotte, J. R.; Hercules, D. M.; Vergne, M. J.; Long, T. E. *Journal of the American Chemical Society* **2002**, *124*, 8599.
(128) Yamauchi, K.; Lizotte, J. R.; Long, T. E. *Macromolecules* **2003**, *36*, 1083.
(129) Bowman, C. N.; Peppas, N. A. *Macromolecules* **1991**, *24*, 1914.

(130) Anseth, K. S.; Decker, C.; Bowman, C. N. *Macromolecules* **1995**, *28*, 4040.
(131) Guymon, C. A.; Dougan, L. A.; Bowman, C. N. *Photopolymerization* **1997**, *673*, 16.
(132) Guymon, C. A.; Bowman, C. N. *Macromolecules* **1997**, *30*, 5271.
(133) Guymon, C. A.; Shao, R.; Holter, D.; Frey, H.; Clark, N. A.; Bowman, C. N. *Liquid Crystals* **1998**, *24*, 263.
(134) Kannurpatti, A. R.; Anseth, J. W.; Bowman, C. N. *Polymer* **1998**, *39*, 2507.
(135) Goodner, M. D.; Bowman, C. N. *Macromolecules* **1999**, *32*, 6552.
(136) Young, J. S.; Bowman, C. N. *Macromolecules* **1999**, *32*, 6073.
(137) Russell, G. T.; Napper, D. H.; Gilbert, R. G. *Macromolecules* **1988**, *21*, 2133.
(138) Russell, G. T.; Gilbert, R. G.; Napper, D. H. *Macromolecules* **1993**, *26*, 3538.
(139) Berl, V.; Huc, I.; Khoury, R. G.; Lehn, J. M. *Chemistry-a European Journal* **2001**, *7*, 2798.
(140) Ilhan, F.; Gray, M.; Rotello, V. M. *Macromolecules* **2001**, *34*, 2597.
(141) Mammen, M.; Shakhnovich, E. I.; Deutch, J. M.; Whitesides, G. M. *Journal of Organic Chemistry* **1998**, *63*, 3821.
(142) Simanek, E. E.; Isaacs, L.; Li, X. H.; Wang, C. C. C.; Whitesides, G. M. *Journal of Organic Chemistry* **1997**, *62*, 8994.
(143) Kim, C.; Lee, S. J.; Lee, I. H.; Kim, K. T.; Song, H. H.; Jeon, H.-J. *Chemistry of Materials* **2003**, *15*, 3638.
(144) Yang, Z. H.; Cao, T. B.; Chen, J. Y.; Cao, W. X. *European Polymer Journal* **2002**, *38*, 2077.
(145) Zhang, Y. J.; Yang, S. G.; Guan, Y.; Miao, X. P.; Cao, W. X.; Xu, J. *Thin Solid Films* **2003**, *437*, 280.
(146) Manabu Mizutani, T. M. *Journal of Biomedical Materials Research* **2002**, *61*, 53.
(147) Matsuda, T.; Mizutani, M. *Macromolecules* **2000**, *33*, 791.
(148) Matsuda, T.; Mizutani, M.; Arnold, S. C. *Macromolecules* **2000**, *33*, 795.
(149) Mizutani, M.; Arnold, S. C.; Matsuda, T. *Biomacromolecules* **2002**, *3*, 668.
(150) Mizutani, M.; Matsuda, T. *Biomacromolecules* **2002**, *3*, 249.
(151) Mizutani, M.; Matsuda, T. *Journal of Biomedical Materials Research* **2002**, *61*, 53.
(152) Nakayama, Y.; Matsuda, T. *Journal of Polymer Science Part a-Polymer Chemistry* **1992**, *30*, 2451.
(153) Nakayama, Y.; Matsuda, T. *Journal of Polymer Science Part a-Polymer Chemistry* **1993**, *31*, 3299.
(154) Minsk, L. M.; VanDeusen, W.; Robertson, E. M. U.S. Patent # 2,670,285, 1954.
(155) Minsk, L. M.; VanDeusen, W.; Robertson, E. M. U.S. Patent # 2,670,286, 1954.
(156) Minsk, L. M.; VanDeusen, W.; Robertson, E. M. U.S. Patent # 2,670,287, 1954.

(157) Robertson, E.; Deusen, W.; Minsk, L. *Journal of Applied Polymer Science* **1959**, *2*, 308.
(158) L. M. Minsk, J. G. S., W. P. Van Deusen, & J. F. Wright *Journal of Applied Polymer Science* **1959**, *2*, 302.
(159) Decker, C.; Bianchi, C. *Polymer International* **2003**, *52*, 722.
(160) Baret, V.; Gandini, A.; Rousset, E. *Journal of Photochemistry and Photobiology a-Chemistry* **1997**, *103*, 169.
(161) Gandini, A.; Belgacem, M. N. *Progress in Polymer Science* **1997**, *22*, 1203.
(162) Fang, S. W.; Timple, H. J.; Gandini, A. *Polymer* **2002**, *43*, 3505.
(163) L. M. Minsk, W. P. V. D., & E. M. Robertson U.S. Patent # 2,670,286, 1954.
(164) Nishikubo, T.; Iizawa, T.; Shiozaki, Y.; Koito, T. *Journal of Polymer Science Part a-Polymer Chemistry* **1992**, *30*, 449.
(165) L. M. Minsk, W. P. V. D., & E. M. Robertson U.S. Patent # 2,670,285, 1954.
(166) L. M. Minsk, W. P. V. D., & E. M. Robertson U.S. Patent # 2,670,287, 1954.
(167) E. Robertson, W. D., L. Minsk *Journal of Applied Polymer Science* **1959**, *2*, 308.
(168) Murase, S.; Kinoshita, K.; Horie, K.; Morino, S. *Macromolecules* **1997**, *30*, 8088.
(169) Lazarev, V. V.; Barberi, R.; Iovane, M.; Papalino, L.; Blinov, L. M. *Liquid Crystals* **2002**, *29*, 273.
(170) Kawatsuki, N.; Goto, K.; Kawakami, T.; Yamamoto, T. *Macromolecules* **2002**, *35*, 706.
(171) Kawatsuki, N.; Goto, K.; Yamamoto, T. *Liquid Crystals* **2001**, *28*, 1171.
(172) Kawatsuki, N.; Kawakami, T.; Yamamoto, T. *Advanced Materials* **2001**, *13*, 1337.
(173) Kawatsuki, N.; Matsuyoshi, K.; Hayashi, M.; Takatsuka, H.; Yamamoto, T. *Chemistry of Materials* **2000**, *12*, 1549.
(174) Sapich, B.; Stumpe, J.; Krawinkel, T.; Kricheldorf, H. R. *Macromolecules* **1998**, *31*, 1016.
(175) Tung, C. H.; Ying, Y. M.; Yuan, Z. Y. *Journal of Photochemistry and Photobiology a-Chemistry* **1998**, *119*, 93.
(176) Jantas, R.; Wodka, T.; Janowska, G. *Polimery* **2001**, *46*, 812.
(177) Andreopoulos, F. M.; Beckman, E. J.; Russell, A. J. *Journal of Polymer Science Part a-Polymer Chemistry* **2000**, *38*, 1466.
(178) Andreopoulos, F. M.; Deible, C. R.; Stauffer, M. T.; Weber, S. G.; Wagner, W. R.; Beckman, E. J.; Russell, A. J. *Journal of the American Chemical Society* **1996**, *118*, 6235.
(179) Economy, J.; Andreopoulos, A. G. *Polymers for Advanced Technologies* **1996**, *7*, 561.
(180) Yujun Zheng, M. M., Sarita V. Mello, Mustapha Mabrouki, Fotios M. Andreopoulos, Veeranjaneyulu Konka, Si M. Pham, and Roger M. Leblanc *Macromolecules* **2002**, *35*, 5228

(181) Zheng, Y. J.; Andreopoulos, F. M.; Micic, M.; Huo, Q.; Pham, S. M.; Leblanc, R. M. *Advanced Functional Materials* **2001**, *11*, 37.
(182) Abdel-Mottaleb, M. M. S.; De Feyter, S.; Gesquiere, A.; Sieffert, M.; Klapper, M.; Mullen, K.; De Schryver, F. C. *Nano Letters* **2001**, *1*, 353.
(183) Tao, J.; Liu, G. *Macromolecules* **1997**, *30*, 2408.
(184) Coleman, M. M.; Hu, Y.; Sobkowiak, M.; Painter, P. C. *Journal of Polymer Science Part B-Polymer Physics* **1998**, *36*, 1579.
(185) Hu, Y.; Gamble, V.; Painter, P. C.; Coleman, M. M. *Macromolecules* **2002**, *35*, 1289.
(186) Tao, J.; Liu, G.; Ding, J.; Yang, M. *Macromolecules* **1997**, *30*, 4084.
(187) Kawatsuki, N.; Furuso, N.; Goto, K.; Yamamoto, T. *Journal of Photopolymer Science and Technology* **2002**, *15*, 265.
(188) Zahir, S. *Journal of Applied Polymer Science* **1979**, *23*, 1355.
(189) Oh, D. H. C. a. S. J. *European Polymer Journal* **2002**, *38*, 1559.
(190) Choi, D. H.; Cha, Y. K. *Polymer Bulletin* **2002**, *48*, 373.
(191) Coursan, M.; Desvergne, J. P.; Deffieux, A. *Macromolecular Chemistry and Physics* **1996**, *197*, 1599.
(192) Ortyl, E.; Janik, R.; Kucharski, S. *European Polymer Journal* **2002**, *38*, 1871.
(193) Kuckling, D.; Ivanova, I. G.; Adler, H. J. P.; Wolff, T. *Polymer* **2002**, *43*, 1813.
(194) Brahmbhatt, D. I.; Singh, S.; Patel, K. C. *European Polymer Journal* **1999**, *35*, 317.
(195) Ciamician, G.; Silber, P. *Berichte der Deutschen Chemischen Gesellschaft zu Berlin* **1902**, *35*, 4128.
(196) Chen, Y.; Chen, K. H. *Journal of Polymer Science Part a-Polymer Chemistry* **1997**, *35*, 613.
(197) Chen, Y.; Chou, C. F. *Journal of Polymer Science Part a-Polymer Chemistry* **1995**, *33*, 2705.
(198) Chen, Y.; Geh, J. L. *Polymer* **1996**, *37*, 4473.
(199) Chen, Y.; Geh, J. L. *Polymer* **1996**, *37*, 4481.
(200) Chen, Y.; Hong, R. T. *Journal of Polymer Science Part a-Polymer Chemistry* **1997**, *35*, 2999.
(201) Chen, Y.; Jean, C. S. *Journal of Applied Polymer Science* **1997**, *64*, 1749.
(202) Chen, Y.; Jean, C. S. *Journal of Applied Polymer Science* **1997**, *64*, 1759.
(203) Chen, Y.; Lin, J. J. *Journal of Polymer Science Part a-Polymer Chemistry* **1992**, *30*, 2699.
(204) Chen, Y.; Saigo, K.; Yonezawa, N.; Tachibana, K.; Hasegawa, M. *Bulletin of the Chemical Society of Japan* **1987**, *60*, 3341.
(205) Chen, Y.; Shiao, M. T. *Bulletin of the Chemical Society of Japan* **1992**, *65*, 3423.
(206) Chen, Y.; Wu, J. D. *Journal of Polymer Science Part a-Polymer Chemistry* **1994**, *32*, 1867.
(207) de Melo, J. S.; Fernandes, P. F. *Journal of Molecular Structure* **2001**, *565*, 69.

(208) Delzenne, G. A.; Laridon, U. *36th Congress International De Chimie Industrielle* **1967**, *3*, 373.
(209) Demelo, J. S. S.; Becker, R. S.; Macanita, A. L. *Journal of Physical Chemistry* **1994**, *98*, 6054.
(210) Fang, J. Y.; Whitaker, C.; Weslowski, B.; Chen, M. S.; Naciri, J.; Shashidhar, R. *Journal of Materials Chemistry* **2001**, *11*, 2992.
(211) Fischer, J.; Henry, R.; Hoover, J.; Lindsay, G.; Stenger-Smith, J.; Chafin, A. P. USA Pat #5212269, 1993.
(212) Hammond, G. S.; Stout, C. A.; Lamola, A. A. *Journal of the American Chemical Society* **1964**, *86*, 3103.
(213) Hasegawa, M.; Saigo, K.; Katsuki, H.; Yonezawa, N.; Kanoe, T. *Journal of Polymer Science: Polymer Chemistry Edition* **1983**, *21*, 2345.
(214) Hoffmann, R.; Wells, P.; Morrison, H. *Journal of Organic Chemistry* **1971**, *36*, 102.
(215) Horaguchi, T.; Hosokawa, N.; Tanemura, K.; Suzuki, T. *Journal of Heterocyclic Chemistry* **2002**, *39*, 61.
(216) Jackson, P. O.; Bergmann, G.; Hogg, J. H. C.; O'Neill, M.; Hindmarsh, P.; Kelly, S. M.; Clark, G. F. *Synthetic Metals* **2002**, *127*, 95.
(217) Jackson, P. O.; O'Neill, M.; Duffy, W. L.; Hindmarsh, P.; Kelly, S. M.; Owen, G. J. *Chemistry of Materials* **2001**, *13*, 694.
(218) K. Gnanaguru, N. R., K. Venkatesan, and V. Ramamurthy *Journal of Organic Chemistry* **1985**, *50*, 2337.
(219) Kawata, H.; Ichikawa, S.; Kumagai, T.; Niizuma, S. *Tetrahedron Letters* **2002**, *43*, 5161.
(220) Krauch, C.; Farid, S.; Schenck, G. *Chem. Ber.* **1966**, *99*, 625.
(221) Lewis, F. D.; Barancyk, S. V. *Journal of the American Chemical Society* **1989**, *111*, 8653.
(222) Moorthy, J. N.; Venkatesan, K. *Journal of Organic Chemistry* **1991**, *56*, 6957.
(223) Moorthy, J. N.; Venkatesan, K. *Journal of Materials Chemistry* **1992**, *2*, 675.
(224) Morrison, H.; Curtis, H.; McDowell, T. *Journal of the American Chemical Society* **1966**, *88*, 5415.
(225) Obi, M.; Morino, S.; Ichimura, K. *Chemistry of Materials* **1999**, *11*, 656.
(226) Ohkawa, K.; Shoumura, K.; Yamada, M.; Nishida, A.; Shirai, H.; Yamamoto, H. *Macromolecular Bioscience* **2001**, *1*, 149.
(227) Ree, M.; Kim, S. I.; Lee, S. W. *Synthetic Metals* **2001**, *117*, 273.
(228) Saigo, K.; Chen, Y.; Fujioka, K. *Chemistry Letters* **1988**, 647.
(229) Saigo, K.; Chen, Y.; Yonezawa, N.; Kanoe, T.; Tachibana, K.; Hasegawa, M. *Macromolecules* **1986**, *19*, 1552.
(230) Saigo, K.; Shiwaku, T.; Hayashi, K.; Fujioka, K.; Sukegawa, M.; Chen, Y.; Yonezawa, N.; Hasegawa, M.; Hashimoto, T. *Macromolecules* **1990**, *23*, 2830.
(231) Saigo, K.; Yonezawa, N.; Sekimoto, K.; Hasegawa, M.; Ueno, K.; Nakanishi, H. *Bulletin of the Chemical Society of Japan* **1985**, *58*, 1000.

(232) Schonberg, A.; Latif, N.; Moubasher, R.; Awad, W. *Journal of the Chemical Society* **1950**, 374.
(233) Tian, Y. Q.; Akiyama, E.; Nagase, Y.; Kanazawa, A.; Tsutsumi, O.; Ikeda, T. *Macromolecular Chemistry and Physics* **2000**, *201*, 1640.
(234) Yamamoto, H.; Kitsuki, T.; Nishida, A.; Asada, K.; Ohkawa, K. *Macromolecules* **1999**, *32*, 1055.
(235) Yonezawa, N.; Yoshida, T.; Hasegawa, M. *Journal of the Chemical Society-Perkin Transactions 1* **1983**, 1083.
(236) Yoshiki Chujo, K. S., and Takeo Saegusa *Macromolecules* **1990**, *23*, 2693.
(237) Hugel, T.; Holland, N. B.; Cattani, A.; Moroder, L.; Seitz, M.; Gaub, H. E. *Science* **2002**, *296*, 1103.
(238) Shimoboji, T.; Ding, Z. L.; Stayton, P. S.; Hoffman, A. S. *Bioconjugate Chemistry* **2002**, *13*, 915.
(239) Kawatsuki, N.; Matsuyoshi, K.; Yamamoto, T. *Macromolecules* **2000**, *33*, 1698.
(240) Rennert, J. J. *Photographic Science and Engineering* **1971**, *15*, 60.
(241) Graley, M.; Reiser, A.; Roberts, A. J.; Phillips, D. *Macromolecules* **1981**, *14*, 1752.
(242) Ichimura, K.; Akita, Y.; Akiyama, H.; Kudo, K.; Hayashi, Y. *Macromolecules* **1997**, *30*, 903.
(243) Kim, H. T.; Park, J. K. *Polymer Bulletin* **1998**, *41*, 325.
(244) Jackson, P. O.; Karapinar, R.; O'Neill, M.; Hindmarsh, P.; Owen, G. J.; Kelly, S. M. Proceedings of SPIE-The International Society for Optical Engineering, 1999; p 38.
(245) Joshi, A.; Enholm, E. J. *Abstracts of Papers of the American Chemical Society* **2002**, *223*, B243.
(246) Assaid, I.; Hardy, I.; Bosc, D. *Optics Communications* **2002**, *214*, 171.
(247) Kimura, T.; Kim, J.-Y.; Fukuda, T.; Matsuda, H. *Macromolecular Chemistry and Physics* **2002**, *203*, 2344.
(248) Park, S. Y.; Park, H. Y.; Lee, H. S.; Park, S. W.; Park, D. W. *Optical Materials* **2002**, *21*, 331.
(249) Micic, M.; Zheng, Y.; Moy, V.; Zhang, X.-H.; Andreopoulos, F. M.; Leblanc, R. M. *Colloids and Surfaces* **2003**, *27*, 147.
(250) Chae, B.; Lee, S. W.; Ree, M.; Jung, Y. M.; Kim, S. B. *Langmuir* **2003**, *19*, 687.
(251) Oriol, L.; Pinol, M.; Serrano, J. L.; Tejedor, R. M. *Journal of Photochemistry and Photobiology a-Chemistry* **2003**, *155*, 37.
(252) Furumi, S.; Otomo, A.; Yokoyama, S.; Mashiko, S. *Thin Solid Films* **2003**, *438-439*, 85.
(253) Pirrung, M. C.; Pieper, W. H.; Kaliappan, K. P.; Dhananjeyan, M. R. *Proceedings of the National Academy of Sciences of the United States of America* **2003**, *100*, 12548.
(254) Lee, S. W.; Kim, S. I.; Lee, B.; Choi, W. Y.; Chae, B.; Kim, S. B.; Ree, M. *Macromolecules* **2003**, *36*, 6527.

(255) Balaji, R.; Grande, D.; Nanjundan, S. *Reactive & Functional Polymers* **2003**, *56*, 45.
(256) Esen, H.; Kusefoglu, S. H. *Journal of Applied Polymer Science* **2003**, *89*, 3882.
(257) Trenor, S. R.; Lizotte, J. R.; Love, B. J.; Long, T. E. *In Preparation* **2004**.
(258) Trenor, S. R.; Lizotte, J. R.; Love, B. J.; Long, T. E. *In Preparation* **2004**.
(259) Rabe, J. P.; Buchholz, S. *Science* **1991**, *253*, 424.
(260) De Feyter, S.; Gesquiere, A.; Abdel-Mottaleb, M. M.; Grim, P. C. M.; De Schryver, F. C.; Meiners, C.; Sieffert, M.; Valiyaveettil, S.; Mullen, K. *Accounts of Chemical Research* **2000**, *33*, 520.
(261) Gesquiere, A.; Abdel-Mottaleb, M. M.; De Feyter, S.; De Schryver, F. C.; Sieffert, M.; Mullen, K.; Calderone, A.; Lazzaroni, R.; Bredas, J. L. *Chemistry-a European Journal* **2000**, *6*, 3739.
(262) Decker, C. *Journal of Coating Technology* **1987**, *59*, 97.
(263) L . Plambeck, J. U.S. Patent # 2,760,863, 1956.
(264) Yourick, J. J.; Bronaugh, R. L. *Journal of Applied Toxicology* **1997**, *17*, 153.
(265) Jakubiak, R.; Bunning, T. J.; Vaia, R. A.; Natarajan, L. V.; Tondiglia, V. P. *Advanced Materials* **2003**, *15*, 241.
(266) *Coumarins: Biology, Applications, and Mode of Action*; O'Kennedy, R.; Thornes, R. D., Eds.; John Wiley & Sons, 1997.
(267) Killard, A. J.; O'Kennedy, R.; Bogan, D. P. *Journal of Pharmaceutical and Biomedical Analysis* **1996**, *14*, 1585.
(268) Nielson, B. E. In *The Biology and Chemistry of the Umbelliferae*; Heywood, V. E., Ed.; Academic Press: London, 1971.
(269) Murray, R. D. H.; Mendez, J.; Brown, S. A. *The Natural Coumarins: Occurence, Chemistry and Biochemistry*; John Wiley & Sons: New York, 1982.
(270) Eckardt, T.; Hagen, V.; Schade, B.; Schmidt, R.; Schweitzer, C.; Bendig, J. *Journal of Organic Chemistry* **2002**, *67*, 703.
(271) Zhang, R. F.; Zheng, H. P.; Shen, J. C. *Synthetic Metals* **1999**, *106*, 157.
(272) Izquierdo, M. E. F.; Granados, J. Q.; Mir, V. M.; Martinez, M. C. L. *Food Chemistry* **2000**, *70*, 251.
(273) Yamazaki, H.; Tanaka, M.; Shimada, T. *Journal of Chromatography B* **1999**, *721*, 13.
(274) Jones, G.; Rahman, M. A. *Journal of Physical Chemistry* **1994**, *98*, 13028.
(275) Jones, G.; Jackson, W. R.; Choi, C.-y.; Bergmark, W. R. *Journal of Physical Chemistry* **1985**, *89*, 294.
(276) Stathatos, E.; Lianos, P.; Stangar, U. L.; Orel, B. *Chemical Physics Letters* **2001**, *345*, 381.
(277) Cohen, B.; Huppert, D. *Journal of Physical Chemistry A* **2001**, *105*, 7157.
(278) Kovac, B.; Novak, I. *Spectrochimica Acta Part a-Molecular and Biomolecular Spectroscopy* **2002**, *58*, 1483.
(279) de Melo, J. S. S.; Becker, R. S.; Macanita, A. L. *Journal of Physical Chemistry* **1994**, *98*, 6054.

(280) Moriya, T.; Anzai, H. *Bulletin of the Electrotechnical Laboratory* **1982**, *46*, 431.
(281) Becker, R. S.; Chakravorti, S.; Gartner, C. A.; Miguel, M. D. *Journal of the Chemical Society-Faraday Transactions* **1993**, *89*, 1007.
(282) Hoshiyama, M.; Kubo, K.; Igarashi, T.; Sakurai, T. *Journal of Photochemistry and Photobiology a-Chemistry* **2001**, *138*, 227.
(283) Park, S. W.; Seo, B. S.; Kim, E. H.; Kim, D. H.; Paeng, K. J. *Journal of Forensic Sciences* **1996**, *41*, 685.
(284) Keating, G. J.; O'Kennedy, R. In *Coumarins: Biology, Applications, and Mode of Action*; O'Kennedy, R., Thornes, R. D., Eds.; John Wiley & Sons: New York, 1997.
(285) Semple, S. J.; Nobbs, S. F.; Pyke, S. M.; Reynolds, G. D.; Flower, R. L. P. *Journal of Ethnopharmacology* **1999**, *68*, 283.
(286) Weinmann, I. In *Coumarins: Biology, Applications, and Mode of Action*; O'Kennedy, R., Thornes, R. D., Eds.; John Wiley & Sons: New York, 1997.
(287) Casley-Smith, J. R.; Casley-Smith, J. R. In *Coumarins: Biology, Applications, and Mode of Action*; O'Kennedy, R., Thornes, R. D., Eds.; John Wiley & Sons: New York, 1997.
(288) Ebbinghaues, S. W.; Mohler, J. L.; Marshall, M. E. In *Coumarins: Biology, Applications, and Mode of Action*; O'Kennedy, R., Thornes, R. D., Eds.; John Wiley & Sons: New York, 1997.
(289) Mohler, J. L.; Williams, B. T.; Freeman, J. A.; Marshall, M. E. In *Coumarins: Biology, Applications, and Mode of Action*; O'Kennedy, R., Thornes, R. D., Eds.; John Wiley & Sons: New York, 1997.
(290) Piler, N. B. In *Coumarins: Biology, Applications, and Mode of Action*; O'Kennedy, R., Thornes, R. D., Eds.; John Wiley & Sons: New York, 1997.
(291) Thornes, R. D. In *Coumarins: Biology, Applications, and Mode of Action*; O'Kennedy, R., Thornes, R. D., Eds.; John Wiley & Sons: New York, 1997.
(292) Zlabinger, G. J. In *Coumarins: Biology, Applications, and Mode of Action*; O'Kennedy, R., Thornes, R. D., Eds.; John Wiley & Sons: New York, 1997.
(293) Clark, S. L.; Porter, T. F.; West, F. G. *Obstetrics and Gynecology* **2000**, *95*, 938.
(294) Hirsh, J.; Fuster, V.; Ansell, J.; Halperin, J. L. *Journal of the American College of Cardiology* **2003**, *41*, 1633.
(295) Pisklak, M.; Maciejewska, D.; Herold, F.; Wawer, I. *Journal of Molecular Structure* **2003**, *649*, 169.
(296) Yu, D. L.; Suzuki, M.; Xie, L.; Morris-Natschke, S. L.; Lee, K. H. *Medicinal Research Reviews* **2003**, *23*, 322.
(297) Fujiwara, M.; Shiokawa, K.; Kawasaki, N.; Tanaka, Y. *Advanced Functional Materials* **2003**, *13*, 371.
(298) Mal, N. K.; Fujiwara, M.; Tanaka, Y. *Nature* **2003**, *421*, 350.
(299) Knoevenagel, E. *Berichte der Deutschen Chemischen Gesellschaft zu Berlin* **1904**, *37*, 4461.
(300) Song, A. M.; Wang, X. B.; Lam, K. S. *Tetrahedron Letters* **2003**, *44*, 1755.
(301) Schroeder, C. H.; Link, K. P. *Journal of the American Chemical Society* **1953**, *75*, 1886.

(302) Wiener, C.; Schroeder, C. H.; Link, K. P. *Journal of the American Chemical Society* **1957**, *79*, 5301.
(303) Laufer, M. C.; Hausmann, H.; Hölderich, W. F. *Journal of Catalysis* **2003**, *218*, 315.
(304) Van, T. N.; Debenedetti, S.; De Kimpe, N. *Tetrahedron Letters* **2003**, *44*, 4199.
(305) Bigi, F.; Carloni, S.; Ferrari, L.; Maggi, R.; Mazzacani, A.; Sartori, G. *Tetrahedron Letters* **2001**, *42*, 5203.
(306) Bigi, F.; Chesini, L.; Maggi, R.; Sartori, G. *Journal of Organic Chemistry* **1999**, *64*, 1033.
(307) Maggi, R.; Bigi, F.; Carloni, S.; Mazzacani, A.; Sartori, G. *Green Chemistry* **2001**, *3*, 173.
(308) Ahmad, M.; King, T. A.; Ko, D. K.; Cha, B. H.; Lee, J. M. *Optics and Laser Technology* **2002**, *34*, 445.
(309) Singh, S.; Kanetkar, V. R.; Sridhar, G.; Muthuswamy, V.; Raja, K. *Journal of Luminescence* **2003**, *101*, 285.
(310) Wheelock, C. *Journal of the American Chemical Society* **1959**, *81*, 1348.
(311) Mantulin, W.; Song, P. *Journal of the American Chemical Society* **1973**, *95*, 5122.
(312) Singh, T. S.; Rao, B. S. M.; Mohan, H.; Mittal, J. P. *Journal of Photochemistry and Photobiology a-Chemistry* **2002**, *153*, 163.
(313) Oh, J. K.; Wu, J.; Winnik, M. A.; Craun, G. P.; Rademacher, J.; Farwaha, R. *Journal of Polymer Science Part a-Polymer Chemistry* **2002**, *40*, 1594.
(314) Ammar, H.; Fery-Forgues, S.; El Gharbi, R. *Dyes and Pigments* **2003**, *57*, 259.
(315) Aihara, S.; Hirano, Y.; Tajima, T.; Tanioka, K.; Abe, M.; Saito, N.; Kamata, N.; Terunuma, D. *Applied Physics Letters* **2003**, *82*, 511.
(316) Murase, S.; Teramoto, M.; Furukawa, H.; Miyashita, Y.; Horie, K. *Macromolecules* **2003**, *36*, 964.
(317) Tanaka, I.; Inoue, Y.; Ishii, N.; Tanaka, K.; Izumi, Y.; Okamoto, S. *Displays* **2002**, *23*, 249.
(318) Sharma, V. K.; Saharo, P. D.; Sharma, N.; Rastogi, R. C.; Ghoshal, S. K.; Mohan, D. *Spectrochimica Acta Part a-Molecular and Biomolecular Spectroscopy* **2003**, *59*, 1161.
(319) Ström, K. T. *Berichte der Deutschen Chemischen Gesellschaft zu Berlin* **1904**, *37*, 1383.
(320) Anet, R. *Chemistry & Industry* **1960**, 897.
(321) Anet, R. *Canadian Journal of Chemistry* **1962**, *40*, 1249.
(322) Brett, T. J.; Alexander, J. M.; Stezowski, J. J. *Journal of the Chemical Society-Perkin Transactions 2* **2000**, *6*, 1105.
(323) Shim, S. C.; Jeong, B. M.; Paik, Y. H. *Bulletin of the Korean Chemical Society* **1992**, *13*, 684.
(324) Belfield, K. D.; Bondar, M. V.; Liu, Y.; Przhonska, O. V. *Journal of Physical Organic Chemistry* **2003**, *16*, 69.
(325) Lamola, A. A. *Journal of the American Chemical Society* **1966**, *88*, 813.

(326) Suzuki, Y.; Hasegawa, M. *Journal of Polymer Science Part C-Polymer Letters Edition* **1973**, *11*, 173.
(327) Takahashi, H.; Sakuragi, M.; Hasegawa, M.; Takahashi, H. *Journal of Polymer Science Part a-Polymer Chemistry* **1972**, *10*, 1399.
(328) Kim, H. C.; Kreiling, S.; Greiner, A.; Hampp, N. *Chemical Physics Letters* **2003**, *372*, 899.
(329) Michl, J.; Thulstrup, E. *Spectroscopy with Polarized Light: Solute Alignment by Photoselection, Liquid Crystal, Polymers, and Membranes Corrected Software Edition*; John Wiley & Sons: New York, 1995.
(330) Chung, T.-S. *Thermotropic Liquid Crystal Polymers: Thin-film Poly Chara Blends*; Technomic Pub Co, 2001.
(331) McArdle, C. B. *Side Chain Liquid Crystal Polymers*; Kluwer Academic Publishers, 1990.
(332) Plate, N. A. *Liquid-Crystal Polymers (Specialty Polymers)*; Plenum Pub Corp, 1993.
(333) Mantia, F. P. L.; La, F. P. *Thermotropic Liquid Crystal Polymer Blends*; Technomic Pub Co, 1993.
(334) Acierno, D.; Collyer, A. A. *Rheology and Processing of Liquid Crystal Polymers*; Chapman & Hall, 1996.
(335) Collyer, A. A. *Liquid Crystal Polymers: From Structures to Applications*; Elsevier Applied Science, 1992.
(336) Kishore, G. a. K. *Macromolecules* **1995**, *28*, 806.
(337) Schadt, M.; Seiberle, H.; Schuster, A. *Nature* **1996**, *381*, 212.
(338) Schadt, M.; Schmitt, K.; Kozinkov, V.; Chigrinov, V. *Japanese Journal of Applied Physics Part 1-Regular Papers Short Notes & Review Papers* **1992**, *31*, 2155.
(339) Schadt, M.; Seiberle, H.; Schuster, A.; Kelly, S. M. *Japanese Journal of Applied Physics Part 2-Letters* **1995**, *34*, L764.
(340) Hindmarsh, P.; Owen, G. J.; Kelly, S. M.; Jackson, P. O.; O'Neill, M.; Karapinar, R. *Molecular Crystals and Liquid Crystals Science and Technology Section a-Molecular Crystals and Liquid Crystals* **1999**, *332*, 2949.
(341) Tian, Y. Q.; Kong, X. X.; Nagase, Y.; Iyoda, T. *Journal of Polymer Science Part a-Polymer Chemistry* **2003**, *41*, 2197.
(342) Tian, Y. Q.; Akiyama, E.; Nagase, Y. *Journal of Materials Chemistry* **2003**, *13*, 1253.
(343) Li, W. J.; Lynch, V.; Thompson, H.; Fox, M. A. *Journal of the American Chemical Society* **1997**, *119*, 7211.
(344) Tlenkopatchev, M. A.; Fomine, S.; Fomina, L.; Gavino, R.; Ogawa, T. *Polymer Journal* **1997**, *29*, 622.
(345) Fomine, S.; Delgado, C.; Fomina, L.; Gavino, R.; Ogawa, T. *Macromolecular Chemistry and Physics* **1997**, *198*, 3065.
(346) M. Uchida, T. I. a. K. F. In *CAS*; European Patent Office: Japan, 1995.
(347) Fomine, S.; Fomina, L.; Sanchez, C.; Ortiz, A.; Ogawa, T. *Polymer Journal* **1997**, *29*, 49.

(348) Fomine, S.; Perez, H.; Fomina, L.; Tlenkopatchev, M.; Ogawa, T. *Macromolecular Chemistry and Physics* **1997**, *198*, 1679.
(349) Cardona, C. M.; Jannach, S. H.; Huang, H.; Itojima, Y.; Leblanc, R. M.; Gawley, R. E.; Baker, G. A.; Brauns, E. B. *Helvetica Chimica Acta* **2002**, *85*, 3532.
(350) Fomine, S.; Rivera, E.; Fomina, L.; Ortiz, A.; Ogawa, T. *Polymer* **1998**, *39*, 3551.
(351) Lu, Z. Y.; Yuan, T. S.; Chen, Y. L.; Wei, X. Q.; Zhu, W. G.; Xie, M. G. *Chinese Chemical Letters* **2002**, *13*, 674.
(352) Lang, J. M.; Drickamer, H. G. *Journal of Physical Chemistry* **1993**, *97*, 5058.
(353) Palmans, A. R. A.; Smith, P.; Weder, C. *Macromolecules* **1999**, *32*, 4677.
(354) Gilat, S. L.; Adronov, A.; Fréchet, J. M. J. *Journal of Organic Chemistry* **1999**, *64*, 7474.
(355) Serin, J.; Schultze, X.; Adronov, A.; Fréchet, J. M. J. *Macromolecules* **2002**, *35*, 5396.
(356) Adronov, A.; Fréchet, J. M. J.; He, G. S.; Kim, K. S.; Chung, S. J.; Swiatkiewicz, J.; Prasad, P. N. *Chemistry of Materials* **2000**, *12*, 2838.
(357) Lee, L. F.; Adronov, A.; Schaller, R. D.; Fréchet, J. M. J.; Saykally, R. J. *Journal of the American Chemical Society* **2003**, *125*, 536.
(358) Zheng, Y. J.; Micic, M.; Mello, S. V.; Mabrouki, M.; Andreopoulos, F. M.; Konka, V.; Pham, S. M.; Leblanc, R. M. *Macromolecules* **2002**, *35*, 5228
(359) Chujo, Y.; Sada, K.; Saegusa, T. *Macromolecules* **1990**, *23*, 2693.
(360) Chujo, Y.; Sada, K.; Saegusa, T. *Macromolecules* **1990**, *23*, 2636.
(361) Trenor, S. R.; Long, T. E.; Love, B. J. *Macromolecular Chemistry and Physics* **2004**, *205*, 715.
(362) Yamamoto, H. *Macromolecules* **1986**, *19*, 2476.
(363) Yamamoto, H.; Hirata, Y.; Tanisho, H. *International Journal of Biological Macromolecules* **1994**, *16*, 81.
(364) Yamamoto, H.; Ikeda, K.; Nishida, A. *Polymer International* **1992**, *27*, 67.
(365) Yamamoto, H.; Miyagi, Y.; Nishida, A.; Takagishi, T.; Shima, S. *Journal of Photochemistry* **1987**, *39*, 343.
(366) Yamamoto, H.; Nishida, A. *Polymer International* **1991**, *24*, 145.
(367) Yamamoto, H.; Nishida, A. *Bulletin of the Chemical Society of Japan* **1988**, *61*, 2201.
(368) Yamamoto, H.; Nishida, A. *Journal of Photochemistry and Photobiology a-Chemistry* **1988**, *42*, 149.
(369) Yamamoto, H.; Nishida, A. *Macromolecules* **1986**, *19*, 943.
(370) Yamamoto, H.; Nishida, A.; Kawaura, T. *International Journal of Biological Macromolecules* **1990**, *12*, 257.
(371) Yamamoto, H.; Nishida, A.; Shimozawa, T. *Journal of the Chemical Society-Perkin Transactions 2* **1989**, 1477.
(372) Yamamoto, H.; Nishida, A.; Takimoto, T.; Nagai, A. *Journal of Polymer Science Part a-Polymer Chemistry* **1990**, *28*, 67.
(373) Matsuda, T.; Mizutani, M.; Arnold, S. C. In *USPTO* USA Patent # 6,423,818, 2002.

(374) Ballesteros, O. G.; Maretti, L.; Sastre, R.; Scaiano, J. C. *Macromolecules* **2001**, *34*, 6184.
(375) Jones, G.; Jimenez, J. A. C. *Journal of Photochemistry and Photobiology B-Biology* **2001**, *65*, 5.
(376) Haupt, K.; Mayes, A. G.; Mosbach, K. *Analytical Chemistry* **1998**, *70*, 3936.
(377) Graf, C.; Schartl, W.; Fischer, K.; Hugenberg, N.; Schmidt, M. *Langmuir* **1999**, *15*, 6170.
(378) Haupt, K.; Dzgoev, A.; Mosbach, K. *Analytical Chemistry* **1998**, *70*, 628.
(379) Bruggemann, O.; Haupt, K.; Ye, L.; Yilmaz, E.; Mosbach, K. *Journal of Chromatography A* **2000**, *889*, 15.
(380) Lindenblatt, G.; Schartl, W.; Pakula, T.; Schmidt, M. *Macromolecules* **2001**, *34*, 1730.
(381) Lindenblatt, G.; Schartl, W.; Pakula, T.; Schmidt, M. *Macromolecules* **2000**, *33*, 9340.
(382) Schmidt, R.; Alt, H. G.; Ebenhoch, J. *Journal of Applied Polymer Science* **2001**, *80*, 613.
(383) Schmidt, R.; Alt, H. G.; Ebenhoch, J. *Journal of Applied Polymer Science* **2001**, *80*, 281.
(384) Even, P.; Chaubet, F.; Letourneur, D.; Viriot, M. L.; Carre, M. C. *Biorheology* **2003**, *40*, 261.
(385) Allonas, X.; Fouassier, J. P.; Kaji, M.; Miyasaka, M.; Hidaka, T. *Polymer* **2001**, *42*, 7627.
(386) Yang, Y. Y.; Feng, S. J.; Li, C. D.; Lao, L.; Wang, S. F.; Huang, W. T.; Gong, Q. H. *Journal of Photopolymer Science and Technology* **2002**, *15*, 83.
(387) Singh, A.; Ma, D. C.; Kaplan, D. L. *Biomacromolecules* **2000**, *1*, 592.
(388) Yongyuan, Y.; Shujing, F.; Chengde, L.; Le, L.; Shufeng, W.; Wentao, H.; Qihuang, G. *Journal of Photopolymer Science and Technology* **2002**, *15*, 83.
(389) Walshe, M.; Howarth, J.; Kelly, M. T.; Okennedy, R.; Smyth, M. R. *Journal of Pharmaceutical and Biomedical Analysis* **1997**, *16*, 319.
(390) Goss, B. *International Journal of Adhesion and Adhesives* **2002**, *22*, 405.
(391) Wolff, T.; Goerner, H. *Physical Chemistry Chemical Physics* **2004**, *6*, 368.
(392) Yu, X.; Scheller, D.; Rademacher, O.; Wolff, T. *Journal of Organic Chemistry* **2003**.
(393) Yu, X. L.; Wolff, T. *Langmuir* **2003**, *19*, 9672.
(394) Chen, X.; Smid, J. *Langmuir* **1996**, *12*, 2207.
(395) Kelly, S. M.; Owen, G. J.; O'Neil, M.; Jackson, P. O. World Patent #WO 0055151, 2000.
(396) Lee, S. W.; Kim, S. I.; Lee, B.; Kim, H. C.; Chang, T.; Ree, M. *Langmuir* **2003**, *19*, 10381.
(397) Falk, B. J.; Vallinas, S. M.; Crivello, J. V. *Journal of Polymer Science Part a-Polymer Chemistry* **2003**, *41*, 579.
(398) Peinado, C.; Salvador, E. F.; Baselga, J.; Catalina, F. *Macromolecular Chemistry and Physics* **2001**, *202*, 1924.

(399) Peinado, C.; Salvador, E. F.; Alonso, A.; Corrales, T.; Baselga, J.; Catalina, F. *Journal of Polymer Science Part a-Polymer Chemistry* **2002**, *40*, 4236.
(400) Peinado, C.; Allen, N. S.; Salvador, E. F.; Corrales, T.; Catalina, F. *Polymer Degradation and Stability* **2002**, *77*, 523.
(401) Bosch, P.; Fernandez-Arizpe, A.; Catalina, F.; Mateo, J. L.; Peinado, C. *Macromolecular Chemistry and Physics* **2002**, *203*, 336.
(402) Zumbrum, M. Ph.D. Dissertation, Virginia Polytechnic Institute and State University, 1990.
(403) Minsk, L. M.; Smith, J. G.; Deusen, W. P. V.; Wright, J. F. *Journal of Applied Polymer Science* **1959**, *2*, 302.
(404) Ngai, T.; Wu, C. *Macromolecules* **2003**, *36*, 848.
(405) Skoog, D. A.; Holler, F. J.; Nieman, T. A. In *Saunders Golden Sunburst Series*; 5th ed.; Publishing, S. C., Ed.; Harcourt Brace College Publishing: Philadelphia, 1998.
(406) Kovacs, A. J.; Gonthier, A. *Kolloid Zeitschrift & Zeitschrift fuer Polymere* **1972**, *250*, 530.
(407) Buckley, C. P.; Kovacs, A. J. *Colloid and Polymer Science* **1976**, *254*, 695.
(408) Kovacs, A. J.; Straupe, C. *Journal of Crystal Growth* **1980**, *48*, 210.
(409) Cheng, S. Z. D.; Wunderlich, B. *Macromolecules* **1989**, *22*, 1866.
(410) Cheng, S. Z. D.; Wu, S. S.; Chen, J. H.; Zhuo, Q. H.; Quirk, R. P.; Vonmeerwall, E. D.; Hsiao, B. S.; Habenschuss, A.; Zschack, P. R. *Macromolecules* **1993**, *26*, 5105.
(411) Pearce, R.; Vancso, G. J. *Macromolecules* **1997**, *30*, 5843.
(412) Huang, X. D.; Goh, S. H. *Macromolecules* **2001**, *34*, 3302.
(413) Beekmans, L. G. M.; Meer, D. W. v. d.; Vancso, G. J. *Polymer* **2002**, *43*, 1887.
(414) Hoffman, J. D. *Polymer* **1983**, *21*, 3.
(415) Hoffman, J. D. *Polymer* **1982**, *23*, 656.
(416) Hoffman, J. D. *Macromolecules* **1986**, *19*, 1124.
(417) Hoffman, J. D.; Miller, R. L. *Macromolecules* **1988**, *21*, 3038.
(418) Appel, M.; Fleischer, G. *Macromolecules* **1993**, *26*, 5520.
(419) Armistead, J. P.; Hoffman, J. D. *Macromolecules* **2002**, *35*, 3895.
(420) Trenor, S. R.; Shultz, A. R.; Love, B. J.; Long, T. E. *Chemical Reviews* **2004**, *In Press*.
(421) Gnanaguru, K.; Ramasubbu, N.; Venkatesan, K.; Ramamurthy, V. *Journal of Organic Chemistry* **1985**, *50*, 2337.
(422) Wu, C.; Ngai, T. *Polymer* **2004**.
(423) Bunsen, R. W.; Roscoe, H. E. *Ann. Phys.* **1859**, *108*, 234.
(424) Martin, J. W.; Chin, J. W.; Nguyen, T. *Progress in Organic Coatings* **2003**, *47*, 292.
(425) Schindl, A.; Rosado-Schlosser, B.; Trautinger, F. *Hautarzt* **2001**, *52*, 779.
(426) Hamilton, J. F. In *The Theory of the Photographic Process*; 4th ed.; James, T. H., Ed.; Macmillan Publishing Co., Inc.: New York, 1977.
(427) Halm, J. *Notices R. Astron. Soc.* **1922**, *82*, 473.
(428) Ahmad, H.; Yaseen, M. *Polymer Engineering and Science* **1979**, *19*, 858.

(429) Levy, G. C.; Rinaldi, P. L.; Dechter, J. J.; Axelson, D. E.; Mandelkern, L. In *Polymer Characterization by ESR and NMR*; Woodward, A. E., Bovey, F. A., Eds.; ACS: Washington, D.C., 1980; Vol. 142.
(430) Grulke, E. A. In *Polymer Handbook*; Brandrup, J., Immergut, E. H., Grulke, E. A., Eds.; John Wiley & Sons: New York, 1999.
(431) Webb, J. H. *Journal of the Optical Society of America* **1933**, *23*, 157.
(432) Nakano, S.; Endo, T. *Progress in Organic Coatings* **1993**, *22*, 287.
(433) Keller, P. *Chemistry of Materials* **1990**, *2*, 3.
(434) Peacock, A. J. *Polymer Communications* **1987**, *28*, 259.
(435) Keller, R. C. *Rubber Chemistry and Technology* **1988**, *61*, 238.
(436) Plambeck Jr., L. U.S. Patent # 2,760,863, 1956.
(437) Dowbenko, R. In *Handbook of Pressure Sensitive Adhesive Technology*; 2nd ed.; Satas, D., Ed.; Van Nostrand Reinhold: New York, 1989.
(438) Ebe, K.; Seno, H.; Horigome, K. *Journal of Applied Polymer Science* **2003**, *90*, 436.
(439) Trenor, S. R.; Huyck, R. H.; Long, T. E.; Love, B. J. *In Preparation* **2004**.
(440) Greenly, R. Z. In *Polymer Handbook*; Brandrup, J., Immergut, E. H., Grulke, E. A., Eds.; John Wiley & Sons: New York, 1999.
(441) Odian, G. *Principles of Polymerization*; 4th ed.; John Wiley and Sons, Inc.: New York, 2004.
(442) McKee, M. G.; Wilkes, G. L.; Colby, R. H.; Long, T. E. *Macromolecules* **2004**, *37*, 1760.
(443) Reneker, D. H.; Chun, I. *Nanotechnology* **1996**, *7*, 216.
(444) Fong, H.; Chun, I.; Reneker, D. H. *Polymer* **1999**, *40*, 4585.
(445) Deitzel, J. M.; Kleinmeyer, J.; Harris, D.; Tan, N. C. B. *Polymer* **2001**, *42*, 261.
(446) Deitzel, J. M.; Kosik, W.; McKnight, S. H.; Tan, N. C. B.; DeSimone, J. M.; Crette, S. *Polymer* **2002**, *43*, 1025.
(447) Hohman, M. M.; Shin, M.; Rutledge, G.; Brenner, M. P. *Physics of Fluids* **2001**, *13*, 2201.
(448) Grafe, T.; Graham, K. *International Nonwovens Journal* **2003**, *12*, 51.
(449) Matthews, J. A.; Wnek, G. E.; Simpson, D. G.; Bowlin, G. L. *Biomacromolecules* **2002**, *3*, 232.
(450) Gupta, P.; Wilkes, G. L. *Polymer* **2003**, *44*, 6353.
(451) Kenawy, E.-R.; Layman, J. M.; Watkins, J. R.; Bowlin, G. L.; Matthews, J. A.; Simpson, D. G.; Wnek, G. E. *Biomaterials* **2003**, *24*, 907.
(452) Zong, X.; Kim, K.; Fang, D.; Ran, S.; Hsiao, B. S.; Chu, B. *Polymer* **2002**, *43*, 4403.
(453) Zeng, J.; Hou, H.; Wendorff, J. H.; Greiner, A. *Polymer Preprints (American Chemical Society, Division of Polymer Chemistry)* **2003**, *44*, 174.
(454) Greiner, A.; Zeng, J.; Wendorff, J. H.; Hou, H. 226th ACS National Meeting, New York, NY, United States, 2003.
(455) Chiche, A.; Stafford, C. 27th Annual Meeting of The Adhesion Society, Wilmington, N.C., 2004; p 42.

VITA

Scott Russell Trenor

Scott Russell Trenor was born in March 1976 in West Palm Beach, Florida and lived in Wellington, Florida. After graduating from Wellington Community High School in 1994, he pursued his undergraduate studies in Materials Science and Engineering at the University of Florida, receiving a Bachelor of Science degree in 1998 with a minor in Chemistry. During his undergraduate career, he was a 5-time recipient of the National Science Foundation Undergraduate Research and Scholarship award.

In January 1999, Scott began studies in graduate school at Virginia Polytechnic Institute and State University in Materials Science and Engineering. He studied in the fields of adhesives and biomaterials under the guidance of Dr. Brian Love and received a Masters of Engineering in the fall of 2001. Following the Master's degree Scott joined the newly formed Macromolecular Science and Engineering Program to pursue a Doctorate of Philosophy. Scott was married to Julie P. Martin in January of 2004. Following graduation, Scott will join the Adhesives, Sealants and Coatings Division of KRATON Polymers in Houston, Texas.